Ionisation Studies on Some Small Molecules

Wei-Xian Peng

Department of Physics and Astronomy

The University of Glasgow

Presented as a thesis for the degree of Doctor of philosophy in the University of Glasgow

To

Mum and Dad

Husband and Sons

Acknowledgements

I would like to thank the following people for their contributions, assistance and friendship during the course of this work.

Dr. K W D Ledingham, my supervisor, for his encouragement and guidance throughout the period of my studies and his confidence in my abilities.

Prof. R Ferrier, for his constant and always friendly approach and for his sincere support in getting me financial support jointly with Dr. Ledingham.

Dr. R P Singhal, for his helpful advice and discussion in many aspects associated with the project.

Dr. R. Jennings, for his humour and cheerful talk whenever we meet each other.

Dr. A Marshall and Dr. A Clark for their advice and assistance in the earlier stage of my experimental work.

Dr. J Sander for his kindness and friendship.

Mr. T. McCanny and Mr. R. Maxwell for their technical assistance.

Miss C McIntyre for her valuable assistance in all aspects, her constant enthusiasm and care to me that makes me feel warm all the time during my stay in Glasgow.

My research colleagues, Dr. Ronger Zheng, Dr. Weijie Jia and Mr. C T J Scott for their friendly assistance in my earlier stage of my studies, Mr. Shiliang Wang for friendship, Mr. R. Deas, Mr. H C Kilic and Mr. D J Smith for helpful collaboration.

Mary Shearer and Brian Swann for their constant friendship and support.

Dr. C. Raine for his help in computer skills.

CVCP for an ORS.

The University of Glasgow for a scholarship.

Rutherford Appleton Laboratory for providing femtosecond laser facilities

Summary

The work of this thesis targeted the applications of a well established laser spectroscopic technique-REMPI; particuarly a laser-based procedure for the trace detection of environmentally sensitive molecules NO_X (x=1,2) and carbon monoxide (CO). The thesis also explores a new laser mass spectrometry technique-femtosecond mass spectroscopic trace analysis. The thesis consists of seven chapters which cover the fundamental concepts and principles (chapter 1), theories (chapter 2), instrumentation (chapter 3), the main experimental results of this work (chapter 4, 5 and 6) and future plans (chapter 7).

Chapter 1 introduces the fundamentals and some related basic concepts, photodissociation and predissociation, introduction to laser spectroscopy analysis and ionisation of atoms and molecules in intense laser fields. This chapter will help the reader to understand later chapters. The principle of mass spectrometry has been included in chapter 3 and 4 and therefore not mentioned in this chapter .

Chapter 2 deals with some theoretical work. Firstly a brief review of the historical background of multiphoton ionisation has been given. Thereafter the basic ionisation schemes of atoms and molecules has been described and the results of perturbation theory were quoted and the rate equations of MPI deduced.

Chapter 3 describes the instrumentation, including: - conventional laser light sources, laser pulse energy detector, ion detector, LeCroy 9304 175 MHz digital oscilloscope, time-of-flight (TOF) mass spectrometer and ultrafast laser system.

Chapter 4 has reviewed the technologies of NO_X detection, introduced the REMPI spectroscopy of NO_X, described the experimental methodology used in this thesis and reported the results of trace analysis of NO_X at atmospheric pressure conditions using a simple ionisation chamber. The wavelength dependence of the ion signal around 226 nm and 382 nm have been investigated. The sensitivity of the ion signal size for different gases and wavelengths have been determined and the related limits of detection (LODs) have been deduced.

In **chapter 5**, a brief description of the CO molecule and a short review about the REMPI spectroscopy of CO has been given. An optical spectroscopic fingerprint at 230 nm has been presented and the characteristics of the spectroscopic structure has

been explained. The results of the sensitive detection using this fingerprint have been reported. The result includes the measurements of LODs for CO in the air and CO in nitrogen and the level of CO in a real urban air sample. A combined analysis using both optical and mass spectroscopy is very helpful to explain the unknown peaks of the optical spectra. A spectrum showing a gas mixture of NO_2, CO and air in the wavelength region of 224-232 nm is given. This indicates that using one simple gas container (ionisation chamber) and the same dye, three gases (NO_2, CO and O_2) can be detected.

Chapter 6 concerns the ionisation of small molecules in intense laser fields in the femtosecond time regime. In particular the results for NO_2 and CO_2 ionisation have been analysed and additionally the ionisation of NO (fragmented from NO_2) and CO have been also analysed. The influence on ion yields of laser wavelengths, photon polarisation and power densities have been investigated. It turns out that for NO_2, there is a competition between the ID (ionisation followed by dissociation) and DI (dissociation followed by ionisation) processes which depends on laser wavelengths and other factors. However for CO_2 molecules, the ID process is always dominant in this thesis indicating that the lifetime of the dissociative energy levels of this molecule are at least less than 100 fs.

Chapter 7 proposes the future work which should be carried out and some ideas which might be verified. Therefore this chapter is an exciting one.

All the data in this thesis were analysed by the author. The data for the chapter 4 and 5 were taken at our home laboratories by the author and the data for the chapter 6 were taken at the Rutherford Appleton Laboratory (RAL) in collaboration with my Glasgow collegues and with considerable assistance from RAL collegues.

Contents

Chapter 1

Related Fundamentals

This chapter aims at introducing the basic concepts and principles which are related to the research work of this thesis.

1.1 Some related basic concepts

1.1.1 Laser characteristics (Andrews, 1992)

1.1.1.1 Coherence

The initially most widely acclaimed attribute of the laser, the coherent nature of its emission, is in general only indirectly relevant to spectroscopic applications. The extent of the correlation in phase between the photons in a laser beam is characterised by a coherence length l_c, which is the inverse of the line-width as expressed in wave number terms (Demtröder, 1981):

$$l_c = \frac{1}{\Delta\tilde{\nu}} \qquad (1.1.1.1.1)$$

While typical semiconductor lasers have coherent lengths of about 1 mm, l_c values of up to 1 km are achievable in ring dye lasers. The spectroscopic significance of l_c values, however, lies much more in their reflection of the extent of monochromaticity rather than coherence. The coherent nature of laser light is also characterised by its photon distribution. The probability of finding N photons in a volume that on a time average contains a mean number M is given by the Poisson distribution (London, 1973):

$$P_N = \frac{M^N e^{-M}}{N!} \qquad (1.1.1.1.2)$$

A number of so-called coherence spectroscopies do exist that are invariably studied with laser light. Some of these, such as self-induced transparency and photon echo, relate to pulse propagation characteristics and are generally not observable in normal chemical media. The coherence of the laser photons in this thesis is relevant only in the sense that it enables short (mode-locked) pulses to be created.

1.1.1.2 Collimation

The physically narrow beam diameter and small divergence of a typical laser beam are useful attributes in certain types of application, both in the laboratory and in the field. Most laser beams are well collimated with no more than a milliradian divergence, and most of the intensity occurs within a few micron-scale cross section.

The exact distribution of intensity within a laser beam is determined by the mode structure, and in the simplest case consists of an essentially Gaussian distribution. Since there is no hard edge to the beam, its diameter w is usually defined at the transverse distance at which the intensity drops to $1/e^2$ (13.5%) of its central peak value. Quantum uncertainty considerations show that any such beam can in general only be focused down to a diffraction limit where its diameter is the same order as the wavelength. In fact, the focused beam waist w_0 is determined by the relation

$$w_0 = \frac{2M^2\lambda}{\pi\theta} \qquad (1.1.1.2)$$

Where λ is the wavelength and θ is the angle of convergence of the focused beam. The quantity M^2 is called beam quality parameter, and has a diffraction-limited value of unity for a fundamental Gaussian-mode beam. In practice, M^2 values below 1.2 are regarded as optimum.

The tight focusing afforded by lasers is especially significant for micro-sampling applications, where sample volumes of the order of 1 μl are entirely feasible. Indeed in laser-based methods for the analysis of matrix-assisted laser desorbtion/ionisation (MALDI), sample volumes of 0.5 μl are possible (Peng, W.X., 1996). In the microanalysis of non uniform solids such as minerals or corroded metals, the precision of the laser beam as a probe is also significant, especially where it is used for the ablation of a small region of surface analysis. In conjunction with conventional or laser-based spectroscopic detection, this affords a useful technique for characterising the composition of heterogeneous solids. Scanning a focused laser beam over the surface enables different areas to be analysed, typically with micron

resolution; where high-power pulses are used to ablate successive layers of such materials, the analysis additionally provides depth profiling data. The ability to deliver laser beams into optical fibres also facilities a number of biological applications such as remote fibre fluorimetry.

The other extreme of scale in remote sensing is represented by the various spectroscopic varieties of lidar (light detection and ranging), in which atmospheric species are targeted by a ground-based laser system and identified telescopically by their optical response. These techniques, which depend crucially on the very small divergence of the beams delivered by most large laser system. They are of particular value in the study of industrial chimney gases and atmospheric pollutants and are currently much in vogue in connection with the study of stratospheric ozone depletion.

1.1.1.3 Intensity

For a wide variety of spectroscopic applications, far more important than collimation is the high intensity often associated with laser output. There are in fact several parameters in terms of which the high photon flux delivered by lasers can be characterised.

Higher output powers can be achieved by pulsing techniques, based on the simple fact that the power is increased if a given energy E is delivered within a decreased time. Here the pulse energy is an equally important consideration, and the corresponding power $W = \frac{dE}{dt}$. A good idea of the pulse power is obtained by dividing the pulse energy by the pulse length. The average power is the energy per pulse multiplied by the number of pulses per second.

The best measure of the intensity actually experienced by a sample, however is the *irradiance*, which is the power delivered per unit cross sectional area of the beam. It is principally the small dimensions of the beam that give rise to the very high irradiance delivered by laser sources. A good CW argon ion laser, for example, produces an irradiance of about 10^7 Wcm^{-2}. As mentioned earlier, this intensity can be greatly increased by focusing to the diffraction limit; in this instance irradiance of about 10^{13} Wcm^{-2} can be achieved, representing 10^{10} times higher than that of a typical sunlight on the earth's surface.

In terms of the irradiances produced by pulsed lasers, the highest figures are obtained through use of mode-locking and allied techniques, characterised by pulses measured on the picosecond (10^{-12} s), or even femtosecond (10^{-15} s) time scale. Intensities of the order of 10^{14} Wcm^{-2} are readily attainable from a focused mode-locked argon laser, for example, representing a light flux equal to that to be found in the interior of stars. Intensities as high as 10^{19} $W\,c\,m^{-2}$ are now being considered. Spectroscopically, such high intensities prove useful for both the identification of weak spectral features and the study of intrinsically weak process.

1.1.1.4 Monochromaticity

It is the high degree of monochromaticity of laser light that carries the most significance for spectroscopic applications, with the continual advances in cavity design reflected in a gradual reduction in achievable laser linewidth. The parameter that most effectively characterises the degree of monochromaticity is the quality factor Q, defined as the ratio of the laser emission frequency to its linewidth. It is also expressible as the coherence length divided by the emission wavelength:

$$Q = \frac{\nu}{\Delta\nu} = \frac{l_c}{\lambda} \qquad (1.1.1.4)$$

In absorption-based laser spectroscopy this parameter represents an upper limit on the achievable resolution, which in practice may be reduced by other features of the instrumentation. Quality factors of 10^7 or even higher are not uncommon in the lasers most widely used for spectroscopy.

The impact of the continued improvements in source monochromaticity is well illustrated by the tremendous developments that have taken place in high-resolution electronic spectroscopy based on dye lasers, where resolutions of below 0.1 cm^{-1} are now routinely attainable. With suitable instrumentation frequency-stablised ring dye lasers can in fact offer a spectral resolution better than 10^{-5} cm^{-1}, corresponding to Q values of about 10^{11}. In the infrared region tunable diode lasers can offer linewidths of less than 10^{-3} cm^{-1}, albeit over a limited spectral range, providing a means for the collection of high-resolution vibrational and rotational spectra.

1.1.1.5 Pulsing (Andrews,1992)

Time-resolved studies constitute an increasingly significant area of application for laser spectroscopy. Principally, this reflects the progressive and remarkable reduction

in achievable pulse duration, particularly with regard to the mode-locked lasers producing what have become well known as ultra short (subpicosecond) pulses. These lasers operate by establishing a phase relationship between a large number of longitudinal modes within the laser. With N_L modes in a cavity of optical length L that a pulse repetition frequency is obtained, which is written as:

$$f = \frac{c}{2L} \tag{1.1.1.5.1}$$

typically around 100 MHz, and a pulse duration given by

$$\Delta t = \frac{4\pi L}{(2N_L + 1)c} \tag{1.1.1.5.2}$$

where c is the speed of light. Pulse lengths are now down to the femtosecond scale. There is an inevitable price to pay for the time resolution thus achieved, however, and this is a loss of spectral resolution in accordance with the inexorable operation of the quantum mechanical umcertainty principle. Nonetheless, such pulses are very significant for the study of ultrafast processes.

It is not a coincidence that as far as genuine chemistry is concerned most such processes directly involve interaction with light. The reason is simply that the range of atomic motion over picosecond and subpicosecond times is necessarily very limited, and only unimolecular processes such as electron transfer or bond fission can occur on such a time scale. Mostly, such processes require a substantial input of energy, and photo-absorption thus provides a convenient initiation stage. In fact, the primary processes of vision and of photosynthesis have both been shown to occur on a picosecond time scale.

To take advantage of the high resolution potential afforded by laser spectroscopy, it is, of course, necessary to minimise the effects of phenomena such as collision broadening and Doppler broadening in the sample. This can be accomplished by a number of means, including molecular beam methods (Bernstein, 1982) and the utilisation of various kinds of nonlinear optical effects such as saturation and two-photon absorption. Such studies are not primarily of analytical importance, but they are unparalleled in the wealth of fine structure they can reveal for the detailed characterisation of molecular systems and their chemical reactions.

It has been seen that how the various characteristics of laser sources may be exploited for spectroscopic applications. It is now appropriate to consider the physics of laser interactions in more detail and to understand better the basis for each specialised type of laser spectroscopy. To do so, it is important to focus on which factors determine the possibility of spectroscopically useful coupling between the laser radiation and the atoms and molecules of the sample.

1.1.2 Interactions with laser photons (Andrews, 1992)

The characteristic features of the various kinds of laser spectroscopy, in terms of both their instrumentation and the distinctive analytical information they provide, are largely determined by two considerations. The first concerns the physical nature of the basic processes by which laser interacts with samples (e.g., by photoabsorption or light scattering). Generally, such interaction results in the promotion of sample species such as atoms, ions or molecules to excited energy levels. The secondary processes that occur subsequently to the sample excitation (e.g. molecular fragmentation or fluorescence) represent the other factor determining the spectroscopic methodology.

The issues involved in determining whether a given sample molecule, for example, will undergo a spectroscopically useful transition through its interaction with a given laser beam can be enumerated as follows. First and perhaps most fundamentally, there is the question of the likelihood of the molecule being struck by the necessary number of photons. For most types of spectroscopy, a single photon induces the molecular transition, but where nonlinear interactions are involved, two or more laser photons may need to transverse the molecule almost simultaneously. Next, the laser photon needs to have an appropriate energy to accommodate the desired transition. There are also selection rules to be satisfied, in terms of both molecular symmetry and photon polarisation. Finally in the case where sample molecules are not in free rotation, the orientation of sample also has a bearing on whether the required transition can occur. Each of these factors is now given in more detail.

1.1.2.1 Spatial consideration

First the probability of finding a single photon in the volume of space V_1 occupied by an atom, molecule, or chromophore (i.e., the species that is of spectroscopic interest) has to be considered. For laser light whose intensity fluctuations approximate to a

Poisson distribution, the result for the mean photon number M is given by (Andrews, 1990)

$$M = \frac{IV_1\lambda}{hc^2} \qquad (1.1.2.2.1)$$

where I is the beam irradiance and λ is its wavelength. At first sight it is surprising to find how small M generally is. The probability of finding a laser photon traversing a sample molecule under typical laboratory conditions can be illustrated by considering a sample of water (mean molecular volume $V_1 = 3\text{x}10^{-29}$ m^3) irradiated by a 10^{15} Wcm^{-2} pulse from a mode-locked argon laser operating at a wavelength of 488 nm. Using equation (1.1.2.1), it can be found that $M = 2.5\times10^{-4}$. In other words, one molecule in 4000 has a photon passing through the volume it occupies at any given instant time.

The average time each photon takes to pass through any given molecule is given by $t = V_1^{1/3} / c$; the mean interval between photons, $\tau = t / M$, is therefore

$$\tau = \frac{hc}{IV_1^{2/3}\lambda} \qquad (1.1.2.1.2)$$

In the example given earlier, $t=10^{-18}$ s (10^{-3} fs) and τ=4 fs.

If one asks the question what is the probability of finding two photons absorbed by the molecule simulataneously, one needs to evaluate $\langle N(N-1)\rangle$, (Craig, 1984). The (N-1) factor arises because after detecting one photon there are only (N-1) left. Here the answer is $\langle N(N-1)\rangle$=M^2, which incidentally reveals the quadratic dependence of two-photon absorption on light intensity.

1.1.2.2 Energetics

Given a sample molecule with the correct number of photons present, all other issues concern whether or not a spectroscopic transition can occur. For processes involving only the absorption of a single laser photon, the laser photon energy $h\nu = E_f - E_i$ must obviously match the difference between two quantum states of the molecule, $E_f - E_i$, as in figure 1.1.2.2.1a. The extension of this energy conservation principle to single-beam n-photon absorption processes, as figure 1.1.2.2.1b,

$$nh\nu = E_f - E_i \qquad (1.1.2.2.1)$$

follows. It is important to note that multiphoton absorption of this nonresonant kind is a concerted rather than a multistep process, as there is no physically identificial intermediate stage between the absorption of successive photons. For other processes, where emission of light also contribute to the overall transition, as in Raman effect (Figure 1.1.2.2.1c), or where two or more laser beams interact in sample molecules, as in four-wave mixing processes (Figure 1.1.2.2.1d), laser wavelength again plays an important role, but one that is often more subtle.

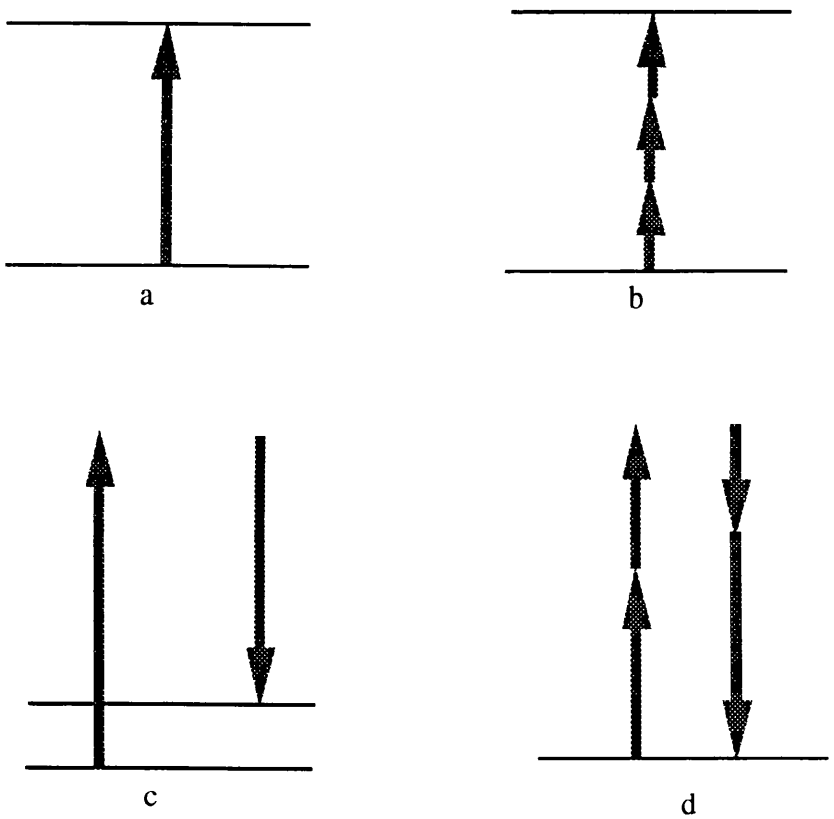

Figure 1.1.2.2.1 Energy level diagrams for (a) single-photon absorption, (b) nonresonant three-photon absorption, (c) nonresonant (Stokes) Raman scattering, (d) nonresonant four-wave mixing.

It is not generally necessary in processes involving photons of two or more different frequencies for the energy of any lesser number of photons from a given source to satisfy equation (1.1.2.2.1c). Overall energy conservation simply demands that the difference between the sum of the absorbed and emitted photon energies equals a molecular transition energy. However, when equation (1.1.2.2.1) is also satisfied, it

generally transpires that the rate of laser-induced transitions increases markedly, often by many orders of magnitude. This situation is known as *resonance enhancement,* and examples of resonance in multiphoton absorption and Raman scattering are illustrated in figure 1.1.2.2.2a and b.

The reason for resonance behaviour can be understood on the basis of the time-energy uncertainty principle:

$$\Delta E \Delta t \geq \hbar \qquad (1.1.2.2.2)$$

For simplicity one can focus on the case of multiphoton absorption. When resonance conditions are absent, as in figure 1.1.2.2.1b, then after absorption of the first laser photon the molecule exists in a state with a large ΔE. Accordingly, it can exist in such a state only if further absorptions restore energy conservation within a very short time. For example, if there is no appropriate state within 8,000 cm^{-1} of the photon wavenumber, another photon must arrive within a window of 1 fs for energy conservation not to be measurably violated.

However, if the first photon is near resonance with a real molecular state, as in figure 1.1.2.2.2a, then the intermediate state has a small ΔE and can exist for much longer. This greatly increases the probability that the next photon will arrive within the necessary window. In the limit where exact resonance occurs and ΔE is zero, there is no longer any temporal constraint, because the intermediate state can be physically populated by single-photon absorption. Then the multiphoton process can take place in two stages, with an arbitrary time interval between absorption of the first photon and subsequent radiative interactions that complete the processes. Similar arguments can be applied to other types of resonance processes.

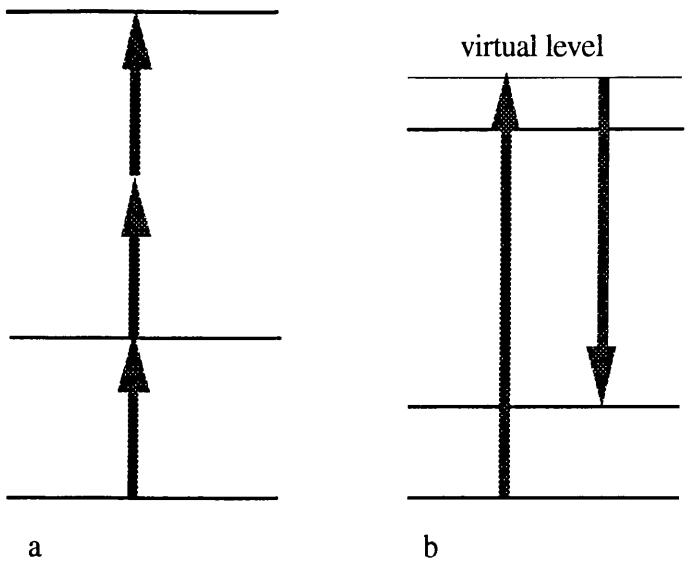

Figure 1.1.2.2.2 Energy levels for (a) three photon absorption with single photon resonance, (b) resonance (Stokes) Raman scattering.

1.1.3 Transition strength and quantum selection rules

If a photon or photons of the right energy to match the gap between two molecular states are present at a given sample molecule, there still only a finite and usually small probability that transition will occur and contribute to the generation of a spectral feature. Normally, each radiative interaction occurs by an electric dipole coupling with the photon electric field, and the quantum mechanical transition moment dictates the strength of coupling. Symmetry restriction may entirely rule out any such coupling between the radiation and the molecule, though often a much weaker coupling mediated by magnetic dipole or electric quadruple interactions permits such "forbidden" interactions to occur with a probability reduced by a factor of 10^4 or more.

The quantum mechanical selection rules for conventional photon absorption are well known and apply with equal force to laser-induced single-photon absorption. Probably the most familiar is the Laporte selection rule for centrosymmetric molecules, which allows transitions only between states of opposite parity, gerade (g) $\leftrightarrow$ ungerade (u). Each successive stage in a multiphoton process is also subject to the same rules, given that each radiative interaction almost invariably occurs by the same electric dipole coupling. However, the product selection rules depart substantially from the normal results; for example, if an even number of photons is

involved, as in Raman scattering, two-photon absorption, and four-wave mixing, then the section rules $g \leftrightarrow g$ and $u \leftrightarrow u$ apply. In fact, for molecules of reasonably high symmetry, far more states can be accessed by multiphoton processes than those show up in conventional single photon spectra. Halpern et al (1980) calculated the rotational line intensity factors for two- and tree-photon excitation of diatomic molecules belong to Hund'd case (a) intermediate and (b)-(c) coupling schemes. (Hund's casees a, b and c are refer to Steinfield, 1974)

1.1.4 Polarisation effect

Photon polarisation is also involved in the selection rules for processes involved in more than one photon. This contrasts strongly with the case of single-photon absorption, where, at least for isotropic media, there is essentially no dependence on beam polarisation. Such dependence as does exist arises only for optically active (chiral) compounds and is associated with the interference of magnetic dipole and electric quadruple interactions. These weak effects produce the small polarisation dependence that is manifest in the phenomena of circular dichroism and optical rotation.

For two-photon and higher-order processes, the spectra of reasonably symmetrical molecules display a marked dependence on polarisation. This is well known in connection with Raman scattering, where depolarisation ratio measurements, which reflect a dependence on the relative polarisations of the laser input and the scattered beam, also yield further information on excited state symmetries (Long, 1977). Tjossem et al observed the spectra of the two-photon transition $B^1\Sigma^+ \leftarrow X^1\Sigma^+$ of CO molecules using both linear and circular polarisation, the shape of the spectra at different polarisation are completely different, see figure 1.1.4.

Laser beam polarisation plays an obvious role in the orientational effects displayed by anisotropic media such as crystals, liquid crystals, and surfaces. However, it should be noted that strong laser pumping can induce anisotropy in an isotropic liquid sample.

Also in laser ionisation mass spectroscopy in intense laser fields, employing proper laser polarisation, the kinetic energies of the fragment ions can be measured (Normand et al, 1991).

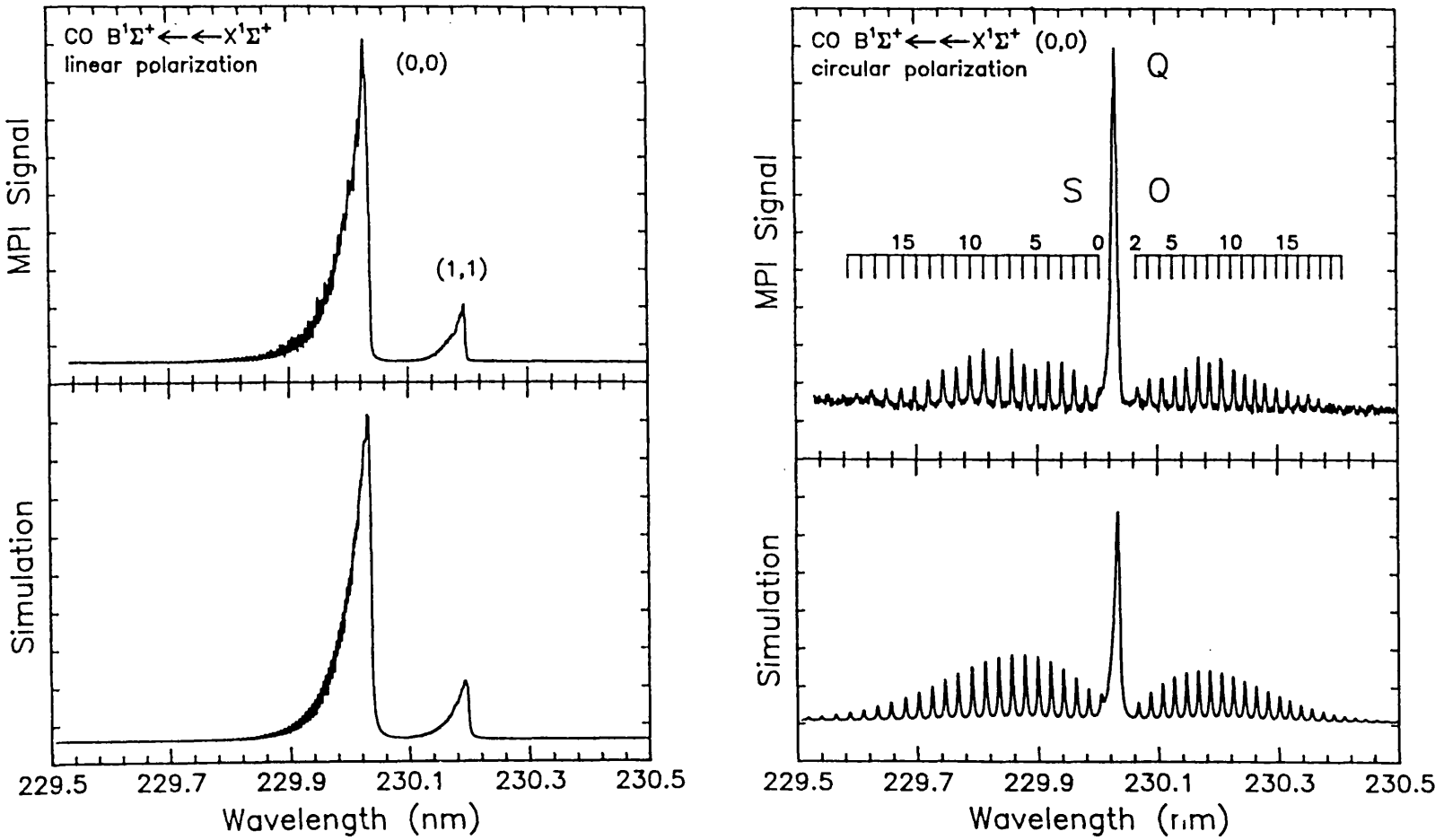

Figure 1.1.4 Spectra of the two-photon $B^1\Sigma^+$–$X^1\Sigma^+$ band of carbon monoxide taken with linear polarised light (left) and circular polarised light (from Tjoseem, 1989)

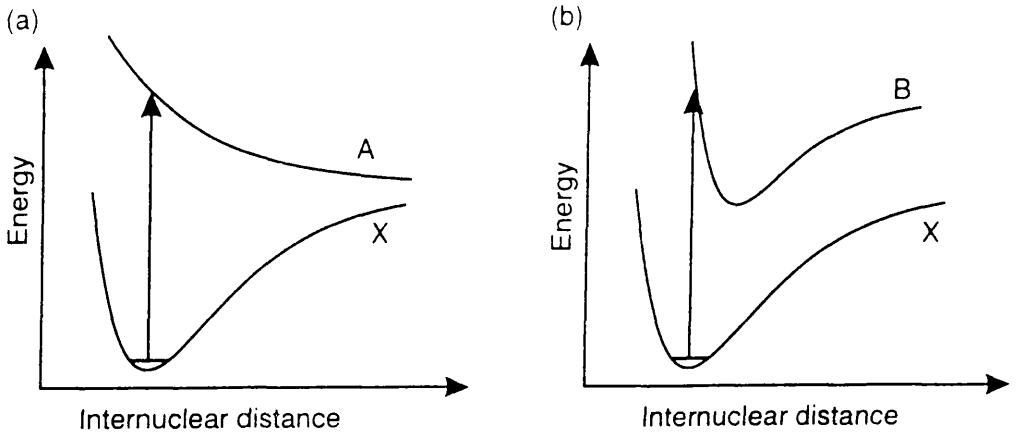

Figure 1.2.1 Absorption to (a) an unbound state at an energy greater than its dissociation energy, and (b) a bound state.

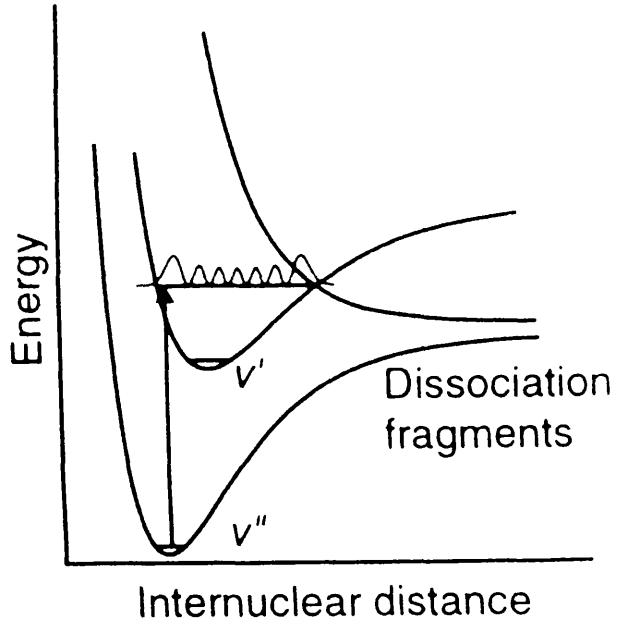

Figure 1.2.2 Potential energy curves for a typical diatomic molecules showing the crossing that leads to predissociation

1.2 Photodissociation and predissociation (Wayne and Wayne, 1996)

1.2.1. Photodissociation

Optical dissociation may come about either if absorption occurs so that the excited species possesses energy greater than its own dissociation energy, or if the absorption occurs to an unbound, repulsive state. Both possibilities are shown in figure 1.2.1. In either case, the molecule will dissociate, and any excess energy may be taken up by the fragments as translational energy. Because this translational energy is effectively continuous, the spectrum beyond the point at which dissociation occurs becomes a continuum. If the upper state is bound, then at longer wavelengths (i.e. lower energies) the spectrum may be banded, corresponding to different vibration levels in the upper state. These level become progressively closer together, until the continuum is reached: the energy corresponding to the onset of the continuum--the convergence limit--is the dissociation energy to the products.

Complete removal of an electron, photoionisation can also be regarded as a form of photodissociation, yielding dissociation products of an ion and an electron

$$AB + h\nu \rightarrow AB^* \rightarrow AB^+ + e. \qquad (1.2.1)$$

1.2.2 Predissociation

Another route to fragmentation exists; the process involves population of an excited state *below* its dissociation limits, and its subsequent radiationless transition to populate another state *above* the dissociation limit of that second state. The phenomenon is referred to as *predissociation.*

Predissociation in a diatomic molecule can be explained in terms of the crossing potential energy curves of figure 1.2.2. Absorption populates the upper bound curve at an energy above that where the repulsive curve cross it. Subject to the quantum mechanical requirements for radiationless transition the system may thus cross to the repulsive state, which falls apart to yield the atomic fragments.

1.3 Introduction to laser spectroscopy analysis

The laser-based analysis can be divided into two categories: laser spectroscopic techniques and non-laser-spectroscopic ones. This thesis involve both of them. Chapters 4 and 5 deal with laser ionisation spectroscopy and chapter 6 deals with

ionisation in intense laser fields which is a laser non-spectroscopic technique, but it is a kind of laser mass spectroscopic technique. Only the laser spectroscopy-based analytical problems have been mentioned in this paragraph.

1.3.1 Introduction to laser spectroscopy

Lasers have received much recognition in various fields of science and technology. In some fields (medicine, material processing, commerce, defence etc.) the application of laser light has proved unexpectedly successful. In other fields (spectroscopy, metrology, photochemistry) there are a lot of new areas to be started. It took a decade in the 1960s to complete even the more obvious applications of lasers in spectroscopy. This was due to the fact that the first pulsed and continuous-wave lasers operated at a limited number of discrete frequencies of visible and near infrared ranges. At the same time, most of the methods of atomic and molecular spectroscopy require that the laser radiation frequency should coincide with the frequency of a definite quantum transition between two energy levels of the studied atom or molecule. Late in the 1960s, various methods of generating coherent light with a tunable frequency began to develop rapidly. So it was in that period that the methods of laser spectroscopy began to progress.

In the 1970s thousands of researchers got involved in the studies on laser spectroscopy making use of the technology of quantum electronics. In that period international conferences on laser spectroscopy and tunable lasers were held regularly. Several monographs on general principles of laser spectroscopy (ed. by Walther, 1976; Demotroder, 1981) and many monographs on different trends in laser spectroscopy were published over a short period of time. The analytical applications of laser spectroscopy, of course, are highly effective and rapidly developing. In the 1980s, resonant ionisation spectroscopy (RIS) became a very popular sensitive analytical technique. An international symposium series-RIS- started from 1984. Since then the proceedings of RIS are published regularly and monographs concerning laser analysis appeared widely (e.g.: ed. by Letokhov, ed. by Vertes et al). The laser spectroscopic analysis technique used in this thesis is RIS-based analysis, either using a ionisation chamber or a mass spectrometer.

1.3.2 Spectroscopy and quantum mechanics

Spectroscopy is basically an experimental subject and is concerned with the absorption, emission, or scattering of electromagnetic radiation by atoms or

molecules. It can be seen from figure 1.3.2 that electromagnetic radiation covers a wide wavelength range from radio waves to γ-rays and the atoms or molecules may be in the gas, liquid, or solid phase or, of great importance in surface chemistry, absorbed on solid surfaces.

The wavelength range dealt with in this thesis is only in the UV and visible because of the availability of laser facilities. There are many laser spectroscopic techniques. According to the means of detection, they can be termed by: absorption spectroscopy, fluorescence spectroscopy, ionisation spectroscopy and photo-electron spectroscopy and in addition, Raman spectroscopy. Of those techniques, only laser ionisation spectroscopy is involved in this thesis.

Quantum mechanics, on the other hand is a theoretical subject relating to many aspects of physics and chemistry, but particularly to spectroscopy (Hollas, 1992). The theoretical work of the application of quantum mechanics is beyond the scope of this thesis, however some important results have been employed to explain the experimental results, e.g., the line shape of the transition of CO molecule at 230 nm (chapter 5, paragraph 5.5.1).

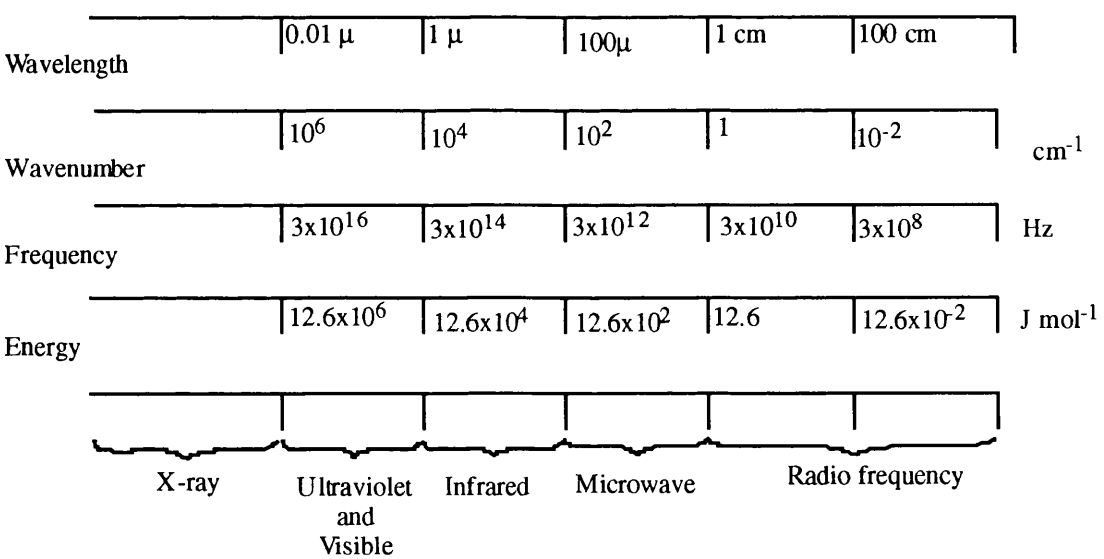

Figure 1.3.2 The electromagnetic spectrum

1.3.3 The basic problems of laser spectroscopy

The characteristics of laser radiation have provided the potential for solving the basic problems of spectroscopy which are to obtain necessary spectral and time resolution, sensitivity and selectivity.

1.3.3.1 Spectral resolution

The resolution of the classical methods of atomic and molecular spectroscopy in the gas phase was usually limited by the instrumental resolution of the spectrometer. This limitation is particularly noticeable in the IR region where the resolution of only a limited number of unique spectrometers reaches 0.01 cm^{-1}. These numerical parameters should be compared with the Doppler width of vibrational-rotational absorption lines of molecular gases which is about 10^{-3} cm^{-1}.

Tunable lasers with a narrow radiation line, particularly injection IR lasers and dye lasers in the visible region (in combination with nonlinear frequency conversion in the near UV and near IR regions), have allowed realisation of the ultimate spectral resolution of linear spectroscopy which is determined by the real absorption spectrum of the sample without any influence by the spectral instrument. However, for the purpose of quantitative analysis in this thesis, the spectral resolution is not as important as in optical spectroscopy. Instead, the resolution of a mass spectrometer seems more important.

1.3.3.2 Temporal resolution

The temporal resolution in pre-laser kinetic spectroscopy was, at best, about 10^{-8} s due to the use of pulsed flash-lamps and a Kerr-cell shutter. The creation in the late 1960s of ultrashort pulse lasers which employ the effect of synchronisation of a great number of modes of wide spectral range laser (Shapiro, S.L., 1977) has culminated in a great progress in the methods of laser picosecond spectroscopy. In recent years further progress has been made in the generation femtosecond pulses down to 11 fs from a Ti:sapphire laser (Stingl et al, 1994). Ultrashort laser pulses with a tunable frequency enable selective excitation of a considerable fraction of molecules to a definite quantum state and picosecond resolution of primary photophysical and photochemical processes with excited molecules. Progress in the generation of ultrashort laser pulses with the capacity for controlling pulse width and tunability has made it possible to observe a chemical reaction directly while fragments are either

encountering or escaping each other. The femtosecond dynamics of the transition-state region and the clocking of fragment separation in real time using femtosecond transition-state spectroscopy (FTS) have been reviewed by Zewail, A.H. (1990). Observations of molecular vibration and rotation have also been reported using femtosecond lasers (Dantus, M., 1990).

1.3 3.3 Sensitivity

Although all the spectral information is contained in one atom or one molecule, real measurements of spectra are possibly only with a great number of particles in the sample (approximately from 10^{10} to 10^{20} for different methods and objects) because the sensitivity of all the spectral methods is very limited. So the problem of increasing the sensitivity of the spectroscopic methods has also been very important for analytical applications. The method of photoionisation laser spectroscopy based on resonance stepwise photoionisation of atoms and molecules enables detection of single atoms and molecules (Letokhov, V.S., 1976)

1.3 3.4 Selectivity

In analysing a real sample, selectivity is also of critical importance; that is the ability to detect the presence of atoms or molecules of definite sorts in their mixtures. The potentialities of optical spectroscopy in this respect have always been limited. For the most part, this holds true for the analysis of condensed media characterised by broad absorption lines which have low information capacity. The spectral analysis of molecules is then often performed after preliminary separation of these molecules by, for example, chromatography.

The use of laser radiation has, firstly, made it possible in some cases to simplify optical spectra of molecules, for example the fluorescence spectra of molecules in low-temperature matrix, and has increased the selectivity of analysis. Secondly, the spectra of multistep laser excitation of atoms and molecules are characterised by a far higher selectivity than ordinary absorption spectra. Finally, higher sensitivity laser methods can be easily combined with such well known methods of analysis such as chromatography, mass spectrometry, etc. Therefore the high selectivity of the methods of laser spectroscopy in combination with a high sensitivity is extremely valuable for analysis purposes.

In this thesis, chapter 4 and 5 deal with laser-based optical spectroscopic analysis, while the work in chapter 6 does not contain optical spectroscopic features due to the effect of intense laser fields. The phenomena of atoms and molecules in the intensive laser fields will be introduced in the next paragraph.

1.4 Ionisation of atoms and molecules in intense laser fields

The behaviour of molecules in intense laser fields is an area of active investigation. Multiphoton ionisation (MPI) and above-threshold ionisation (ATI) occur in molecules just as in atoms (Allendof, S.W. and Szoke, A., 1991; Verschuur, J.W.J., et al, 1989; ; Helm, H., et al, 1991; Strickland, D.T. et al, 1992; Gibson, G.N., et al, 1991; Zavriyev, A. et al. 1990). Additional degrees of freedom in molecules lead to some new phenomena as well. An example is above-threshold dissociation (ATD), in which the internuclear electronic potentials are mixed by the laser field at points of multiphoton resonance, causing the molecule to dissociate via several possible channels corresponding to the absorption of one, two, or more photons (Zavriev, 1993).

The experiments involving the interaction of atoms with intense laser fields have traditionally been divided into two regimes, multiphoton and tunnelling. In the former, laser ionisation can be described by perturbation theory, whereas in the latter ionisation can be described by introducing the Keldysh γ parameter (Keldysh, 1965),

$$\gamma = \left(\frac{V}{2U}\right)^{1/2} \tag{1.4.1}$$

where V is the zero-field ionisation potential and U is the ponderomotive potential of the laser. The ponderomotive potential is the average kinetic energy acquired by an electron in the laser field and is given by

$$U(eV) = 9.33 \times 10^{-14} I(W/cm^2)\lambda(\mu m) \tag{1.4.2}$$

According to Augst, S. et al (1989), the multiphoton regime corresponds to $\gamma > 1$, whereas $\gamma < 1$ corresponds to the tunnelling regime. While Ilkov et al (1992) proposed to define the tunnelling regime with the aid of the following two criteria

$$\gamma < 0.5 \tag{1.4.3}$$

$$F < F_{BSI} = \frac{\left(\frac{1}{2}E_0\right)}{Z} \tag{1.4.4}$$

Where F_{BSI} is the barrier suppression ionisation field (BSI), in atomic units, and can be viewed classically as the case when the electron simply 'passes over' the fully suppressed atomic potential. It can be obtained by setting equal the Coulomb barrier saddle point $2\sqrt{ZF}$ and the electron binding energy $E_0 = \frac{Z^2}{2n^{*2}}$ for state with m=0 in neglecting the Stark shift, where m is a magnetic quantum number.

Most of the experimental studies of laser-induced ionisation have demonstrated ion production occurring in the regime of $\gamma > 1$, while some experiment using an Infrared laser (e.g. CO_2 laser, at 10.6 μm) indicated that the ion production can occur in the regime of $\gamma \leq 0.5$ (Walsh, T.D. et al, 1994). Most cases in Chapter 6 in this thesis indicated that the involved ionisation is in the multiphoton ionisation regime, although some cases indicated that the ionisation is in between multiphoton and tunnelling regimes.

Previous research on molecules under very intense light fields has concentrated on phenomena such as multi-ionisation kinetics (Boyer et al, 1989; Hatherly et al, 1994; Purnell, et al, 1994), velocity (Cornaggia et al, 1990; Lavancier et al, 1991; Normand, et al, 1991) and angular (Hatherly, et al 1990) distributions of photofragmented ions (Stankiewicz, et al, 1993; Cornaggia et al, 1994; Frasinski at al, 1994). In recent yeas, some effort towards to quantitative analysis using femtosecond laser has started (Becher et al, 1994; He and Becker, 1996, 1997; Ledingham et al, 1997). For applications, it is desirable to know the ion yield of neutrals under the influence of a high-intensity light field, because the ion yield directly influences the sensitivity and quantification of analytical methods. The ion yields depend on both laser beam and molecular properties. From the laser beam aspect, the main influence are power density, frequency, polarisation, and pulse width; from the molecular aspect, the response to the laser field is generalised by an overall quantity, the n-photon cross section. The work of this thesis only deals with the laser beam aspect, mainly the influence of laser intensity, polarisation, frequency etc. (Chapter 6).

References:

Allendof, S.W. and Szoke, A., (1991)
High-intensity multiphoton ionisation of H_2, *Phys. Rev A* **44,** pp.518-534

Andews, D.L. (1990)
Applied laser spectroscopy, VCH publishers, Inc.

Andews, D.L. (1992)
Lasers in chemistry, 2nd, Springer, Berlin.

Augst, S., Strickland, D., Meyerhofer, D.D., Chin, S.L., and Eberly, J.H. (1989)
Tunneling ionisation of noble gases in a high-intensity laser field, *Phys. Rev. Lett.* , **63**, pp. 2212-2215

Becker, C.H. and Hovis, J.S. (1994)
Surface analysis by phtoionisation at very high laser intensities, *J. Vac. Sci. Technol. A* **12 (4)**, pp. 2352-2356

Bernstein, R.B. (1982)
Chemical Dynamics via molecular beam and laser techniques, Clarendon, Oxford.

Boyer, K., Luk, T.S., Solem, J.C. and Rhodes, C.K. (1989)
Kinetic-energy distributions of ionic fragments producing subsecond multiphoton ionisation of N_2, *Phys. Rev. A* **39,** pp. 1186-1192

Craig, D.P. and Thirrunamachandran, T. (1984)
Molecular quantum elctrodynymics, Academic, New York.

Demtröder, W. (1981)
Laser spectroscopy , Springer series in chemical physics, 5, Berlin

Dantus, M., Bowman, R.M. and Zewail, A.H. (1990)
Femtosecond laser observations of molecular vibration and ritation, *Nature,* **343,** pp. 737-739

Frasinski, L.J., Codling K., Hartherly, P., Barr, J., Ross, I.N. and Toner, W.T. (1987)
Femtosecond dynamics of multielectron dissociative ionisation by use of picosecond laser, *Phys. Rev Lett.*, **58,** pp. 2424

Gibson, G.N., Freeman, R.R. and McIlrath (1991)
Dynamics of the high-intensity multiphoton ionisation of N_2, *Phys. Rev Lett.*, **67,** pp. 1230-1233

Hatherly, P.A., Frasinski, L.J., Codling, K., Langly, A.J. and Shaikh, W. (1990)
The angular-distribution of atomic ions follow the multiphoton ionisation of carbon-monoxide, *J. Phys. B -At. Mol. Opt.,* **23**, L291-

Hatherly, P.A., Stankiewicz, M., Codling, K., Frasinski, L.J. and Cross, G.M. (1994)
The multielectron dissociation ionisation of molecular -iodine, *J. Phys. B-At. Mol. Opt.*, **27**, pp. 2993-300

Helm, H., Dyer, M.J. and Bizzants (1991)
Simplication of photoelectron-spectra of H_2 in intense laser fields, *Phys. Rev. Lett.*, **67,** pp. 1234-1237

Hollas, J.M. (1992)
Modern spectroscopy, John Wiley and Sons, Biddles Ltd, Great Britain.

Ilkov, F.A., Decker, J.E. and Chin, S.L. (1992)
Ionisation of atoms in the tunneling regime with experimental evidence using Hg atoms, *J. Phys. B-At. Mol. Opt. Phys.* **25**, (1992) pp. 4005-4020

Khundakar, L.R and Zewail, A.H. (1990)
Ultrafast molecular reaction dynamics in real-time: progress over a decase, *Annu.Rev.Phys. Chem.*, 41, pp.15-90

Letokhov, V.S. (1985)
Laser analytical spectrochemistry, IOP publishing Ltd, Adam Hilger, UK.

Letokhov, V.S. (1976)
Future applications of selective laser photophysics and photochemistry, Tunable lasers and their applications, ed by Mooradian, A., Jaeger and Stockseth, P., *Proc. Int. Conf., Loen, Norway, Springer Series in Optical Sciences,* **13**, Berlin

Long, D.A. (1977)
Raman spectroscopy, McGraw-Hill, New York

Peng, W.X. (1996)
MALDI mass-spectrometry analysis of human hemoglobin, *Chemi.Res. Chin.Univ.*,**12**, no.1, pp.44-49

Purnell, J., Snyder, E.M., Wei, S., and Calstleman, Jr, A.W. (1994)
Ultrafast laser-induced couloumb explosion of clusters with high charge states, *Chem. Phys. Lett.* **229**, pp.333-339 (1994)

Shapio, S. L. (1977)
Ultroshort light pulses 1977, Springer Series (Berlin) "Topics in applied physics", **18**

Stankiewiecz, Frasinski, L.J., Cross, G.M., Hatherly, L.J., Codling, K., Langly, A.J. and Shaikh, W. (1993)
Dissociative ionisation of N_2 and CO using intense laser at 248 and 305 nm, *J. Phys. B-At. Mol. Opt.*, **26,** pp.2619-2626

Steinfield, J.J. (1974)

Molecular and radiation, *An introduction to modern molecular spectroscopy*, Harper and Row, publishers, USA

Stingl, A., Spielman,C.a nd Kraus, F. (1994)

Generation of 11-fs pulses from a Tisaphpphire laser without the use of prism, *Optics Lett.*,**19**, PP.204-206

Strickland, D.T., Beadoin, Y., Dietrich and Corkum (1992)

Optical studies of inertially confined molecular-iodine ions, *Phys. Rev. Lett.*, **68**, pp. 2755-2758

Verschuur, J.W.J., Noordam, L.D. and Linden van den Heuvell, H.B. (1989)

Anomalies in above-threshold ionisation observed in H_2 and its fragments, *Phys. Rev. A*, **40**, pp. 4383-4391

Vertes, A. (1993)

Laser ionisation mass analysis, *Chemical analysis*, **124,** John Wiley and Sons, INC. USA

Walsh, T.D.G., Ilkov, F.A., Decker, J.E. and Chin, S.L. (1994)

The tunnel ionisation of atoms, diatomic and triatomic molecules using intense 10.6 μm radiation, *J. Phys. B-At. Mol. Opt. Phys.* **27**, (1994) pp. 3767-3779

Walther, H. (1976)

Laser spectroscopy of atoms and molecules, Spriger series *'Topics in applied physics'*, **2**, Berlin

Wayne, C.E. and Wayne, R.P (1996)

Photochemistry, Oxford University Press Inc, New York15

Wilson, J and hawkes, J.F.B. (1987)

Lasers: Principles and Applications, Prentice Hall Ltd, London

Zewail, A.H. (1989)

Transition-state spectroscopy, Abstracs of papers of the American Chemical Society, 198, PP. 56-Phys.

Chapter 2

MPI Process

2.1 Introduction

The term multiphoton ionisation (MPI) is quite generally applied to any atomic and molecular system in which multiple photons are absorbed to take the system above its first ionisation potential with resultant ion formation. A spectrum of a multiphoton process often displays quite different information from a normal single photon spectrum because of different selection rules and transition intensities. Entirely new states are seen in multiphoton spectra that provide a much more complete understanding of the exited state structure of atoms and molecules. MPI comprises nonresonant and resonant processes. If molecules were excited to an intermediate state (an excited state, or a Rydberg state) by absorbing one or more photons first and then absorbing additional one or more photons to form ions, then the process is termed resonant multiphoton ionisation or resonant enhanced multiphoton ionisation (REMPI). Such process will often be described as an (n+m) REMPI, implying that the excitation involves a coherent (i.e. simultaneous) n-photon absorption to reach the resonant intermediate state of the neutral and that a further m photons need to be absorbed to cause the ionisation process. REMPI processes have found wide applications in the following research fields: (1) excited-state spectroscopy and dynamics, (2) the study of photoionization and subsequent events originating from an excited state, and (3) ultrasensitive detection. In this thesis, for ultrasensitive detection, only one colour REMPI process has been involved, since two or more colour REMPI process needs more expensive lasers and laboratory area, although they can provide more information, such as the saturation situation in the ionisation step. Therefore the theoretical consideration for MPI in this chapter only refers to a one colour laser.

The types of experimental observations using MPI can be: (a) the intensity of ionisation is measured as a function of laser wavelength, so-called laser wavelength dependence; (b) the amount of ionisation as a function of laser intensity, so-called

laser power dependence; or (c) the photoelectron energy spectrum. The experimental work of this thesis only comprise type (a) and (b), therefore the theoretical consideration is only linking with such types.

2.2. Historical background of MPI process

The first work on multiphoton processes can be dated as far back as the beginning of quantum theory when Goeppert-Mayer (1931) published a theoretical paper on simultaneous two-photon absorption. Because of the lack of a proper intense monochromatic light source, such an experiment could only be imagined. The advent of the powerful Q-switched ruby laser in the early 1960s and its capability to create breakdown in gases has sparked a strong interest in explaining the physical mechanism that created the first few free electrons followed by cascade ionisation, i.e., breakdown (Chin, 1970; Morgan, 1975). Almost immediately multiphoton ionisation itself became a separate subject of its own because of the challenge of predicting (Keldysch, 1965), isolating, and observing such a highly improbable phenomena. Voronov and Delone (1965) were the first to observe multiphoton ionisation of rare-gas atoms followed by the French Saclay group (Agostini et al., 1968). Initially the work of different groups concentrated mainly on proving the existence of such nonresonant multiphoton phenomena. Soon the question of resonant multiphoton ionisation was asked, studied and understood. A new method, resonance ionisation spectroscopy (RIS), was developed (Hurst, G. S. et al., 1975) for the study of long-lived excited states using a laser resonant photoionisation technique. All atomic transitions between the ground state and some excited states, with the exception of He and Ne, may be resonantly excited with commercially available tunable dye lasers. The RIS technique was first used to demonstrate the one-atom detection with Cs by Hurst, G.S. et al. (1977a, 1977b). Nowadays RIS has become a well known research branch and found wide use in many fields. A very good collection of RIS data has been made by Saloman, E.B. (1990, 1991, 1992, 1993).

Earlier work on molecular MPI was reported by Collins et al. (1973) on CS_2, and by Lineberger and Patterson (1972) on two-photon photodetachment of negative ions. The demonstration of multiphoton ionisation as a new spectroscopic tool is credited to Johnson and co-workers (1975) for work on NO, and to Dalby and co-workers (Petty et al., 1975) for work on I_2, both in 1975. One of the earlier molecular studies on resonant two photon ionisation (R2PI) was reported by Mainfray and co-workers

(Held et al., 1972) on the detection by time-of-flight mass analysis of Cs_2^+ in an atomic beam of Cs. Work on similar easily ionised systems followed (Granneman et al., 1977). A great step forward in two-laser R2PI was made by Letokhov and co-workers (Andreyev et al., 1977) on two-step photoionisation of formaldehyde, quickly followed in the next year by mass-analysed R2PI of various molecules in molecular beams. Bernstein and co-workers (Zandee et al., 1978) reported REMPI with mass analysis of I_2 and also benzene (Zandee and Bernstein, 1979a, b).

REMPI can easily be combined with supersonic molecular beams allowing considerable simplification of molecular spectra due to the cooling of internal degrees of freedom, as first shown by Zakheim, D.S. and Johnson, P.M. (1978) for NO. Benzene and several halobenzenes expanded in a free jet were studied by Murakami, J. et al., who found the technique sensitive to as few as ten ions per laser pulse. Many other studies of supersonic beam spectroscopy have been reported e.g. by Miller, J.C., (1986) and by Hippler, M. et al., (1990).

REMPI combined with time-of-flight mass spectrometry has been more and more used for ultra-sensitive analysis. Schindler, R.N. and co-workers reported the mass spectrometric in-situ determination of NO_2 in gas mixtures (Benter, T. et al., 1995). Looney, J.P. et al. (1993) reported the measurement of CO pressures in the UHV regime. Sausa, R.C. and co-workers reported monitoring of vapour-phase nitro compounds (Lemire, G.W. et al., 1993). Ledingham, K.W.D. and co-workers reported the detection of aromatic molecules (Clark, A. et al., 1993a, 1993b; Marshall, A. et al., 1991; Marshall, A. et al., 1992). Weickhardt, C. et al. (1994) and Franzen, J. et al. (1995) reported time-resolved multicomponent analysis of exhaust gas.

Ionisation chambers were the first and simplest detectors for REMPI spectroscopy in molecules, with benzene the first polyatomic molecules to be reported (Johnson, P.M., 1975). REMPI spectra of NO (Johnson, P.M. et al., 1975) and I_2 (Petty et al., 1975) were published previously in the same year and, interestingly, these three molecules have been studied continuously since then. Recently, the ionisation chamber REMPI spectroscopy has been used for trace gas analysis at Glasgow (Peng, W.X. et al., 1995; Marshall, A. et al, 1994); Edinburgh (Pfab, J., 1995), US Army Laboratory (Simeonsson, J.B. et al., 1994) and C.N.R.S. (Guizard, S. et al., 1989).

Multiphoton spectroscopy and multiphoton ionisation methods, including REMPI, have been reviewed in considerable detail in their various aspects (Johnson, P.M. and Otis, C.E., 1981; Lin, S.H. et al., 1984; Schlag, E.W. and Neusser, H.J., 1983; Ashfold, M.N.R., 1986; Ashfold, M.N.R. and Prince, J.D., 1988; Ashfold, M.N.R., 1993; Goodman, L. and Philis, J., 1992; Letokhov, V.S., 1987). Recent reviews by Ashfold et al. cover MPI and REMPI spectroscopy of small molecules and free radical species (Ashfold, M.N.R., 1986 and Ashfold, M.N.R. et al. 1993). The book by Letokhov provides a broad view of the subject that includes the theory, a detailed account of single particle detection, atomic MPI and its applications to the detection of rare isotopes as well as diagnostic applications of atomic and molecular MPI in chemistry and physics (Letokhov, V.S., 1987).

In atmospheric chemistry the spectroscopy, kinetics, and photochemistry of atmospheric constituents, reactive intermediates, and air pollutants are promising area where the REMPI technique facilitates new research. The potential of this technique for the chemical analysis and ultratrace detection of atmospheric species has also become interesting and remains to be fully exploited.

The availability of intense lasers (with intensity larger than 10^{13} W/cm^2) makes high order MPI possible and molecules with high ionisation potential and low photodissociation limits can be detected intact. For example, NO_2 molecule has high ionisation potential and a low dissociative energy level compared to other diatomic and triatomic molecules (see chapter 6) and parent NO_2 peak can still be observed. With the development of high power ultrashort pulse laser, new questions and new challenges such as above-threshold ionisation, free-free transitions, multiply charged ion creation, resonance with autoionising states, very intense laser field effect (tunnelling), femtosecond ionisation have been extensively studied. The advent of femtosecond laser has opened new era for ultrafast photoionization spectroscopy. A number of femtosecond multiphoton ionisation experiments on small molecules, such as CO, CO_2, NO, NO_2 and medium mass nitro-aromatic molecules have been conducted at Glasgow University for studying the pathways and the mechanism of ionisation of the molecules under intense laser radiation (Ledingham, K.W.D. et al, 1995; Singhal, R.P. et al.; 1996).

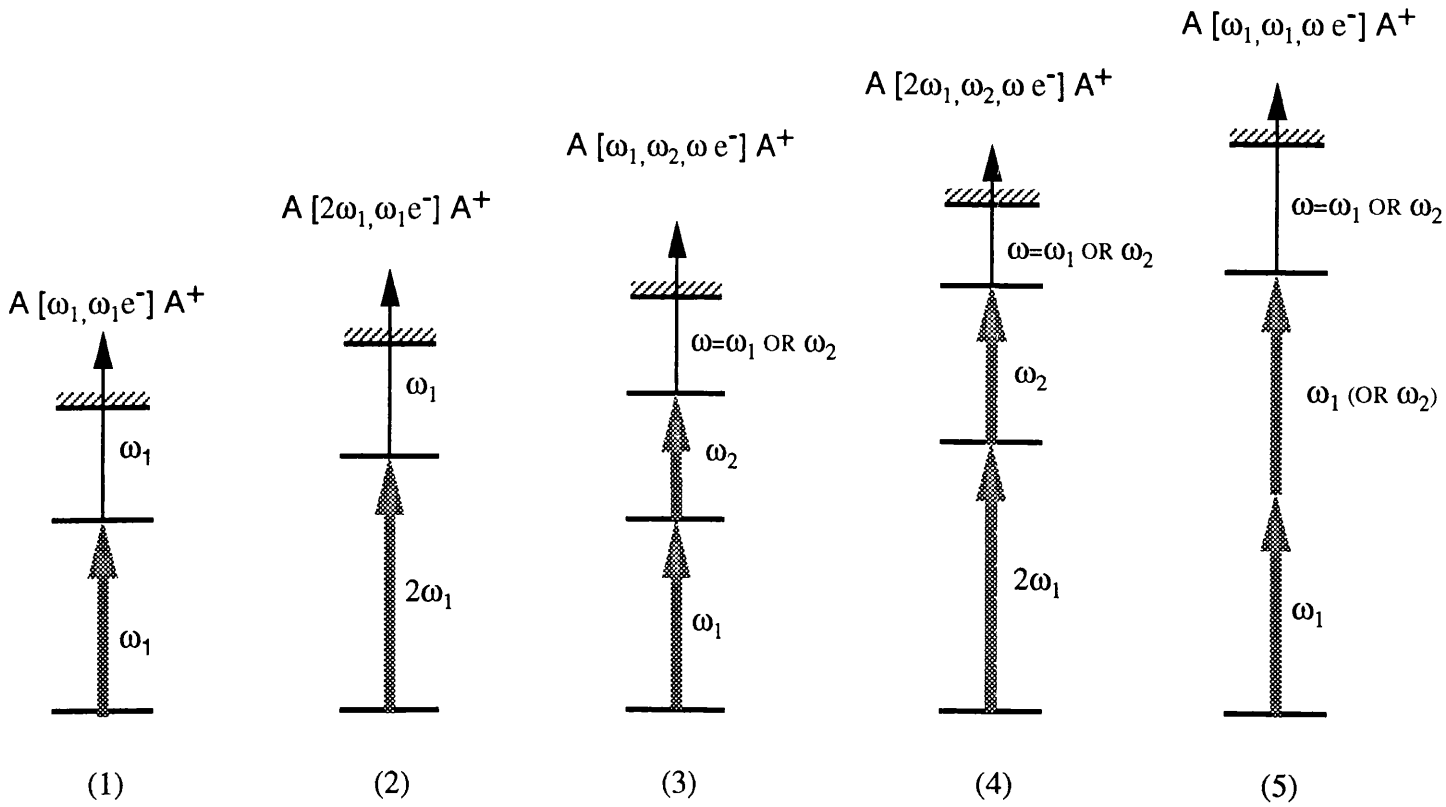

Figure 2.3 Five RIS schemes which can ionize every elements in the Periodical Table exept helium and neon

2.3 Resonant ionisation spectroscopy of atoms

Hurst et al. have proposed five basic ionisation schemes according to the relative energy positions of the intermediate states to the continuum (1979). These are shown in figure 2.3. In the first scheme a level exists at an energy that is more than half the value required to ionise the atom. Hence the atom can be ionised by two photons from the same dye laser, with the first photon being resonant. In the second scheme the output of the tunable dye laser must be frequency doubled to resonantly excite the atom, which is then ionised by a photon from the more intense fundamental beam. For atoms with higher ionisation potentials, more than two excitation steps can be used. Scheme 3 involves two resonant absorption processes which are effected by photons of different wavelengths from different laser beams. Ionisation is achieved by absorbing a photon of either wavelength. In scheme 4, we have a similar process to scheme 3, but the first absorption is effected by a frequency doubled photon. Finally, scheme 5 involves a two-photon resonant absorption which proceeds through a short lived virtual state of the atom, with ionisation accomplished by a single photon absorbed from the same laser pulse. The disadvantage of this method is that the absorption cross section through a virtual state is very small compared to single photon resonant absorption, so in general schemes of this sort are less efficient than corresponding schemes where resonant absorption is involved. Finally, one distinct advantage of this method lies in the fact that states which are forbidden by electric dipole selection rules for single photon transition may be studied.

2.4 Resonant ionisation processes of molecules

The situation of resonant multiphoton ionisation with molecules is much more complicated then that with atoms. Actually, in spite of the fact that selective laser photoionisation of atoms has been extensively developed, the method of laser photoionisation spectroscopy cannot be directly transferred to molecules for the following reasons:

(1) The excited states of polyatomic molecules are of much more complicated nature, and molecular absorption spectra often have little structure. This makes it much more difficult to realise photoionisation of polyatomic molecules with high selectivity.

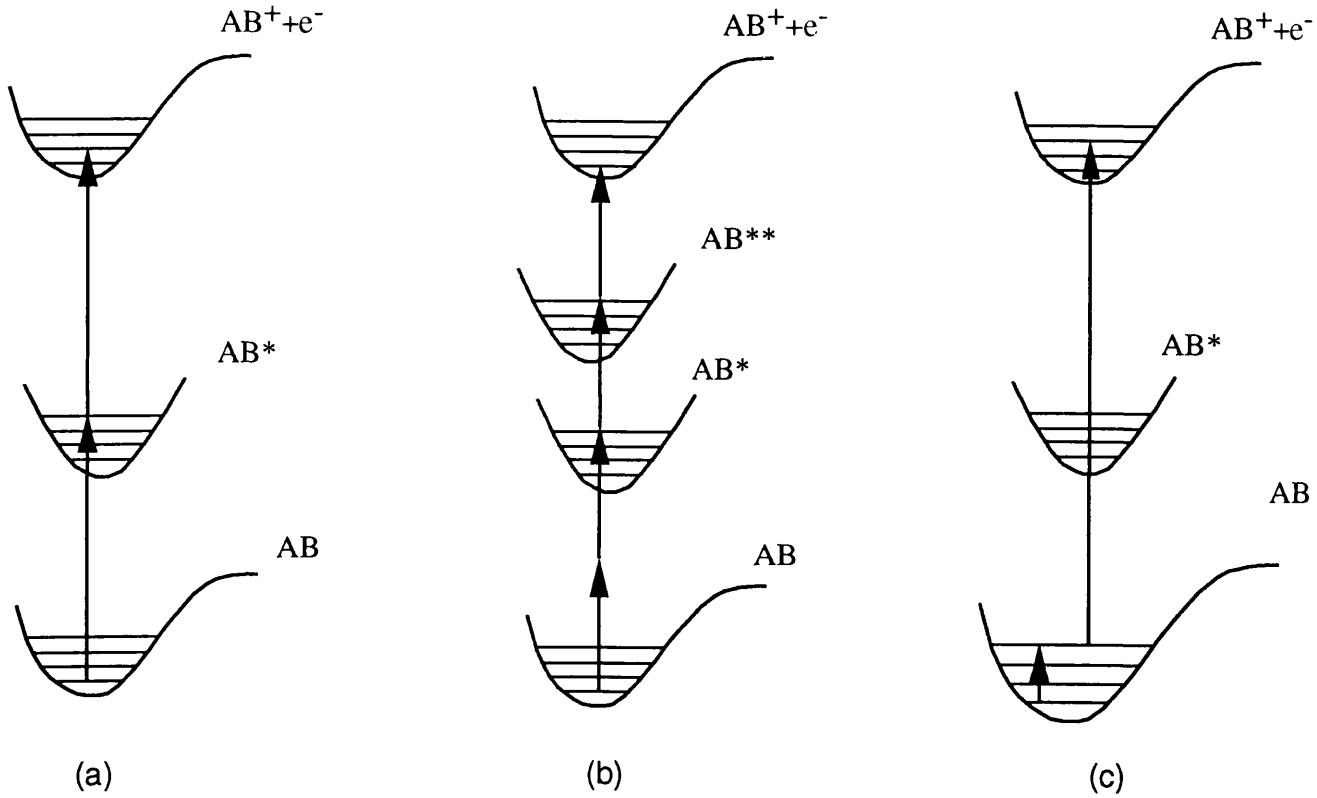

Figure. 2.4 Schemes of molecular REMPI:
(a) via an intermediate electronically excited state (two-color REMPI)
(b) via an intermediate two-photon resonant excitation (multiphoton ionisation).
(c) via a vibrationally excited state (IR-UV photoionisation).

(2) In contrast to atoms, molecules in intermediate states can undergo different photophysical and photochemical transformation (for example, photodissociation), which can compete with the photoabsorption and photoionisation processes.
(3) The products of photoionisation of polyatomic molecules, especially with the use of intense laser radiation, can be very diverse, and this essentially requires the use of the mass-spectrometric technique of analysis and detection of photoions.

Several basic schemes of multistep excitation, shown in a simple manner in figure 2.4, can be used for resonance photoionisation of molecules.

2.5 The results of perturbation theory (Park, D.H., 1983)

Multiphoton processes are usually described by the lowest nonvanishing order of time-dependent perturbation theory. A generalised expression for multiphoton ionisation transition probability can be written as

$$W^{(n)} = \sigma_n F_n(I) \tag{2.5}$$

where n is indicative of the number of laser photons of given energy needed to ionise the species. $F_n(I)$ is a function of the laser intensity and for a nonresonant process is given by perturbation theory as I^n. Also included in $F_n(I)$ is information about the temporal coherence of the laser. σ_n is the cross section of the nth-order process (units cm^{2n} sec^{n-1}) and contains all of the atomic and molecular information. The main feature of the cross section is a matrix-element summation involving all states of the system, including the continuum. A simple I^n dependence for an n-photon transition holds only when no intermediate resonances exist (i.e. non-resonant). With the introduction of resonances the intensity dependence goes as I^{n_0}, where n_0 is usually a non-integer number less than n. Above 10^{35} photons/cm^2 sec perturbation theory is no longer valid because at these intensities electric field exceeds the binding energy of an electron to the nucleus.

On the other hand, Lambropoulos (1976) has estimated the minimum photon flux necessary to observe multiphoton effects as ~10^{20} photons/cm^2sec. With typical laser intensities of 10^9 W/cm^2= 2 x $10^{-16} I/\lambda$ perturbation theory should be valid.

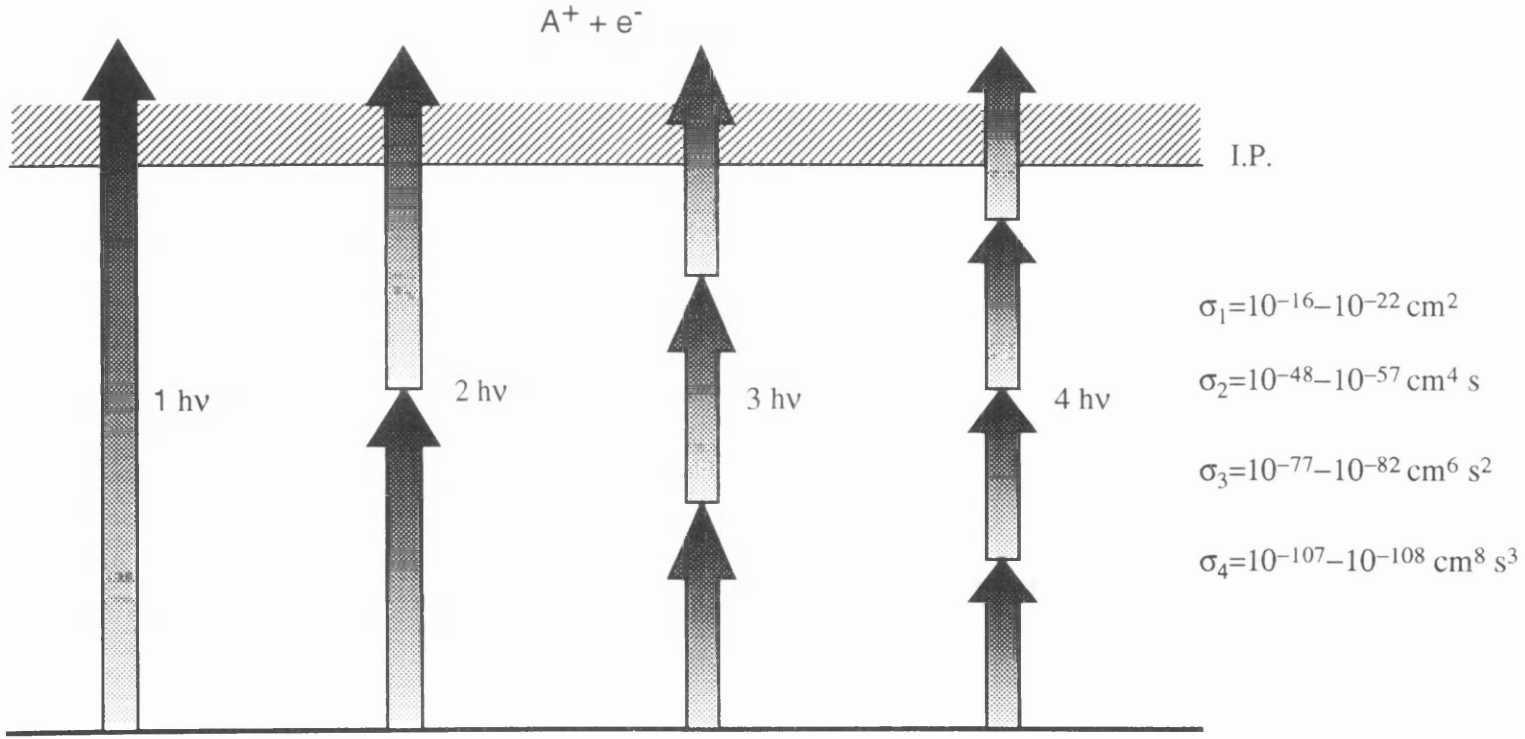

Figure 2.6.1 Cross sections of non-resonant MPI

2.6 . Cross sections

Before attempting to record a multiphoton spectrum, there are some basic molecular parameters that must be kept in mind: the magnitude of typical cross-sections, so that one can estimate the laser intensity which will be needed for the experiment to be undertaken.

2.6.1 Absorption cross sections of non-resonant multiphoton ionisation of atoms

(refer to Mainfray, G. and Macus, C., 1984)

For simplicity, only the 2-photon ionisation of an atom with laser frequency ω and an intensity I is considered first (Gold, 1969). If an energy -conserving first-order transition were possible., the 1-photon transition would take place at a rate $w = \sigma_1 I$, where, σ_1, the 1-photon absorption cross section, is typically 10^{-17} cm^2. A second photon can be absorbed if it is incident within the time T, which is regarded as the time spent by the atom in a laser-induced virtual excited state. This time T is of the order of an optical cycle, i.e. an order of the inverse of laser frequency, ω^{-1}, typically 10^{-15} s. Again the rate of the second event is $\sigma_1 I$ so that the overall rate for the 2-photon ionisation will be

$$w \cong \sigma_1 I \omega^{-1} \sigma_1 I \qquad 2.6.1)$$

Therefore $\sigma_2 = w / I^2 \cong 10^{-49} cm^4 s$.

As far as 3-photon ionisation processes are concerned, let us first return to the simple argument which lead to an order of magnitude estimate for σ_2.

$$w \cong \sigma_1 I T \sigma_1 I T \sigma_1 I \qquad 2.6..2)$$

Therefore,

$$\sigma_3 = w / I^3 \cong 5 \times 10^{-81} cm^6 s^2 \qquad (2.6.3)$$

Figure 2.6.1 shows the typical values of the cross section of non-resonant multiphoton ionisation.

From these small numbers it is apparent that very high light fluxes are needed in order to achieve a significant transition probability, σI^n. Typical nanosecond pulsed dye lasers have pulse powers of around 10^5 watts (1 mJ in a 10^{-8} sec pulse, about

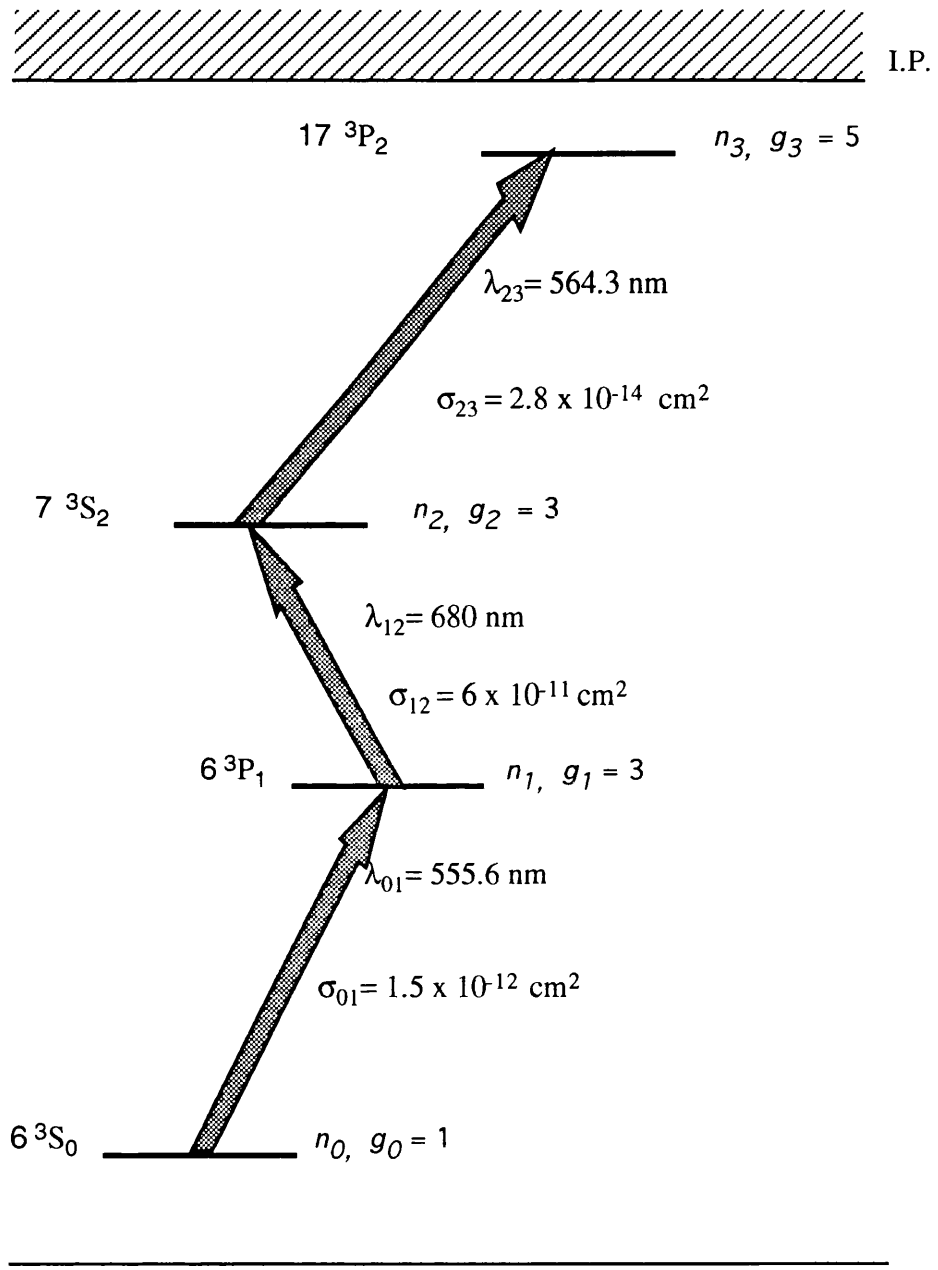

Figure 2.6.2 Three photon resonant excitation scheme of Yb atoms

10^{23} photons/sec or 10^{15} photons/pulse). In order to have a 10^{-2} transition possibility in each laser pulse, the focal area must then be about 3 x 10^{-4} cm^2 for a radius of about 100 μ.

2.6.2. Resonant excitation cross section of resonant multiphoton process

By tuning the laser frequency, the multiphoton ionisation rate of atoms or molecules can be made to exhibit a typical resonant character when the energy of an integral number of photons approaches the energy of an allowed atomic transition. Ionisation rate W increases drastically while retaining a finite value because of damping terms arising from the coupling of the resonant state with the ground state and the continuum. The absorption cross section of a single photon resonant transition between state b and a is given by (Letokhov et al., 1978):

$$\sigma = \frac{g_b}{g_a}\frac{\lambda^2}{2\pi}\frac{A_{ba}}{\Delta\omega} \tag{2.6.4}$$

where λ is the wavelength of the resonant absorption transition, A_{ba} is the Einstein transition coefficient between the initial state and the resonant state (calculated with Hartree-Fock code if necessary), $\Delta\omega$ is the spectral linewidth of the transition, g_a and g_b are the degeneracy factors of the upper and lower levels. Let us take an example for estimating the order of magnitude of resonant absorption cross sections of atoms. Let us apply this formula to the three step-excitation resonant transitions of $6^3P_1 - 6^3S_0$, $7^3S_1 - 6^3P_1$ and $17^3P_2 - 7^3S_1$ of Yb atoms, see figure 2.6.2. The Einstein coefficients for these two transitions are well known: $A(6^3P_1 \rightarrow 6^3S_0)$=1.2 x 10^6 sec^{-1}, $A(7^3S_1 \rightarrow 6^3P_1)$=$10^8$ sec^{-1}. Suppose the transition linewidth is 0.01 cm^{-1}, then the values of the corresponding transitions: σ_{6S-6P}=1.5 x 10^{-12} cm^2 and σ_{6P-7S}=6 x 10^{-11} cm^2. Singhal, R.P. et al. (1989) measured the absorption cross section of the third step excitation $17^3P_2 - 7^3S_1$ with $A(17^3P_2 \rightarrow 7^3S_1)$= 9940 s^{-1}, they obtained a value of σ_{7S-17P}=2.8 x 10^{-14} cm^2, which is consistent with the order of 10^{-14} cm^2 give by Letokhov, V.S. (1987).

2.6.3. Photoionisation cross section

Typical atomic photoionisation cross section is $\sigma_{ion} = 10^{-17} - 10^{-18} cm^2$ (Bekov, G.I., 1978). Typical molecular photoionisation cross section is $\sigma_{ion} = 10^{-17} - 10^{-19} cm^2$ (Boesl, U., 1991).

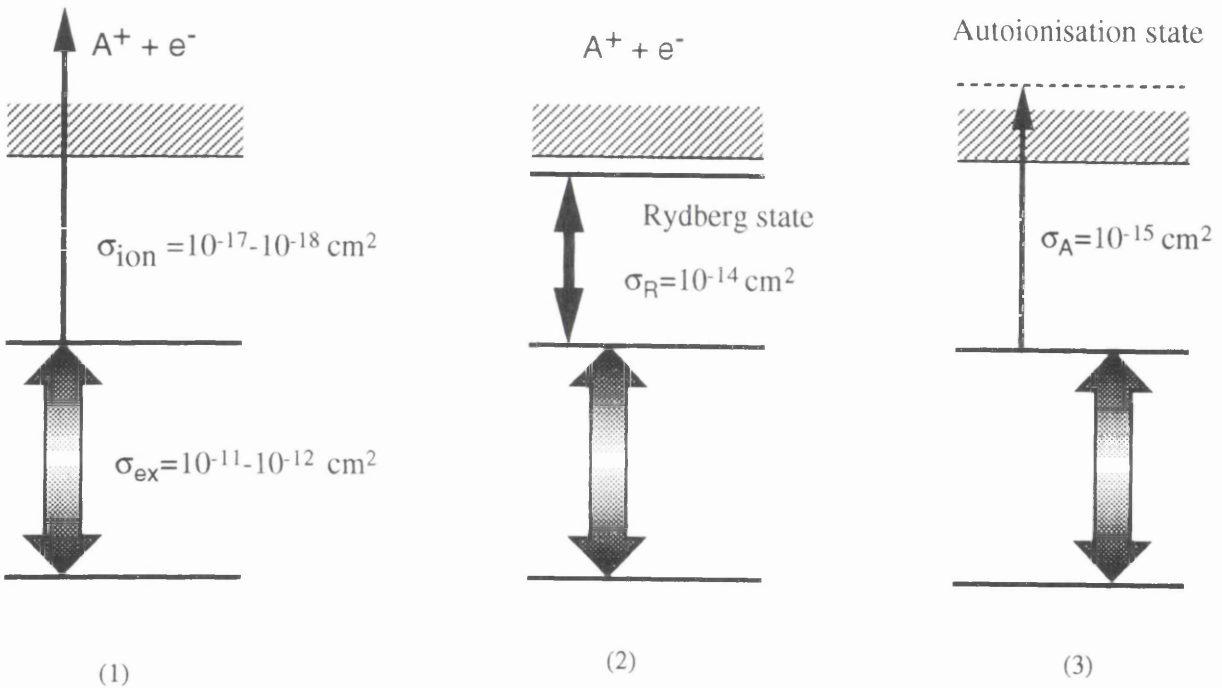

Figure 2.6.3 Multiphoton resonant excitation.
(1) Stepwised resonant ionisation.
(2) Resonant multiphoton absorption and ionization via a Rydberg state
(3) Ionisation via an autoionisation state.

In order to provide a clear picture concerning the above mentioned cross sections, a diagram figure 2.6.3 was produced corresponding to resonance excitation.

2.7 Mechanisms of photoionisation

In multiphoton ionisation, extensive fragmentation can be provided either by increasing the laser power density or by varying the wave length chosen by ionisation.

The actual photodissociation may occur through two different mechanisms; that is either the ladder-switching processes (Diets, W. et al; 1982; Bosel, U. et al. 1980), or ladder-climbing (Stiller, S.W. and Johnson, M.V., 1985 and Gobeli, D.A., 1985). In the case of ladder switching, the molecular ion is initially produced by resonant two photon ionisation (R2PI) or by one of other MPI processes. As the laser power is increased, subsequent absorption of additional photons may occur, resulting in excitation to a state that dissociates, producing ionic (and) neutral fragments. The ionic fragments may absorb subsequent photons, producing yet smaller ionic fragments. In the case of ladder climbing, the neutral molecules may simultaneously absorb several photons and reach an autoionic level and produce neutral or ionic fragment species. Figure 2.7. shows a generalised picture of these two MPI mechanisms. Firstly the molecule can absorb a number of photons resonantly or nonresonantly to reach a dissociative state below the ionisation level. If the laser pulse length is longer than the lifetime of the state then the molecule fragments to form neutral molecules. Depending on the intensity, these fragments may absorb further photons within the initial laser pulse duration to ionise or further fragment. This process is followed by ionisation (DI), i.e. dissociation first and then ionisation. On the other hand if the laser pulse is very much shorter than the lifetime of the dissociative state then the up pumping rate may be so high that the ionisation level is reached. The manifold of ion states can absorb further photons and fragment. Alternatively the molecule can be pumped via a series of autoionisation levels to some highly excited state of the molecule which then fragments to ions. These two variants result in ionisation followed by dissociation (ID) or ladder climbing. Many molecules fragment by ID alone e.g. the aromatics while others e.g. the nitro compounds and the organometallic molecules by the DI route. Often the two mechanisms compete, with ladder climbing becoming more dominant as the pulse width decreases. It is possible also that ladder switching can occur from the ionic manifold of states if the lifetime of the states are shorter than the laser pulse width. In

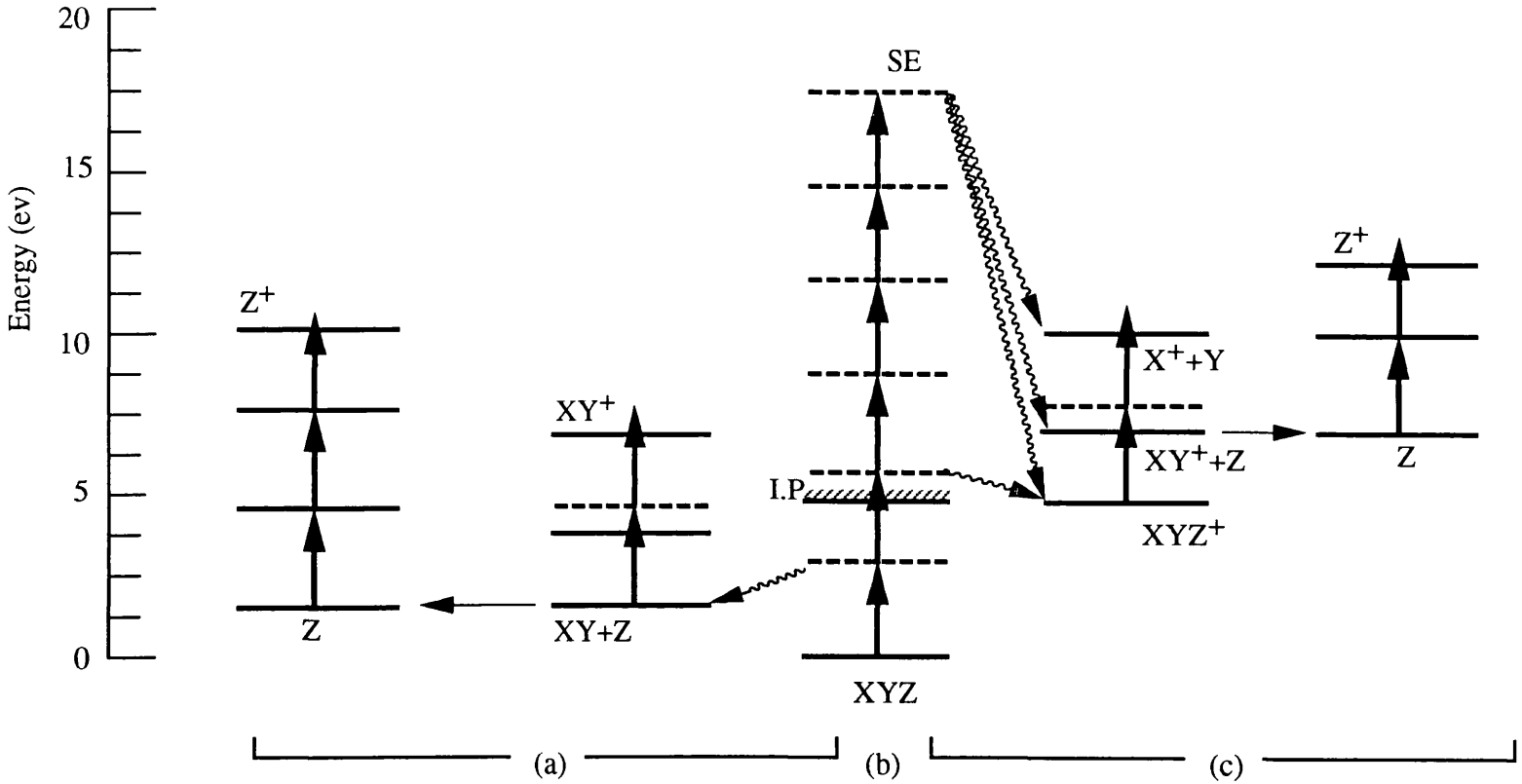

Figure 2.7 Ladder climbing and two kinds of ladder switching models of molecules (follow K.W.D. Ledingham , 1996)
(a) Ladder switching to neutral fragments.
(b) Ladder climbing to a superexcited state.
(c) Ladder switching to ionic fragments.

this case both the ion and the neutral fragments can absorb further photons. For analytical purposes, DI fragmentation is of little use since neither the parent nor the structurally discriminatory ions are formed.

2.8 Rate equations

The possible utilisation of MPI as an analytical technique depends on a full understanding of the dynamics of the process. At the laser power mentioned above, no transition can be considered in isolation, however. A complete picture of all possible excitation pathways in the molecule would have to include the various Raman processes, harmonic generation, Rabi cycling, ionisation, photodissociation, radiationless transitions, etc.

The proper description of multiphoton ionisation dynamics depends, in part, on the phase coherence of the laser field and of the system under study. The most general treatment of MPI dynamics is provided by the equations of motion for the density matrix of the system. If the coherence of the system-laser field is completely preserved then a fully quantum mechanical approach is appropriate. Population rate equation, however, arise from the other extreme when the coherence properties play insignificant role in the dynamics. The rate equations of resonant multiphoton ionisation for atoms have been generally studied by Swain, S. (1979) and for molecules by Johnson, P.M. and Otis, C.E. (1981). The rate equations are also developed to allow the inclusion of the more complex kinetic processes that can occur with molecular species. The resulting differential rate equations can be easily solved if a simplified model of the laser pulse is adopted. For better understanding the kinetics of multiphoton ionisation, a simple model is first treated in paragraph 2.8.1 (simple MPI). In this model only parent molecule's population variations are considered, while the population changes of a dissociative product from the parent molecules have been ignored. For the application of the theory of rate equations, a more complicated model (MPI with a dissociative product) which covers both multiphoton ionisation and dissociation is proposed in paragraph 2.8.2 and which will be applied to the ionisation and dissociation of NO_2 molecules in intense laser fields in chapter 6.

2.8.1 Rate equations for simple MPI

The model for a simple MPI without considering the ionisation of the dissociative product of a parent molecule is schematically depicted in figure 2.8.1.

According to Zakheim and Johnson (1980), the rate equations for a three-level, n+m REMPI process, where n photons are required to excite the molecule from the g-ground state to the r-intermediate resonant state and m-photons are needed to ionise the r-state to the continuum i-state, are

$$\frac{dN_g}{dt} = -aN_g + \phi N_r \tag{2.8.1.1}$$

$$\frac{dN_r}{dt} = aN_g - AN_r \tag{2.8.1.2}$$

$$\frac{dN_i}{dt} = bN_r \tag{2.8.1.3}$$

where $\phi = (a + \frac{1}{\tau})$ and $A = (a + \frac{1}{\tau} + k_p + b)$.. The individual rate constants are the n-photon stimulated absorption (emission) constant a (= $\sigma_n F^n$), the m-photon ionisation constant b (= $\sigma_m F^m$), in which σ is the appropriate cross section and F is the laser flux (photons $cm^{-2}s^{-1}$), lifetime of the resonant intermediate state τ and predissociation rate of the resonant intermediate state k_p. N_g, N_r and N_i are the number of molecules in the ground state, resonant intermediate state and ionic state respectably. Inspection of (2.8.1.3) shows that N_r must first of all be found if the ionisation yield is to be calculated.

$$\frac{d^2N_r}{dt^2} = a\frac{dN_g}{dt} - A\frac{dN_r}{dt} \tag{2.8.1.4}$$

Inserting (2.8.1.1) and (2.8.1.2) into (2.8.1.4) and rearranging it, we get a second order differential equation for N_r,

$$\frac{d^2N_r}{dt^2} + (a + A)\frac{dN_r}{dt} + a(A - \phi)N_r = 0 \tag{2.8.1.5}$$

which, if all molecules were considered to be in their ground states when the laser pulse was 'switched on' (i.e., $N_g = N_0$ and $N_r = N_i = 0$ at t=0), gives

$$N_r(t) = \frac{aN_0}{(\gamma_+ - \gamma_-)}\left[e^{\gamma_+ t} - e^{\gamma_- t}\right] \tag{2.8.1.6}$$

where N_0 is the total number of molecules within the laser beam volume and

$$\gamma_\pm = -\lambda \pm [\lambda^2 - \omega^2]^{\frac{1}{2}} \tag{2.8.1.7}$$

where $$2\lambda = a + A \tag{2.8.1.8}$$

and $$\omega^2 = a(A - \phi) \tag{2.8.1.9}$$

Under the approximation of square wave, i.e. assuming the laser pulse has a flat top temporal profile of pulse length T, we have from (2.8.1.3),

$$N_i(T) = b\int_0^T N_r(t)dt \tag{2.8.10}$$

which gives, upon integration,

$$N_i(T) = \frac{abN_0}{\gamma_+ - \gamma_-}\left[\frac{1}{\gamma_+}\left(e^{\gamma_+ T} - 1\right) - \frac{1}{\gamma_-}\left(e^{\gamma_- T} - 1\right)\right] \tag{2.8.1. 11}$$

for the number if ions produced after the passing of the laser pulse through N_0 ground state molecules.

The above expression simplifies in the limits of high and low laser fluxes. The two limiting forms are considered below.

(1) High flux conditions

When the stimulation, predissociation and ionisation process occur very rapidly compared to the laser pulse length, i.e. when $a, b, k_p >> \frac{1}{T}$, the numbers $\gamma_+ T$ and $\gamma_- T$ become very large and negative, and the exponential terms in (2.8.1.11) tend to zero, giving,

$$N_i(T) = \frac{ab}{\gamma_+ \gamma_-}N_0 = \left(\frac{b}{b + k_p}\right)N_0 \tag{2.8.1.12}$$

Two separate cases need to be considered.

Case 1. When the ionisation rate, b >> resonant state decay rate, k_p, We have,

$$N_i(T) = N_0 \tag{2.8.1.13}$$

In this case, every molecule in the laser beam volume is converted into an ion. This is known as saturation of the (n+m) process - the depletion of the ground state population in the focal region - which is commonly defined as $W_k t_L \geq 1$. Here W_k is the probability for the k th order process and t_L is the laser pulse duration. Although the sensitivity is maximised under these conditions, the spectral selectivity of the intermediate state is desirable.

Case 2. When the intermediate state decay rate, k_p>> ionisation rate, b, then,

$$N_i(T) = \left(\frac{\mathrm{b}}{k_p}\right) N_0 = \left(\frac{\sigma_m F^m}{k_p}\right) N_0 \tag{2.8.1.14}$$

It can be shown that (Letokhov, V.S., 1987) very high ionisation efficiencies may be attained in the laser beam volume provided the following two conditions on the laser fluence, φ, and flux, F, holds;

$$\varphi \geq \varphi_{sat} = \frac{1}{\sigma_{ion}} \tag{2.8.1.15}$$

and

$$F \geq F_{sat} = \frac{1}{2\sigma_{exe} t_L} \tag{2.8.1.16}$$

where σ_{exe} and σ_{ion} are the excitation and ionisation cross sections respectively. The quantities F_{sat} and φ_{sat} are called the saturation flux and fluence respectively.

(2). Low flux conditions

In the opposite limit when $\mathrm{a,b},k_p << \frac{1}{t_L}$, the exponential terms in (2.8.11) can be expanded using the binomial theorem, and when taken to the term of 2nd order in t_L, we have,

$$N_i(T) = \frac{1}{2}\mathrm{ab} N_0 t_L{}^2 = \frac{1}{2}\sigma_n \sigma_m F^{n+m} N_0 t_L{}^2 \tag{2.2.16}$$

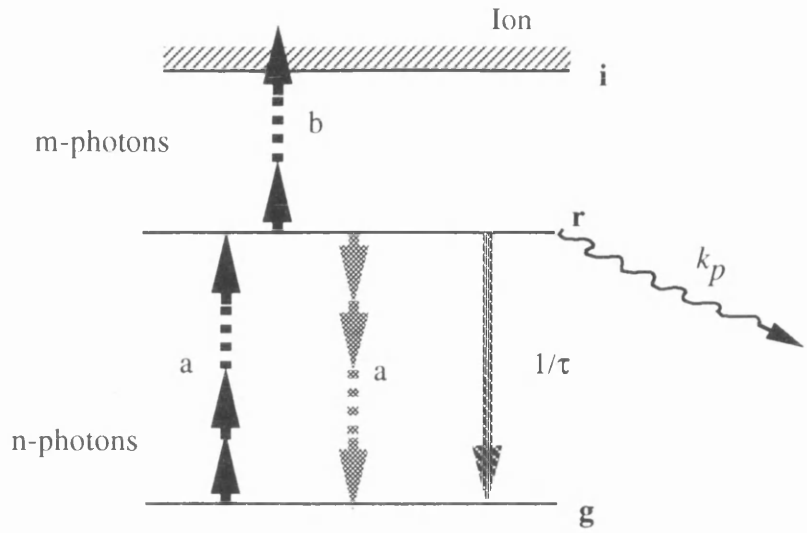

Figure 2.8.1 Population rate scheme of (m+n) REMPI. In the figure, g, r and i correspond to the population in the ground, intermediate, and ionization states respectively, and a, b and k_p represent rate constants for the steps of stimulated n-photon absorption/emission, m-photon ionization and predissociation respectively. The intermediate state lifetime is τ.

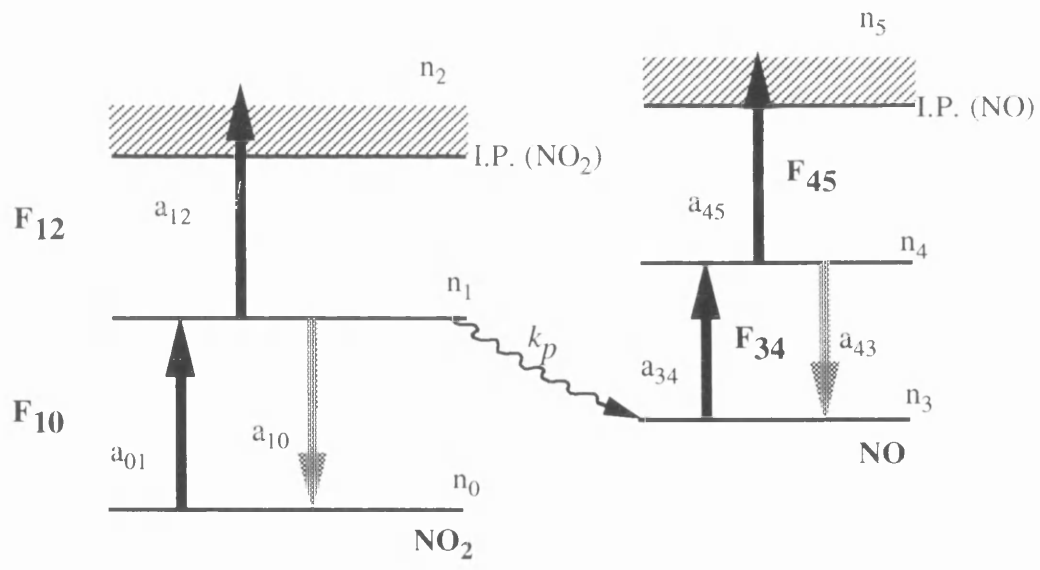

Figure 2.8.2 A model for the multiphoton ionisation and dissociation of the NO_2 molecules and its dissociative product NO in an intense laser field.

This equation shows the ionisation yields to be dependent on the (n+m)th power of the laser flux, which agrees with the result predicted by perturbation theory.

2.8.2. Rate equations for the MPI of a molecule with a dissociative product

Singhal et al (1989) developed a four level population rate equation model and code for a resonant ionisation process. With a modification to take into account the competition between up-pumping and dissociation, the same model was applied to investigate the yields of NO_2 and NO ions and their ratios when NO_2 was irradiated by 375 nm 50 fs laser pulse (Singhal et al., 1996) and by 375 nm 90 fs laser pulse (Singhal et al., 1997). A diagram for the model is shown in figure 2.8.2 in which both NO_2 parent and the dissociative product NO were involved in the MPI processes in an intense laser field. In this model, Singhal et al. assume that spontaneous emission may be neglected due to the short duration of laser pulses. The corresponding equations to the figure 2.8.2 are quoted as follows:

$$\frac{dn_0}{dt} = -a_{10}n_0 + a_{10}n_1 \qquad (2.8.2.1)$$

$$\frac{dn_1}{dt} = a_{01}n_0 - (a_{12} + a_{10} + k_p)n_1 \qquad (2.8.2.2)$$

$$\frac{dn_2}{dt} = a_{12}n_1 \qquad (2.8.2.3)$$

where n_o is the number of NO_2 molecules in its ground state, n_1 is the number of NO_2 molecules in its excited state, n_2 is the number of NO_2^+ produced and $a_{01} = \sigma_{01m_{01}} F_{01}^{\ m_{01}}$, $a_{10} = \alpha_{10}a_{01}$ and $a_{12} = \sigma_{12m_{12}} F_{12}^{\ m_{12}}$. In this model, the statistical weights of each states are taken to be unity and therefore $a_{10} = a_{01}$. k_p is the predissociation rate of the neutral NO_2 parent molecule in its excited state, m_{ij} is the number of photon to be absorbed to introduce relevant transition and F is the laser flux.

The initial number of the neutral NO in its ground state is determined by k_p as a results of the dissociation of the parent molecule in its excited state. Therefore the rate equations for the neutral NO can be written as

$$\frac{dn_3}{dt} = k_p n_1 - a_{34}n_3 + a_{43}n_4 \qquad (2.8.2.4)$$

$$\frac{dn_4}{dt} = a_{34}n_3 - a_{43}n_4 - a_{45}n_4 \tag{2.8.2.5}$$

$$\frac{dn_5}{dt} = a_{45}n_4 \tag{2.8.2.6}$$

where n_3 is the number of neutral NO in its ground state, n_4 is the number of neutral NO in its excited state, n_5 is the number of NO^+ ions and $a_{34} = \sigma_{34m_{34}} F_{34}^{\ m_{34}}$, $a_{45} = \sigma_{45m_{45}} F_{45}^{\ m_{45}}$ $a_{43} = \alpha_{43}a_{34}$ and $a_{45} = \sigma_{45m_{45}} F_{45}^{\ m_{45}}$. The statistical weights of each states are taken to be unity and therefore $a_{43} = a_{34}$.

This model suggests a more complicated but a general solutions for the populations of each states. Solutions for this equations were made using the initial conditions of $n_0 = N_0$, $n_1 = 0$, $n_2 = 0$, $n_3 = 0$, $n_4 = 0$ and $n_5 = 0$ at t=0. The N_0 is the initial number of neutral parent molecule in its ground state.

The initial equation set, eqs. (2.8.2.1)-(2.8.2.3) for the NO_2 parent can be simplified to give a second order differential equation in n_1

$$\frac{d^2n_1}{dt^2} + B\frac{dn_1}{dt} + Cn_1 = 0 \tag{2.8.2.7}$$

The equation (2.8.2.7) has two real positive roots γ_i leading to a general solution $n_1(t)$,

$$n_1(t) = \sum_{i=1}^{2} \beta_i \exp(-\gamma_i t) \tag{2.8.2.8}$$

which determines the number of excited NO_2 molecule. Insert equation (2.8.2.8) into equation (2.8.2.3) and integrate it, the number of the NO_2^+ ions can be determined by

$$n_2(t) = a_{12}\sum_{i=1}^{2} (\beta_i / \gamma_i)[1 - \exp(-\gamma_i t) \tag{2.8.2.9}$$

where γ_i, i=1,2, are determined to be $\gamma_{1,2} = (-B \pm (B^2 - 4C)^{1/2}) / 2$ with $B = a_{01} + a_{10} + k_p + a_{12}$ and $C = a_{01}(a_{12} + k_p)$. β_i are determined using initial conditions to be $\beta_{1,2} = \pm N_0 a_{01} / (\gamma_2 - \gamma_1)$.

The dissociation rate, k_p, of the parent molecules determine the number of the dissociation product, NO, in its ground state and the number of neutral NO products,

n_4, changes as a function of time due to equation (2.8.2.4). The general solution for the equation set (2.8.2.4)-(2.8.2.6) for calculating the number of NO ions is obtained by solving a third order differential equation in n_5 :

$$\frac{d^3n_5}{dt^3} + P\frac{d^2n_5}{dt^2} + Q\frac{dn_5}{dt} - a_{34}a_{43}k_p n_1 = 0 \qquad (2.8.2.10)$$

Where n_1 is given by equation (2.8.2.8).

With $y \equiv \frac{dn_5}{dt}$, equation (2.8.2.10) can be written as

$$\frac{d^2y}{dt^2} + P\frac{dy}{dt} + Qy = \sum R_i \exp(-\gamma_i t) \qquad (2.8.2.11)$$

Solving this differential equation,

$$n_5(t) = \sum_{i=1}^{4} (\delta_i / \gamma_i)[1 - \exp(-\gamma_i t)] \qquad (2.8.2.12)$$

can be obtained, where $\gamma_{1,2}$ are the same as above, $\gamma_{3,4} = (-P \mp (P^2 - 4Q)^{1/2}) / 2$ and $P = a_{34} + a_{43} + a_{45}$ and $Q = a_{34}a_{45}$. δ_i with i =1,2,3,4 are determined using initial conditions as $\delta_1 = R_1 / (Q - P\gamma_1 + \gamma_1^2)$ with $R_1 = a_{34}a_{45}k_p\beta_1$, $\delta_2 = R_2 / (Q - P\gamma_2 + \gamma_2^2)$ with $R_2 = a_{34}a_{45}k_p\beta_2$, $\delta_3 = [\delta_1(\gamma_1 - \gamma_4) + \delta_2(\gamma_2 - \gamma_4)] / (\gamma_4 - \gamma_3)$ and $\delta_4 = -\delta_3 - (\delta_1 + \delta_2)$. The $n_5(t)$ in equation (2.8.2.12) is the number of NO ions obtained.

Using this rate equation model, the analysis of the dissociative ionisation of the molecule NO_2 dealing with a single bond dissociation, the NO_2^+/NO^+ ratio gives a significant information about the competition between the ionisation of the parent molecule and the dissociation through this bond (Ledingham et al., 1995, Singhal et al., 1996). Therefore the ratio of n_2 / n_5 can be calculated using equations (2.8.2.9) and (2.8.2.12).

2.9 Concluding remarks

Certain aspects of the use of kinetics to model multiphoton ionisation dynamics have been presented. A feature that has to be properly accounted for in any dynamical description is the saturation effect and its consequences. When kinetic saturation of the ionisation step occurs, the multiphoton absorption is the rate-limiting step and the

resonant behaviour is then controlled by that step and by any spontaneous processes. The work of Crance and Fenenile (1977) indicates that absorption cross sections can be estimated in this regime. However the resonant signal shape will be broadened over the true molecular shape, due to lifetime broadening. When the interaction volume can't be taken as a cylinder, the geometric saturation appears. At high intensity, the power dependence goes as $I^{1/2}$ no matter how many photons are involved in the ionisation (Cervenan and Isenor, 1975). When the signal is saturated on-resonance, the off-resonance signal (there is usually some nonresonant or continuum background) still has a high order of nonlinearity and the background signal will catch up to the resonant signal until it is saturated too. A great loss of spectroscopic information occurs when there is saturation. This situation should be avoided for spectroscopic measurements, but not for sensitivity measurements.

In general, MPI is a very good tool to study atoms and molecules. This tool has been used in Glasgow for trace gas phase molecule detection. The following table lists some values which are described in detail later.

Table 2.9. The MPI (REMPI) processes which have been used at Glasgow.

Trace molecules	REMPI process	Laser wavelength	Laser energy	Detection limit
NO in N_2	1+1	226 nm	50 μJ	2-3 ppb
NO_2 in Air	2+1	226 nm	150 μJ	10-15 ppb
NO in N_2	2+1	382 nm	3 mJ	200 ppt
NO_2 in Air	1+2+1	382 nm	3 mJ	10 ppb
CO in N_2	2+1	230 nm	50 μJ	1 ppm
CO in Air	2+1	230 nm	200 μJ	0.6 ppm
C_6H_6	1+1	260 nm	260 μJ	5 ppb

References:

Agostini, P. , Fabre, F., Mainfray, G., and Manus, C. (1968)
U-5-multiphoton ionization of hydrogen and rare gases, *IEEE J. Quatum Electron.* **QE-4**, 667-669

Arckerhalt, J.R. and Shore, B.W. (1977)
Rate equations versus Bloch equations in multiphoton ionization, *Phys. Rev. A* **16**, pp. 277-282

Andreyev, V.S., Antonov, V.S., Knyazev, I.N., and Letkhov, V.S. (1977)
Two-step photoionization of H_2CO by measurement of N_2- and H_2-lasers and measurement of the lifetime of its $^1A_2$ state, *Chem. Phys. Lett.* **45**, pp. 166-168

Ashfold, M.N.R. (1986)
Multiphoton probing of molecular Rydberg states, *Molec. Phys.* **58**, PP. 1-20

Ashfold, M.N.R. and Prince, J.D. (1988)
Multiphoton process in molecular gases, *Contemp. Phys.* **29**, pp. 125-157

Ashfold, M.N.R., Clement, S.G., Howe, J.D. and Western, C.M. (1993)
Multiphoton ionization spectroscopy of free-radical species, *J. Chem. Soc. Faraday Trans.* , **89**, PP. 1153-1172

Bekov, G.I., Letokhov, V.S., Matveev, O.I. and Mishin, V.I. (1978)
Ionisation detection of single atoms by laser radiation using Rydberg states, *Sov. Phys. JETP* , **48** (6), pp. 1052-1057

Boesl, U. (1991)
Multiphoton excitation and mass-selective ion detector for neutral and ion spectroscopy, *J. Phys. Chem.*, **95**, pp. 2949-2962

Boesl, U., Neusser, H.J., Schlag, E.W., (1980)
Visible and UV multiphoton ionisation and fragmentation of polyatomic molecules, 31*J. Chem. Phys.*, **72**, 4327-4333

Benter, T., Liesner, M., Sauerland, V., and Schindler, R.N. (1995)
Mass spectrometric in-situ determination of NO_2 in gas mixures by resonance enhanced multiphoton ionization, *Fresenius J. Anal. Chem.* **351**, pp. 489-492

Cervenan, M.R., Isenor, N.R. (1975)
Multiphoton ionization yield curves for Gaussian laser beams, *Opt. Commun.* **13**, pp. 175-178

Chin S.L. (1970)
Direct experimental evidence of multiphoton ionization of impurities as the inraction process of laser-induced gas break down, *Can. J. Phys.*, **48,** pp. 1314-1317

Clark, A., Kosmidis, C., Ledingham, K.W.D., Marshall, A., Sander, J., and Singhal, R. P. and Cambell, M., (1993a)
Resonat ionization of oxygen and hydrogen atoms following laser-inhanced photodisociation of nitrobenze vapour, *J. Phys. B: At. Mol. Opt. Phys.*, **26**, L655-L670

Clark, A., Ledingham, K.W.D., Marshall, A., Sander, J., and Singhal, R. P., (1993b)
Attomole detection of nitroaromatic vapours using resonance enhanced multiphoton ionization mass spectrometry, *Analyst,* **118**, pp. 601-607

Collins, C.B., Johnson, B.W., Popescu, D., Musa, G., Pascu, M.L., and Popescu, I. (1973)
Multiphoton ionization of molecular cesium with tunable dye laser, *Phys. Rev. A* **8**, pp. 2197-2201

Crance, M. and Fenenile, S. (1977)
Resonant multiphoton ionization induced by pulsed excitation, *Phys. Rev. A* **16**, pp. 1587-1591

Diets, W.; Neusser, H.J.; Bosel, U., Schlag, E.W., Lin, S.H., (1982)
A model for multiphoton ionization mass spectroscopy with application to Benzene, *Chem. Phys.*, **66**, 105-127

Franzen, J., Frey, R. and Nagel, H. (1995)
Fast monitoring of motor exhaust components by resonant multiphoton ionization and time-of-flight mass-spectrometry, *J. Mol. Struc.*, **347**, pp. 143-151

Gavrilla, M. (1992)
Atoms and molecules in intense fields, Academic Press

Gobeli, D.A. and ElSayed, M.A. (1985)
Studies of rapid dynamics of 2,4-Hexadiyne by the pump-pump picosecond laser mass-spectrometric technique, *Proceddings of the society of photo-optical instrumentation engineers,* **533**, pp. 72-77

Gold, A (1969)

Two-photon spectroscopy, Quantum optics, Glauber, R.J., ed., Italian physics society course **42**, Academic, New York, pp.397-420

Goodmam, L. and Philis, J., (1992)

Multiphoton absorption spectroscopy, In Andrew, D.L. ed. *Applied Laser Spectroscopy*, VCH, New York, pp. 319-364

Granneman, E.H.H., Klewer, M., Nienhus, G., and Vander Weil, M.J. (1977)

Two-photon ionization of calsium via the 7 $^2P_{1/2, 3/2}$ intermidiate states, *J. Phys. B* **10**, pp 1625-1632

Guizard, S., Chapolard, D., Horani, M. and Cauyacq, D., (1989)

Detection of NO traces using resonantly enhanced multiphoton ionization: A method for monitoring atmosphereic pollutants, *Appl. Phys.* **B 48**, pp. 471-477

Held, B., Maifray, G., and Morellec, J. (1972)

Multiphoton ionization probability of potassum atoms at 1.06 μ and 0.53 μ, *Phys. Lett. A* **39**, 57-58

Hippler, M., Yates, A.J. and Pfab, J. (1990)

Ultra-trace analysis of NO by high resolution laser fluoresence and ionization spectroscopy, *Inst. Phys. Conf. Ser.* No.113: Section 9, pp. 303-306

Hurst, G.S., Payne, M.G., Kramer, S.D. and Young, J.P. (1979)

Resonance ionisation spectroscopy and one-atom detection, *Reviews of modern physics*, **51**, pp. 767-819

Hurst, G.S., Payne, M.G., Nayefeh, M.H. and Young, J.P. (1977a)

A demonstration of one-atom detection, *Appl. Phys. Lett.*, **30**, pp. 229-231

Hurst, G.S., Payne, M.G., Nayefeh, M.H. and Young, J.P. (1977b)

One-atom detection using resonant ionisation spectroscopy, *Phys. Rev. A* **15**, pp. 2283-2291

Hurst, G.S., Payne, M.G., Nayefeh, M.H., Judish, J.P., and Wagner, E.B. (1975)

Saturated two-photon resonance ionisation of He(2 ^{1}S)*, *Phys. Rev. Lett.*, **35**, pp. 82-85

Johnson P.M (1975)

Multiphoton ionization spectroscopy, *J. Chem. Phys.* **62**, 4562-4563

Johnson P.M. and Otis, C.E., (1981)

Molecular multiphoton spectroscopy with ionization detection,*Ann. Rev. Phys. Chem.* ,**32**, pp. 139-157

Lambropoulos, P. (1976)
Topics on multiphoton process in atoms, Adv. At. Mol. Phys. **12**, pp. 87-164

Ledingham, K.W.D. and Singhal, R.P.
High intensity laser mass spectrometry - A review, accepted by *Int. J. Mass. Spectr.*

Ledingham, K.W.D. (1995)
Multiphoton ionisation and laser mass spectrometry, in ed by Andrews, D.L. and Demidov, A.A., Plenum Press, New York, PP. 199-227

Lemire, G.W., Simeonsson, J.B., Sausa, R.C. (1993)
Monitoring of vapor-phase nitro-compounds using 226-nm radiation-fragmentation with subsequent NO resonance-enhanced multiphoton ionization detection, *Anal, Chem.* **65**, pp. 529-533

Letokhov, V.S. , Mishin, V.I., and Puretzky, A.A., Prog. (1977)
Selective photoionization of atoms by laser radiation and ita applications, *Quantum. Electron.* **5**, pp. 139-203

Letokhov, V.S. (1987)
Laser Photoionization Spectroscopy, Academic Press, London

Lin, S.H., Fujimura Y., Neusser, H.J., and Schlag, E.W. (1984)
Multiphoton Spectroscopy of Molecules, Academic Press, New York

Lineberger, W.C., and Patterson, T.A. (1972)
Two photon photodetechment spectroscopy: The $C_2^{-2}\Sigma$ states, *Chem. Phys. Lett.* **13**, pp. 40-44

Looney, J. P., Harrington, J.E., Smyth, K.C., O'Brian, T.R., and Lucatorto, T.B. (1993)
Measurement of CO pressure in the ultrahigh vacuum regime using resonance-enhanced multiphoton-ionization time-of-flight mass spectrometry, *J. Vac. Sci. Tevhnol. A* **11(6)**, pp. 3111-3120

Mainfray, G. and Macus, C., (1984)
"Normal" multiphoton ionization of atoms, in ed. by Chin, S. L. and Lambropoulos "Multiphoton ionisation of atoms", Academic, London, pp. 7-34

Maker, P.D., Turhune, R.W., and Savage, C.M. (1964)
Quantum Electronics, Columbia Univ. Press, New York, pp. 1559

Marshall, A., Clark, A., Jennings, R., Ledingham, K.W.D. and Singhal, R.P., (1991)
Resonant two-photon ionization for detection of aromatic molecules. *Mass. Sci. Technol.*, **2**, pp. 1078-1082

Marshall, A., Clark, A., Jennings, R., Ledingham, K.W.D., J. Sander and Singhal, R.P., (1992)
Laser induced dissociation ionization and fragmentation process in nitroaromatic molecules, *Int. J. Mass Spec. Ion Proc.*, **116**, pp. 143-156

Marshall, A., Clark, A., Deas, R. M., Kosmidis, C., Ledingham, K.W.D., Peng, W., Singhal, R.P. (1994)
Sensitive atmospheric pressure detection of nitroaromatic compounds and NO_X (x=1,2) molecules in an ionization chamber using resonance-enhanced multi-photon ionization, *Analyst,* **119**, pp. 1719-1724

Miller, J. C.(1986)
Ultrasensitive, Isotopically selective detection of nitric oxide by multiphoton ionisation in a supersonic beam, *Anal. Chem.*, **58**, pp. 1703-1705

Morgan, C. G. (1975)
Laser-induced breakdown of gases, *Rep. Phys. Prog.* **38**, pp. 621-665

Murakami, J., Ito, M., and Kaya, K. (1980)
Multiphoton ionization spectra of benzene, fluorobenzene, and chlorobenzene resonat with S_0-S_1 transitions by use of nozzle beam method, *J. Chem. Phys.* **72**, 3263-3270

Parker. D.H., (1983)
Laser ionisation spectroscopy and mass spectroscopy, in Kliger, D.S. ed. , Unltrasensitive laser spectroscopy, pp.234-309

Peng, W.X., Ledingham, K.W.D., Marshall, A., Singhal, R.P. (1995)
Urban air pollution monitoring: Laser-based procedure for the detection of NO_X gase, *Analyst,* **120**, pp. 2537-2542

Petty, G., Tai, C., and Dalby, F.W. (1975)
Nonlinear resonant photoionization in molecilar iodine,*Phys. Rev. Lett.* **34,** pp. 1207-1209

Pfab, J. (1995)
Laser-induced fluorecence and ionization spectroscopy of gas phase species, In Clark, R.J.H. and Hester, R.E. ed. *Spectroscopy in environmental science*, pp. 149-222

Saloman, E.B. (1990)
A resonance ionisation spectroscopy/resonance ionisation mass spectroscopy data service, I-Data sheets for As, B, Cd, C, Ge, Au, Fe, Pb, Si and Zn, *Spectrochimica Acta* **45B** , Nos. 1/2, pp. 37-83

Saloman, E.B. (1991)
A resonance ionisation spectroscopy/resonance ionisation mass spectroscopy data service, II-Data sheets for Al, Ca, Cs, Cr, Co, Cu, Kr, Mg, Hg and Ni, *Spectrochimica Acta* **46B** , No. 3, pp. 319-378

Saloman, E.B. (1992)
A resonance ionisation spectroscopy/resonance ionisation mass spectroscopy data service, III-Data sheets for Sb, Bi, P, Na, and Sn, *spectrochimica Acta* **47B** , No. 4, pp. 517-543

Saloman, E.B. (1990)
A resonance ionisation spectroscopy/resonance ionisation mass spectroscopy data service, IV-Data sheets for Be, In, Li, K, Rb, Ag, Ti and v and an update of the datasheet for Ni, *Spectrochimica Acta* **48B** , No. 9, pp. 1139-1203

Scheck, I. and Jortner, J. (1985)
Bloch equation and kinetic equations in multiphoton ionization,*Chem. Phys.* **97**, pp.1-11

Schlag, E.W. and Neusser, H.J. (1983)
Multiphoton mass-spectroscopy, *ACC. Chem. Res.* **16**, pp. 355-360

Singhal, R.P., Land, A.P., Ledingham, K.W.D. and Towrie, M. (1989)
Population rare equations modelling of a resonant ionisation process, *J. Anal. At. Spec.*, **4,** pp. 599-603

Singhal, R.P., Kilic, H.S., Ledingham, K.W.D., Kosmidis, C., McCanny, T (1996)
Multiphoton ionization and dissociation of NO_2 by 50 fs laser pulses, *Chem. Phys. Lett*, **253**, pp.81-86

Singhal, R.P. (1997)
Private communication

Simeonsson, J. B., Lemire, G.W., Sausa, R.C. (1994)
Laser-induced photofragmentation/photoionization spectrometry: A method for detection ambient oxides of nitrogen, *Anal. Chem.*, **66**, pp. 2272-2278

Stiller, S.W. and Johnson, M.V. (1985)
Compititive fragmentation processes in multiphoton ionisation-The role of ladder switching, *J. Phys.Chem.*, **89**, pp. 2717-2719

Swain, S. (1979)
A simple model for multiphoton ionization, *J. Phys. B* **12**, pp. 3201-3228

Voronnov, G.S., and Delone, N.B. (1966)
Many-photon ionization of the Xenon atom by Ruby laser radiation, *Sov. Phys. JETP* Engl. Trans. **23**, pp. 54-58

Weickhardt, C., Boesl, U., and Schlag, E.W. (1994)
Laser mass spectroscopy for time-resolved multicomponent analysis of exhaust gas, *Anal. Chem.*, **66**, pp. 1062-1069

Zakheim, D.S. and Johnson, P.M. (1978)
Two- and three-photon resonances in the four-photon ionization spectrum of nitric oxide at low temperature, *J. Chem.. Phys.* **68**, pp. 3644-3653

Zakheim, D.S. and Johnson, P.M. (1980)
Rate equation modeling of molecular multiphoton ionization dynamics,*Chem.. Phys.* **46**, pp. 263-272

Zandee, L., and Bernstain, R.B. (1979a)
Laser ionization mass spectrometry extensive fragmentation via resonance-enhanced multiphoton ionization of a molecular benzene beam, *J. Chem. phys.* **70**, pp. 2574-2575

Zandee, L., and Bernstain, R.B. (1979b)
Resonance-enhanced multiphoton ionization and fragmentation of molecular beams: NO, I_2, benzene, and butadiene, *J. Chem. phys.* **71**, pp. 1359-1371

Zandee, L.Bernstain, R.B., and Linchtin, D.A. (1978)
Vibronic/mass spectroscopy via multiphoton ionization of a molecular beam: the I_2 molecule,*J. Chem. phys.* **69**, pp. 3427-3429

Chapter 3

Instrumentation

3.1 Introduction

The principle of the instrumentation for this thesis can be described by the block diagram shown in Figure 3.1. However some units can be exchanged when the conditions differ, i.e. ion chamber is used for atmospheric conditions and a mass spectrometer in vacuum. In addition the laser may be changed from nanosecond to femtosecond regime.

In the nanosecond regime, the laser light source consists of a TE-860 XeCl excimer laser, a Lumonics EPD-330 Dye laser and an Inrad Model 5-12 second harmonic generation autotracking system.

In the femtosecond regime, the laser light source consists of a system of ultrafast laser pulses including optics for frequency doubling and changing pulse lengths from 100 fs to 3 ps.

The ion detectors are different for atmospheric pressures and vacuum conditions. For the former an ionisation chamber is used and for the latter an electron multiplier mounted inside a time-of-flight mass spectrometer is used.

The digital oscilloscope is used for both signal monitoring and storage of mass spectra.

The data acquisition system consists of a boxcar integrator, a computer interface and a Macintosh micro computer.

The laser power, specifically the laser pulse energy, was monitored by a J3 pyroelectronic joulemeter or a Gentec joulemeter.

All the above-mentioned units will be described in some detail in the following paragraphs.

3.2 Laser light sources

3.2.1 Lumonics TE-860 -3 Excimer laser

Excimers (The term excimer comes from Excited dimer) are molecules which are bound in their excited states but are unstable in their electronic ground states. Typical of such materials are the rare gas halides such as ArF, KrF and XeCl. The different gases operate at different wavelength regions.

The laser pumping cycle of an excimer can be understood as a bound-free system. The electronic ground state of such molecules have a mainly repulsive potential in the ground state with a shallow Van der Waal's minimum. The well depth of the ground state is less than the thermal energy kT at room temperature (see figure 3.2.1.a) (Demtroder, 1982). These systems are therefore highly unstable in their ground state and dissociate rapidly on a time scale of 1-10 ps. They do however form bound excited states and provided the number density of reactant molecules is sufficiently high, a population inversion may easily be achieved due to the absence of a ground state population. A transition between the excited bounded state and the dissociative ground state results in the emission of radiation which constitutes the laser output. The tunability range depends on the slope of the repulsive potential and on the internuclear positions of the classical turning points in the excited vibrational levels. The tuning range of excimer laser is very small.

The Lumonics TE-860-3 is an excimer laser for which the gases F_2, ArF, KrCl, XeCl, N_2, XeF, N_2^+, F and CO_2 can be used as laser gain media. Those media can generate laser radiation with wavelengths from VUV to UV. The laser medium used in this laboratory is XeCl. The typical output parameters of such a laser are displayed in table 3.2.1.

The TE-860-3 excimer laser can be used as a direct UV radiation source or used to pump a dye laser to generate tuneable laser radiation due to its high intensity and high repetition working frequencies.

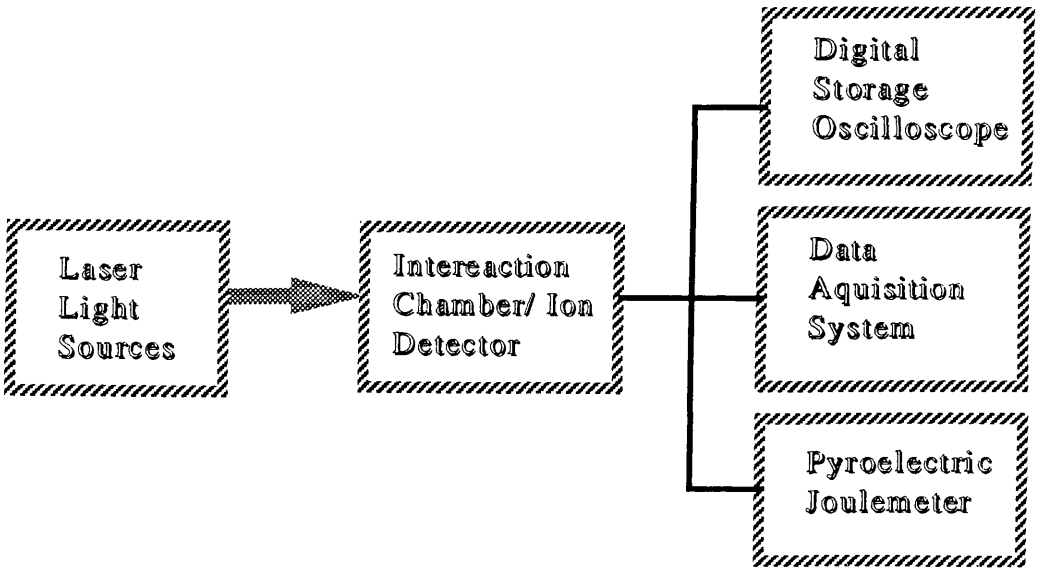

Figure 3.1 A block diagram for the experimental setup.

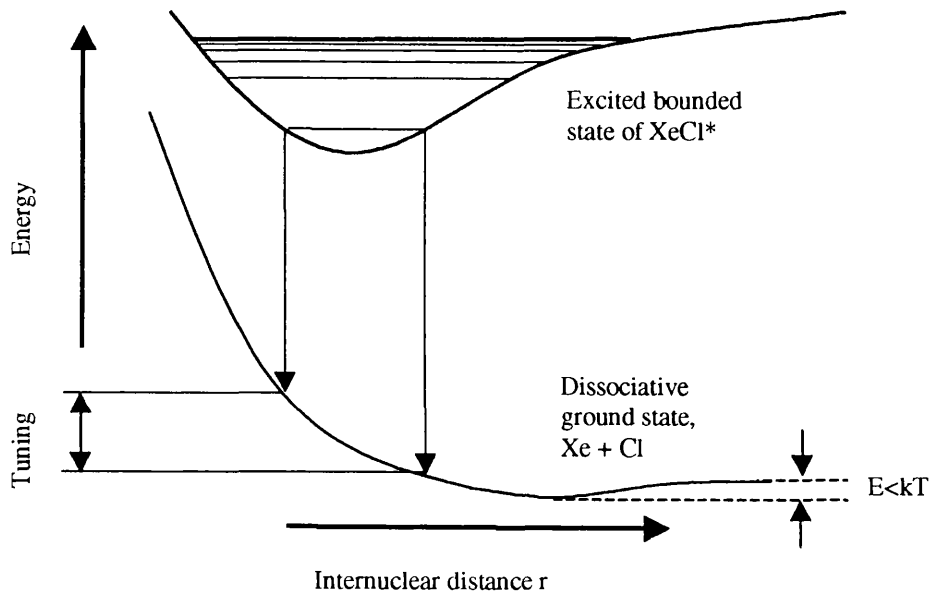

Figure 3.2.1 A schematic diagram of an excited state and the ground state of an excimer molecule

Table. 3.2.1 The performance parameters of the Lumonics TE-860-3 excimer laser

Wavelength	308 nm
Pulse length	4-12 ns
Beam size	8 mm x 12 mm
Beam divergence	2.4 x 6 mrad
Maximum repetition rate	70 - 80 Hz
Average pulse energy	70 mJ
Pulse to pulse stability	5%

3.2.2 Dye laser system

The dye laser system in this laboratory consists of Lumonics EPD-330 dye laser itself, an Inrad Autotracker II and a Lumonics EPD-60 Compuscan. The function of the Autotracker is to double the frequency of the laser pulse generated by the Lumonics EPD-330 and keep the phase matching condition when scanning the dye laser source. The function of the Lumonics EPD-60 Compuscan is to set or scan the wavelength of the Lumonics EPD-330 dye laser by controlling the rotation of the tuning mirror in the dye laser cavity through a stepping motor.

3.2.2.1 Basic principle of dye laser

Dye lasers are still the most widely used tuneable light sources because their operating range can extend from 300 nm to 1.2 μm depending on the pumping laser and the appropriate dye.

Organic dye molecules are the lasing species and are dissolved in an appropriate solvent and circulated by a pump through the lasing volume. These molecules absorb short wavelength light from a pumping laser, and fluoresce at longer wavelength (see figure 3.2.2.1 a).

Figure 3.2.2.1 b shows a typical dye energy level structure of dye molecules with singlet bands S_0, S_1 and triplet bands T_1. When dye molecules in a liquid solvent are irradiated with visible or UV light, high vibrational levels of the excited state S_1 are populated by optical pumping from thermally populated rovibronic levels in the S_0 ground state. Induced by collisions with solvent molecules, the excited dye molecules undergo very fast radiationless transitions into the lowest vibrational level of S_1 with relaxation times of 10^{-11} - 10^{-12} s. This level is depopulated by either

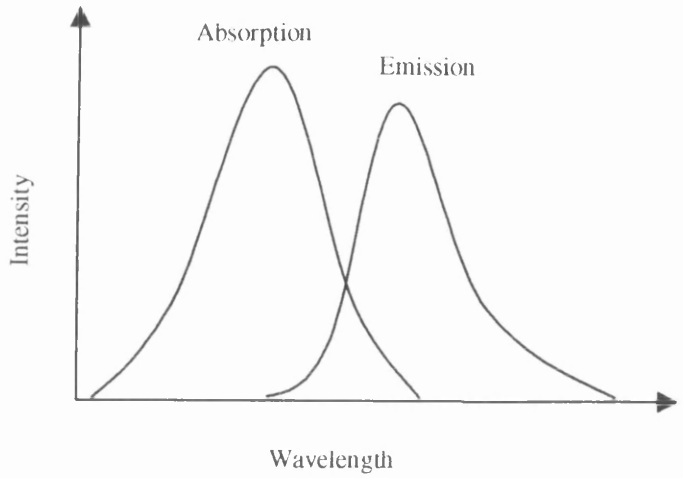

Figure 3.2.2.1.a. A schematic diagram shows the shift of dye emission spectrum shifted towards redder than absorption spectrum

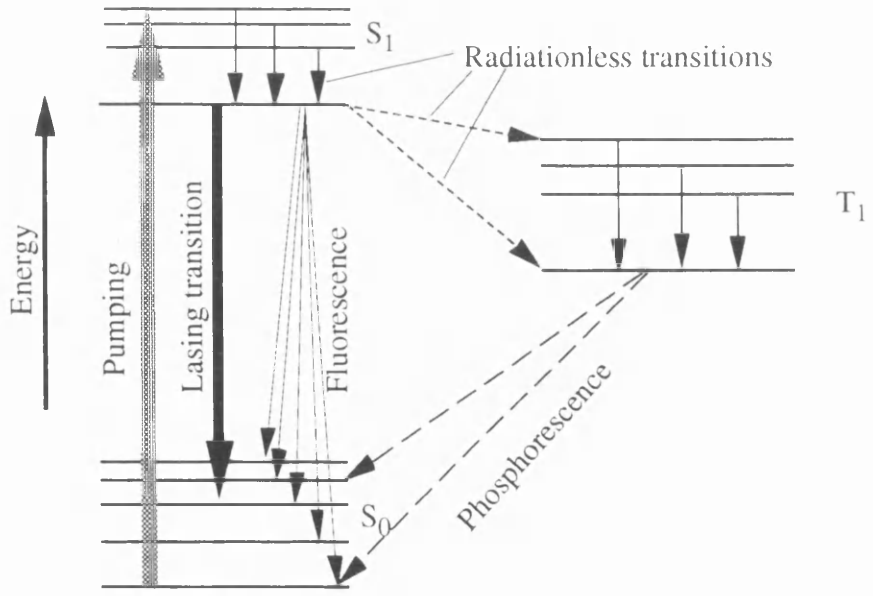

Figure 3.2.2.1 b Schematic energy level diagram and pumping cycle in dye molecules

spontaneous emission into different rovibronic levels of S_0 or by radiationless transitions into a lower triplet state T_1 (intersystem crossing). Lasing action normally takes place between the bottom levels of S_1 to the top levels of S_0 because of the Frank-Condon principle. The latter are sufficiently far above the bottom of the ground state for them to be almost empty at room temperature. Thus the dye laser is a four level system and the threshold is reached at a very small population inversion.

The absorption losses in the active dye medium are mainly caused by the following two effects:

a) The intersystem crossing transitions $S_1 \rightarrow T_1$ not only diminishes the population of the states in the ground state band and therefore the attainable inversion, but they also lead to an increased population of the triplet state T_1. What is more, the triplet absorption spectrum of the transition from T_1 to a higher triplet state T_m partly overlaps with the singlet fluorescence spectrum which results in additional absorption losses for the dye laser radiation. Because of the long lifetimes of molecules in the lowest triplet state, which can only relax into the S_0 ground state by slow phosphorescence or by collisional deactivation, the population density of T_1 may become undesirably large. To overcome this problem, the dye laser was circulated through the dye cells in order to rapidly remove the dye molecules in T_1 state from the lasing volume. Another advantage of circulating is to avoid dye overheating which can cause the dye itself to decompose.

b) For many dye molecules the absorption spectra which correspond to the transitions from the optically pumped singlet state S_1 to still higher states S_m partly overlap with the gain profile of the laser transition from S_1 to S_0. These losses are inevitable.

3.2.2.2 EPD-330 dye laser

The dye laser used in this laboratory is a Lumonics EPD-330 and its optical layout is shown in figure 3.2.2.2. The Luminous EPD-330 dye laser was pumped by a Lumonics TE-860-3 excimer laser. The excimer laser beam passed through a beam splitter and about 10% of the pulse energy was focused into the oscillator dye cell. This initiated laser action, while the remainder of the pump beam was time delayed and focused into an amplifier dye cell, where the oscillator beam caused further stimulated emission from the excited dye molecules and boosted the oscillator power

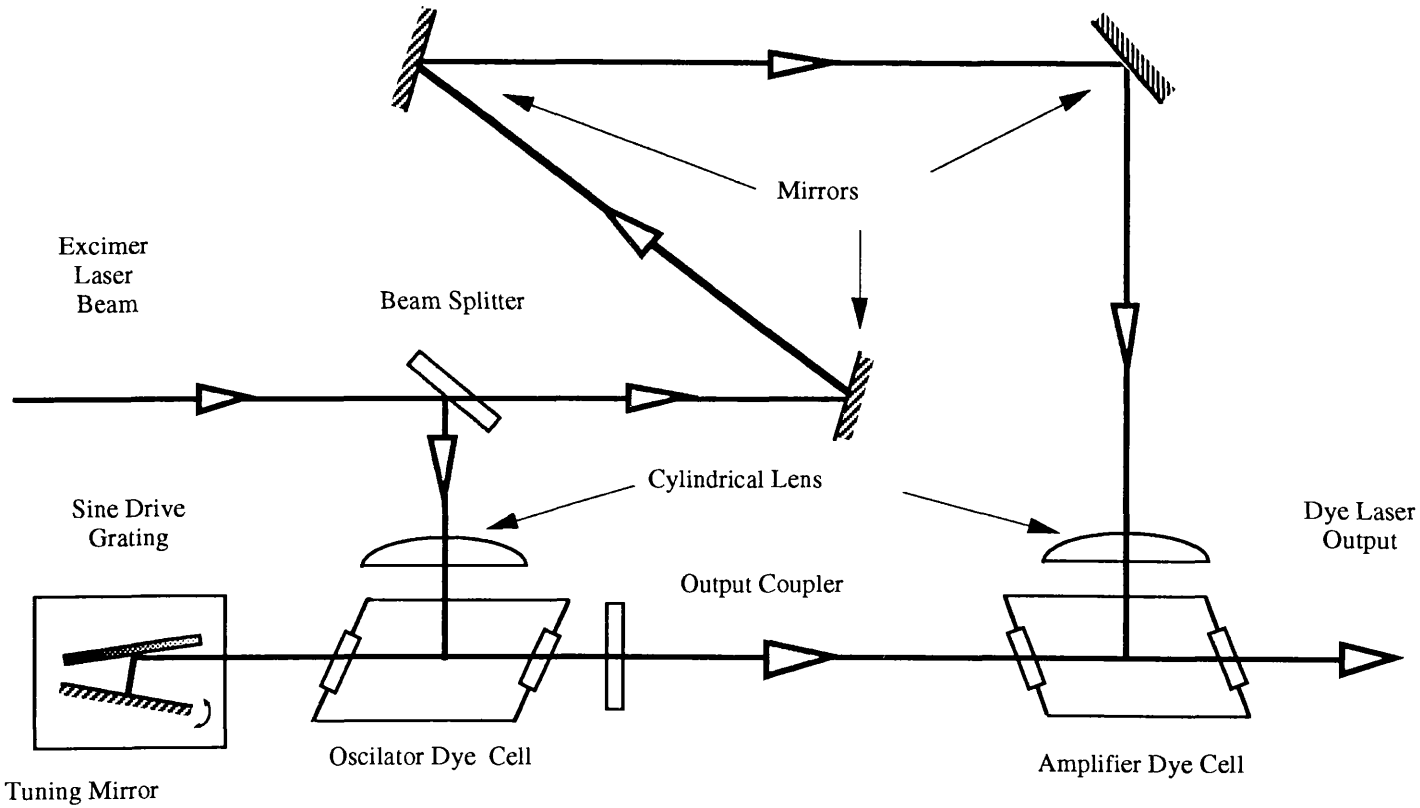

Figure 3.2.2.2. EPD-330 dye laser optical layout

by a factor of about 15. at the peak of the gain curves for most dye used, output pulse energies of 5 -10 mJ were easily obtained.

Wavelength tuning through out the dye gain profile was achieved by using the tuning mirror facing to the holographic grating in the sine drive . The grating was arranged at grazing incidence under an angle $\alpha \approx 90^{o}$ against the grating normal. At a wavelength λ the first diffraction order is reflected from the grazing incidence grating into the direction β determined by the grating equation (Demtroder, 1982)

$$\lambda = d(\sin\alpha + \sin\beta) \approx d(1 + \sin\beta) \qquad (3.2.2.2)$$

where d is the grating constant, β is the angle between the grating normal and the first order reflected light.

Typical output beam parameters of the Lumonics EPD-330 dye laser are listed in Table 3.2.2.2.

Table 3.2.2.2. Performance parameters of EPD-330 dye laser

Tuning range	320-950 nm
Pulse length	4-12 ns
Beam size	2 mm x 2 mm
Beam divergence	< 1 mrad
Spectral linewidth	< 0.2 nm
Average pulse energy	5-10 mJ
Pulse to pulse stability	5%
Polarisation	>5% vertical

3.2.3. Autotracker

The Inrad Autotracker II is a stand-alone servo system for frequency mixing and second harmonic generation of pulsed laser source in nonlinear crystals. The active feedback of the system accommodates wavelength changes due to active dye laser scanning and compensates for bulk crystal temperature produced by either ambient or laser induced heating.

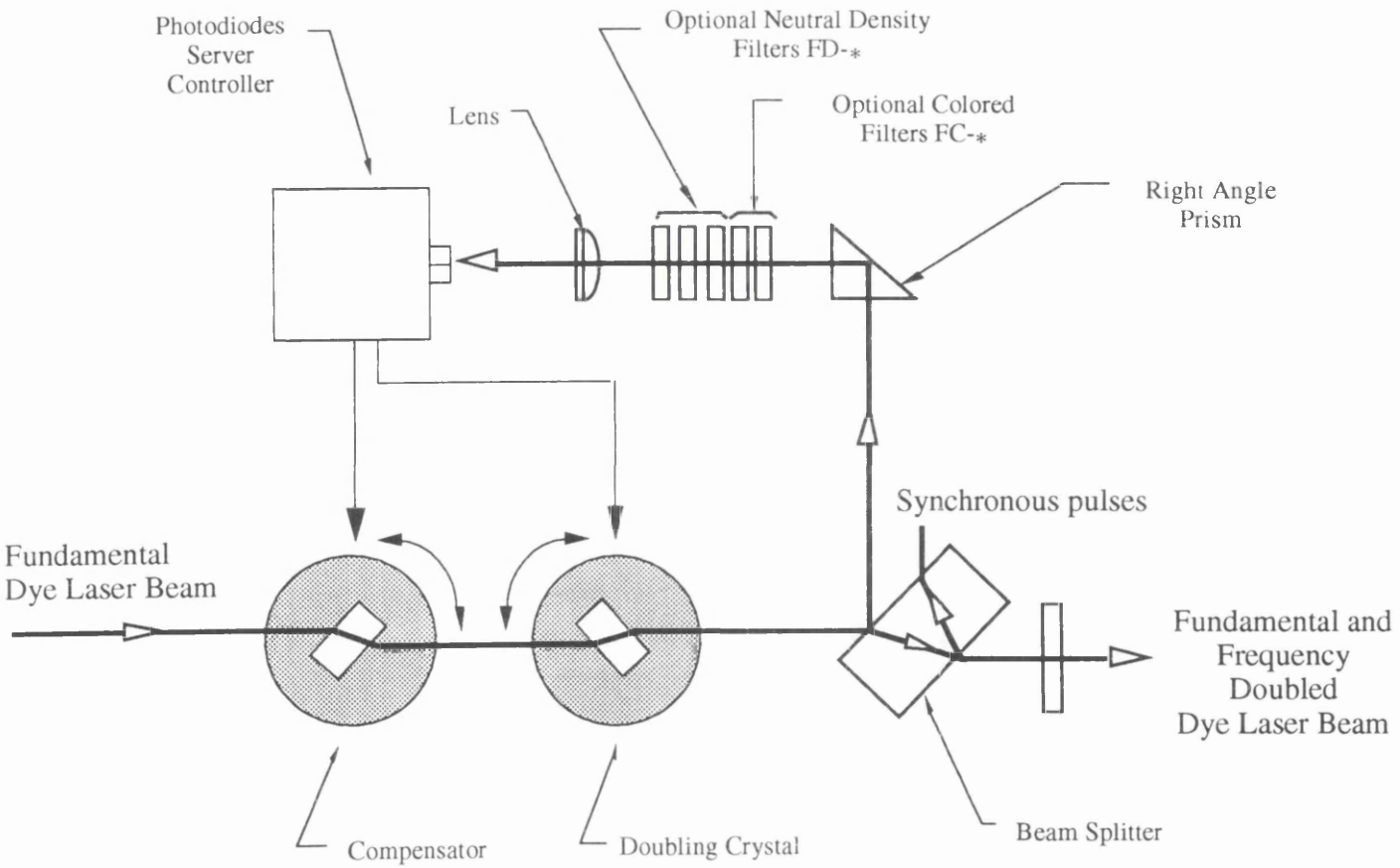

Figure 3.2.3. Schematic Diagram of Inrad Autotracker II system

The standard system consists of an electronic control unit and an optical assembly (see figure 3.2.3)

The fundamental laser beam is directed through a compensator and then a frequency doubling crystal. The compensator is for correcting any displacement that the beam may suffer on passing through the doubling crystal. A variety of frequecy doubling crystals exist such as BBO (see Eimerl et al., 1987), KDP etc. which have different optimum wavelength regions in which they operate.

The control unit receives signals generated by sensors in the optical assembly, processes that information, and controls the angle of the crystal mount.

Beam sampling generates the signals used to control the servomotor. Less than 1% of the harmonic beam is directed toward the balance sensor by one surface of an uncoated fused silica beamsplitter. The other surface of the beam splitter directs light into a photodiode to provide a synchronisation pulse. The sampled beam undergoes elevation by one of three FR-* subassemblies (for pictorial simplicity, they are not showing in the diagram).

After making a right angle turn, the beam undergoes filteration and attenuation by FC-* plug-ins. The FR-* and/or FC-* units filter the sampled beam so that the appropriate wavelength impinges on the balance sensor. The FD-* units attenuate the sampled beam to a workable level. A focusing lens reduces the beam diameter to a size commensurate with the balance sensor which provides the photodiodes PD1 and PD2 signals required for servo tuning.

3.2.4 EPD-60 scan control system (compuscan)

The EPD-60 microprocessor-based scan control system adds to the EPD-50 motor drive and permits fully programmable scanning of the EPD-330 laser by a keyboard (see figure 3.2.4).

The motor drive consists of a stepping motor together with a micro-step drive module offering extremely smooth motion. This motor drive unit controls the rotation of a mirror in the optical cavity which alter the angle of the laser incident upon the holographic grating. The angle of incidence upon the grating determines the lasing wavelength which is most efficient.

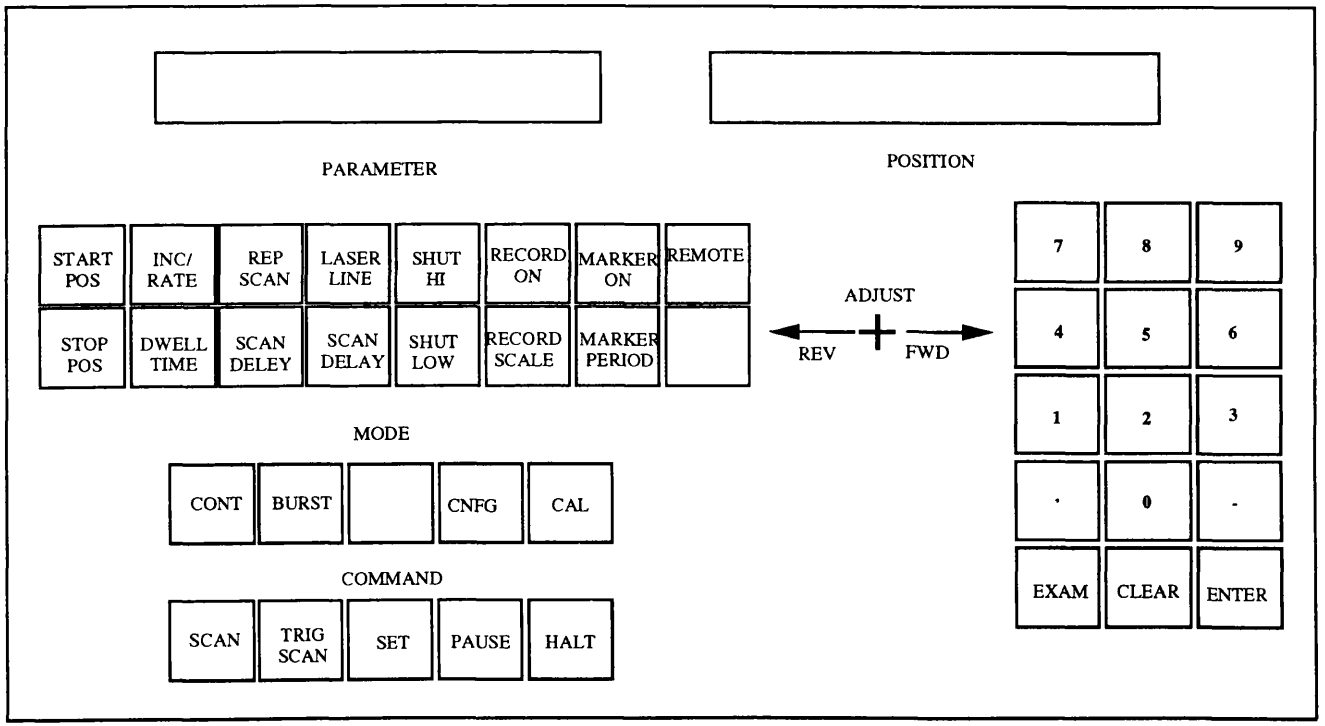

Figure 3.2.4. Compuscan Keyboard and Display

Once calibrated, the system will follow all wavelength changes, constantly updating in Å. Two modes of scanning are possible i.e. continuous or burst, as well as a toggle switch which allows manual control over the wavelength position. The system also has the ability to remove any backlash from the wavelength drive, before carrying out any wavelength scan to ensure reliable and accurate wavelength measurements.

3.2.5. Laser power attenuator

A Newport variable attenuator was used in the experiments performed in this laboratory. The unit consists of two pairs of counter-rotating quartz plates arranged in zero beam deviation configuration. Upon rotation of the plates, the angle of incidence is changed and therefore the degree of attenuation is altered in accordance with the Fresnel relations. When properly aligned the unit covered a dynamic range of 100%-10%. A schematic of the instrument is shown in figure 3.2.5.

3.3 Laser pulse energy detectors

3.3.1 Molectron Pyroelectric Joulemeter

The laser pulse energy detector used to measure UV light in this laboratory is J3 pyroelectric joulemeter which is a calibrated, fast response pulsed energy detector. The operation of the device relies on the absorption of the laser pulse energy by a thin crystal of lithium tantalite. On absorbing laser radiation, the crystal is rapidly heated and becomes electrically polarised. This polarisation produces a surface charge which is collected, electrically integrated and observed as a voltage pulse across 50 ohms. The peak height of the signal is then proportional to the absolute energy in the pulse. The energy calibrations varies from model to model, e.g. J3-09 being 1.25 V/mJ and J4-09 being 0.79 V/mJ. The main features of J3 Pyroelectric joulemeters are shown in table 3.3.1.

Table 3.3.1 The main features of J3 Pyroelectric joulemeters

Pulse repletion rate	Single pulse up to 4 kHz
Sensitivity	3 nJ
Wavelength range	From UV to Far IR
Pulse width	From ps to 250 ms
Active diameter	9 mm
Energy damage threshold	0.05 Joules/ cm^2

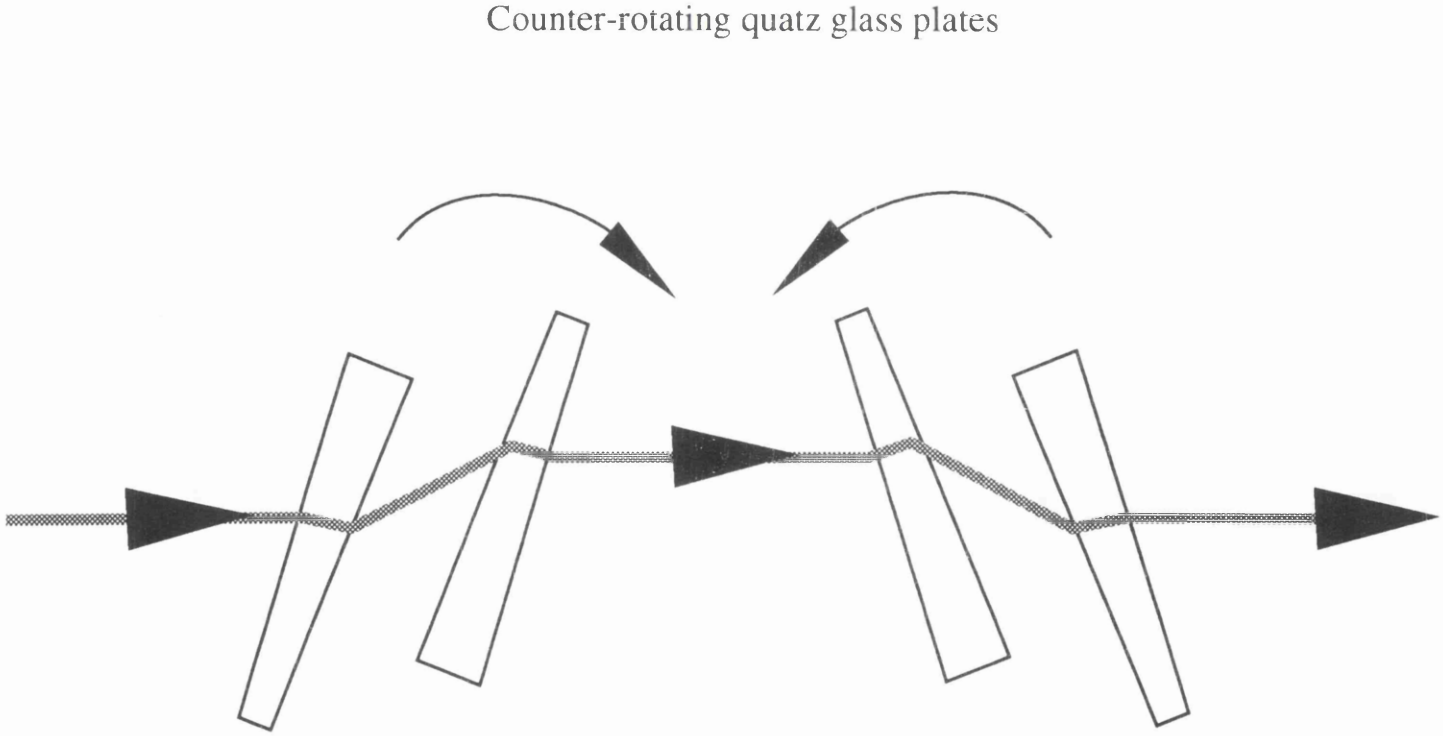

Figure 3.2.5. A schemetic diagram of a Newport optical attenuator

3.3.2 Gentec Joulemeter

The gentec model ED-200 Fast-Response Joulemeter produced by Canadian Gen-Tec Inc. is a sensitive thermal detector intended for the measurement of pulsed laser energies at rates up to 3 per second. It is suitable for use with oscilloscope, fast recorders and peak-reading solid state volt meters having input resistance of 1 megohm or lager. The body of the joulemeter is made of aluminium, ensuring an unusually high degree of rejection of electromagnetic interference. In this thesis work it was used to monitor the output power of the excimer laser pulse. Its optical and electrical characteristics are shown in table 3.3.2.

Table 3.3.2 Optical and electrical characteristics of Gentec Joulemeter

Output	> 5 V/J into 1 megohm load resistance
Maximum incident energy	2 Joules
Accuracy	better than 10%
Response time	5 ms
Recover time	0.3 s
Load resistance	1 MΩ or larger
Spectral response	uniform from visible up to 30 μm

3.4 Ion detectors

Ionisation detectors are different for the measurements at atmospheric pressure and vacuum condition. A simple ionisation chamber which contains just a pair of parallel plates in a diecast box was used as an ion detector at atmospheric pressure and a Time-of-Flight (TOF) system with an electronic multiplier was used as ion detectors at vacuum pressure. The former collects the all ions produced by a laser pulse without distinguishing their mass numbers. The latter separated the ions into bunches according to their different flight times corresponding to their mass to charge ratio M / Z, where M is the mass of an ion and Z is the charge number of the ion, and collected the ions by an electronic multiplier.

3.4.1 Ionisation chamber

The ionisation chamber is fitted with quartz windows for laser access. Ports for vacuum pumping and gas flow were added to allow dilution experiments to be performed. The ionisation chamber and gas sample dilution system is shown in

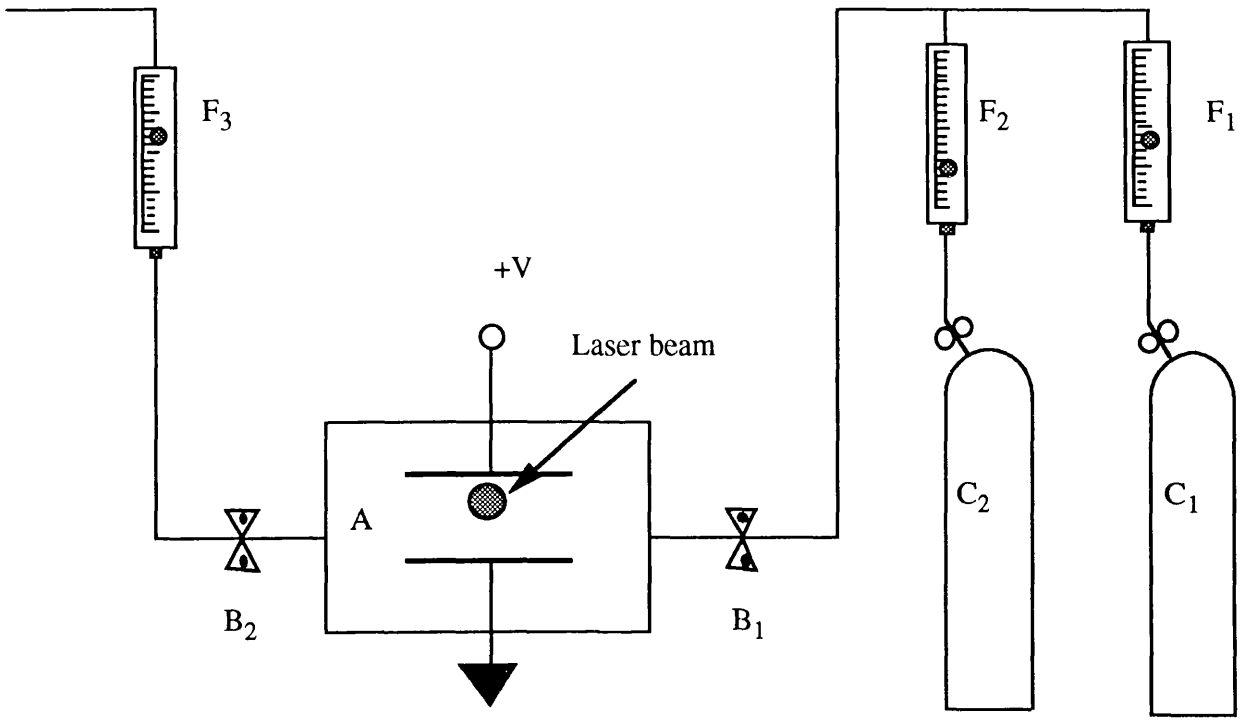

Figure 3.4.1. Gas dilution system. A-Ion chamber, $B_{1/2}$-Gas flow valves, C_1-Balance gas, C_2-Analyte gas, $F_{1/3}$-Flow meters with regulator

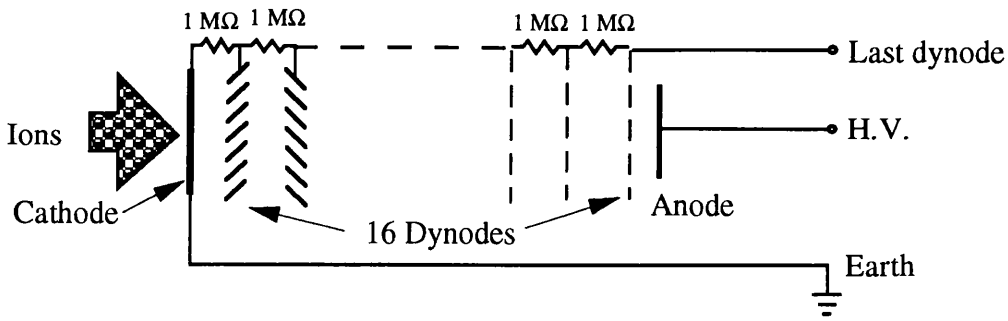

(a) Thorn-EMI 642/3 electron multiplier tube

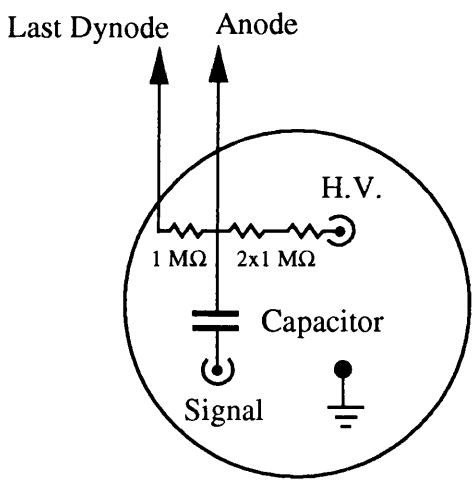

(b) External electric connection for the tube

Figure 3.4.2 (a) The structure of Thorn-EMI 642/3 multiplier tube,
(b) External electric connections for the tube

figure 3.4.1. Two meters F_1 and F_2 are put in the gas inlet side of the ion chamber, one for monitoring analyte gas or sample gas flow rate, another for monitoring the diluting gas flow rate. The third meter F3 is put in the exhaust side of the chamber, from the reading of this meter one can monitor the leaking of the gas flow system and adjust the concentration equilibrium inside the chamber.

3.4.2 Electron multiplier

A model Thorn-EMI 642/3 electron multiplier with 16 dynodes is used for ion detection in the vacuum circumstances under the pressures lower than 10^{-4} torr. The detector works on the principle that an ion strikes the dynode releasing two electrons. The liberated electrons are accelerated through an electric field and strike more dynodes thus resulting in an avalanche effect. The net gain of this system is about 10^7. Figure 3.4.2 shows the internal electrical structure and the external electric connection for this electron multiplier. Ion signals were observed across 50 ohms in order to preserve the resolution of the system.

3.5 Time-of-Flight mass spectrometer (TOF-MS)

3.5.1 The principle of TOF-MS

TOF-MS is not a new technique. It has been improved a lot since its inception by Stephens (1934), typically in ion source (e.g. Wiley and Maclaren, 1955). Many scientists reported and reviewed the development and applications of TOF MS, e.g. Price and Milnes (1984); Cotter (1992); Bosel et al (1994) and Mamyrin (1994).

The time-of-flight mass spectrometer is essentially a drift tube in which short pulses of ions are produced at one end and are collected at the other. They are separated into packets according to their mass to charge ratios, and arrived at the ion detector at different times (figure 3.5.1).

If during the pulse all the ions are given the same energy or momentum the time at which they arrived at the end of the drift tube will depend on their velocity and hence on their masses

$$UZe = \frac{1}{2}Mv^2$$

i.e.

$$v = \sqrt{2U\frac{Ze}{M}} \qquad (3.5.1.1)$$

where υ is the velocity, U is the potential of the acceleration field, and Z / M is the charge to mass ratio of the ions in the unit of electron charge magnitude. If L is the drift length then

$$t = L\sqrt{\frac{M}{2UZe}} \tag{3.5.1.2}$$

or mass to charge ratio

$$M / Z = \frac{2Ue}{L^2}t^2 \tag{3.5.1.3}$$

The resolution, R, of a TOF spectrometer is given by

$$R = \frac{M}{\Delta M} = \frac{1}{2}.\frac{t}{\Delta t} \tag{3.5.1.4}$$

where Δt is the FWHM of the ion peak at time t in TOF spectrum and ΔM is the FWHM of the mass peak at M in the corresponding mass spectrum.

3.5.2 The main factors which define the resolution of a mass spectrometer

In TOF mass spectrometry, the ideal situation arise when ions of the same M / Z ratio are formed in an infinitely thin volume which is perpendicular to the acceleration field, and with no initial kinetic energy, then all ions with the same M / Z would arrive at the detector at precisely the same time, and the available mass resolution would be defined entirely by the electrical characteristics of the ion detector.

However, in reality, the initial spatial, temporal and velocity distributions of the laser produced ions can cause time spread and therefore limit the resolving power of the instrument (see figure 3.5.2).

Initial temporal distribution The effect of initial temporal distribution is caused by the finite length of the ionising laser pulse. Each isomass packet will therefore have a temporal spread of at least this value (the laser pulse length) at the detector position. Figure 3.5.2 (a) shows two identical ions formed at different times. Because they have the same velocities , the time interval remains constant as they exit the drift tube and are recorded by the detector. It can be seen from the definition of the mass

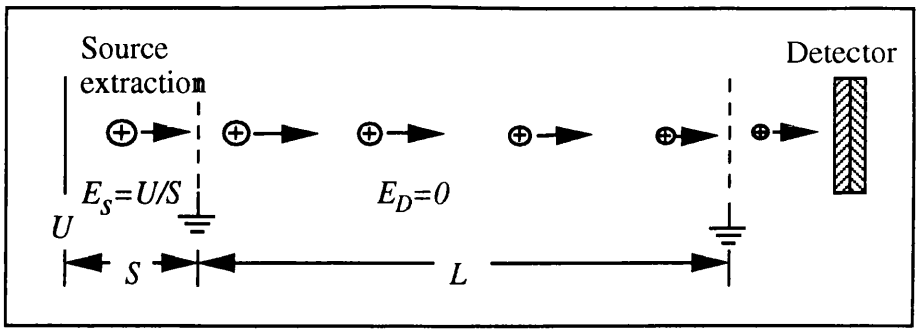

Figure 3.5.1 The principle of a Time-of-Flight mass spectrometer

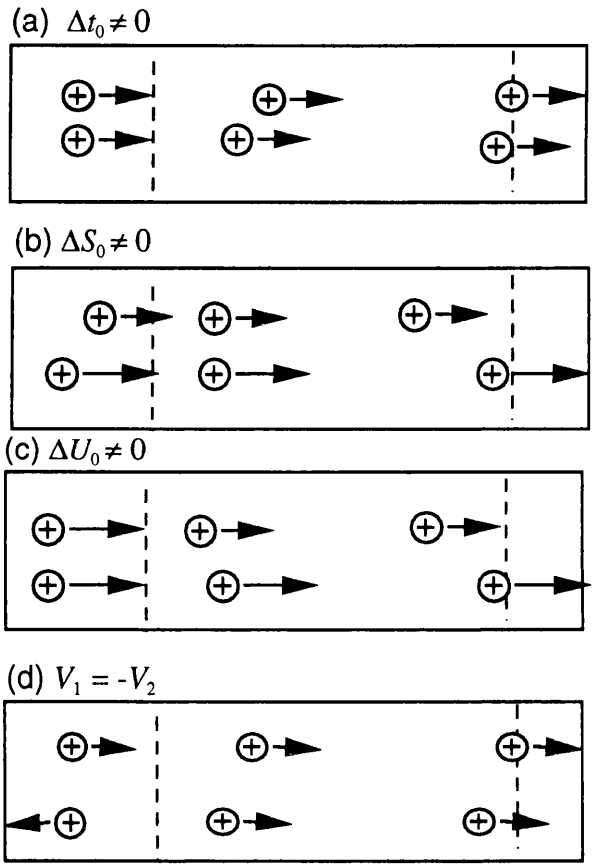

Figure 3.5.2 Effects of initial time, space, and kinetic energy distributions on mass resolution, after Cotter 1992).
(a) Two ions formed at different times. (b) Two ions formed at different location in the ion extract field. (c) Two ions formed with diffrent initial kinetic energies. (d) Two ions with the same initial kinetic energy that have initial velocities in opposite directions.

resolution of TOF spectrometer that mass resolution can be improved by extending the flight time (t). This can be accomplished by reducing the acceleration voltage or increasing the drift tube length. Because high acceleration voltages improve ion transmission and energy focusing, longer flight lengths have been common.

Spatial distribution. In the interaction area of the laser and molecular beams, the isomass ions formed in different positions of the laser beam undergo different acceleration potential. Figure 3.5.2 (b) shows two ions of the same mass that have the same initial kinetic energy but are formed in different locations along the direction of the electric field. The ions formed towards the rear of the ion source falls through a large electrical potential and is accelerated to a higher kinetic energy than the formed near the front of the source. The extraction field can be adjusted so that these ions will be coincident at a space focus plane (SFP). Space focusing is achieved by using relatively low (<1 kV) extraction voltages. The spatial distribution can be also reduced by focusing the laser beam in the ion formation region.

Initial kinetic energy distributions. In figure 3.5.2 (c) two ions of the same mass are formed in the same location but with different kinetic energies. The difference in their arrival times at the detector increases with flight tube length but can be minimised by using high acceleration voltages. Alternatively, reflectrons are used to compensate for the differences in kinetic energy. In figure 3.5.2 (d), two ions of the same mass have the same initial kinetic energy, but their velocities are in the opposite directions. The ion moving away from the source exit will travel against the field, stop, turn around, and be accelerated to the same energy as the ion moving toward the exit. These two ions will have the same velocity and will, therefore, remain at constant difference in arrival times (equal to the turn-around time Δt of the ion moving away from the detector). Similar to the temporal distribution, the turn around time problem can be minimised by using long flight tubes and high extraction fields.

3.5.3 The TOF mass spectrometer used in this thesis

The mass spectrometer used in this thesis is a type of Wiley and McLaren design linear TOF (Wiley and McLaren, 1955). In this design, the simple ion source used in earlier TOF (e.g. Stephens 1946) has been replaced by double field (ion formation region and ion acceleration region) ion source. Figure 3.5.3 shows the components layout of the TOF used in this thesis. The length of the drift tube is about 1.2 meters. The ion source consists of a pusher plate and extraction optics with the second optic

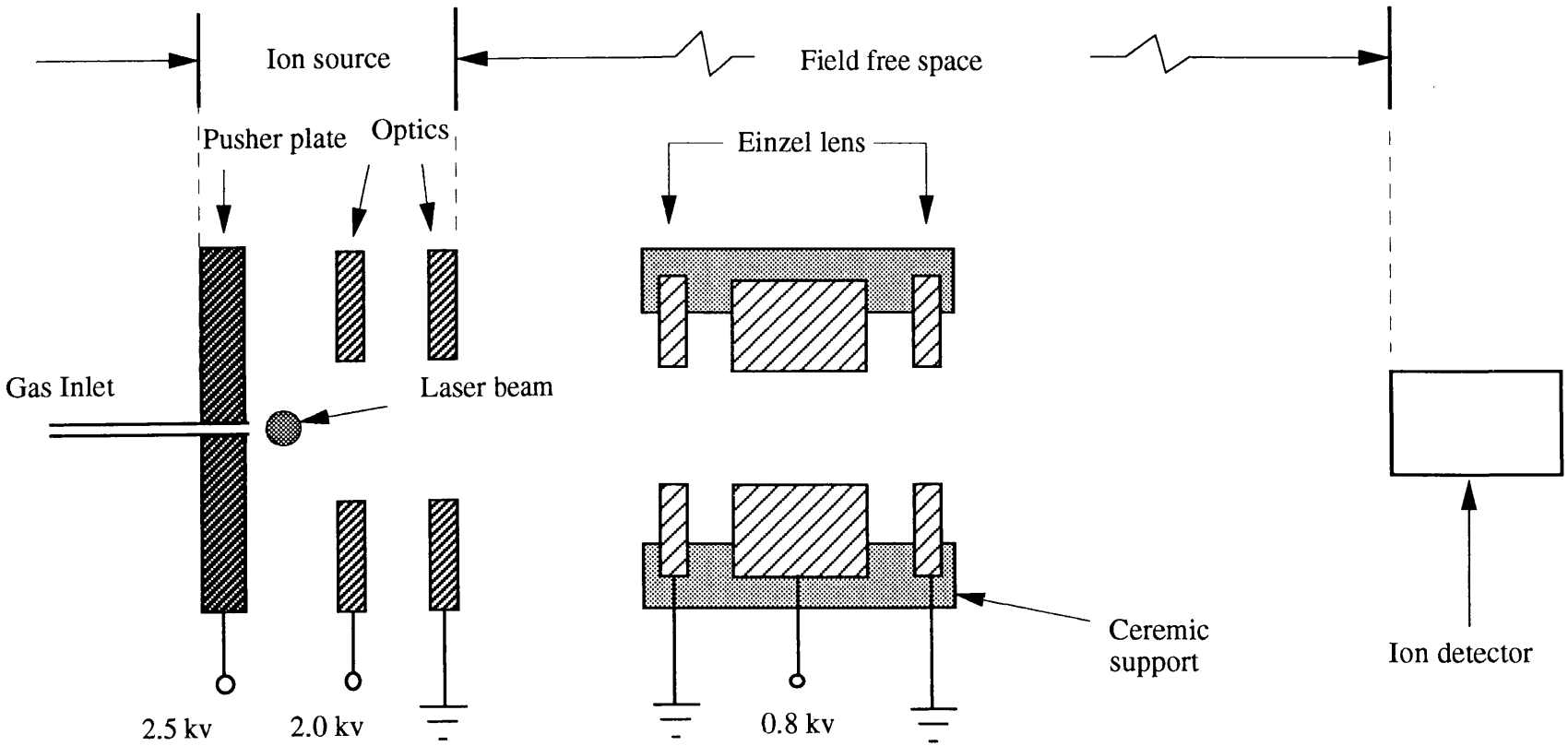

Figure 3.5.3 The linear TOF mass spectrometer components layout in this lab

earthed. The ratio between the two field strengths can be adjusted to reduce the time spread. The Einzel lens placed on the way of ion drift path is for focusing the ions to avoid the ions with an initial vertical velocity flying beyond the receiving scope of the detector. The resolution of this mass spectrometer is 200 at 100 Da.

3.6 Data acquisition

The instruments for recording optical spectra include a Model SR 250 gated integrator and boxcar averager module, a Model SR 245 Computer Interface module and a Macintosh IIfx micro computer running with a software LabView 2.

The instrument for recording mass spectra is just a LeCroy 9304 QUAD 175 MHz Digital Oscilloscope which was used to monitor the transient ion signal from the ion detector and store them into its build-in memories, memory card or floppy disk.

The recorded waveforms, e.g. mass spectra, can be translated into PC files by using a programme called 93REM and processed using a PC graph package, e.g. Excel, or a Macintosh graph package, e.g. MacDraw Pro, after translating PC files into Macintosh files.

3.6.1 Model SR 250 Gated Integrator and Boxcar Averager module

The Stanford Research (SR) Systems Inc. produced Model SR 250 Gated Integrator and Boxcar Averager module consists of a gated generator, a fast gated integrator, and exponential averaging circuitry. The gated generator, triggered internally or externally, provides an adjustable delay from a few nanoseconds to 100 milliseconds, before it generates a continuously adjustable gate of 2 nanoseconds to 15 milliseconds. The delay may be set by a front panel potentiometer, or automatically scanned by a rear panel input voltage in order to record entire waveformes.

The fast gated integrator integrates the input signal during the gate. The output from the integrator is then normalised by the gate width to provide a voltage which is proportional to the average of the input signal during the sampling gate. This signal is further amplified according to the front panel sensitivity setting. Then it is sampled by a low droop sample and hold amplifier, and output via a front panel BNC connector. This LAST SAMPLE output allows experimenter to do a shot-to-shot analysis of the signal being studied, and makes the instrument a particularly useful component in a computer data acquisition system.

A moving exponential average over 1 to 10,000 samples is available at the AVERAGE OUTPUT. This traditional averaging technique is useful for pulling small signals from noisy background. As one averages many noisy samples of a signal, the average will converge to the mean value of the signal, and the noise will average to zero. In the case of random white noise background, the signal-to-noise ratio increases as the square root of the number of samples in the average. This allows a S/N improvement of a factor of 100 using this technique alone.

3.6.2 LeCroy 9304 QUAD 175 MHz oscilloscope

Architecture. The 9304 produced by LeCroy Corporation is a 175 MHz digital oscilloscope with four channels for signal input and four memories for waveform processing. The instrument features 100 Megasample/s 8-bit flash ADCs for each channel. Waveform acquisition memories consist of 10k data points per channel. Four memories are available for temporary storage and four additional memories are available for waveform zooming and processing. The central processor is a Motorola 68020 microprocessor which performs computations and controls the oscilloscope's operation.

Waveform Mathematics. Any trace A,B,C or D for data processing can be set up as a mathematical function. Waveform negation, identity, addition, subtraction, multiplication and division, as well as summed averaging of up to 1000 waveforms, are standard. The waveform processing options WP01 and WP02 offer a wide range of additional possibilities:

- continuous averaging
- Summed averaging of up to 1 000,000 waveforms
- enhanced resolution by up to 3 bits with filtering
- extreme, i.e. envelope of many waveforms
- mathematical functions, such as integral, derivative, logarithm, exponential, square, square root and sin x/x interpolation.
- Fast Fourier Transform (option WP02), including FFT averaging

The most frequently used Math Type in this thesis work is Average in Summed Average mode. In this mode, waveforms were added with equal weight, whenever the setting number of sweeps is reached, the averaging process stops. The recording

resulted from averaging has a reduced random noise component compared with a single-shot record.

3.7. Femtosencond laser system

The lasers with pulse duration in the femtosecond (10^{-15} s) domain have been developed since the earlier 1980s. With such short pulse, ultrahigh peak power up to $10^{12}/10^{15}$ W is possible. The generation of ultrahigh power can be realised using Chirped Pulse Amplification (CPA) technique. Figure 3.7.1 shows the principle of CPA. The idea of CPA is to initially generate a very short duration pulse. The next step is to stretch its pulse duration, thus significantly reducing its brightness (or peak power). This low brightness optical pulse is then amplified, with the probability of self focusing induced damage significantly reduced. Following amplification, the pulse is recompressed to narrow pulse again and therefore high peak power is achieved. The pulse stretcher can be optical fibre delay line, a pair of gratings, a number of dispersion mirrors, a pair of prisms or various combinations of the above.

The femtosecond laser system used in this thesis is the facility in Rutherford Appleton Laboratory shown in figure 3.7.2. The system consists of a short laser pulse source (a titanium-sapphire oscillator, Spectra-physics Tsunami pumped by a 5-7 W Argon-ion laser with all lines, Spectra-physics 171), a pair of prism pulse width stretcher, an amplifier of three stage dye lasers pumped by a Nd: YAG laser and a SF-10 glass block pulse compressor (Langley et al, 1994).

The short pulse source readily produced an 82-MHz train of pulses with duration of 50 fs and energy 2 nJ at a wavelength of 750 nm. Before amplification, the 750 nm pulses were stretched to about 700 fs in the prism pair in double pass with a prism separation of about 2 m. To maintain good pulse quality in the output beam, a 2-m focal length lens L was used to make the beam waist close to the rear mirror UFM_2 of the stretcher.

The stretched pulses were sent to a three-stage dye-amplifier system and then recompressed by a 145-mm-thick block of SF 10 glass into pulse train with duration of 50 fs and energy of 100 μJ.

The recompressed 50 fs and 100 mJ laser beam was introduced to TOF through a series optics such as polariser, chirping crystals, lenses, BBO (BaB_2O_4, Barium metaborate, a nonlinear optical material discovered by Professor Changtien Chen of

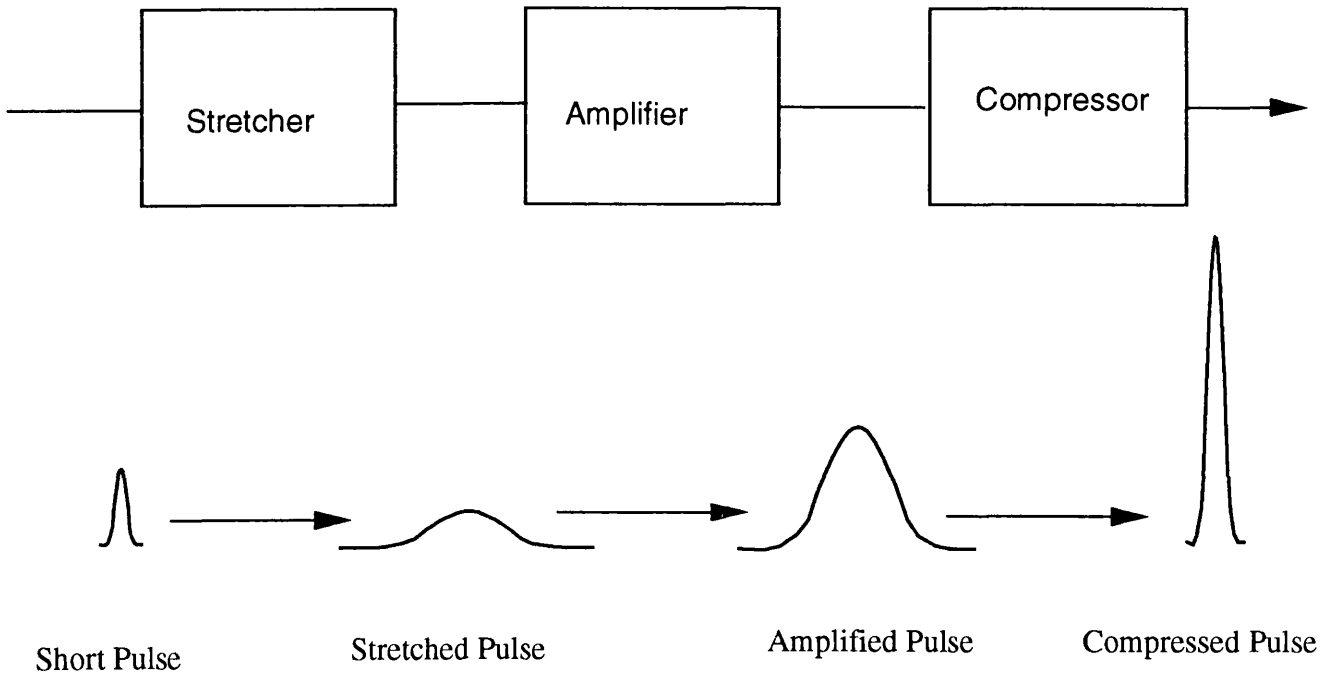

Figure 3.7.1. Principle of Chirped Pulse Amplification

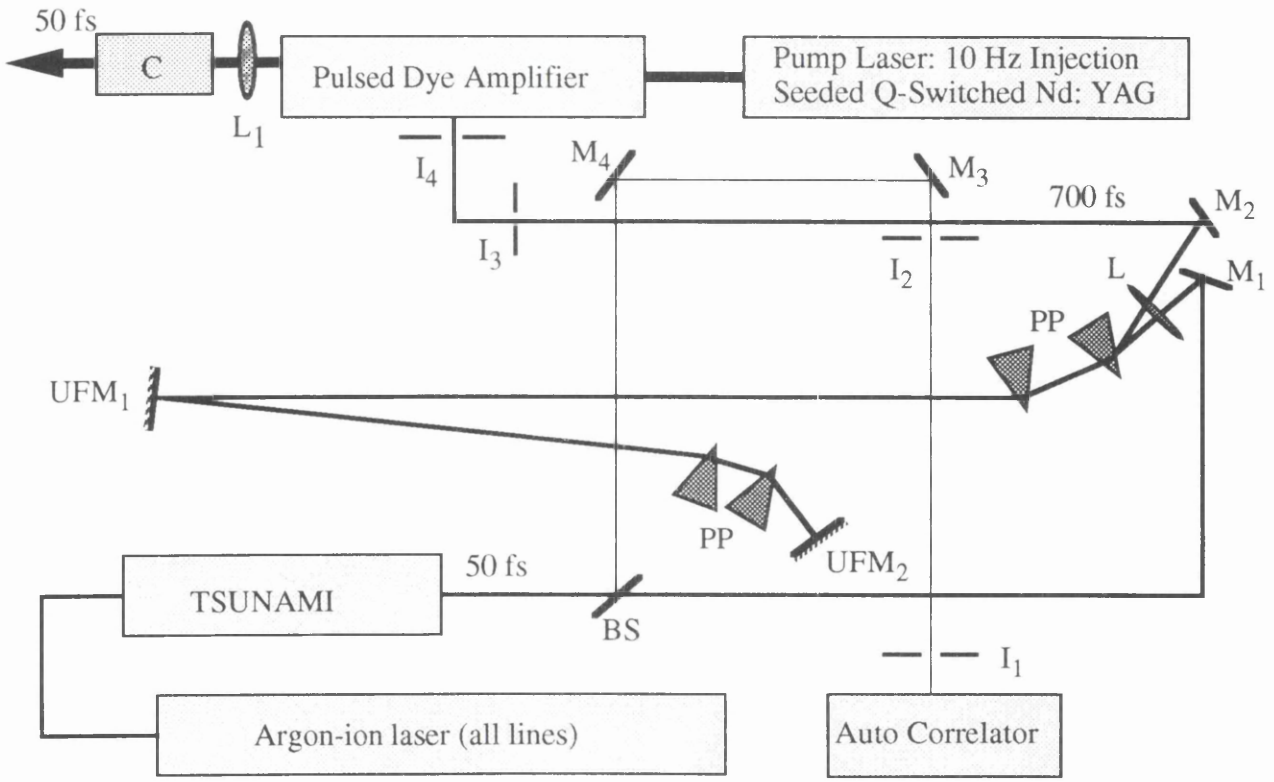

Figure 3.7.2. The LSF femtosecond laser system: 90 fs @ 750 nm, 10 Hz, 100 μJ. In the figure, **BS**: Beam Splitter; $\mathbf{I_{1\text{-}4}}$: Irises; $\mathbf{M_{1\text{-}4}}$: Aluminium Mirrors; **PP**: BK7 Prism Pair; **L**: Long focus length lens; $\mathbf{L_1}$: 1m focus length Lens; $\mathbf{UFM_{1,2}}$: Ultrafast Mirrors; **C**: Glass Compressor SF 10;

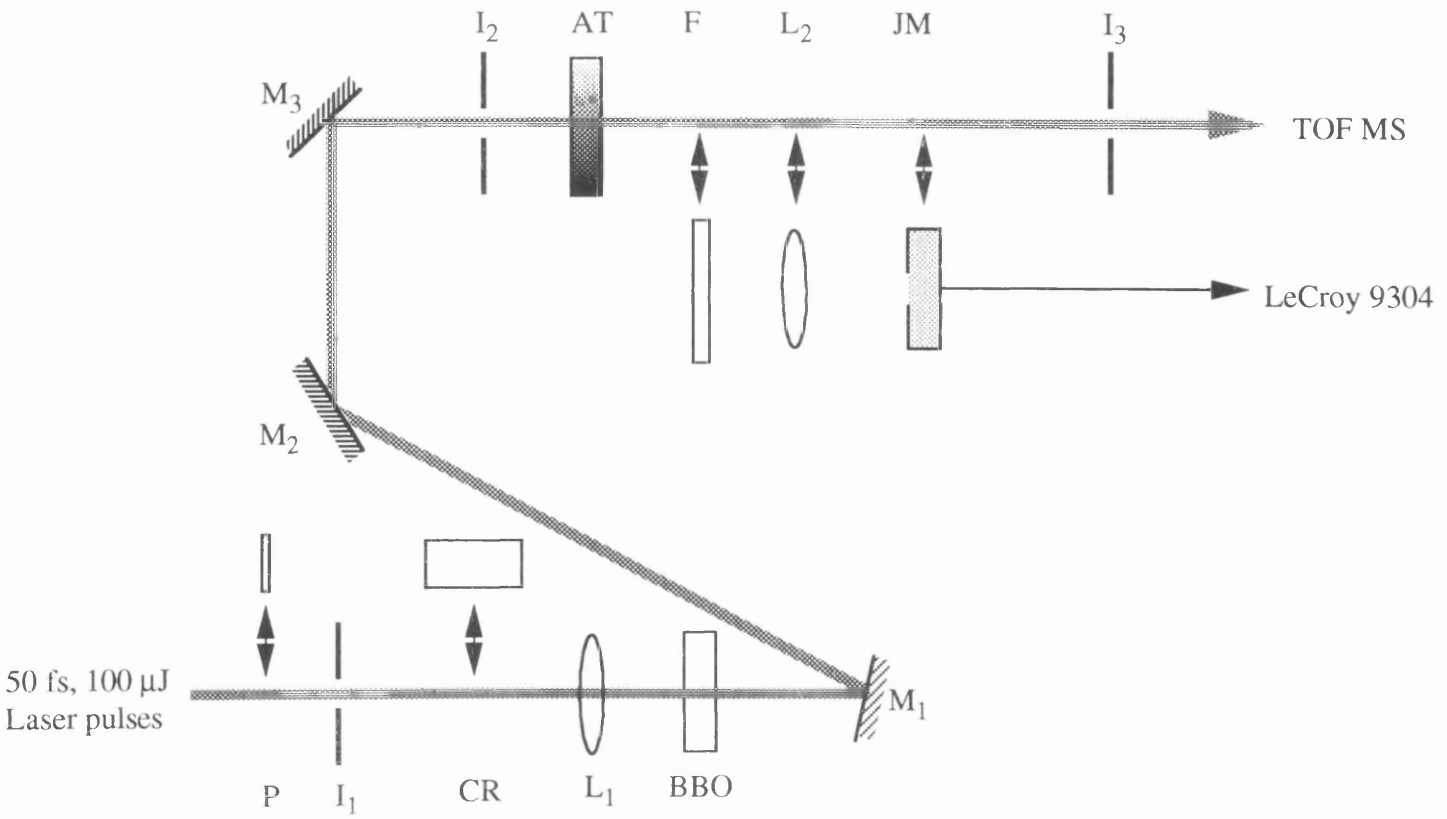

Figure 3.7.3. Femtosecond optics layout. $L_{1\text{-}2}$: Lenses; P: Polarizer; $I_{1\text{-}3}$: Irises; CR: Chirping crystal; $M_{1\text{-}3}$: Mirrors; F: Filter; AT: Attenuator; JM: Joule Meter

the Fujian Institute for research on the Structure of Matter, PR China) operated at 28.7°, mirrors, attenuator and Irises etc for obtaining required polarisation, pulse lengths, frequencies and intensities. The layout of the optics is shown in figure 3.7.3. Several pulse lengths can be obtained by inserting diffrent crystal blocks or their combinations. The 50 fs laser pulses were invariably stretched to about 90 fs at the entrance of TOF by all other optics except stretching crystals.

References:

Boesl, U. (1994)

Laser ion sources for time-of-flight mass spectrometry, *Int. J. mass Spec. and Ion Proc.*, **131**, pp. 87-124

Clark, A (1992)

The application of resonance enhanced multiphoton ionisation mass spectrometry to the detection of aromatic molecules, PhD thesis, Glasgow University, pp. 57-61

Cotter, R.J. (1992)

Time-of flight mass spectrometry for the structural analysis of biological molecules, *Anal. Chem.*, **64,** pp.1027-1039

Eimerl, D., Davis, L. and Velsko, S. (1987)

Optical, mechanical, and thermal properties of barium borate, *J. Appl. Phys.*, **62**, 1968-1983

Langley, A. J, Noad, W.J., Ross, I.N. and Shaikh, W.(1994)

High-brightness femtosecond laser using titanium-sapphire technology and amplification in dyes, *Appl. Opt.*, **33**, pp. 3875-3880

Mamyrin, B.A. (1994)

Laser assisted reflectron time-of-flight mass spectrometry, *Int. J. Mass Spec. and Ion Proc.*, **131**, pp. 1-19

Price, D. and Milnes, G.J. (1984)

Recent development in techniques utilising time-of-flight mass spectrometry, *Int. J. Mass Spec. and Ion Proc.* , pp. 61-68

Wiley, W.C. and McLaren, I.H. (1955)

Time-of-flight mass spectrometer with improved resolution, *Rev. Sci. Instr.*, **26**, pp. 1150-1157

Chapter 4

Trace NO_X Detection by REMPI Spectroscopy at Atmospheric Pressure

4.1. Introduction

One of the applications of REMPI spectroscopy in this laboratory aims at trace NO_X detection in air at atmospheric pressure, since the nitrogen oxides play several important roles in tropospheric chemistry and they are important species for monitoring air quality. The main sources of NO_X in the urban air include combustion of fossil fuels, biomass burning, lightning, oxidation of ammonia and microbial processes in soils. It has been pointed out that (Logan, J. A., 1983) the largest sources of NO_X on a global basis are combustion of fossil fuels at mid-latitudes and biomass burning in the tropics. Therefore, in Britain the main NO_X source in the urban air is expected to be from combustion of fuels. Car emissions now dominate urban air pollution with the concomitant fear that they may be linked to respiratory diseases and this has lead to a recent resurgence of public awareness and concern in urban air quality.

Nitrogen oxides (NO_X, x=1, 2) from car emissions are produced primarily in the form of nitric oxide that rapidly reacts with tropospheric ozone to form nitrogen dioxide.

$$NO + O_3 \rightarrow NO_2 + O_2$$

Nitrogen dioxide rapidly photo dissociates at wave lengths shorter than 400 nm to form nitrogen oxide and atomic oxygen.

$$NO_2 + h\nu \rightarrow NO + O$$

which regenerates ozone.

$$O + O_2 + M\ (catalyst\ usually\ N_2) = O_3 + M$$

Thus nitric oxide forms nitrogen dioxide which in concert with volatile organic compounds (VOC) results in the increase of ground level ozone usually downwind and hence remote from the urban sites of initial formation. In addition NO_2 can combine with atmospheric water vapour to form HNO_3 (acid rain).

The main reason for monitoring air pollution in the UK is to comply with EC directives and this has led to the establishment of several expert committees which have produced a number of publications concerned with various aspects of urban pollution.

The average concentration of NO_2 in American cities is about 35 ppb with similar averages for NO (Logan, J.A. 1983). The concentrations in the UK are similar, although EC directives give guide values as percentiles i.e. a 50 percentile (50% of the readings are lower than this value) is similar to average concentrations. The values in rural areas are about 1-2 ppb. Urban levels of NO_2 (maximum hourly concentrations) greater than 100 ppb are considered to be poor.

NO_X detection has been of interest for many years, (e.g. Halpern et al, 1979; Syage et al, 1987; Hippler et al, 1990; Zhu et al, 1990; Cool et al, 1992; Jeffries et al, 1992; Lemire et al, 1993; Simeonsson et al, 1993; Marshall et al, 1994). Precise measurements of NO_X (NO, NO_2) and NO_X-containing compounds, the sum concentration of NO, NO_2, HNO_3, HNO_2 NO_3, N_2O_3, HO_2NO_2, organic nitrates (e.g., PAN, PPN) and other nitrocompounds, are crucial if a comprehensive understanding of the process that determine the tropospheric levels of these compounds is to be achieved.

Presently, the measurement of NO, NO_2 and other nitrogen oxide compounds at background and pollutant levels (ppt to ppb) remains an important analytical challenge (Sickles, 1992). For NO, the most common method of detection is by chemiluminescent reaction (CL) with O_3. The reaction produces electronically excited NO_2 whose emission intensity is proportional to the initial concentration of NO. Other measurement methods include long path absorption and differential absorption LIDAR (DIAL) (Alden et al, 1983; Edner et al, 1988). For NO_2, the US environmental protection agency (EPA) standard method for measurement is also by CL with ozone; however, prior to measurement, NO_2 must be quantitatively converted to NO by catalytic or photolytic means (Sickles, 1992). Other methods include tunable diode absorption spectrometry (TDLAS), (Schiff et al, 1983);

differential optical absorption spectrometry (DOAS), (Plane et al, 1992); opto-acoustic spectrometry, (Fried et al, 1982); denuder methods and wet chemistry methods. The sensitivity of above mentioned methods for the detection of nitrogen oxide compounds in the atmosphere usually requires that the signal be integrated over time or distance, resulting in a loss of temporal or spatial resolution. Furthermore, the selectivity of these methods is often insufficient to prevent interference effects for low level determinations.

Laser induced fluorescence (LIF) is a highly sensitive and selective technique for the detection of gas phase molecules (Sickles, J.E., 1992). The use of LIF in this aspect dates back to the early work of Sukurai and Broida (Sukurai, K. and Broida, H. P., 1969). They reported that they can detect trace NO_2 at sea level down to 3 ppt. Pfab and co-workers (Hippler et al, 1991) reached a detection limit of 5 ppt of NO in 1 atm of argon with one-photon LIF at 226 nm. Photofragmentation/Laser induced fluorescence (PF/LIF) was used to detected NO_X-containing compounds. The limits of detection (LODs) for various (PF/LIF) techniques are well into ppt for NO, NO_2 and HNO_3 (1985; Bradshaw, J.D. et al, 1985; Sandholm, S.T. et al, 1990).

Laser photoionization (LPI), including non resonant multiphoton ionization and resonant-enhanced multiphoton ionization (REMPI) spectroscopy was proposed as a method for detection atmospheric pollutants as early as 1979 (Brophy and Rettner, 1979). Resonance enhanced multiphoton ionization (REMPI) is generally regarded to offer more sensitivity than LIF for the detection of low concentrations of small molecules since LIF requires high quality photon collection system and the calculation for quantification is rather complicated. REMPI requires simple ion detection system and the ion detection efficiency can be 100%. Some scientists investigate NO_X and NO_X-parent molecules by REMPI in combination with mass spectrometers e.g. Sausa and co-workers (Lemire, G.W. et al, 1993; Simeonson. J.B. et al, 1993; Simeonson. J.B. et al, 1994); Ledingham and co-workers (Marshall, A. et al, 1991; 1992a; 1992b; 1992c; Clark, A et al, 1993b and Ledingham, K W D et al, 1995)

Briefly, the results of selected representative studies are as follows. Brophy and Rettner first demonstrated the feasibility of the approach by using two-photon ionization to detect trace levels (ppm) of aniline in air. Sausa and co-workers have shown that molecular beam sampling with TOF spectrometry can be used to detect NO (8 ppb) at atmosphere pressure by (1+1) REMPI via its $A^2\Sigma^+ \leftarrow X^2\Pi$ (0,0) band

near 226 nm. They also detected NO, NO_2, HNO_3 and $CHNO_2$ at the same wavelength region by laser-induced photofragmentation/photoionization (PF/PI) spectrometry. The limits of detection (LODs) for NO and NO_2 are 1 and 22 ppb respectively.

REMPI has been used at Glasgow for detecting various NO_X and NO_X containing compounds. (Marshall. A. et al, 1991, 1992a, 1992b, 1992c; Clark, A. et al, 1993a, 1993b). The papers mentioned here are mass-spectrometer-based and they are not suited to open atmospheric measurements, therefore not suited to in-situ air pollution monitoring. An ion chamber has been used to detect NO_X at atmospheric pressure (Marshall, A., et al 1994; Peng, W. X. et al 1995). Trace NO_X detection and real time analysis have been performed by this approach for NO A $^2\Sigma^+(v'=0)\leftarrow$X $^2\Pi(v''=0)$ (1+1) REMPI process at 226 nm and C $^2\Pi(v'=0)\leftarrow$X $^2\Pi(v''=0)$ (2+1) REMPI process at 382 nm.

4.2 REMPI spectroscopy of NO and NO_2

NO has been one of the most studied diatomic molecules. A partial energy level diagram and a partial potential energy diagram for NO are shown in figure 4.2.1 (a) (From Herzberg, 1950) and figure 4.2.1 (b) (From McNesby and Okabe, 1964). A very detailed potential curve has been given by Gilmore F.R. (1966). Its ground state X $^2\Pi$ has two spin-orbit components X $^2\Pi_{1/2}$ and X $^2\Pi_{3/2}$. An absorption spectrum of NO is shown figure 4.2.2 (From McNesby and Okabe, 1964). NO was also one of the first molecules for which the REMPI process has been investigated. (Johnson, P.M. et al, 1975; Jackson et al, 1978). A simplified Gilmore diagram with the REMPI schemes used for our experiments is shown in Figure 4.2.3.

The one colour 1+1 REMPI process of A $^2\Sigma^+\leftarrow$X $^2\Pi_{1/2,3/2}$ ($\upsilon'=0,\upsilon''=0$) has been widely investigated by many groups since tunable UV laser wavelength near 226 nm became available (e.g. Zacharias et al, Jacobs et al, 1986; Marshall et al, 1993). Because the NO ionization potential of 9.26 eV (NG et al, 1976) is relatively low and the first electronic excited state A $^2\Sigma^+$ ($\upsilon'=0$)level lies at about 5.48 eV, just above the middle of the ionization energy, this transition has been used to measure vibrational and rotational distributions in ground state NO (Winkler, I.C. et al, 1986) and to detect trace NO molecules in nitrogen (Peng, W.X. et al, 1995). This is a two step process. At the first step, one photon excites NO from ground state X $^2\Pi_{1/2,3/2}$ to the intermediate state A $^2\Sigma^+$ which corresponds to the well known γ (0,0) band (i. e.

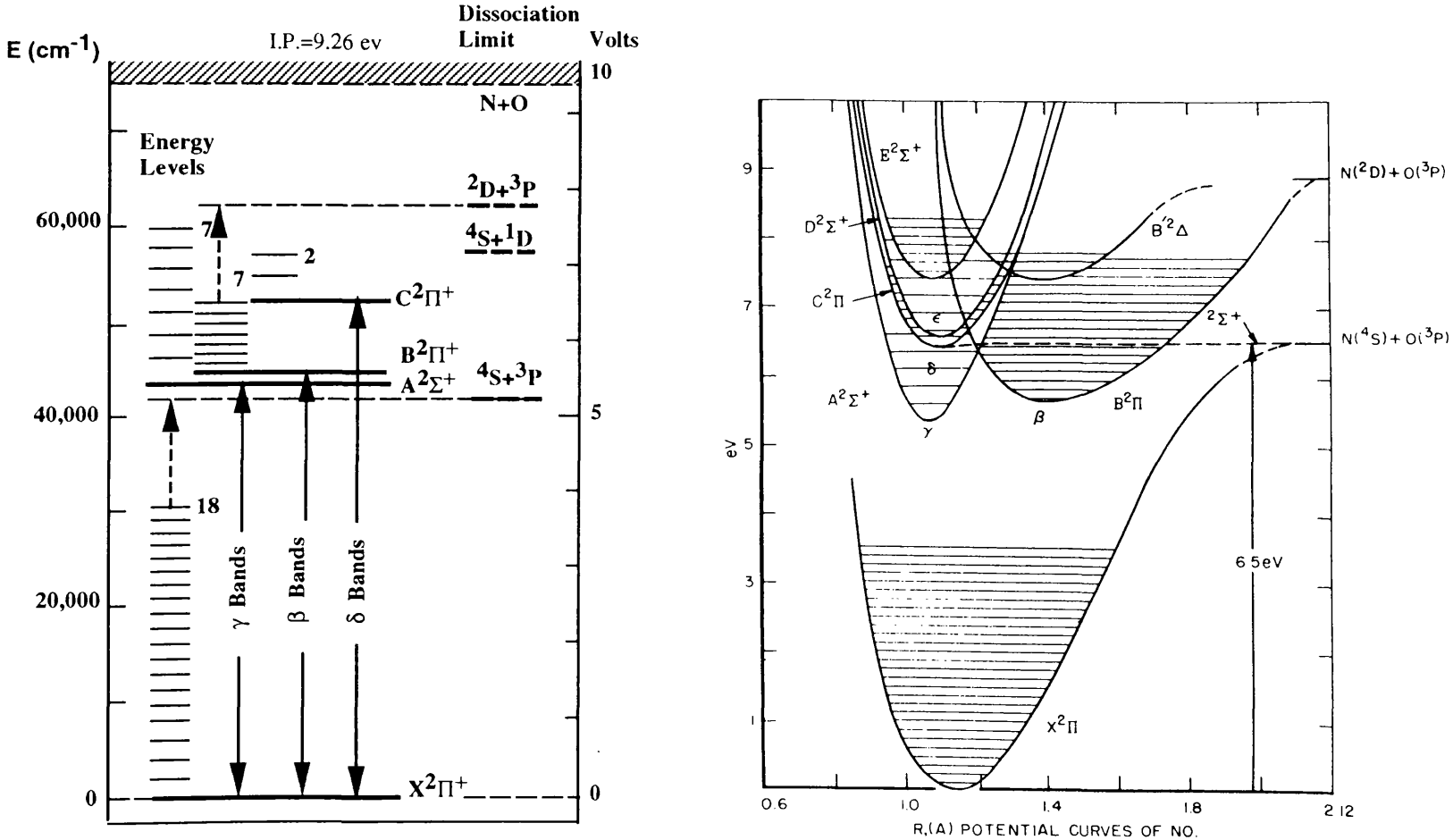

Figure 4.2.1 Partial NO (nitric oxide) Energy Levels (left) which is from Herzberg (1950) and potential curves (right) which is from McNesby and Okabe (1964).

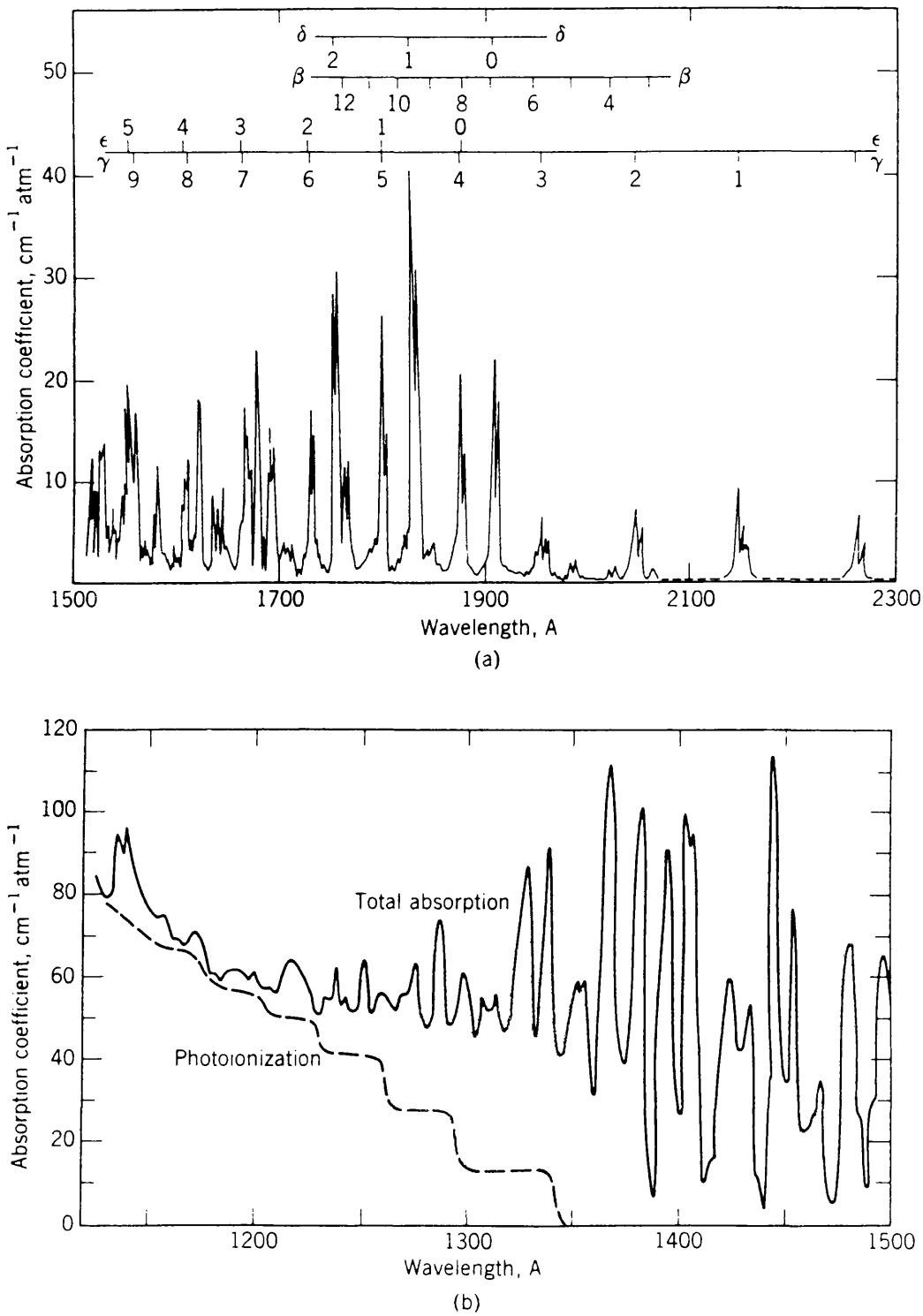

Figure 4.2.2 The absorption spectrum of nitric oxide, NO. The form of the absorption law employed is $I=I_0 \exp(-\alpha pl)$, where p is in atm at 0^0C. From McNesby and Okabe (1964)

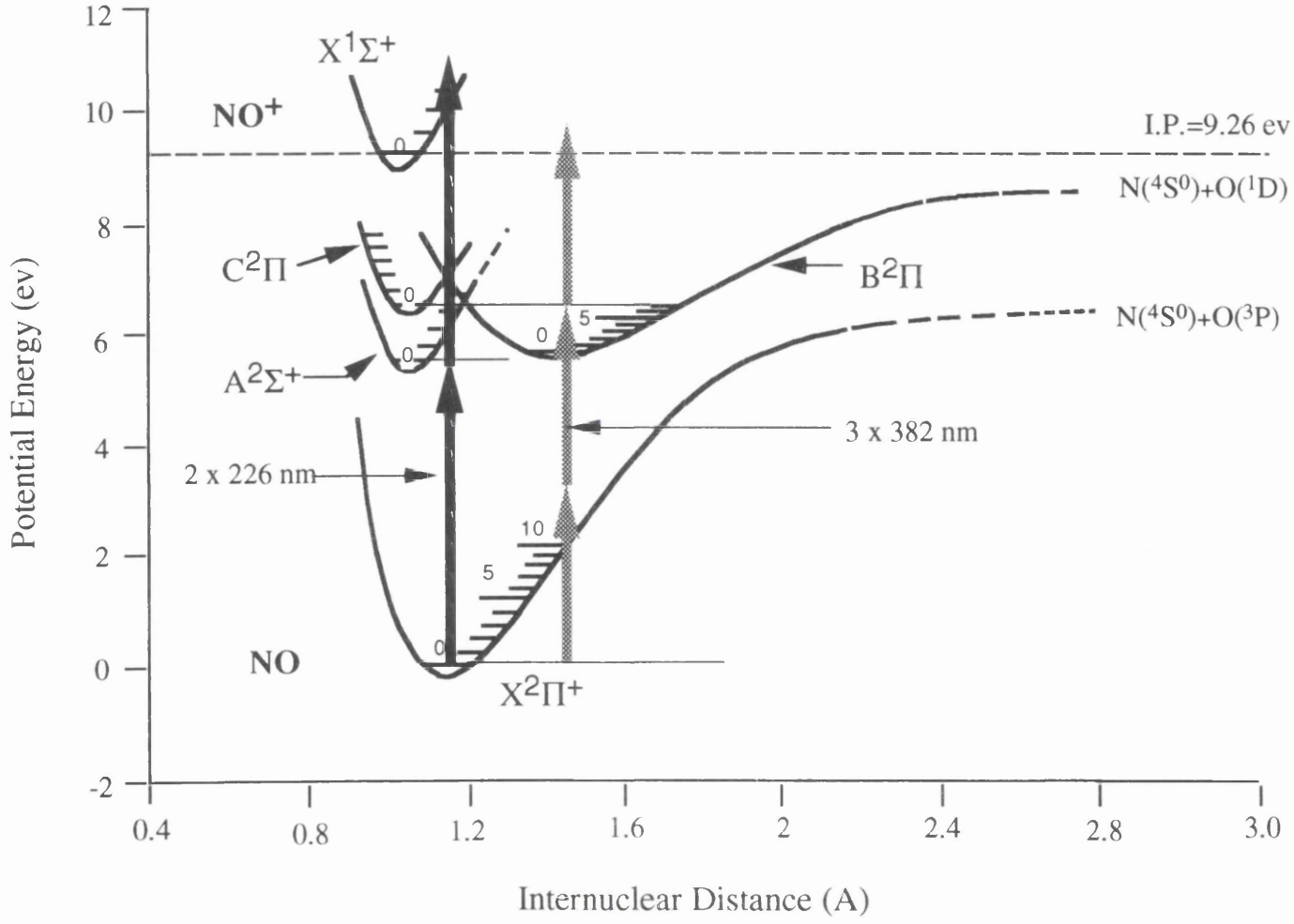

Figure 4.2.3 A simplified Gilmore diagram with the REMPI schemes used for our experiments.

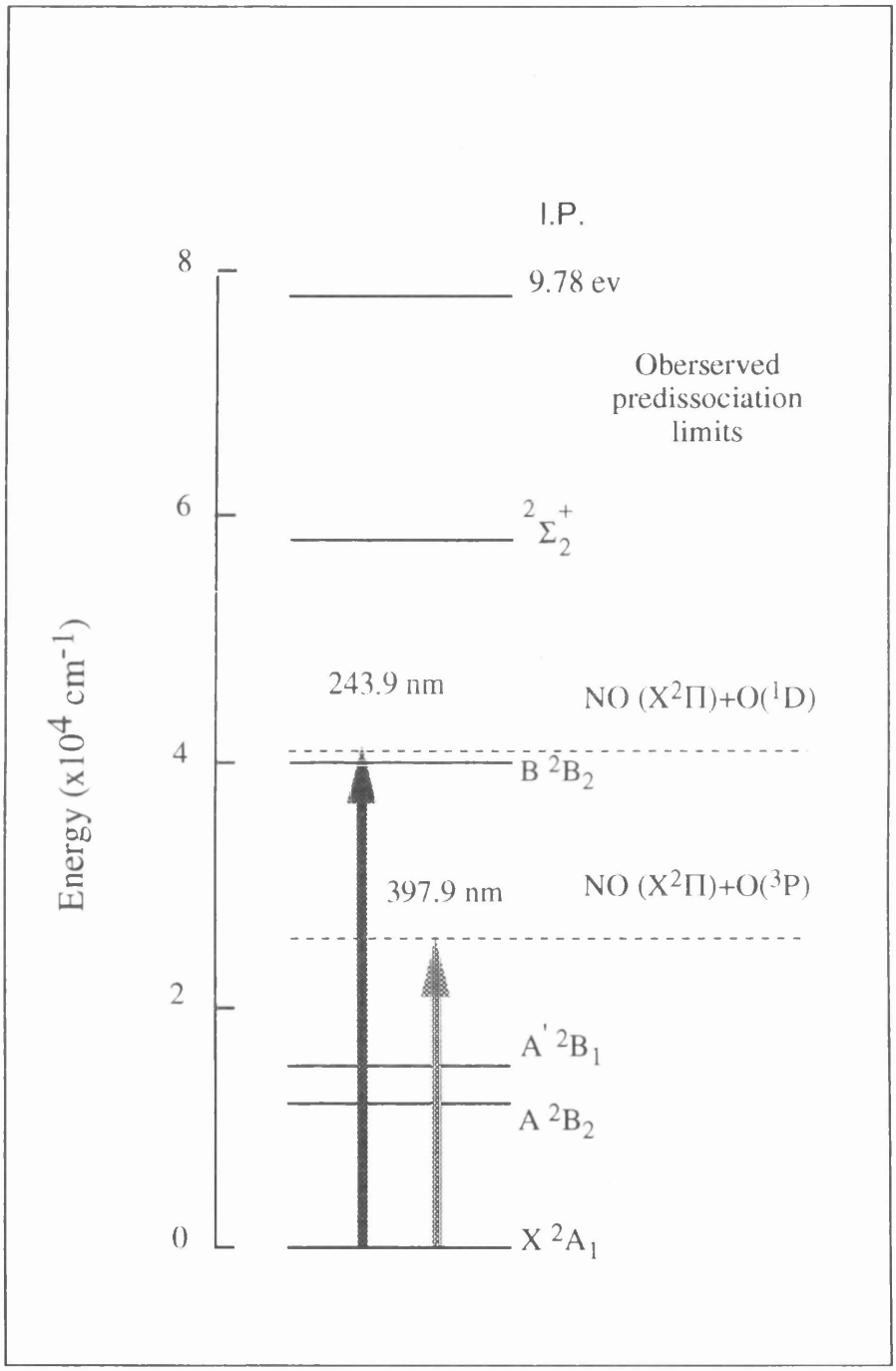

Figure. 4.2.4 A diagram of partial electronic state energy levels and observed dissociation limits for NO_2 molecule.

the band origin, 43906.37 cm^{-1}). This transition is well-known from astrophysical and terrestrial atmospheric observations and from the spectroscopy of flames and combustion products. The absorption of a second photon ionises the molecules.

The C $^2\Pi$ is another widely studied state of NO molecules since it lies at the dissociation limit for the splitting of NO (X $^2\Pi$) into ground state nitrogen and oxygen atoms. The two photon laser absorption spectrum of NO C $^2\Pi$ (υ'=0)←X $^2\Pi_{1/2,3/2}$ (υ"=0) was obtained by observing the fluorescence from C state (Freeman, 1977). The one colour 2+1 REMPI process via intermediate state C $^2\Pi$(υ'=0,3) from ground state X $^2\Pi_{1/2,3/2}$ (υ"=0) has been also investigated by several groups (e. g., Rottke. H. et al, 1985; Miller, J. C., 1986). The C $^2\Pi$(υ'=0)←X $^2\Pi_{1/2,23/2}$ (υ"=0) (2+1) REMPI process at 382 nm was used to carry out NO trace detection by Guizard et al, the detection limit that they reported is 50 ppt NO diluted in pure nitrogen at 560 mbar.

We report here trace NO detection with LOD of 200 ppt at atmospheric pressure. A typical spectrum for this transition taken by the author and used as a fingerprint of NO molecular spectra at 382 nm is described in detail in the experimental section.

NO_2 is a triatomic molecule with several geometric structures. In its ground state, NO_2 is bent and the ONO angle is large (134°15'), falling under the C_{2v} symmetric classification. Its ground state has $^2A_1$ symmetry. Additional low lying electronic states have $^2B_1$, $^2B_2$ and $^2A_1$ symmetries (Morrison et al, 1981). A correlation of orbital energies with ONO bond angle indicates that the $^2B_2$ state should assume a linear geometry , while the other two states are expected to be slightly more bent than the ground state. The interaction between these states caused the complexity of NO_2 molecular spectroscopy and much uncertainty. Photodissociation to NO+O(^{3}P) occurs after the absorption of a photon at wavelengths shorter than 397.9 nm (25130 cm^{-1}) (Douglas and Huber, 1965; Lee and Uselman, 1972). The dissociation lifetime at 397.9 nm has been estimated to be 10^{-13} sec (Robin, 1980). In the near UV the lifetime lies between 70-200 fs depending on the excitation wavelength (Rohlfing, E. A. and Valentini, J.J. 1985). When a photon with wavelength shorter than 243.9 nm (41000 cm^{-1}) is absorbed, a second dissociation limit is reached. Figure 4.2.4 shows a partial electronic state energy levels diagram for NO_2.

When NO_2 absorbs a photon at a wavelength shorter than 397.9 nm from a laser with pulse width of nanoseconds, it dissociates immediately to NO+O(^{3}P) with both

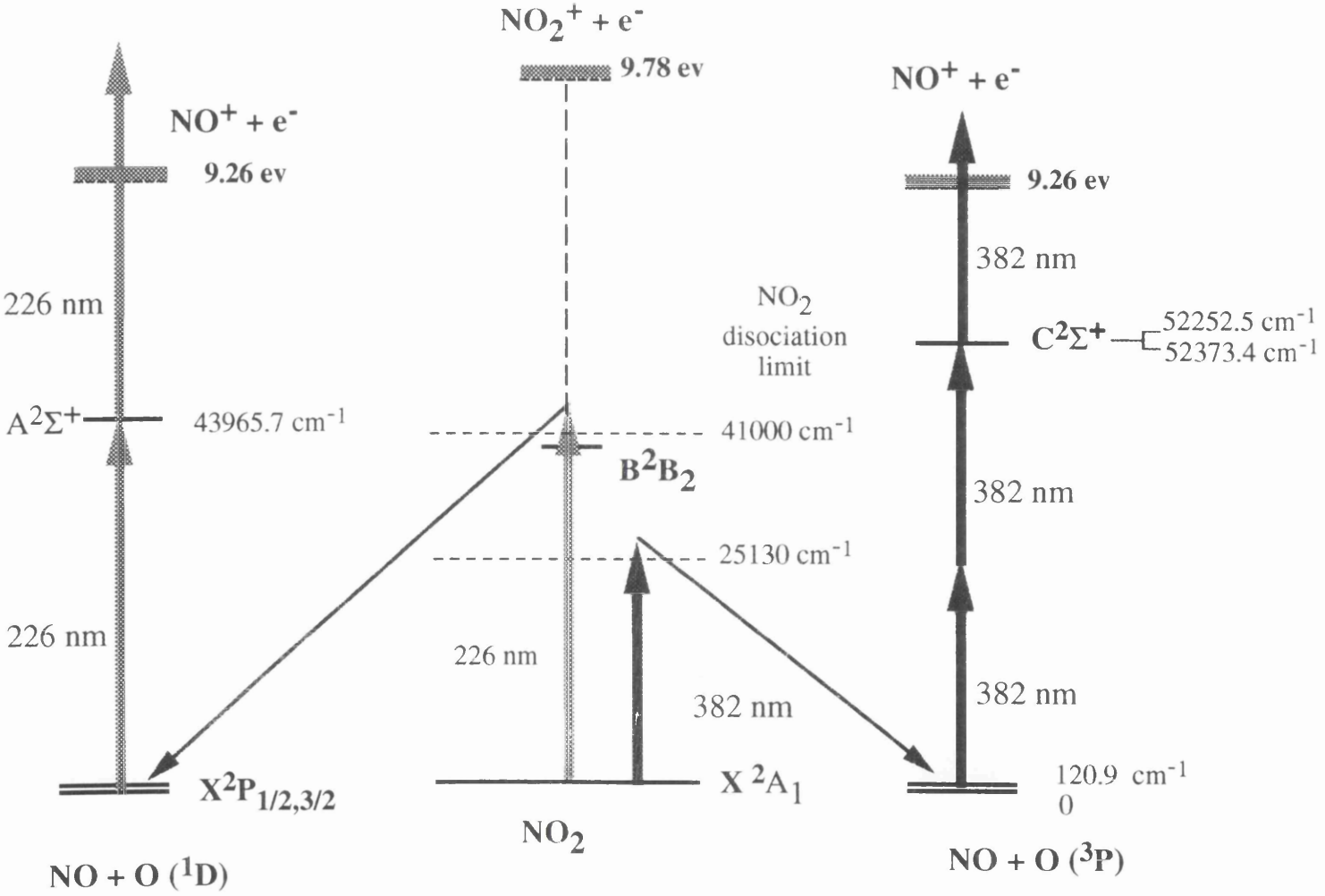

Figure 4.2.5 NO_2 REMPI schemes used in this thesis

fragments capable of absorbing further photons. If the photolysis photon corresponds to a resonance in NO, then a large ionization current pulse is produced if the detector is an ionization chamber or a large NO ion peak at m/z=30 if the detector is a mass spectrometer. For nanosecond laser pulses the probability of producing an NO_2 ion peak (m/z=46) in a spectrometer is very small about 1% or less (Marshall et al, 1992). Thus it is very difficult to distinguish between NO and NO_2 with a nanosecond laser based analytical technique and for real urban samples only the detection of the NO_X species is possible. However it should be pointed out that when lasers with a pulse width of some picoseconds or less are used then the dissociation lifetimes are largely defeated and a sizeable ion NO_2 peak is produced and hence NO_2 can be distinguished (Ledingham et al, 1995).

Figure 4.2.5 shows the schemes of NO_2 photolysis and NO REMPI processes. The detection of NO_2 in this thesis was carried out by detecting NO fragments. A $^2\Sigma^+(\upsilon'=0)$ and C $^2\Pi$ $(\upsilon'=0)$ were chosen as resonant intermediate states for 1+1 REMPI at 226 nm and 2+1 REMPI at 382 nm. The excitation cross-section has been shown to lie between 10^{-16} cm^2 to 10^{-15} cm^2 (Hippler and Pfab, 1995) for the A-state and an estimated excitation cross section for C-state is about 10^{-52} cm^2 (Guizard 1989). The photoionization cross sections have been measured to be $\sigma_i^A=(7.0\pm0.9)$ x 10^{-19} cm^2 (Zacharias et al, 1980) for the A-state and $\sigma_i^c \approx 10^{-54}$ cm^{4}s for the C-state.

4.3. Methodology and experimental

4.3.1 Methodology

The normal laser-based experimental procedure for gas analysis can be summarised by a block diagram figure 4.3.1. A finger print for trace analysis is a spectrum carrying a specific spectroscopic characteristic of the molecule under study and without interference from other molecules and it should be of high sensitivity. The first step to identify the finger print is to find out the strong absorption peak in some available dye laser wavelength region. This can be done by measuring the absorption spectrum in the wavelength region of interest or by finding finding the absorption spectrum needed from the literature and by recording the laser wavelength dependence of ion yields (signal size) in the chosen region from the known absorption spectrum. Both ion signal and laser pulse energy were recorded. For power normalisation of the ion signal wavelength dependence, laser power dependence of

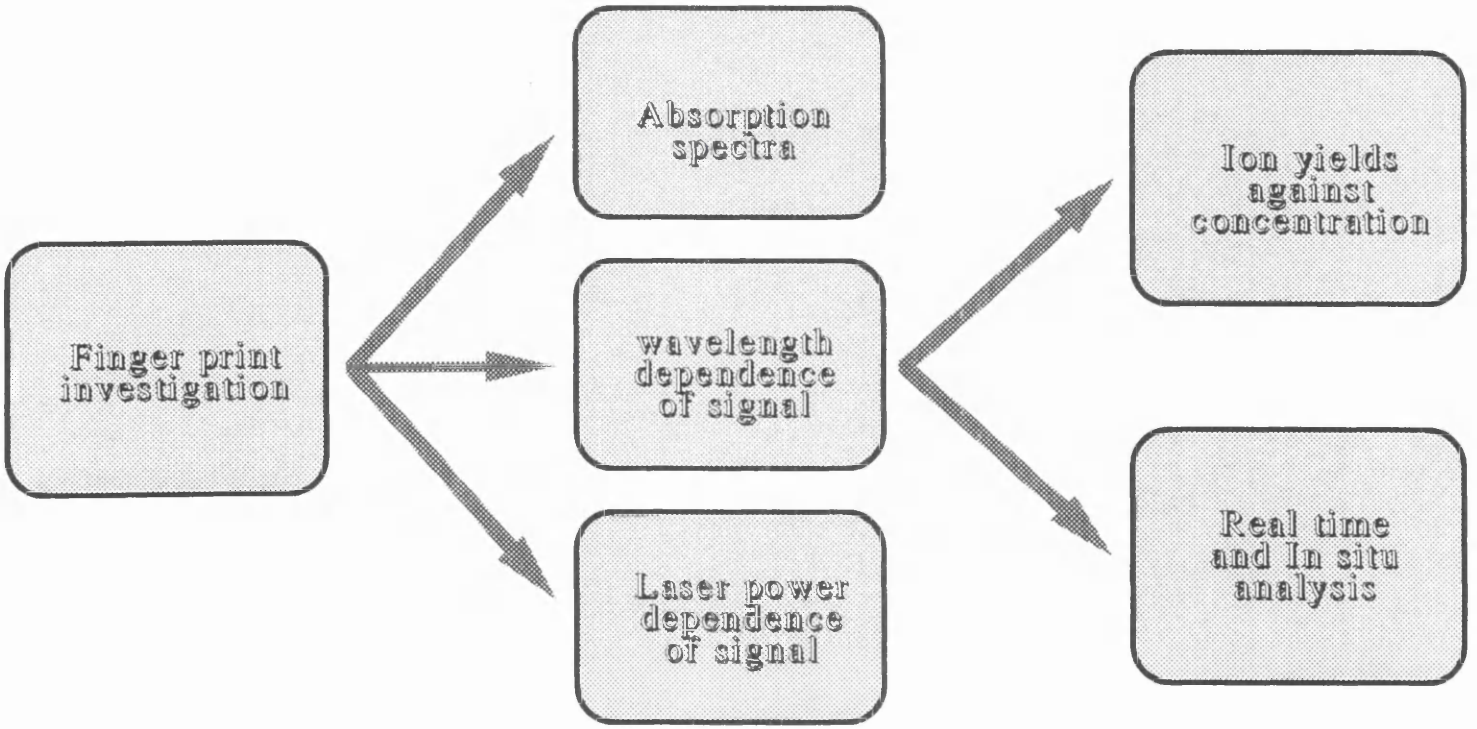

Figure 4.3.1. A block diagram for a laser-based procedure for trace analysis.

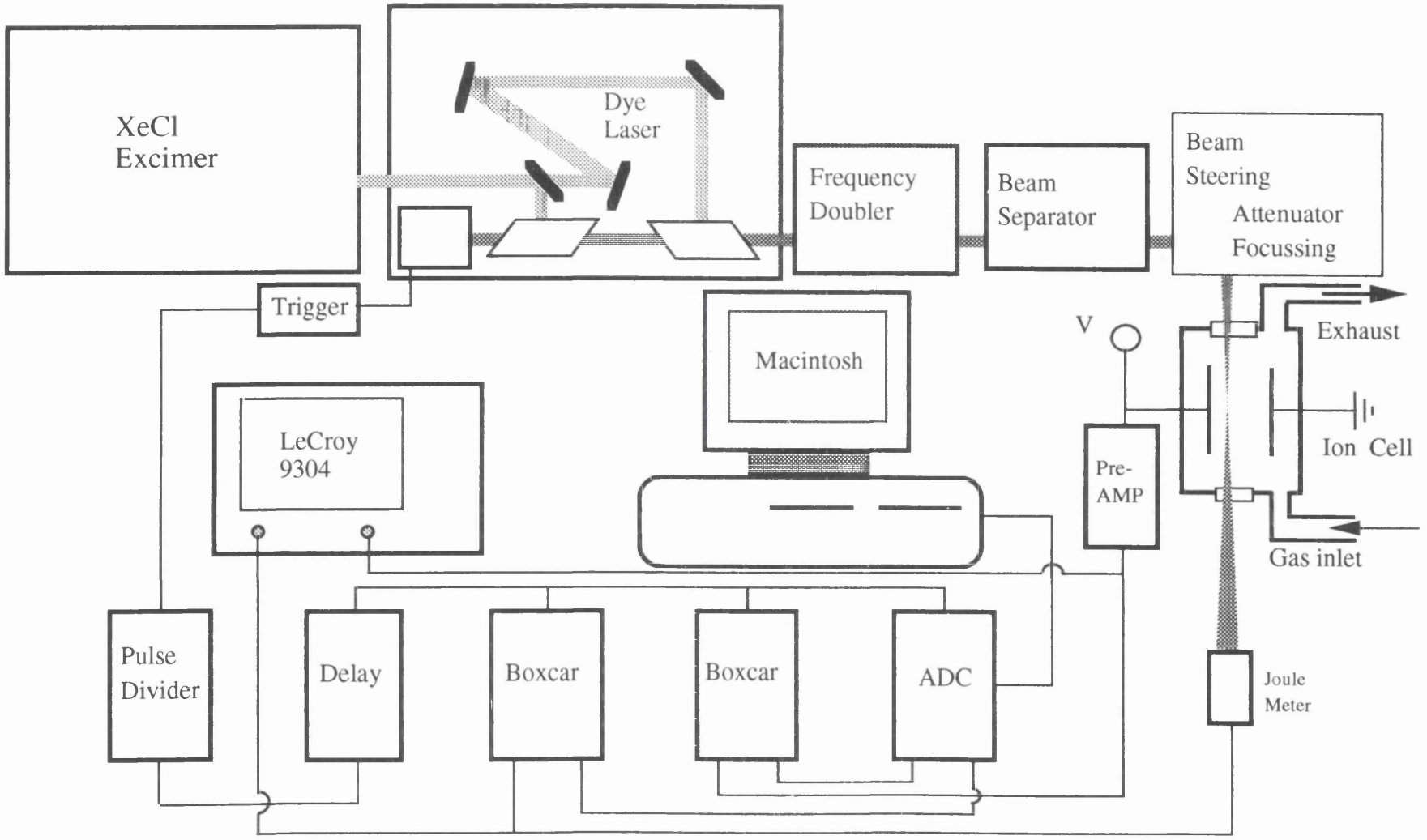

Figure 4.3.2.1 The experimental setup used for NOx detections

ion signal size (ion yields) should be investigated, since the laser intensity can vary considerably because of shot-to-shot fluctuations and because of variations in laser gain when scanning across a dye curve.

A series of curves showing the wavelength dependence of ion signal size was recorded at different analyte concentrations. For each concentration, the same measurements were repeated many times until the spectral intensity approaches a constant value thus reducing the errors caused by concentration fluctuations. A calibration curve can be deduced from these measurements by evaluating the area under these curves and the limit of the detection (LOD) can be determined from the calibration curve. Real (known) time and in situ analysis can be undertaken by sampling urban air and bringing the sample to the laboratory.

A calibration curve for determining the sensitivity which can be reached was deduced from a number of wavelength dependence curves which were taken at different concentrations. Finally real samples were measured and compared with the standard calibrated gases.

4.3.2 Experimental

The experiments concerning the detection of trace NO in nitrogen and trace NO_2 in air were carried out in this laboratory by the author. The experimental setup used for NO_X detection is shown in figure 4.3.2 for taking data in the UV region. Coumarin 47 laser dye was used to span the wavelength range 448-460 nm. UV radiation was obtained by frequency doubling the dye output using a BBO "B" cut crystal. For the spectra taken near 382 nm, BBQ dye was used.

The gases used for quantitative calibration in the experiments were 1 ppm NO_2 seeded in air or 1 ppm NO seeded in nitrogen (BOC special gases) and diluted by high pressure air and pure nitrogen. The gas flow system was described in chapter 3.

The measurements on signal size versus concentration (for measuring calibration curves) were carried out from low to high concentrations instead of the opposite way. In the latter way the chamber must be flushed using balance gas many times until the background signal returns to the same level after the measurement for each concentration. This procedure makes sure that there is no analyte contamination in the chamber. However, with the former way one needs to measure the same spectrum many times until the observed spectral intensities reach about the same level for each

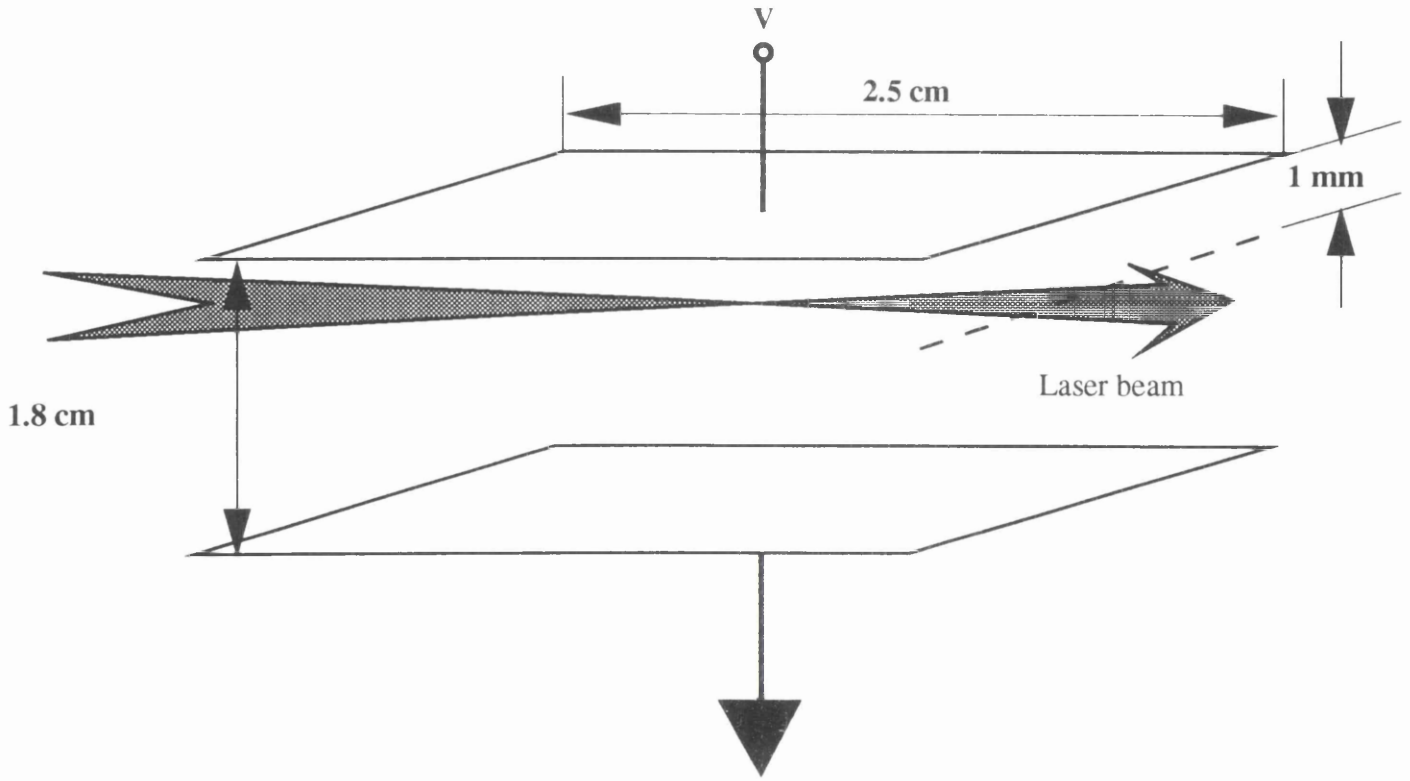

Figure 4.3.2.2. A shematic diagram of the ion chamber

concentration. Thus the errors caused by the concentration fluctuations can be reduced.

Real urban air samples can only be measured in static condition and compared with static calibration gas since the sample amount is limited.

The laser beam was set to pass through the chamber 1 mm beneath the upper electronic field plate with its waist in the centre of the chamber (figure 4.3.2.2). By using a 30 cm focal length quartz lens, the waist of the laser beam can be focused into a diameter of about 0.1 mm. The laser was operated at a repetition rate of 10 Hz. The duration of the laser pulse is about 6 ns.

The voltages applied to the plates ranged between 100 V and 800 V. Ion current pulses were fed through a preamplifier. The amplified signal is fed to a boxcar integrator and then transferred to a microcomputer to be recorded and analysed. The software used for data recording is Lab View 2. The spectroscopic data is processed by using Graph III for Macintosh.

The spectra for NO in nitrogen gas at different concentrations in the wavelength region near 226nm were taken at a laser pulse energy of 50 μJ. The laser pulse energy was measured in the laser beam exit side using a calibrated pyrometer J3-09.

4.4. Results

4.4.1 NO in nitrogen at 226 nm and 382 nm

Figure 4.4.1.1 shows a typical double-headed spectrum of NO γ-band A $^2\Sigma^+(\upsilon'=0)$ $\leftarrow$X $^2\Pi_{1/2,3/2}$ ($\upsilon''=0$) one photon absorption transition at 226 nm. This spectrum has been chosen as the NO fingerprint by many groups (Sausa and co-workers, Pfab and co-workers and this group). Because of the complexity of the rotational structure due to the angular momentum coupling, there are 12 rotational branches associated with each vibrational γ-band: the main branches P_{11}, P_{22}, Q_{11}, Q_{22}, and R_{22} and the satellite branches P_{12}, P_{21}, Q_{12}, Q_{21} , R_{12} and R_{21} . The spectra were scanned from high to low energy or from blue to red, as the band heads occurred in the low energy end of the spectrum in the P_{11}, Q_{11}, P_{22}, and P_{12} branches. Within the spectral resolution of this experiment , four of the branches were degenerate with four others, P_{22} and Q_{12}, Q_{11} and P_{21}, Q_{22} and R_{12}, and R_{11} and Q_{21} . Fortunately, high resolution is not necessary for the purpose of sensitive detection.

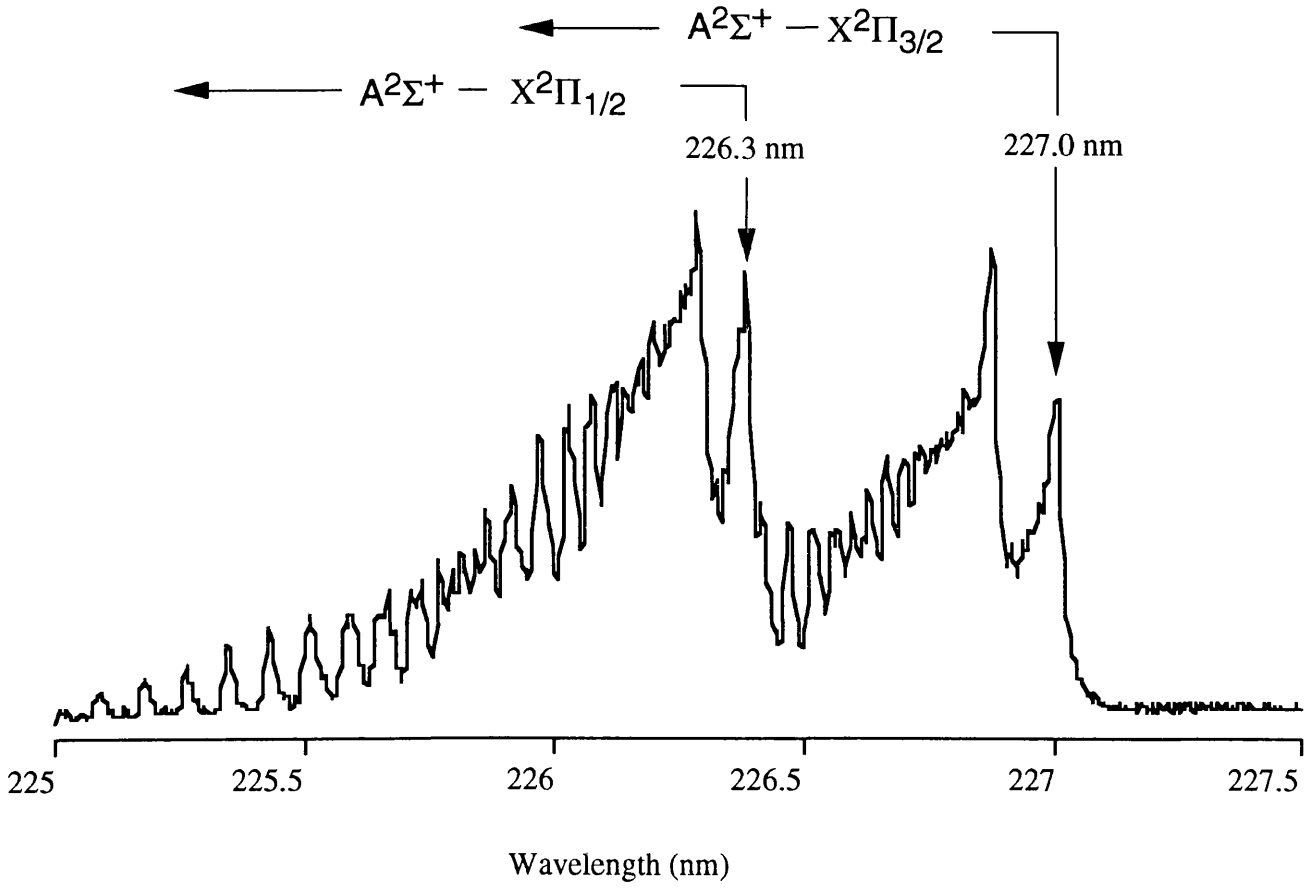

Figure 4.4.1.1 A spectrum of NO for the (1+1) REMPI at 226 nm

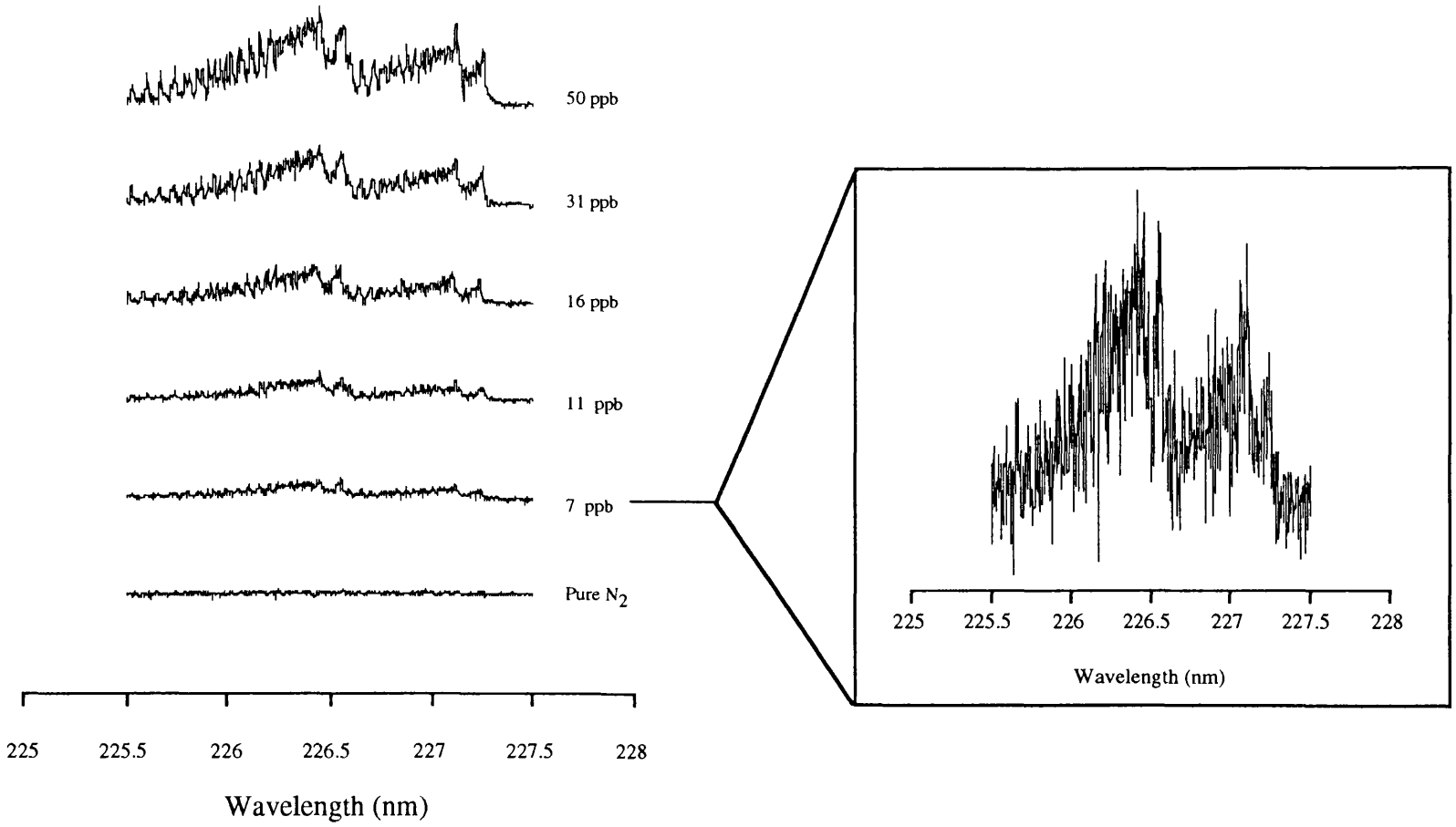

Figure 4.4.1.2 NO Spectra at 226 nm taken with different concentrations at atmospheric pressure using a simple ionisation chamber.

During the course of recording the spectra, a wavelength calibration was carried out using the two sub-band head positions which are 226.29 nm for P_{11} branch and 226.97 nm for P_{21} branch. For determining the limitation of detection of NO in nitrogen at 226 nm, a series of spectra were taken different concentrations using the above mentioned fingerprint, see figure 4.4.1.2. The spectra were taken in single shot mode, i.e. each of the point in the graph corresponds to one laser pulse. The NO is added as an impurity to nitrogen gas rather than air since the long term stability of the calibrant concentration cannot be guaranteed when the NO is added to air. Both ion signal size and laser pulse energy were recorded for each data point. The first step in the analysis of the NO spectra from REMPI is to perform a background subtraction and normalisation of the signal to the laser powers. Background subtraction is necessary, because sometimes the background is different for different NO concentrations. This difference was probably caused by non-resonat multiphoton ionization. If the laser power can be kept constant during the whole process of data taking, then the laser power normalisation is not necessary. The area under each curve after background subtraction is determined, and a relationship between net ion signal size and a series of NO concentrations in nitrogen balance was obtained, as shown in figure 4.4.1.3. It can be seen that the signal size is a linear function of concentration. The lowest level for the detection of NO at twice background level (i.e. signal to noise ratio equals 2) is between 2-3 ppb for this single shot data.

Figure 4.4.1.4. is the spectrum that the author used as the NO fingerprint at 382 nm. This spectrum was mainly contributed by the NO $\delta(0,0)$-band, particularly $\beta(0,7)$-band. As one can see from figure 4.2.1, the energy level of vibrational state C $^2\Pi$ ($\upsilon'=0$) is very close to the state of B $^2\Pi$ ($\upsilon'=7$), therefore the lowest J-members of C $^2\Pi$ ($\upsilon'=0$) are perturbed by B $^2\Pi_{3/2}$ ($\upsilon'=7$). This perturbation has been studied by Achermann and Miescher (1968) and the perturbed eigenvectors as well as the eigenvalues for this state have been calculated.

Figure 4.4.1.5 displays one of the subband heads of the NO δ (0,0)-bands, the transition of C $^2\Pi \leftarrow$ X $^2\Pi_{1/2,}$ with increasing NO concentrations. The data was taken at the wavelength region near 382 nm with a laser pulse energy of 3 mJ and the laser beam focused to a diameter of 0.1 nm . In this case, the laser fluence is 5 x 10^9 W/cm^2 which is in agreement with Guizard's results. A spectrum of pure nitrogen was recorded for the background. In these spectra each point is the average of 10 laser shots. From these recorded spectra one can plot the NO concentration

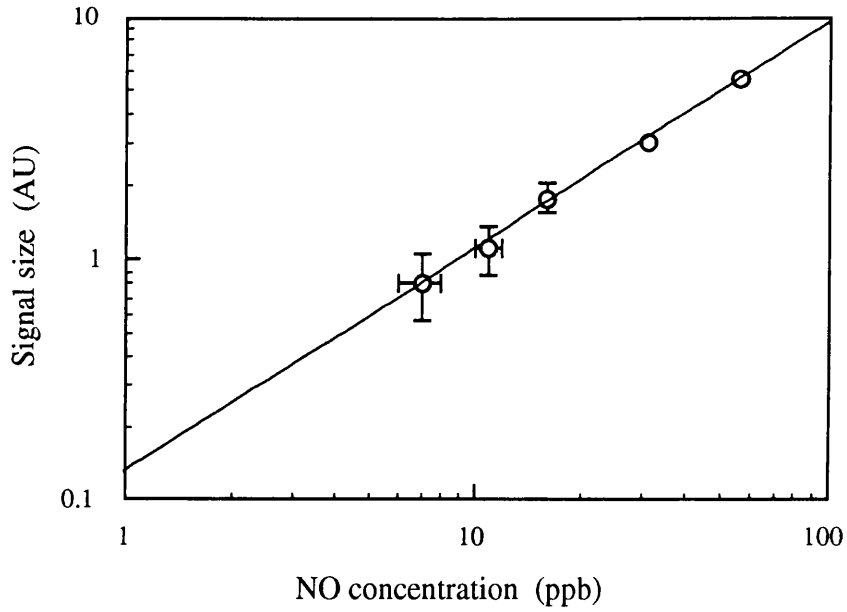

Figure 4.4.1.3 NO ionsignal size versus different concentrations, data taken at 226 nm

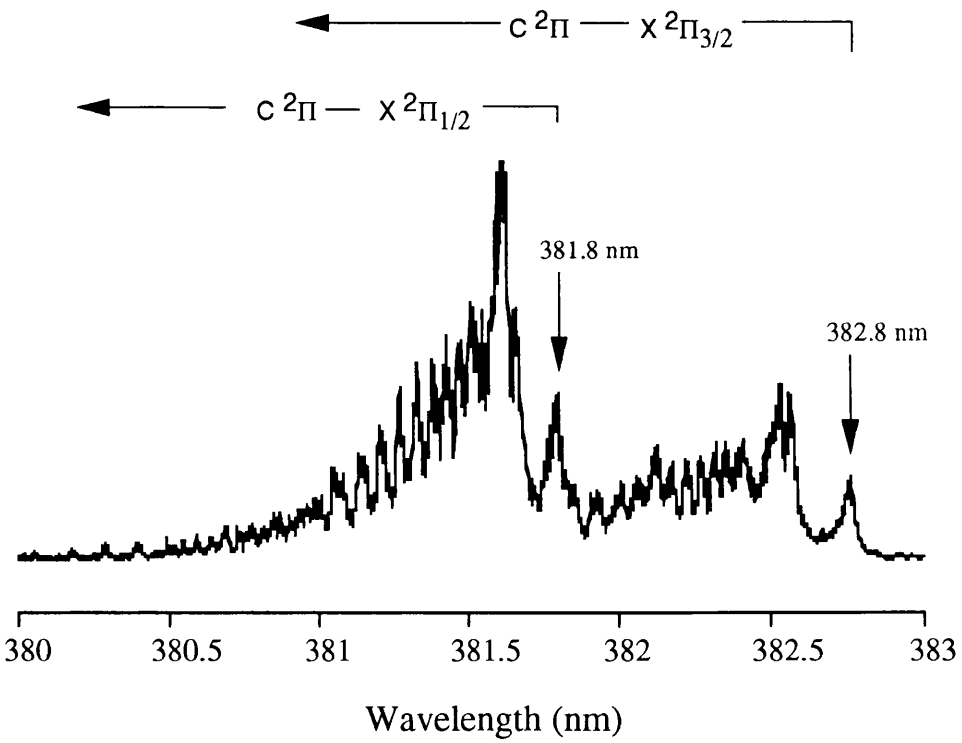

Figure 4.4.1.4 An NO (2+1) REMPI spectrum at 382 nm

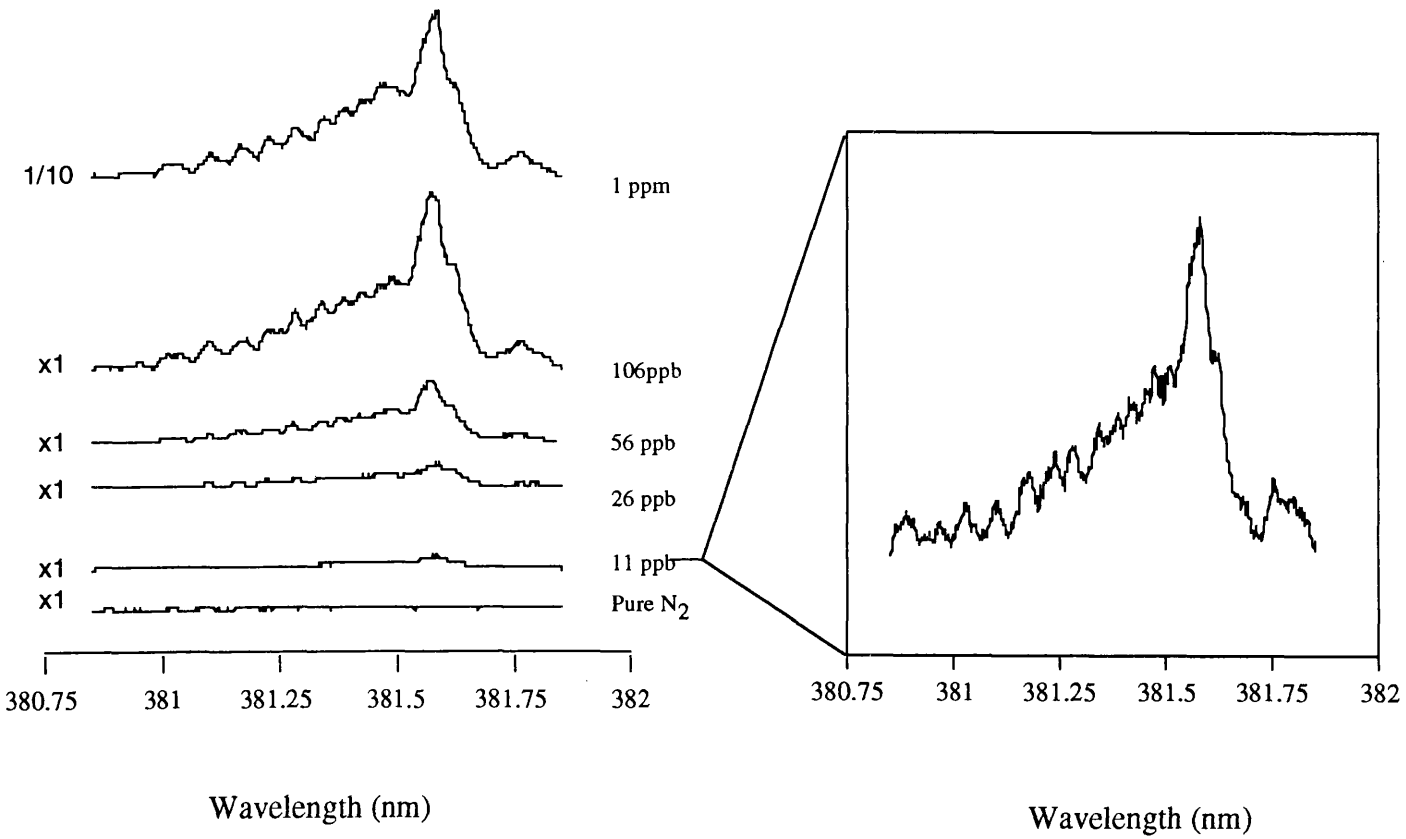

Figure 4.4.1.5 NO spectra at 382 nm with different concentrations, the magnified spectrum is corresponding to 11 ppb NO in nitrogen balance gas.

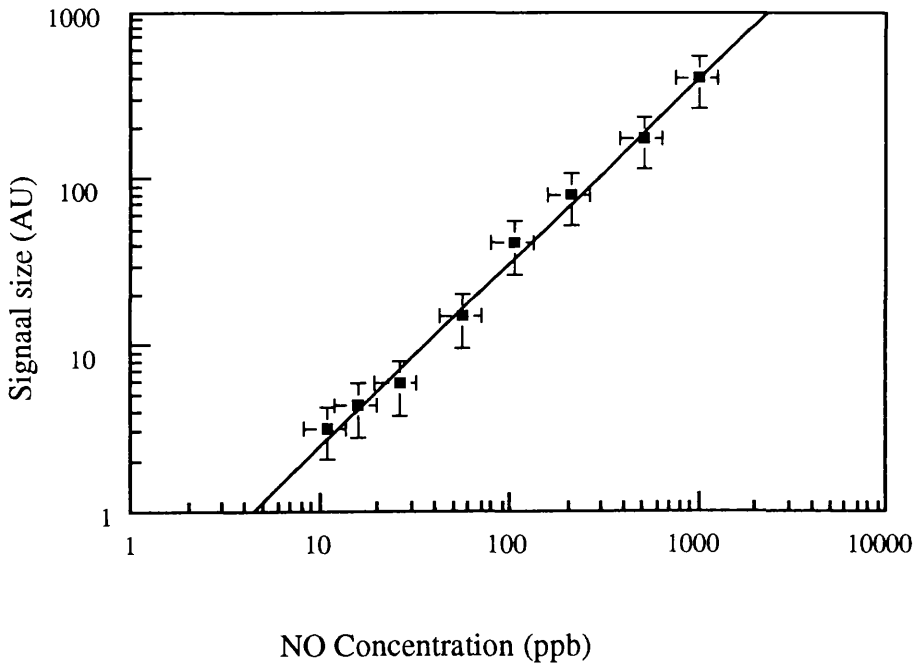

Figure 4.4.1.6 NO ion yields versus NO concentrations, data taken at 382 nm

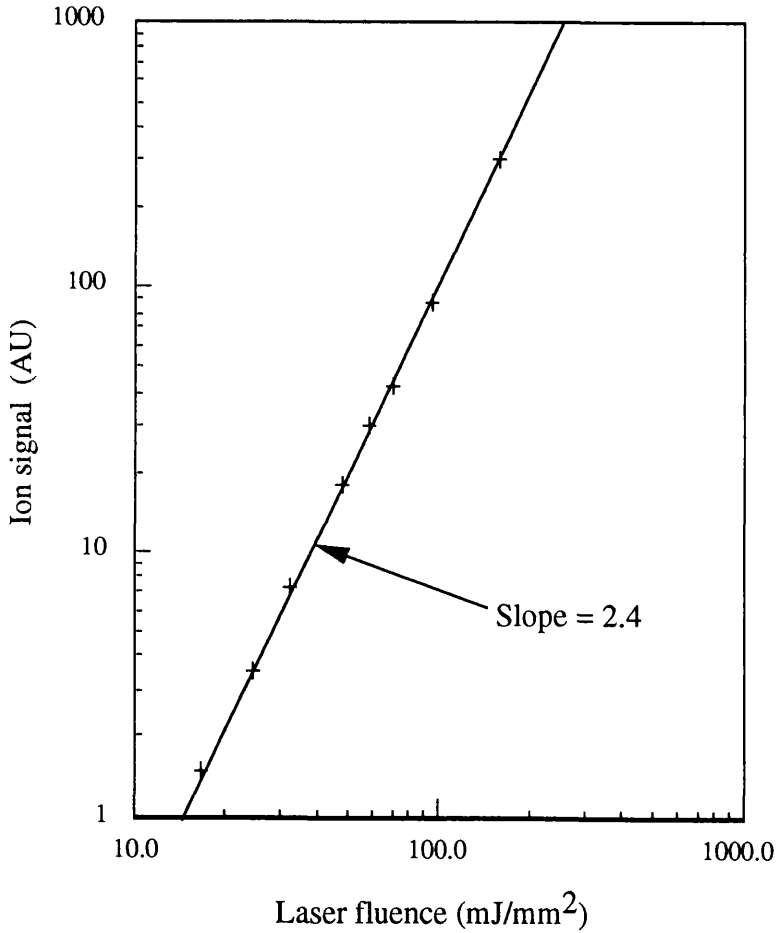

Figure 4.4.1.7 NO ion yields versus laser fluence, data taken at 382 nm.

calibration curve figure 4.4.1.6. The lowest level for NO detection can be deduced from these curves in figure 4.4.1.5 to be 200 ppt, in agreement with the data presented by Guizard et al. The sensitivity for NO at 382 nm is marginally better than 226 nm taken in single shot mode but a greatly improved sensitivity can be expected if averaging is taken over 100 or even 1000 shots although at the expense of a much lower data taking rate.

The laser power dependence of the ion signal size for the strongest line of NO (2+1) REMPI process at 382 nm was investigated. A linear dependence of the NO ion signal on the focused laser output is illustrated in log-log scale diagrams figure 4.4.1.7. In figure 4.4.1.7 the slope of the straight line can be easily determined. The value of this slope is 2.4 which is in between 2 and 3. Slope equals 2 means that the ionization step is saturated. Slope 3 means neither excitation nor ionisation are saturated. This non-integral result is different from Guizard's,-their laser power dependence showed a quadratic relationship. The reason is that they set their laser pulse intensity to make the two photon excitation unsaturated and the ionization step saturated, while in this work both the excitation and the ionisation step is partially saturated.

4.4.2 NO_2 in air at 226 nm and 382 nm

Two spectra of NO_2 in air at different low concentrations, 20 and 50 ppb respectively, are given in figure 4.4.2.1. It was estimated that the lowest concentration for NO_2 in single pulse mode is between 10-15 ppb which is considerably poorer than the lowest NO concentration reached. This might be expected since for NO_2, a (1+1+1) three photon process is required, one to dissociate to NO plus two more at 226 nm to ionize NO.

A series of spectra for NO_2 taken at 382 nm and averaged over 10 shots is shown in figure 4.4.2.2. The lowest concentrations reached was similar at about 10 ppb. The ion yield against concentrations at 382 nm for NO_2 was again linear (figure 4.4.2.3). It can be seen in figure 4.4.2.1 that to some degree, the sensitivity at 226 nm is limited by the strong molecular oxygen peak at about 225 nm (Clark et al, 1993), which is not shared by the spectra taken at 382 nm.

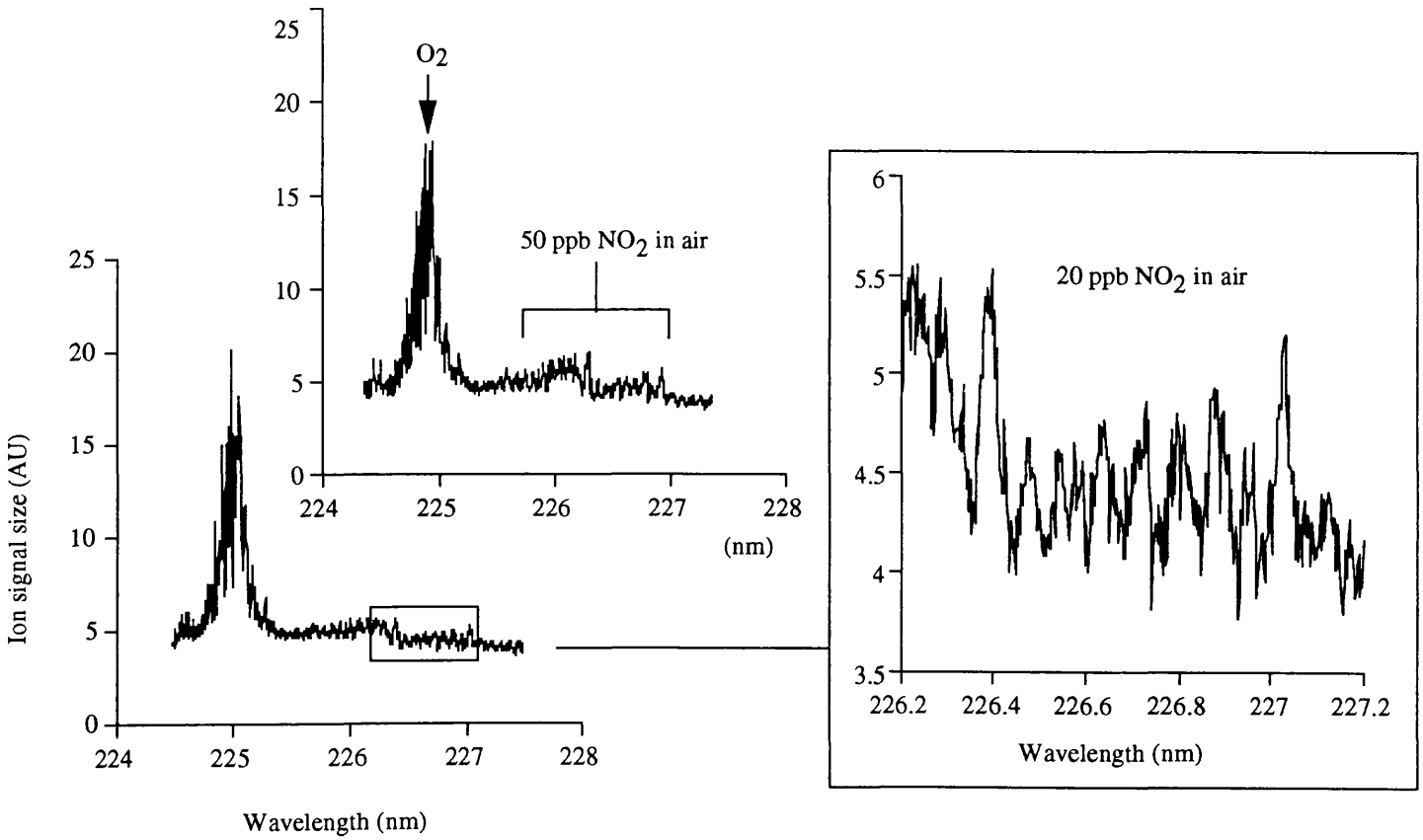

Figure 4.4.2.1 Two spectra for NO_2 in the air at 226 nm. The concentrations are 50 ppb and 20 ppb respectively, the magnified part of the lower trace corresponds to NO_2.

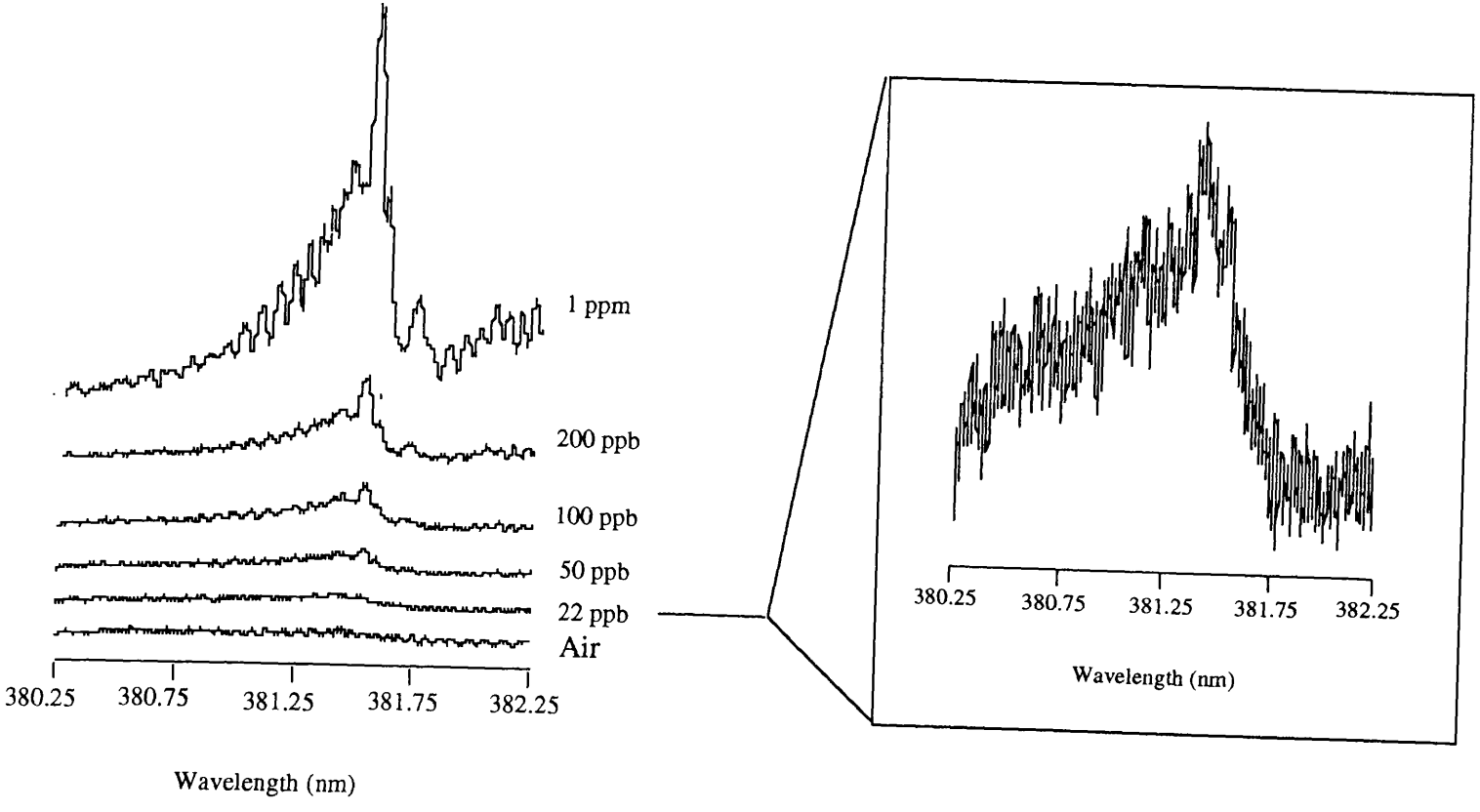

Figure 4.4.2.2 NO_2 Spectra at 382nm with different concentrations in the air, the magnified spectrum corresponds to 22 ppb.

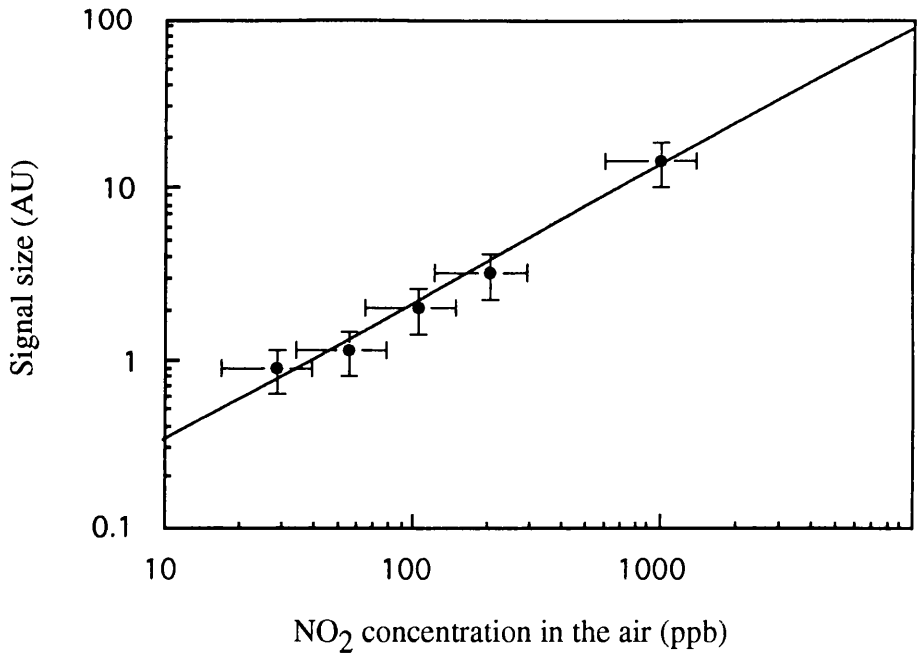

Figure 4.4.2.3 NO (from NO_2) ion yields versus NO_2 concentration, data taken at 382 nm

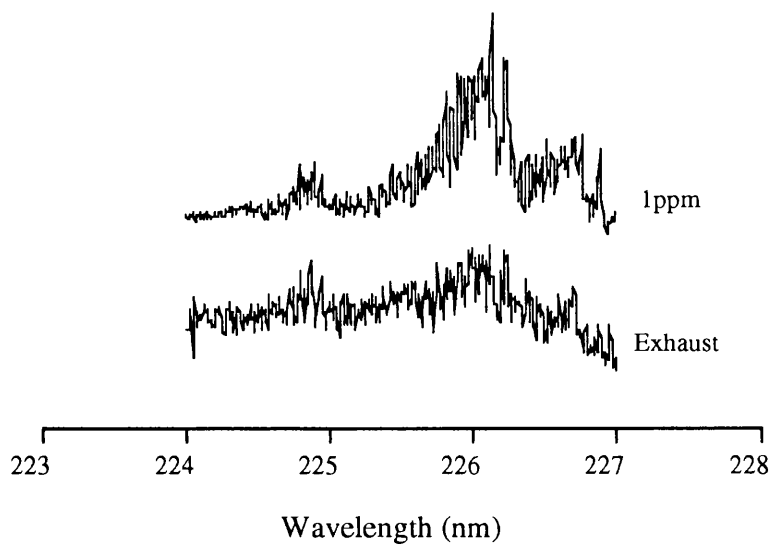

Figure 4.4.3 A comparison of the spectra of 1 ppm NO_2 in the air and the exhaust gas from a car taken in a street in Glasgow.

4.4.3 NO_x in urban air

In order to see whether a simple ionization chamber arrangement could operate with an untreated urban sir sample, the chamber was evacuated and opened for sampling to the real air in a busy street in Glasgow in the rush hour at car exhaust pipe level. It would be expected that the NO_X levels in such a case would be some hundreds of ppb. It can be seen from figure 4.4.11 that the NO_X levels in this work is indeed some hundreds of ppb when compared with a 1 ppm NO_2 in air standard.

4.5. Conclusions and discussions

It has been shown that NO in nitrogen can be detected with a laser based procedure using a simple ionization chamber system with two and three photon absorption processes at both 226 and 382 nm respectively down to sensitivities of a few ppb in single pulse mode. When the pulses were averaged over ten shots at 382 nm, sensitivities of a few hundred ppt could be reached which is well below the currently accepted safety level under current European legislation 72 ppb.

For NO_2, the detection levels were not so low, with about 10 ppb being attainable at 226 nm and with similar sensitivities reached at 382 nm after averaging. The poorer levels of detection were felt to be due to the fact that for NO_2, three and four photon process were necessary at 226 and 382 nm. For both oxides of nitrogen, the advantage of carrying out the analysis at 382 nm is that frequency doubling of the laser fundamental wavelength is unnecessary and that interference from molecular oxygen at 225 nm is eliminated.

At present a single analysis takes about three minutes and hence hundreds of urban air samples can be measured per day when the procedure is automated.

This laser based procedure has advantages of simple setup, easy calibration (on-line gas expansion), high sensitivity (sub-ppb), wide dynamic range (ppb-ppm) and simultaneous multi-component analysis.

Possible error sources for concentration detection are: (1). The fluctuation of laser intensity with time. (2). The gas flow rate fluctuation with time and the flow meter's calibration. The first error can be reduced by keeping the laser power constant as much as possible. To reduce the second error one requires to wait a long time for the

equilibrium and stability of the gas flow rate to be reached and also a more accurate flow meter is needed.

A review of some methods to measure selected NOx gases has been given by Sickles, 1992 (See appendix). A comparison with the data listed by Sickles and published by other investigators has been given in table 4.5.

Table 4.5 Selected Instruments and methods for detecting Oxides of Nitrogen. Table adapted from Sickles, 1992

Species	Methods[a]	Type[b]	Development Stage[c]	Sample Duration	Performance Precision	Performance Accuracy	Performance MDL	Comments
NO	CLM ($NO+O_3$)	I, A, C	C	5 min	≤10%	≤20%	≤9 ppb	—
	CLM ($NO+O_3$)	I, A, C	R	2-60 s	20 ppt	20 ppt	5 ppt	—
	TP-LIF	I, A, C	R	30 s	—	16%	10 ppt	—
	TDLAS	I, A, C	R, C	60 s	—	—	0.5 ppb	40m path length
	TTFMS	I, A, C	L	60 s	—	—	4 ppt	100m path length
	PSD	I, P, IN	C	24 h	—	—	70 ppb-h[d]	—
	LIF[†] (nozzle)	A, C	L	—	—	—	5 ppt	Vacuum
	REMPI[#] (2+1) at 382 nm	A, C	L	—	—	—	50 ppt	NO in N_2
	REMPI[§] (1+1) at 226 nm	A, C	L	—	—	—	1 ppb	NO in Ar
	REMPI[*] (1+1) at 226 nm	A, C	L	—	—	—	2-3 ppb	NO in N_2
	REMPI[*](2+1) ar 382 nm	A, C	L	—	—	—	200 ppt	NO in N_2
NO_2	CLM ($NO+O_3$)	I, A, C	C	5 min	10%	20%	9 ppb	EPA reference method
	CLM ($NO+O_3$)	I, A, C	C	<100 s	20 ppt	30%	10-25 ppt	Uses thermal conventers
	CLM (Luminol)	I, A, C	C	100 s	0.6 ppb	—	10 ppt	Interference: PAN,HNO2,O_3
	TP-LIF	I, A, C	R	2 min	20 ppt	16%	12 ppt	—
	TDLAS	I, A, C	R, C	60 s	—	15%	100 ppt	150m path length
	TTFMS	I, A, C	L	60 s	—	—	0.3 ppt	100m path length
	DOAS	R, A	R, C	12 min	—	10%	4 ppb	800m path length
	DIAL	R, A	R	—	—	—	10 ppb	6km path length
	REMPI[§] (2+1) at 226 nm	A, C	L	—	—	—	22 ppb	NO_2 in air
	REMPI[*] (2+1) at 226 nm	A, C	L	—	—	—	10-15 ppb	NO_2 in air
	REMPI[*](1+2+1) at 382 nm	A, C	L	—	—	—	10 ppb	NO_2 in air

Notations for table 4.5:

a CLM ($NO+O_3$) = Chemiluminescent using $NO+O_3$ reaction;

CLM (Luminol) = Chemiluminescent using reaction with luminol;

TP-LIF = Two photon laser induced fluorescence;

LIF = Laser induced fluorescence;

TDLAS = Tunable diode laser spectroscopy;

TTFMS = Two-tone frequency modulated spectroscopy;

DOAS = Differential optical absorption spectroscopy;

DIAL = Differential absorption lidar

b I = In sit

A = active;

P = Passive;

R =Remote;

C = Continous;

IN = Integrate;

c L = laboratory prototype

R = Research tool

† = Hippler et al., 1990

= Guizard et al., 1989

§ = Simeonsson et al., 1994

* = This work

Appendix:

Other techniques for ambient NO_X detection (Sickles,1992)

This appendix addresses several methods other than laser based REMPI for measuring gaseous pollutants NO_X. Conventionally the most common method to determine NO concentration is chemiluminescence (CLM). Other methods include laser-induced fluorescence (LIF), absorption spectroscopy, and passive collection with subsequent wet chemical analysis.

A.1. Chemiluminescence

CLM can be used to detect several airborne nitrogen-containing species (i. e. NO, NO_2, HNO_2, HNO_3, H_2O_5, PAN, NO_y, etc.). Among these, only NO is detected directly, while the other compounds must be converted in some manner to NO prior to detection.

The principle is based on the detection of the light emitted following the reaction of NO with ozone (O_3). Excess O_3 is added to an air sample containing NO, which is passing through a darkened reaction vessel with infrared reflective walls and a window for viewing by a photo multiplier (PM) tube. The light-emitting species is electronically excited nitrogen dioxide, NO_2^*, a product of the reaction of NO and O_3. This relaxes by photon emission that ranges in wavelength well beyond 600 nm and is centred near 1200 nm. Light is detected by a red sensitive PM tube fitted with optical filters to prevent radiation below 600 nm produced by ozonalysis of other materials from interfering. The intensity of the measured light is proportional to the concentration of NO in the air sample, and the concentration can be determined by calibration with atmospheres of known composition.

The detection of NO_2 employing CLM ($NO+O_3$) does not detect NO_2 directly. Instead it relies on the direct detection of NO, from the conversion of some or all of the NO_2 in the air sample to NO. The resulting NO reacts with O_3 to form NO_2 where fluorescence signal is processed to infer the NO_2 concentration.

Commercial CLM instruments for measuring NO and NO_2 are available. Detection limits of approximately 5 ppb with response times of the order of minutes are claimed by suppliers.

A.2. Laser-Induced Fluorescence (LIF) (Sickles, 1992)

LIF techniques may incorporate single-photon (SP), two-photon (TP), or photofragmentation (PF) schemes. The TP-LIF detection principle requires that a molecule has more than one bonding excited state and can be sequentially pumped into the highest state. If the lifetime of the exited state is short compared to collisional deactivation, then the excited molecule will decay to a more stable state by a fluorescence process. The fluorescence wavelength is shifted relative to that of the pumping wavelengths and thus overcomes noise problems associated with background non-resonant fluorescence. For application to NO, pulsed UV and IR laser light sources are used. Ground-state X $^2\Pi$ is excited to A $^2\Sigma^+$ electronic level using UV laser of 226 nm. Then, using IR wavelengths of 1.06-1.15 μm, the molecule is further pumped to the D $^2\Sigma$ level. The fluorescence resulting from the D $^2\Sigma$ to X $^2\Pi$ transition is monitored at 187-220 nm. By using long-wavelength block filter with solar blind PM tubes, this type of detector discriminates against noise and becomes signal, rather than signal-to-noise, limited. Photon counting and gated-charge integrators are used for signal processing. The intensity of the fluorescence light is related to the concentration of NO in the air sample by calibration with atmospheres of known concentration. Interference from other NO-containing compounds were evaluated, finally only CH_3ONO was found to be potential interference, while NO_2 was not a problem. The sensitivity is defined by integration time (e.g. 1 ppt for 5 min and 10 ppt for 30 s) since photon counting and grated-charge integrators are used for signal processing (Davis et al., 1987).

The detection of NO_2 by LIF is incorporated with its photofragmentation (Rodgers et al, 1980). With this method, NO is measured in one cell using TP-LIF. An XeF excimer laser with output at 353 nm is used in a second cell to photolyze NO_2. The total NO signal in the second cell resulting from ambient and photo fragment NO is measured as NO using TP-LIF. The NO_2 concentration is determined from the difference in signals of the two reaction cells and the partial photolysis.

A.3. Absorption spectroscopy

Absorption spectroscopy encompasses techniques that measure the change in radiance from a source that occurs as a result of absorption by analyte molecules over a known path length. Several techniques, including Fourier transform infrared spectroscopy (FTIR), tunable-diode laser absorption spectroscopy (TDLAS), differential optical absorption spectroscopy (DOAS) and differential absorption lidar (DIAL), have been used to undertake atmospheric measurements. Among these techniques, the TDLAS is a well-developed technique that has been applied to NO, NO_2 and HNO_3. Similar sensitivities have been reported for both remote sensing application using open air path lengths and in situ application using multipass cells (Cassidy and Reid, 1982). The latter configuration has found broad application. As a result in situ TDLAS is a primary focus of this section.

TDLAS employs a tunable diode laser to scan over a narrow wavelength region around a particular absorption line or feature of the gas of interest. High sensitivity is achieved by the high spectral radiance of the diodes and the rapid tenability of the laser. With rapid scanning back and fourth across the absorption line, the absorption appears as an ac signal at twice the frequency and can be sensitively detected by synchronous demodulation. System sensitivities sufficient to measure signal changes of 10^{-5} permit the detection of concentrations less than 10 ppt with a 1-km path length. For analyte molecules that have resolved absorption spectra that are not coincident with other atmospheric constituents, TDLAS is highly specific. Additional information on the operation principles and hardware for TDLAS is provided by Schiff et al. (1983), the detection limit that they reached for NO_X is 0.5 ppb.

Other absorption spectroscopy techniques e.g. differential optical absorption spectroscopy (DOAS) and differential absorption lidar (DIAL) are long-path absorption techniques which have been used for ambient NO_X detection. In DOAS (Platt and Perner, 1983), a Xe high pressure or an incandescent lamp was used with a 1- to 10-km path length. For NO_X, detection limits, target wavelengths are NO, 400 ppt, near 226 nm and NO_2, 100 ppt, near 363 nm. In DIAL, laser is used as the light source. This method employs light of two wavelengths propagated over a given distance at a given intensity. The concentration of the gas species of interest is related to the difference in intensities of the two wavelengths at the receiver. DIAL technique has been applied to the ambient measurement of both NO (Alden et al., 1982) and NO_2 (Edner et al., 1987). Detection limit for this technique is at ppb level.

All above mentioned techniques are active methods, since the light sources used are either laser or strong lamps with the wavelength being artificially selected. The method using natural light or sun light called passive method is omitted here.

References:

Ackermann, F. and Miescher, E. (1968)
Spin-orbit coupling in molecular Rydberg states of the nitric oxide molecule, *Chem. Phys. Lett.* **2**. pp. 351-352

Alden, M., Edner, H., and Svanberg, S. (1982)
laser monitoring of atmospheric NO using ultraviolet differential-absorption techniques, *Opt. Lett.* , **7**, pp. 543-545

Bradshaw, J.D. Rodgers, M.O.; Sanderholm, S.T.; KeSheng, S.; Davis, D.D. (1985)
A two-photon laser-induced fluorescence field instrument for ground and airborne measurements of atmospheric NO, *J. Geophys. Res.*, **90**, pp.12861-12873

Brophy, J.H., Renttner, C.T. (1979)
Laser two-photon ionization spectroscopy: A new method for real-time monitoring of atmospheric pollutants. *Opt. Lett.*, **4** (10), pp. 337-339

Cassidy, D.T., and Reid, J. (1982)
Atmospheric pressure monitoring of trace gases using tunable diode lasers, *Appl. Opt.*, **21**, pp. 1185-1190

Clark, A., Kosmidis, C., Ledingham, K.W.D., Marshall, A., Sander, J., and Singhal, R. P. and Cambell, M., (1993)
Resonant ionization of oxygen and hydrogen atoms following laser-enhanced photodissociation of nitrobenzene vapour, *J. Phys. B: At. Mol. Opt. Phys.*, **26**, L655-L670

Clark, A., Ledingham, K.W.D., Marshall, A., Sander, J., and Singhal, R. P., (1993)
Atomise detection of nitroaromatic vapours using resonance enhanced multiphoton ionization mass spectrometry, *Analyst,* **118**, pp. 601-607

Clark, A., Kosmidiss, C., Deas, R. M., Ledingham, K.W.D., Marshall, A., Sander, J., and Singhal, R. P., (1993)
Resonant ionization of oxygen and hydrogen atoms following laser-induced photodissociation of nitrobenzene vapour, *J. Phys. B: At. Mol. Phys.* **26**, L665-L670

Cool, T.A., Williams, B.A.(1992)
Ultrasensitive detection of chlorinated hydrocarbons by resonance ionization *J. Combus. Sci. Technol.* **82**, pp. 67-69

Davis. D.D., Bradshaw, J.D., Rodgers, M.O., Sandholm, S.T.,and KeSheng, S (1987)
Free tropospheric and boundary layer measurements of NO over the central and the eastern North Pacific Ocean, J. Geophys. Res. **92**, pp. 2049-2070

Douglas, A.E. and Huber, K.P. (1965)
The absorption spectrum of NO_2 in the 3700-4600 A region, *Can. J. Phys.* **43**, pp.74-81

Edner, H., Sunesson, A., Svanberg, S . (1988)
NO plume mapping by laser-radar techniques, *Opt. Lett.* **13** (9), pp. 704-706

Freedman, P.A. (1977)
The two photon absorption spectrum of NO $C^2\Pi$ (v=0)$\leftarrow$$X^2\Pi$ (v=0), *Can. J. Phys.* **55**, pp. 1387-1392

Fried, A. (1982)
A study of measurement interference in the optoacoustic detection of NO_2 by argon-ion laser excitation, *Applied Spectrsc.* **36**, pp.562-565

Gilmore, F.R. (1966)
Potential energy curves for N_2, NO, O_2, and corresponding ions, Memorandum, RM-4034-1-PR

Guizard, S., Chapolard, D., Horani, M. and Cauyacq, D., (1989)
Detection of NO traces using resonantly enhanced multiphoton ionization: A method for monitoring atmosphereic pollutants, *Appl. Phys.* **B 48**, pp. 471-477

Halpern, J.B., Jachson, W.M., McCrary, V. (1979)
Multiphoton sequential photodissociative excitation: a new method of remote atmospheric sensing, *Appl. Opt.* **18** (5), pp. 590-592

Hippler, M., Yates, A.J. and Pfab, J. (1990)
Ultra-trace analysis of NO by high resolution laser fluorescence and ionisation spectroscopy, *Inst, Physi. Conf. Ser.* No. **113,** pp. 303-307

Herzberg, G. (1950)
Molecular spectra and molecular structure: I. Spectra of diatomic molecules, D.Van Norstrand company, Inc, New York.

Hipler, M., Yates, A.J., and Pfab. J. (1991)
Ultra-trace analysis of NO by high-resolution laser fluorescence and ionization spectroscopy, *Inst. Phys. Conf. Ser.* **No. 113**, pp. 303-306

Jackson, W.M. and Lin C. S. (1978)
Competition between multiphoton fluorescence and multiphoton ionization in NO, *J. Chem. Kinet.* , **10**, pp. 945-954

Jacobs, D.C., Madix, R.J., Zare, R.N. (1986)Reduction of 1+1 resonance enhanced MPI spectra to population distributions: Application to the NO A $^2\Sigma^+$←X $^2\Pi$ system, *J. Chem. Phys.*, **85** (10), pp. 5469-5478

Jeffries, J.B., Raiche, G.A., Jusinski, L.E. (1992)
Detection of chlorinated hydrocarbons via laser-atomisation laser-induced fluorescence, *Appl. Phys. B*, Photophysics and laser chemistry, **55**, pp. 76-83

Johnson, P.M., Berman, M.R., and Zakheim, D. (1975)
Nonresonant multiphoton ionization spectroscopy: The four-photon ionization spectrum of nitric oxide, *J. Chem. Phys.*, **62**, pp. 2500-2502

Ledingham, K.W.D. et al (1995)
A comparison of femtosecond and nanosecond multiphoton ionization and dissociation for some nitro-molecules, *Rapid communications in mass spectroscopy*, **9**, pp. 1522-1527

Lee, E.K.C. and Uselman, W.M. (1972)
Molecular predissociation of nitrogen dioxide studied by fluorescence excitation spectroscopy, *Discuss. Faraday Soc.* **53**, pp. 125-131

Lemire, G.W., Simeonsson, J.B., Sausa, R.C. (1993)
Monitoring of vapour-phase nitro-compounds using 226-nm radiation-fragmentation with subsequent NO resonance-enhanced multiphoton ionization detection, *Anal, Chem.* **65**, pp. 529-533

Logan, J.H. (1983)
Nitrogen oxides in the troposphere: Global and Reginal budgets, *J. Geophy. Res* **88** (C15), pp. 10785-10807

Marshall, A., Clark, A., Jennings, R., Ledingham, K.W.D. and Singhal, R.P., (1991)
Resonant two-photon ionization for detection of aromatic molecules. *Mass. Sci. Technol.*, **2**, pp. 1078-1082

Marshall, A., Clark, A., Jennings, R., Ledingham, K.W.D., J. Sander and Singhal, R.P., (1992)

Laser induced fragmentation process in nitrobenzene, *Inst. Phys. Cof. Ser. No 128*: section **5**, pp. 181-184

Marshall, A., Clark, A., Jennings, R., Ledingham, K.W.D. and Singhal, R.P., (1992) Wavelength-dependent laser-induced fragmentation of nitrobenzene, *Int. J. Mass Spec. Ion Proc.*, **112**, pp. 273-283

Marshall, A., Clark, A., Jennings, R., Ledingham, K.W.D., J. Sander and Singhal, R.P., (1992)
Laser induced dissociation ionization and fragmentation process in nitroaromatic molecules, *Int. J. Mass Spec. Ion Proc.*, **116**, pp. 143-156

Marshall, A., Clark, A., Ledingham, K.W.D., J. Sander and Singhal, R.P., (1993)
Laser ionization studies of nitroaromatic and NO_X (x=1,2) molecules in the region 224-238 nm, *Int. J. Mass Spec. Ion Proc.*, **125**, R21-R26

Marshall, A., Clark, A., Deas, R. M., Kosmidis, C., Ledingham, K.W.D., Peng, W., Singhal, R.P. (1994)
Sensitive atmospheric pressure detection of nitroaromatic compounds and NO_X (x=1,2) molecules in an ionization chamber using resonance-enhanced multi-photon ionization, *Analyst,* **119**, pp. 1719-1724

McFarlane, J., Polanyi, J.C., and Shaper, J.G., (1991)
Photodissociation of NO_2 at 248 nm, *J. Photochem. and Photobiol. A: Chem.*, **58**, pp.139-172

McNesby, J.R. and Okabe (1964)
Vacuum ultraviolet photochemistry, Advances in photochemistry, Vol.3, ed. by Noyes, W.A., Hammond Jr., G.S. and Pitts Jr., J.N., Interscience publishers, a division of John Wiley & Sons, New York, pp.157-240

Miller, J.C. (1986)
Ultrasensitive, isotopically selective detection of nitric oxide by multiphoton ionization in supersonic beam, *Anal. Chem.*, **58**(8), pp. 1072-1075

Morrison, R.J.S., Rockney, B.H., and Grant, E.R. (1981)
multiphoton ionization of NO_2: Spectroscopy and dynamics, *J. Chem. Phys.* **75**(6), pp. 2643-2651

NG, C.Y., Mahan, B.H., Lee, Y.T. (1976)
Photoionization with molecular beams. 1. Autoionisation structure of nitric oxide near the threshold, *J. Chem. Phys.* **65,** pp. 1956-1959

Papenbrock, Th.; Stuhl, F.; Muler, K.P.; Rudoph, (1992)
Measurement of gaseous HNO_3 over the Atlantic-ocean. *J. Atoms. Chem.*, **15,** pp. 369-379

Peng, W.X., Ledingham, K.W.D., Marshall, A., Singhal, R.P. (1995)
Urban air pollution monitoring: Laser-based procedure for the detection of NO_X gases, *Analyst,* **120**, pp. 2537-2542

Pfab, J. (1995)
Laser-induced fluorescence and ionization spectroscopy of gas phase species, Spectroscopy in environmental science, Advances in spectroscopy (ed. by Clark R.J.H. and Hester, R.E., John wiley and sons) **24**, pp.149-222

Plane, J. M. C., Nien, C.-F. (1992)
Differential optical-absorption spectrometer for measuring atmospheric trace gases, *Rev. Sci. Instrum.* **63** (3), pp. 1867-1876

Platt, U.F. and Perner, D. (1983)
measurement of atmospheric gases by long path differential UV/visible absorption spectroscopy, Chapter 2.6 In D.K. Killinger and A.Mooradian, eds., Optical and remote laser sensing. Springer-Verlag, New York, pp. 97-105

Rodgers, M.O., Asai, K. and Davis,D.D. (1980)
Photofragmentation/laser-induced fluorescence: A new method for detecting atmospheric trace gases, Appl. Opt., 19, pp. 3597-3605

Rohlfing, E.A. and Valentini, J.J. (1985)
Resonance and pre-resonance Raman-spectroscopy of free-jet-expension cooled molecules, *Abstract of papers of the American Chemical Society,* 188, 1984

Ronbin, M.B. (1980)
Multiphoton fragmentation and ionization, *Appl. opt.* **19**, pp. 3941-3947

Roottke, H. and Zacharias, H. (1985)
Photoionization of single rotational levels in excited $B^2\Pi$, $C^2\Pi$, and $D^2\Sigma^+$ states of $^{14}N^{16}O$, *J. Chem. Phys.*, **83** (10), pp. 4831-4844

Sandholm, S.T.; Bradshaw, J.D.; Dorris, K.S.; Rodgers, M.O.; Davis, D.D. (1990)
An airborne compatible photofragmentation 2-photon laser-induced fluorescence instruments for measuring background troposphere levels of NO, NO_X, and NO_2, *J. Geophys. Res.*, **95**, 10155-10161

Schiff, H. I., Hasti, D.R., Mackey, G.I., Iguchi, T., Ridley, B.A. (1983)
Tunable diode-laser systems for measuring trace gases in tropospheric air, *Environ. Sci. Technol.* **17** (8), A352-A364

Sickles, J. E. (1992)
Sampling and analysis for ambient Oxides of nitrogen and related species, In *Gaseous pollutants,* Nriagu, N.O. Ed., Wiley and Sons, New York, pp. 51-128

Simeonsson, J. B., Lemire, G.W. , Sausa, R.C. (1993)
Trace detection of nitrocompounds by ARF laser photofragmentation ionization spectrometry *Appl. Spectrosc.*, **47**, pp. 1907-1912

Singh, H.B. (1987)
Reactive nitrogen in the troposphere, *Environ. Sci. Technol.* **21** (4), pp. 320-327

Simeonsson, J. B., Lemire, G.W., Sausa, R.C. (1994)
Laser-induced photofragmentation/photoionization spectrometry: A method for detection ambient oxides of nitrogen, *Anal. Chem.*, **66**, pp. 2272-2278

Sukurai, K. and Broida, H.P. (1969),
Spectral study of NO2 fluorescence excited by 11 lines of Argon and Krypton ion lasers, *J. Chem. Phys.*, **50**, pp. 2404-2410

Syage, J. A., Pollard, J.E., Cohen, R.B. (1987)
Ultrasensitive detection of atmospheric constituents by supersonic molecular-beam, multiphoton ionization, mass-spectrometry, *Appl. Opt.*, **26** (17), pp. 3516-3520

Winkler, I.C., Stachnik, R., Steinfield, J.I. and Miller, S. (1986)
Evaluation of 2-photon ionization as a probe of NO ground state population distribution, *Spectrochimia Acta*, **42A**, pp. 339-342

Zacharias, H., Schmiedl, R., Weldge, K.H. (1980)
State selective step-wise photoionization of NO with mass spectroscopic ion detection, *Applied Physics*, **24,** pp.127-133

Zhu, J.Z., Lustig, D., Sofer, I., Lubman, D.M. (1990)
Selective laser-induced resonat 2-photon ionization and fragmentation of substituted nitrobenzene at atmospheric-pressure, *Anal. Chem.*, **62**, pp.2225-2232

Chapter 5

Trace CO Detection by REMPI Spectroscopy

5.1 Introduction

Carbon monoxide (CO) is a dangerous pollutant present in the atmosphere today, especially in metropolitan areas where the density of automobiles is high. Carbon monoxide is both emitted into the atmosphere as a result of combustion processes, and formed from the oxidation of hydrocarbons and other compounds. (The CO content of automobile exhaust can be as high as 10% by volume.) In addition to its harmful and poisonous effects, it is also an important trace gas in the chemistry of the troposphere. It plays an important role in the formation and conversion of other pollutants such as NO, O_3 and NO_2 (Westberg, K. et al., 1971). It can be directly produced in the atmosphere by the oxidation of methane (CH_4) and higher hydrocarbons (Fishman J. and Crutzen P.J., 1978; Warneck, P., 1988). Carbon monoxide is also recognised as one of the most important trace gases in controlling the budget and distribution of the hydroxyl radical (OH), a free radical which exerts a controlling influence on the gas phase chemistry of many atmospheric species. Methane (CH_4), an important 'greenhouse' gas is one such species. Models suggest (Thompson, A. and Cicerone, R.J., 1986; Wofsy, S.C., 1976) that increasing levels of CO in the atmosphere will lower OH concentrations, which in turn will lead to substantial increases in atmosphereic CH_4 and other 'greenhouse' gases. Increasing CH_4 from this and other causes, will in turn lead to further reduction of OH, thus establishing a positive feedback mechanism that could accelerate further increases in CO and CH_4. Although such a decrease in OH cannot be directly confirmed at this time, recent measurements have confirmed an increasing CO background concentration (Rinsland, C.P. and Leaven, J.S. 1985; Khalil, M.A.K. and Rasmussen, R.A., 1988; Dianov-kolokov, V.I. and Yurganov, L.N., 1989; Zander, R. et al., 1989).

Carbon monoxide, although not a 'greenhouse' gas *per se*, can exert yet another influence on global warming through its production and destruction of the 'greenhouse' gas ozone (O_3). Depending upon atmospheric concentrations of nitrogen oxides, CO oxidation can lead to O_3 production (Fisherman, J. and Crutzen, P.J. 1977; Fisherman, J. et al., 1979). The long tropospheric lifetime of CO, moreover, allows it to act as a nearly inert trace for recent anthropogenic inputs (Parrish, D.D. et al., 1991). Simultaneous measurements of CO along with other atmospheric species thus provide an opportunity to learn about the history of the sampled air parcel.

The detection and identification of environmentally sensitive gases at trace levels in the atmosphere pressure has been an issue of great importance. Ozone, nitrogen oxides (NOx) sulphur dioxide (SO_2), carbon monoxide (CO), PM10, benzene, 1,3 butadiene and 25 hydrocarbon species are treated as harmful air pollutants which should be measured for air quality monitoring purpose. Presently, CO can be measured using a variety of techniques including nonspectroscopic and spectroscopic analytical schemes. To the author's knowledge, the CO sensitive detection in the atmosphere have been made using laser photoacoustic spectroscopy (Meyer and Sigrist, 1990), long-path monitoring by infrared resonant absorption spectroscopy (Ku et al., 1975) and differential infrared tunable diode laser absorption spectroscopy (Sachse et al., 1987), gas filter correlation spectroscopy (Fried et al., 1991, ElKarim et al., 1991). CO in the ultrahigh vacuum regime has been measured using REMPI TOF mass spectroscopy (Loony et al., 1993).

This thesis introduces the REMPI schemes of CO in the UV region and reports the CO measurements using both an ionisation chamber and a TOF mass spectrometer.

5.2 CO molecule

Before the CO REMPI spectroscopy is discussed, a brief description about the CO molecule and its spectroscopy will be given.

CO is one of the simplest diatomic molecules and has been the subject of intensive spectroscopic investigation for it is important in various areas. e.g. in astrophysics, surface science and in developing new sources of coherent light. Nearly a hundred years ago, Deslandres undertook the first study of the CO emission spectrum. He observed strong ultraviolet emission bands and called them the Forth Positive System.

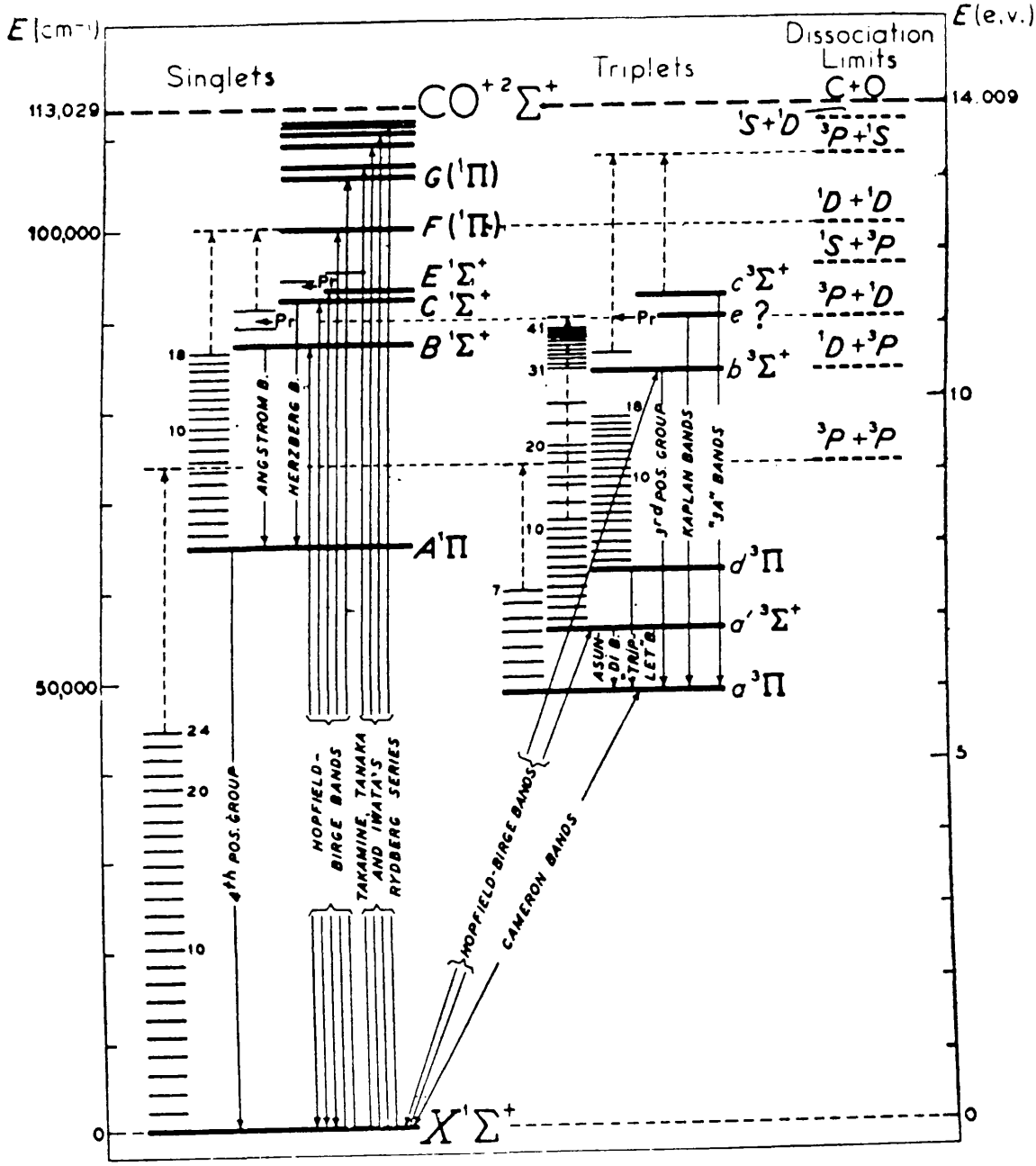

Figure. 5.2.1. Energy level diagram of the CO molecule (from Herzberg, 1950)

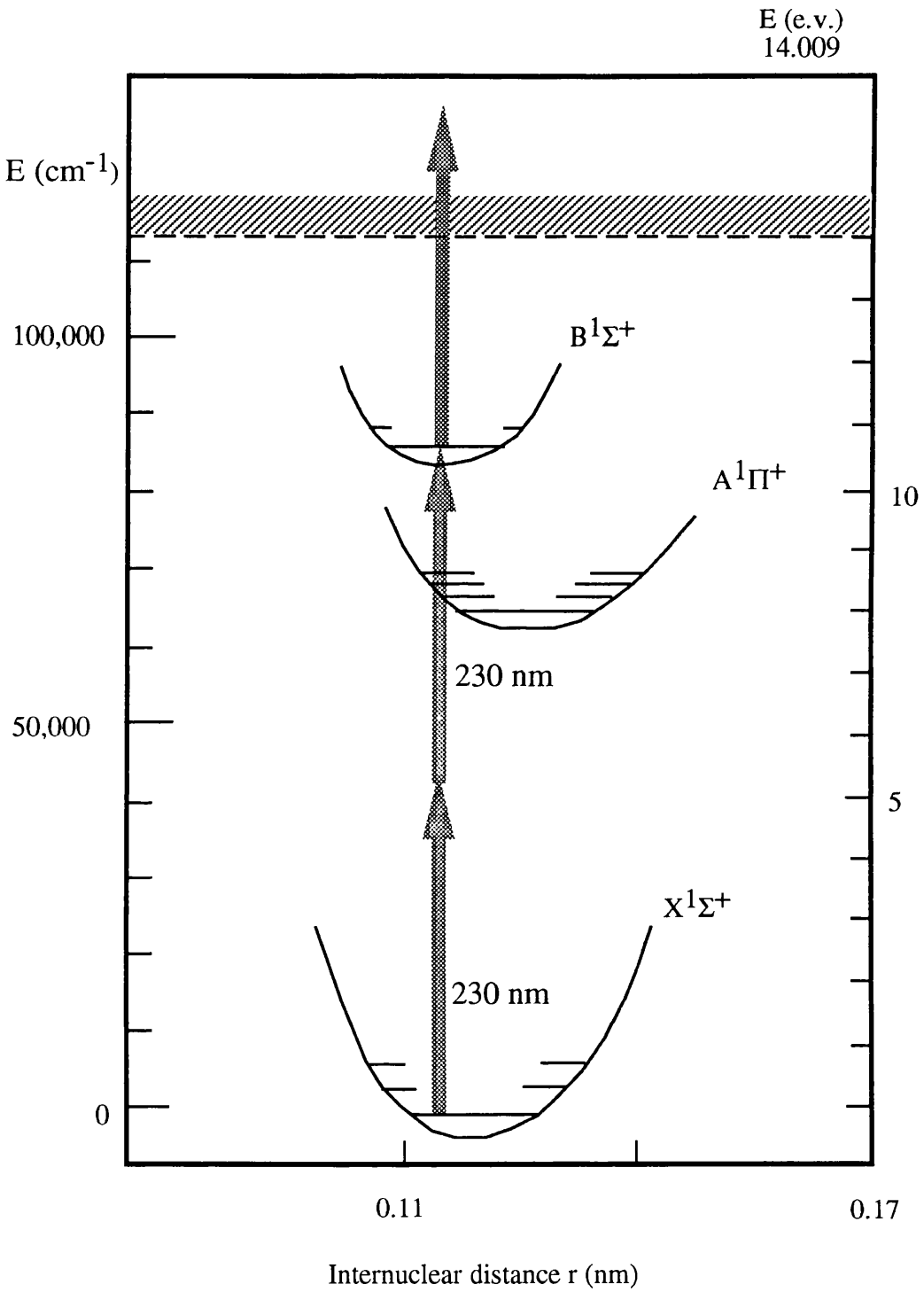

Figure 5.2.2 CO potential energy curves and the 2+1 REMPI scheme at 230 nm.

This system is now identified as the resonant transition between the $(\pi 2p)^4(\sigma 2p)(\pi^* 2p)$ A $^1\Pi$ state and the $(\pi 2p)^4(\sigma 2p)(\pi 2p)^2$ X $^1\Sigma^+$ ground state. Since this pioneer work, many investigations of the CO spectrum have been carried out. Exhaustive references can be found in the monographs of Krupenie (1966), Tilford and Simmons (1972), and the compilation of Herzberg (1950).

The energy level diagram of the CO molecule is shown in figure 5.2.1 (after Herzberg, 1950) and the potential energy curves of some CO singlet states is shown in figure 5.2.2 (a simplified diagram of Wolk, G.L. and Rich, J.W., 1983). The excited electronic states of CO have long been studied in optical absorption and emission. The A $^1\Pi$ and B $^1\Sigma^+$ states have been observed by two-photon ionisation (Zacharias, et al, 1980 and Rottke and Zacharias, 1985), multiphoton techniques including one-colour two-photon absorption (Pratt et al., 1983; Loge et al., 1983); induced fluorescence detection (Loge et al., 1983 and Seitzman et al., 1987); double-resonance excitation B←A←X (Ferrel, et al, 1983; Sha, et al., 1984; Klopotek et al., 1985; Drabbels et al, 1993), and Doppler-free method (Bernheim et al., 1978).

The multiphoton absorption technique via the A and B states has found wide application in detecting CO in both cells and in hydrocarbon flames. In particular, the strong B $^1\Sigma^+$←X $^1\Sigma^+$ two-photon absorption has generated considerable attention as a probe of photodissociation dynamics (Spiglanian, T.A., et al., 1987) in the production of CO^+ and for imaging CO produced in hydrocarbon flame (Seitman et al., 1987; Haumann et al. 1986), as well as air pollutant monitoring (Peng et al., 1997).

Since the ionisation potential of the CO molecule is 14.01 eV and the lowest energy level of B $^1\Sigma^+$ state is about 10.78 eV, three photons with energy of 5.39 eV, i.e. 230 nm, are needed to ionise CO molecules.

5.3 REMPI spectroscopy of CO

To find a spectroscopic fingerprint of CO for the use of trace detection, one needs to investigate its REMPI laser spectroscopy. A number of REMPI schemes have been used to study CO molecules, e. g. using transitions of A $^1\Pi$←X $^1\Sigma^+$ (Jiang et al., 1992, and Pratt et al., 1983 a,b), B $^1\Sigma^+$←X $^1\Sigma^+$ (Loge et al., 1983, Spiglanin et al 1987 and Tjossem et al., 1989), C $^1\Pi$←X $^1\Sigma^+$ (Tjossem et al., 1989 and Koehoven et al., 1993), and E $^1\Pi$←X $^1\Sigma^+$ (Baker et al., Fujii et al., 1989; Hins et al., 1990 and

Koehoven et al., 1993). The reason why we chose a 2+1 REMPI process at 230 nm B $^1\Sigma^+ \leftarrow$ X $^1\Sigma^+$ (two photons for excitation and the third photon for ionization) to conduct CO sensitive detection experiments is because this process can yield strong ionization signals and give a sharp peak.

In general for two photon absorption from $^1\Sigma^+$ to $^1\Sigma^+$ state, three branches O, Q and S (ΔJ = -2, 0, and +2) are allowed, P and R (ΔJ =-1, +1) are forbidden. For the B$\leftarrow$X transition of CO, however, most of the previous (e.g. DiMauro and Miller, 1987) and recent studies (e.g. Drabbels, M et al., 1993) indicate that the O- and S-branches are missing. Only when using strong circularly polarised UV laser, the O- and S-branches can be observed but their intensity is much weaker than the Q-branch (Tjossem et al., 1989). Due to the fact that the rotational constant of the B state (1.96 cm^{-1}, Edelsberg. et al., 1987) is similar to that of the ground state (1.93 cm^{-1}, Herzberg, 1950), the difference in the rotational constants is very small. As a consequence, the Q-branch at least for low J can't be resolved with a normal pulsed dye laser.

The relationship between line frequency and rotational constants for a $^1\Sigma^+ \leftrightarrow ^1\Sigma^+$ transition is given by Drabbels et al.(1993):

$$\nu = T_\upsilon + B'_\upsilon J'(J'+1) - D'_\upsilon J'^2(J'+1)^2 - [B''_0 J''(J''+1) - D''_0 J''^2(J''+1)^2] \qquad (5.3)$$

Where $B'_\upsilon, D'_\upsilon, J'$ and B''_0, D''_0, J''_0 refer to the rotational constants, centrifugal constants and ratational quantum numbers of the upper and groud states, respectively.

Table 5.3 is given below as a reference for some CO molecular constants:

Table 5.3. molecular constants for the $B^1\Sigma^+$ state of different isoyopic species of CO.

		B' (cm^{-1})	D' (cm^{-1})	T_υ (cm^{-1})	τ (ns)
$^{12}C^{16}O$	$\upsilon' = 0$	1.94816	6.8×10^{-6}	86916.15	29.3 (1.6)
$^{13}C^{16}O$	$\upsilon' = 0$	1.86274	6.2×10^{-6}	86916.81	29.6 (1.6)
$^{12}C^{18}O$	$\upsilon' = 0$	1.85553	6.2×10^{-6}	86916.70	29.2 (1.6)

In the above table, τ is the lifetime of $B^1\Sigma^+$ state.

$$\tau = \frac{1}{k_p} = \frac{1}{2\pi\Gamma}$$

where Γ is the linewidth (FWHM) of the transition observed.

5.4 Experimental

Two types of experiments have been conducted for CO molecules, i.e. both in optical spectroscopy and in mass spectroscopy. The apparatus used in the optical spectroscopic experiments is the same as the one used in the experiments for NOx detection and the apparatus used in the mass spectroscopic experiments is shown in figure 5.4. The selective 2+1 REMPI process of B $^1\Sigma^+ \leftarrow$ X $^1\Sigma^+$ (v'=0, v"=0) at 230 nm has been carried out by using a tunable dye laser system. The experiments for the determinations of the limits of detection (LODs) for CO have been conducted using gas samples of 20 ppm CO in the air and 200 ppm CO in nitrogen provided by the Linde Gas UK LTD. The experimental arrangement for these experiments is the same as that used for NO_X detection-using ionisation chambers. It is known that the LOD one can reach, depends on several factors, e.g. laser power, chamber bias voltage and so on. Optimising all the experimental conditions is necessary. The parameters for the sensitive detection for the gas sample of CO (20 ppm) seeded in the air are: laser pulse energy 250 μJ, the chamber bias voltage 200 V, and Boxcar sensitivities of 20 mV or 50 mV. No voltage amplifier or attenuator are needed. The parameters for the sensitive detection for the gas sample of CO (200 ppm) seeded in nitrogen are: laser pulse energy 50 μJ, Boxcar sensitivity 50 mV and the chamber bias voltage 500 V. A voltage attenuator for the input is needed. The laser power dependences of the ion yields have been investigated.

A linear Time-of-Flight Mass Spectrometer was also used to record the mass spectra for an analysis of this sample gas. A real-time in situ measurement of the CO concentration in the urban air of Glasgow has also been made. The structure of the mass spectrometer has been described in chapter 3. The mass spectrometer was pumped by a turbo pump to a base pressure of 10^{-8} Torr. The samples were admitted effusively from the inlet system to the high vacuum system through a needle valve. The sample system could be heated and pumped by a roughing pump to a pressure of 10^{-3} Torr. The inlet line to the high-vacuum chamber could be heated independently as could the entire TOF system.

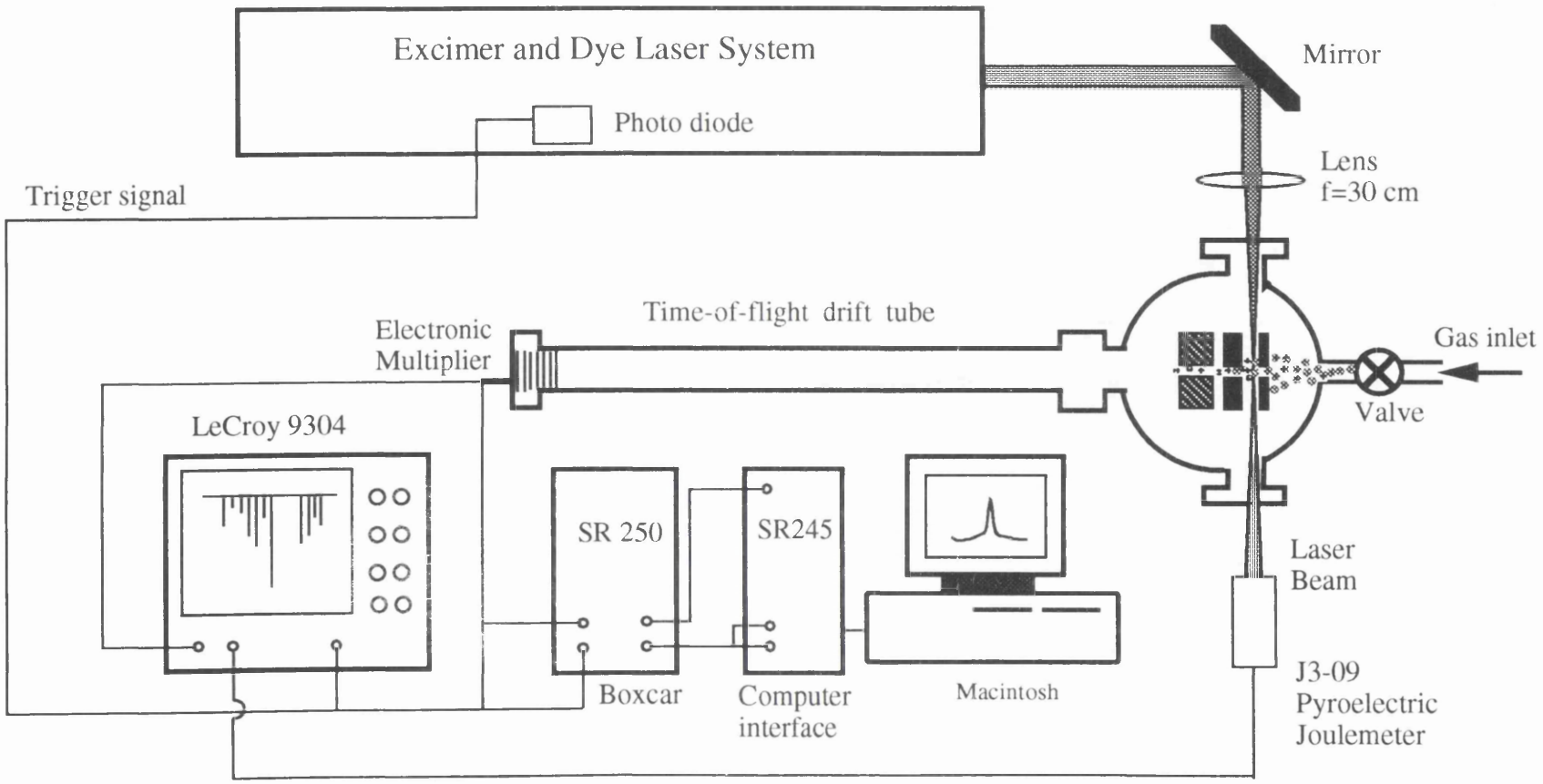

Figuer 5.4 Experimental setup for the gas phase mass spectroscopy

The wavelength calibration of the CO spectrum was performed by recording the spectrum of NO_2 in the air around 226 nm and using its double headed fingerprint to calibrate the compuscan. The mass calibrations of the TOF were carried out using the known mass spectrum of nitrobenzene at 226 nm.

5.5 Results and discussions

5.5.1 The observation of spectrum of the two photon absorption of B $^1\Sigma^+ \leftarrow X\ ^1\Sigma^+$

A typical spectrum corresponding to the B $^1\Sigma^+ \leftarrow$X $^1\Sigma^+$ (0,0) (two photon absorption and one photon ionisation) REMPI process at 230 nm is shown in figure 5.5.1. As can be seen in this figure, only one sharp peak which corresponds to the Q-branch of the transition can be observed. The O and S branches are completely absent. All the rotational lines of the Q-branch are located in a single bandhead with a width of $\Delta\lambda$=0.02 nm. Individual rotational lines could not be resolved using our laser (bandwidth 0.01 nm). This result is in agreement with the observation of DiMauro at al. by looking at the laser-induced fluorescence.

Two photon absorption theory (Bray R.G. and Hochstrasser, R.M., 1976; Chen, K-M and Yeung, E.S, 1978; Mets, F. at al., 1978; Helpern, J.B. et al, 1980) based on rotational line strengths predicts that the oscillator strength of the Q-branch of this transition will vary with the polarisation of the incident laser beam. The measurement of the transition line strengths for the Q-branch using linearly versus circularly polarised light for absorption of two identical photons should yield a polarisation ratio $\sigma_{ll} / \sigma_{cc}$ which is greater than or equal to 4:1. If the polarisation ratio is less than infinity, the O and S branch rotational transitions should also be visible. Tjossem and Smyth (1989) observed these two branches first using circularly polarised light with intensity of I=3x10^8 W/cm^2 at 230 nm. The reason why O and S branches couldn't be observed in the present experiments perhaps is because the polarisation ratio $\sigma_{ll} / \sigma_{cc}$ of our laser is large (about 20).

5.5.2. Wavelength calibration

The Q-head of the transition of B $^1\Sigma^+ \leftarrow$X $^1\Sigma^+$ has been used as the fingerprint to conduct the CO sensitivity experiments. Since the Q-head is very congested and with a very simple appearance, one can't verify it without wavelength calibration. It happens that the NO molecular transition of A $^2\Sigma^+ \leftarrow$X $^2\Pi_{1/2,3/2}$ around 226 nm shares the same wavelength region as that of CO B $^1\Sigma^+ \leftarrow$X $^1\Sigma^+$ when using the laser

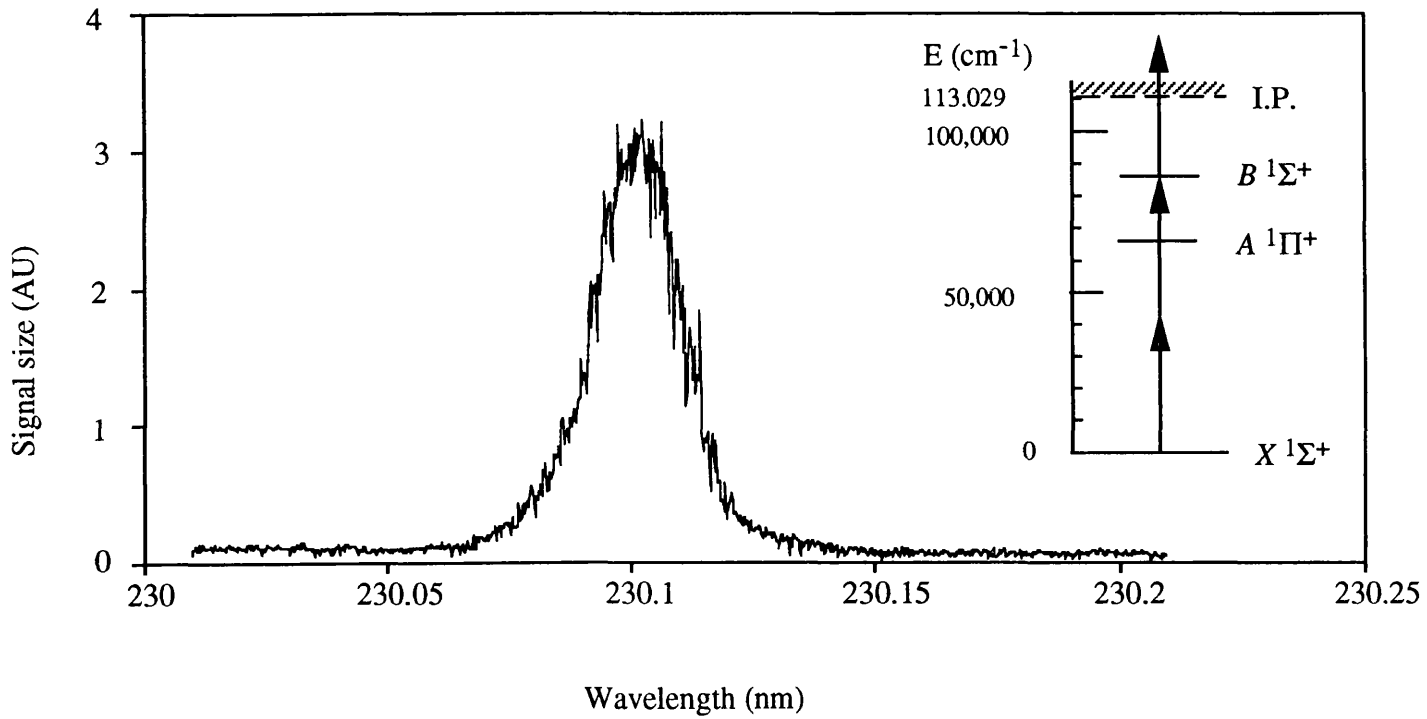

Figure 5.5.1 A recorded CO molecular spectrum. The singly unresolved peak is the Q-head of the two photon transition of B $^1\Sigma^+$--X $^1\Sigma^+$ (v'=0, v"=0) at 230 nm

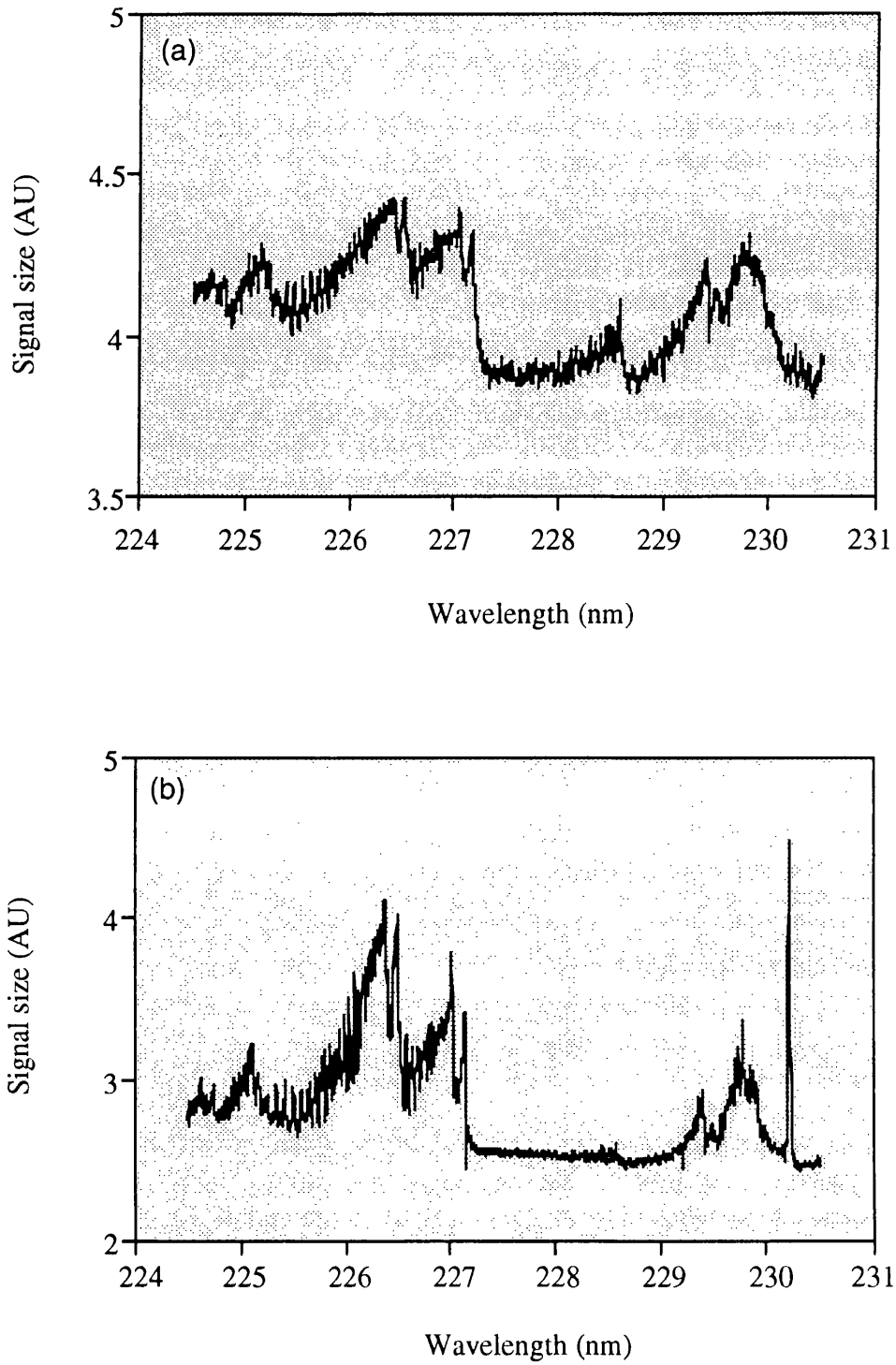

Figur 5.5.2 A comparison between the spectra taken using sample gas NO_2 *in air* and the *gas mixture* of both NO_2 *in air* (a) *and CO in air* (b).

dye LC 4700. Therefore, one can conveniently use the gases of NO or NO_2 as the wavelength calibrants. As was mentioned in chapter 2, the spectrum of NO_2 at 226 nm is actually the spectrum of NO at 226 nm because of the photodissociation of NO_2 molecules by absorbing a photon with a wavelength short than 397.9 nm.

When measuring the sample gas of 20 ppm CO in the air, the gas of 1 ppm NO_2 in the air was used as a calibrant. The wavenumber of the double heads caused by L-S coupling splitting are known to be 44073 cm^{-1} (226.9 nm) for $^2\Sigma^+ \leftarrow X\ ^1\Pi^+_{1/2}$, v (0,0) and 44199 cm^{-1} (226.3 nm) for $^2\Sigma^+ \leftarrow X\ ^1\Pi^+_{3/2}$, v (0,0) respectively. Figure 5.5.2 shows the spectra of the gas mixture of NO_2 in air plus CO in air, the dip on the spectrum is to show the zero level of the photoionisation signal. The sharp high intensity single peak at 230.1 nm in the spectrum corresponds to the two photon absorption transition that was used in the sensitivity experiments.

5.5.3 Sensitive detection of CO at 230 nm

Two series of sensitivity detection experiments have been conducted using gas samples of CO 20 ppm seeded in the air and CO 200 ppm seeded in nitrogen. The curves of ion signal size versus CO concentration are shown in figure 5.5.3.1 and figure 5.5.3.2. As can be seen from both figures a good linear relationship between ion signal and CO concentration within the experimental error exists. The sensitivities derived from these measurements are 0.6 ppm for CO in the air and 1 ppm for CO in nitrogen. The LODs which were obtained are far below the standard recommended by the authorised UK expert panel: 10 ppm (1994).

5.5.4 CO level determination of real urban air sample

The urban air in Glasgow was sampled in a busy commercial area at a time of 1:30 p.m. using the ionisation chamber. The chamber was evacuated in the lab before sampling on the street. Afterwards it was transported to the street whereupon the valve of the chamber was opened to let the urban air in and then the valve was closed.

The sample was measured at 230 nm, comparing the peak area of the spectrum with that of the standard CO gas (from Linder Gas Ltd UK), see figure 5.5.4.1. The CO concentration of the urban air sample was found to be about 2.5 ppm, an amount well

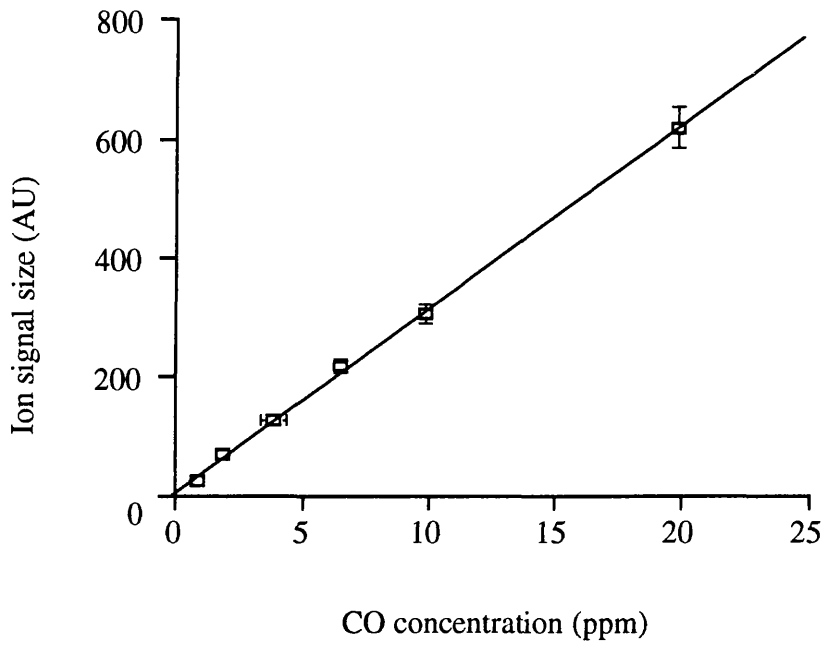

Figure 5.5.3.1 Ion signal size versus CO concentrations for the gas of 20 ppm CO in the air

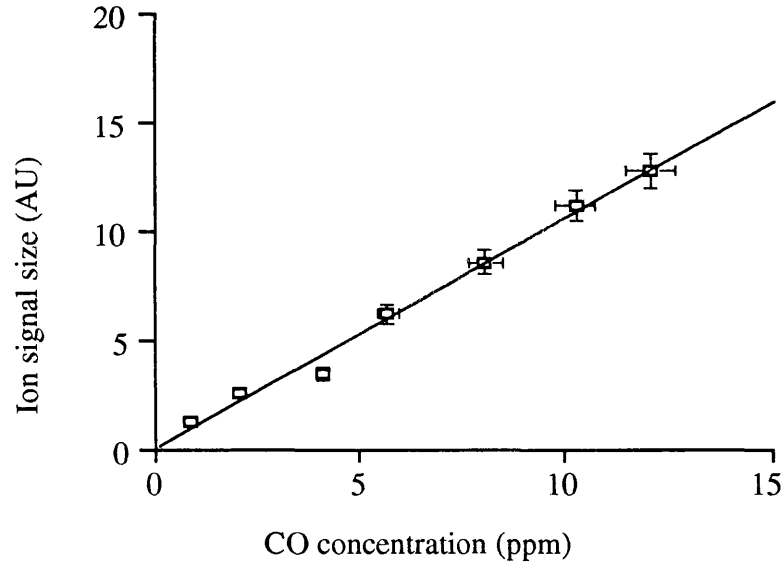

Figure 5.5.3.2 Ion signal size versus concentrations for the gas of 200 ppm CO in N_2. The sample gas was diluted by pure nitrogen with concentration down to under 15 ppm in nitrogen.

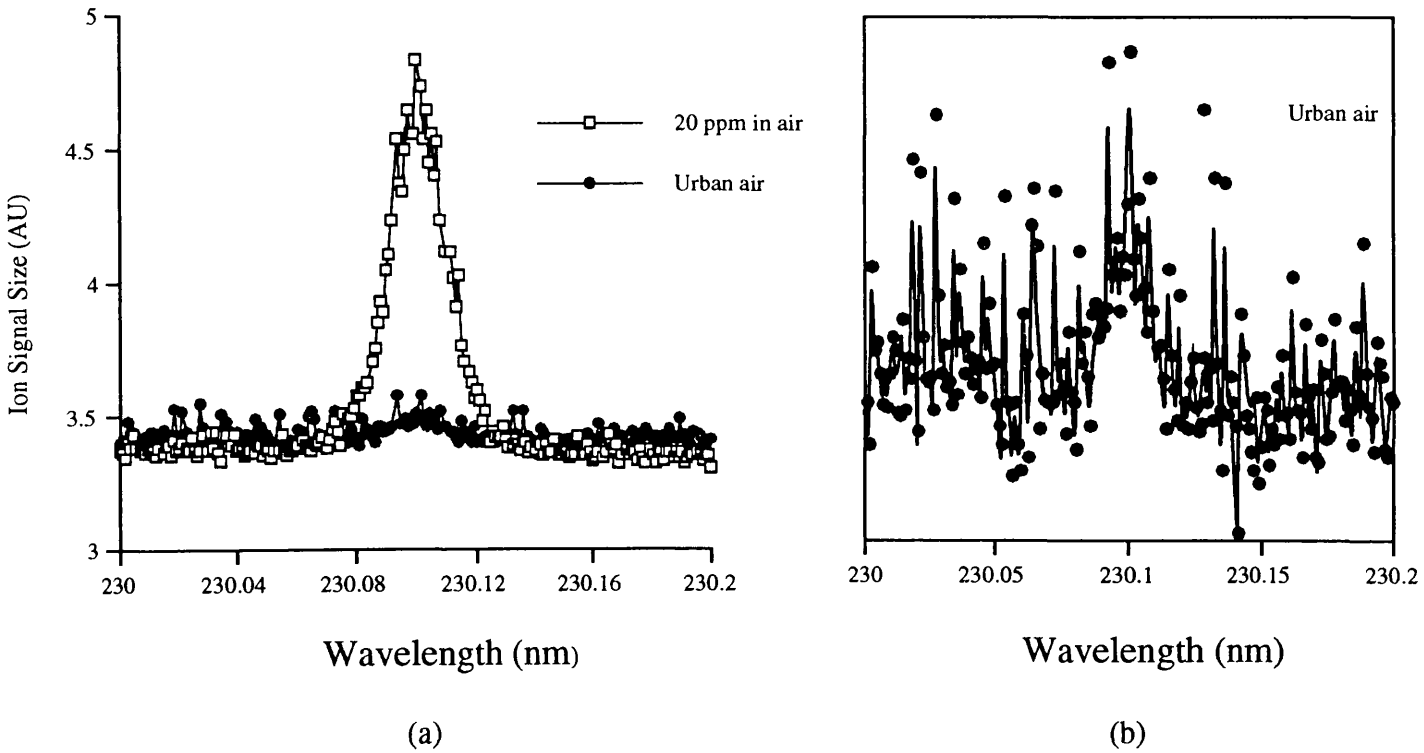

Figure 5.5.4.1 (a) A comparison between 20 ppm CO in the air and the urban street sample, (b) an enlarged diagram of the spectrum for urban air sample. Curve in (b) is obtained by a smoosing procedure.

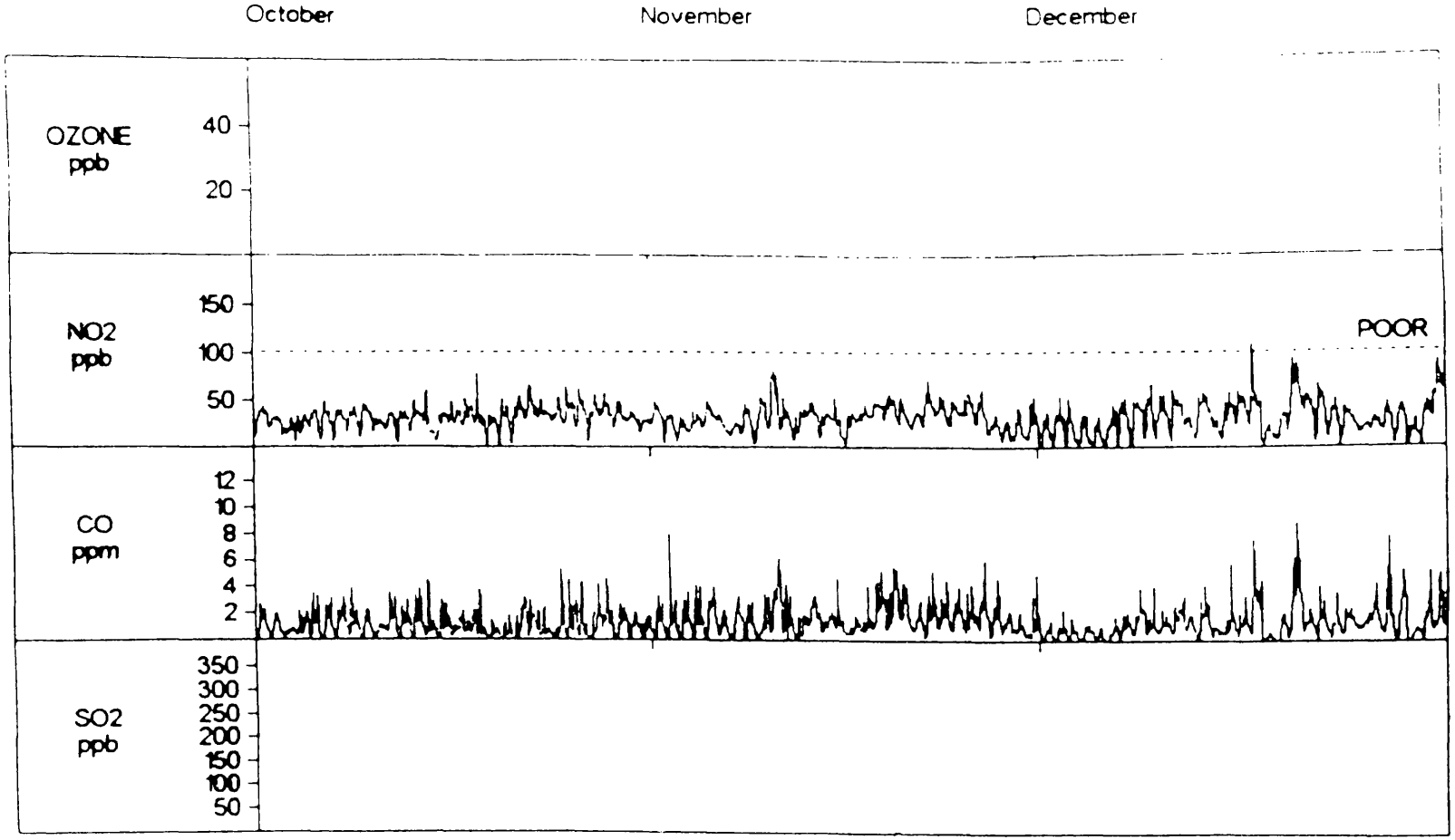

Figure 5.5.4.2. Pollution in Glasgow in 1993. Data supplied by Mr. C. MacDonald on 23rd May 1994. NO_2 was measured by chemiluminiscence and CO by infrared absorption.

below the safety standard of 10 ppm. This is typical of CO pollution in Glasgow (see figure 5.5.4.2)

5.5.5 Mass spectroscopic analysis of the gas of CO in nitrogen

The motivation for conducting CO mass spectroscopic experiment for the gas of 200 ppm CO seeded in nitrogen came from trying to find out the unknown impurities of the sample gas of 200 ppm CO seeded in nitrogen, a product of the UK Linder company. The reason is that when the optical spectra of this sample of gas was recorded, it was found that some extra peaks appeared comparing with the spectrum of the sample gas of CO 20 ppm seeded in the air, see figure 5.5.5.1. By varying the laser wavelength and CO concentration, it was confirmed that the peaks appeared at 230.1 nm on both (a) and (b) belong to CO, but it was uncertain where the peaks 1 and 2 of the curve (b) came from. It was thought that certain impurities were present and a combination of ion chamber and mass spectrometer was used simultaneously in an attempt to identify the impurities. Before determining the mass peaks on the recorded mass spectra, the mass spectrometer must be calibrated. The principle of calibration of the time-of-flight mass spectrometer is rather simple. The time-of-arrival of the ions allowed the determination of unknown masses through the following relationship:

$$\frac{m_1}{m_2} = \left(\frac{t_1}{t_2}\right)^2 \qquad (5.5.5.1)$$

where m is the mass of ions and t is the time of flight. It is preferable that the selection of the mass calibrants should be as close as possible to the mass of the species to be determined.

Nitrobenzene ($C_6H_5NO_2$, Mol. wt. =123) has been chosen as a calibrant for CO gas mass spectra because its photoionisation fragments NO and hydrocarbon groups C_nH_m can give well known mass peaks in the mass region around the CO peak (Kosmidis et al, 1995).

It is supposed that the most probable predissociation pathway of the photochemistry reaction of nitrobenzene at 226 nm is:

$$C_6H_5NO_2 + h\nu \rightarrow C_6H_5 + NO_2 \qquad (5.5.5.3)$$

and

$$NO_2 + h\nu \rightarrow NO + O(^1D) \qquad (5.5.5.4)$$

The evident $C_nH_m^+$ groups are:

C_1 group: C^+, m/z=12; CH^+, m/z=13, CH_2^+, m/z=14; CH_3^+, m/z=15

C_2 group: C_2^+, m/z=24; C_2H^+, m/z=25; $C_2H_2^+$, m/z=26; $C_2H_3^+$, m/z=27

C_3 group: C_3^+, m/z=36; C_3H^+, m/z=37; $C_3H_2^+$, m/z=38; $C_3H_3^+$, m/z=39

C_4 group: C_4^+, m/z=48; C_4H^+, m/z=49; $C_4H_2^+$, m/z=50; $C_4H_3^+$, m/z=51

Figure 5.5.5.2 shows a recorded mass spectrum at 226 nm for the residual nitrobenzene in the mass spectrometer vacuum chamber. In order to see the hydrocarbon peaks clearly the pressure of nitrobenzene in the vacuum chamber was increased.

Once the mass spectrometer has been calibrated, one can determine the unknown mass according to their times of flight.

Figure 5.5.5.3 is a group of mass spectra at different wavelengths. In figure 5.5.5.3, (a) is the spectrum for nitrobenzene at 226 nm . (b) is for the gas 200 ppm CO in nitrogen at 230.1 nm (on resonance). (c) is for CO 200 ppm in nitrogen with a wavelength of 229.87 nm (off resonance) set at peak 1 on figure 5.5.5.1 (b). Figure 5.5.5.3 (d) is a mass spectrum of gas 200 ppm CO in nitrogen with a wavelength, 230.19 nm, at peak 2 on figure 5.5.5.1 (b). From (c) and (d), one can see that there are no extra mass peaks observed other than nitrobenzene background. Moreover, if we set the Boxcar sampling gate at the CO mass peak and then record the optical spectra around 230 nm, we can see that only CO peak appeared on the optical spectra, as figure 5.5.5.4 showed. Both mass and optical analysis where not able to identify the suspected impurities. The explanation for these peaks could be: (1) the impurities which create peaks 1 and 2 are probably some low vapour pressure species which are detectable when in the chamber at atmospheric pressure, but when they were in the vacuum chamber at low pressure they condensed on the inner surfaces of the chamber. (2). The mass of the species is beyond the range of the detector or alternatively the big molecules were fragmented into species which overlapped with the background masses.

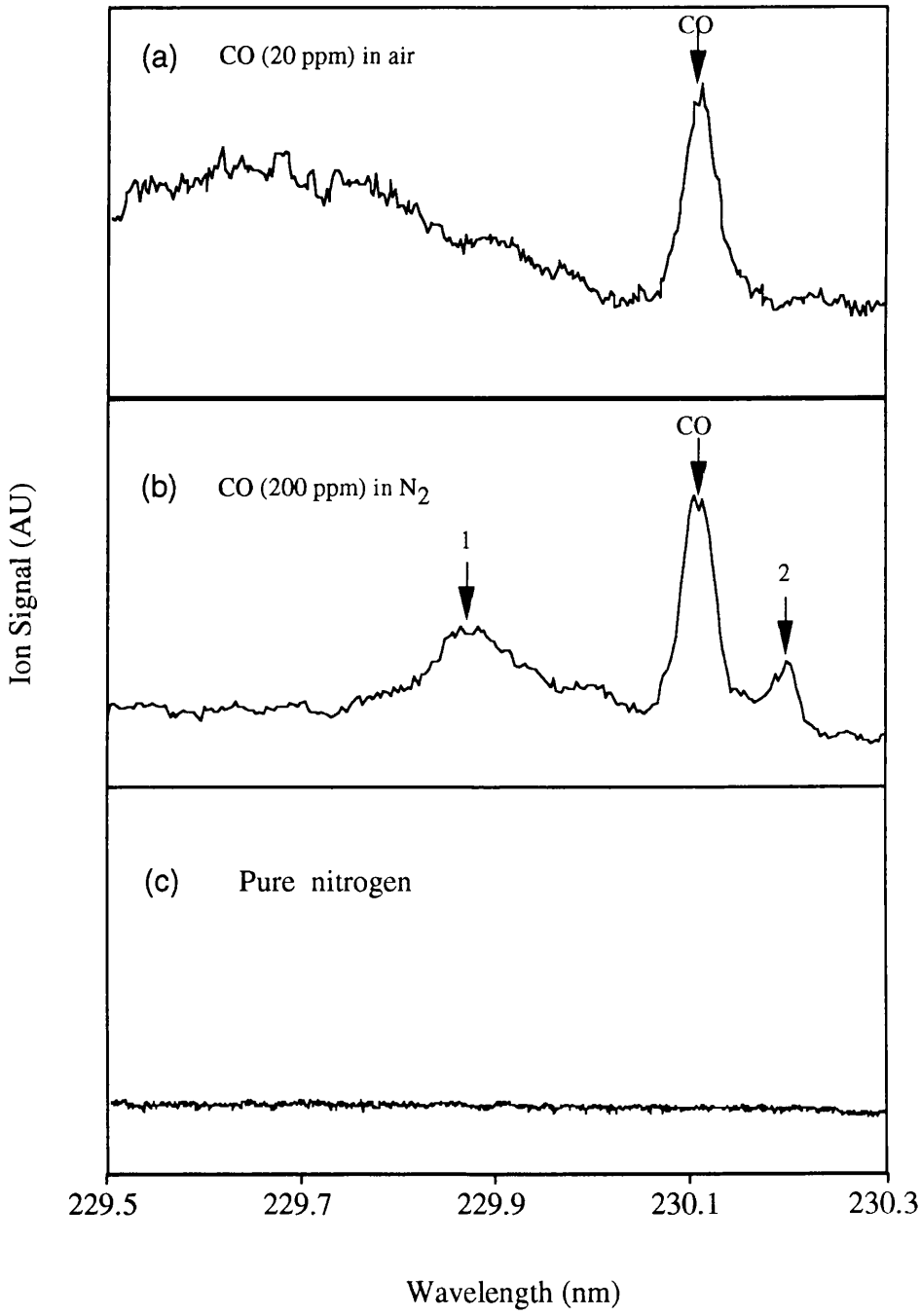

Figure 5.5.5.1 A comparision of the spectra at 230 nm for the gases of 20 ppm CO in air, 200 ppm CO in nitrogen and pure N_2 in an ionisation chamber.

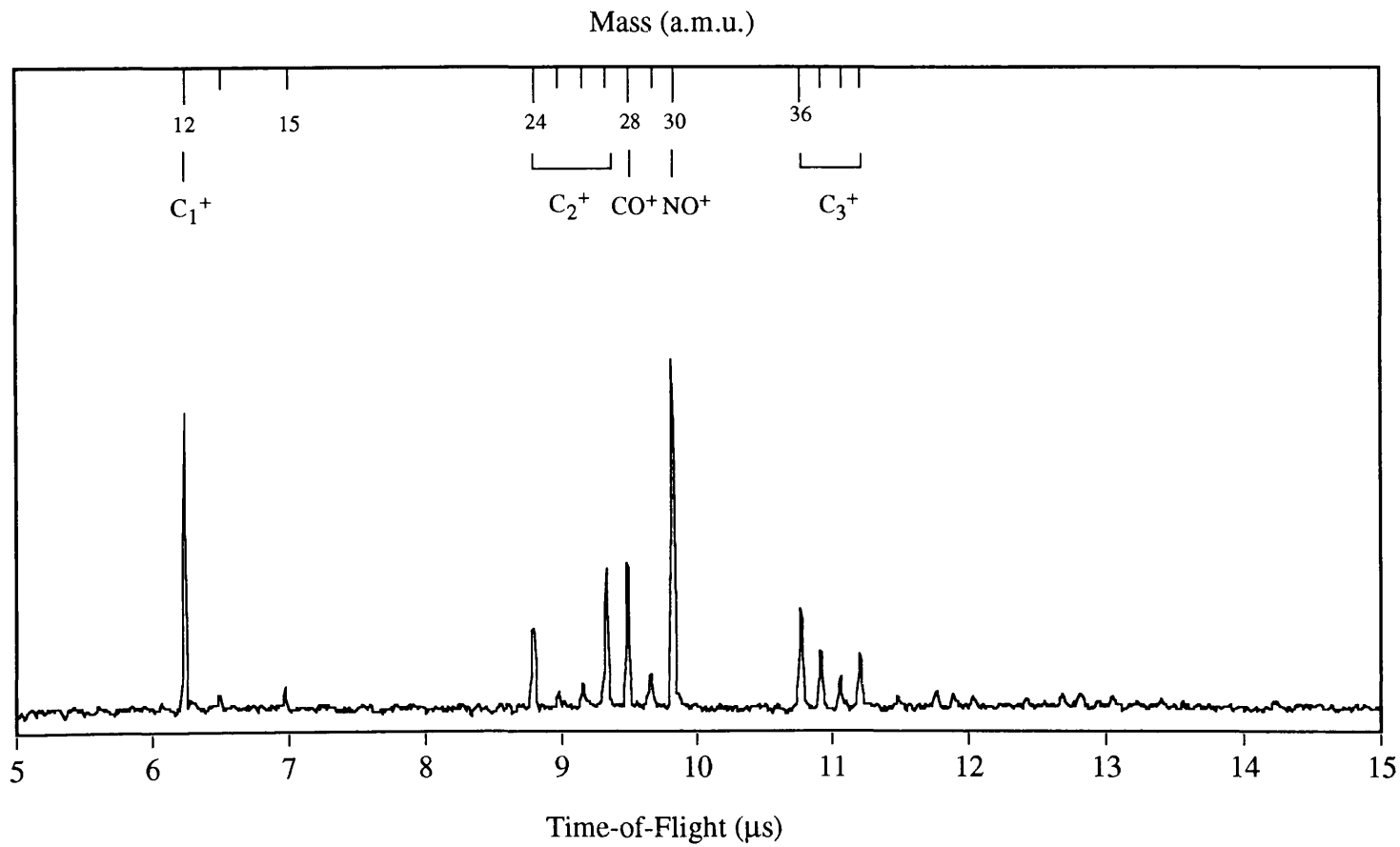

Figure 5.5.5.2 A Time-of-Flight spectrum of nitrobenzene at 226 nm used for mass calibration

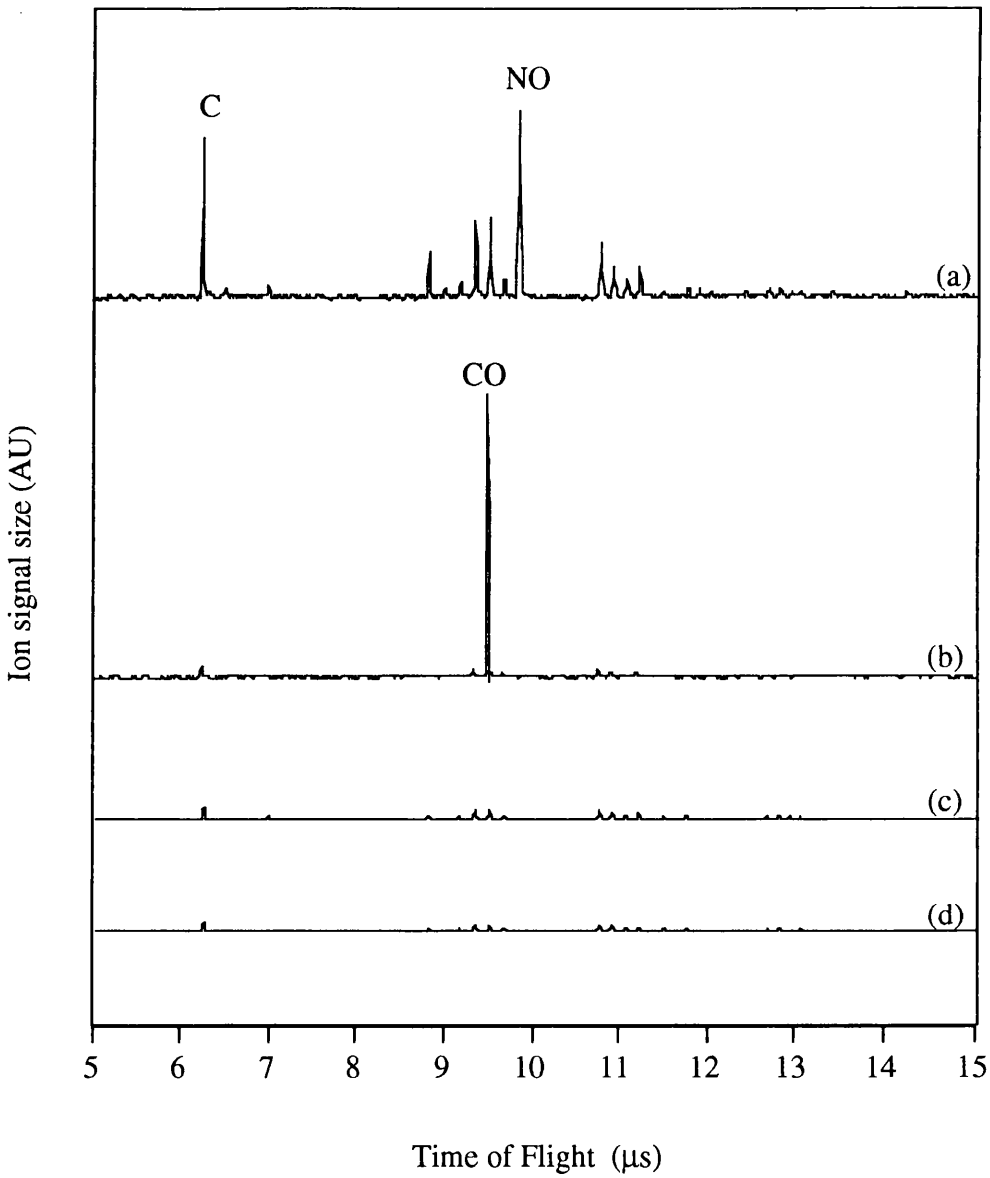

Figure 5.5.5.3 CO mass spectra at different wavelengths. Trace (a) is the mass spectrum of nitrobenzene at 226 nm which gives the mass calibration for all mass spectra in this figure. (b) is the mass spectrum for for the gas of 200 ppm CO in nitrogen with the UV dyelaser set at the CO molecular resonant two-photon absorption wavelength 230.1 nm. (c) is the mass spectrum for the same gas with laser wavelength set at 229. 87 nm which corresponds to the peak 1 on figure 5.5.5.1. (d) is the mass spectrum for the same gas with laser wavelength at 230.19 nm on the peak 2 of figure 5.5.5.1.

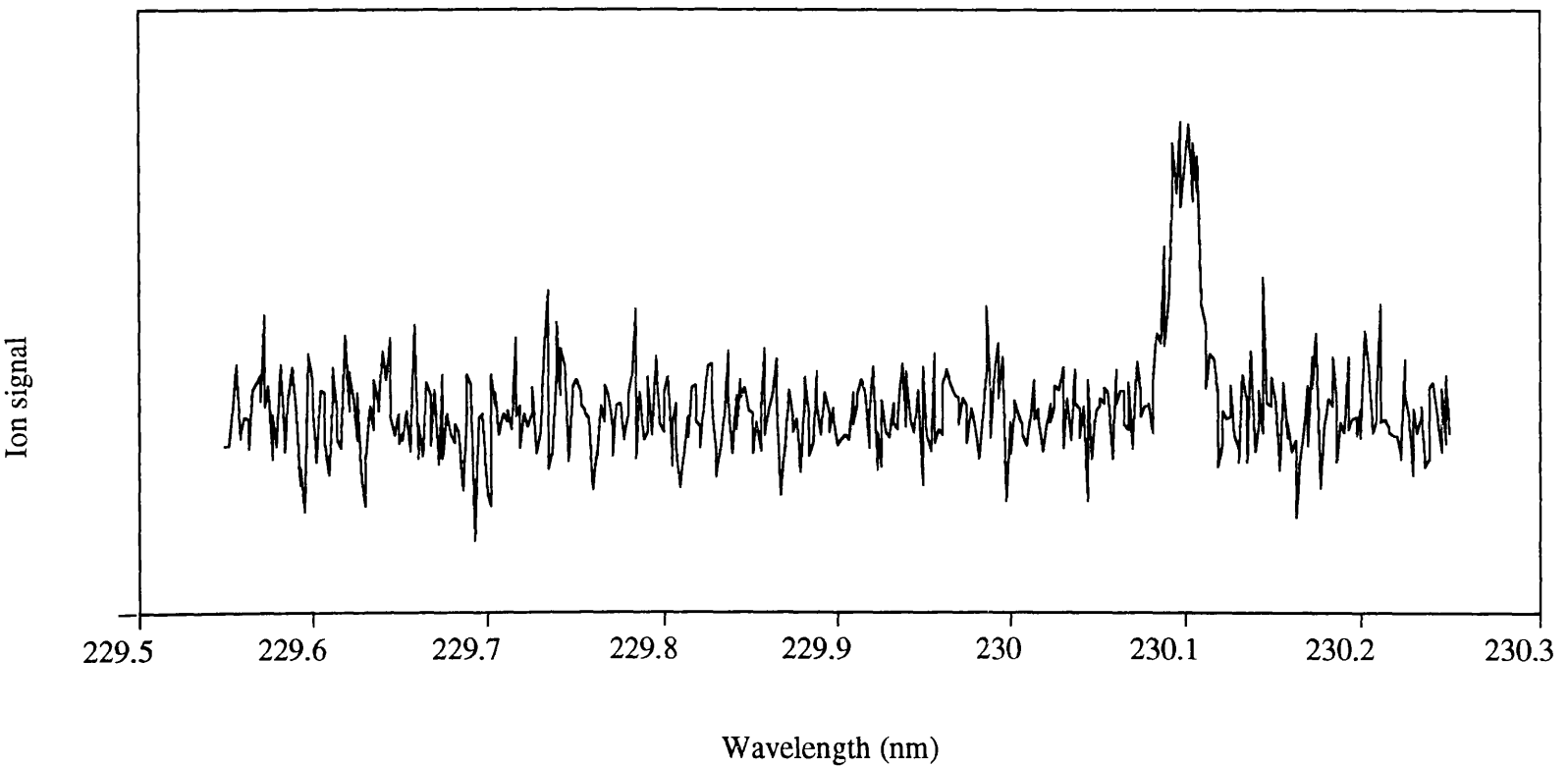

Figure 5.5.5.4 A spectrum around 230 nm of CO molecular spectroscopy taken with the Boxcar samping gate set on CO peak on a mass spectrum.

5.5.6 Laser intensity dependence of CO ion yields at 230 nm

The measurement of the laser intensity dependence of ion yields is normally used as an auxiliary means to study multiphoton process. As was mentioned in chapter 2 it is only for non-resonant multiphoton processes that the laser intensity law follows the relationship of I^n. When one or more resonant intermediate states exist, the power index is usually less than the photon number which is involved in the multiphoton process. Figure 5.5.6.1 shows a graph of ion intensity as a function of laser pulse energy at 230 nm. It can be seen from the figure that the dashed line indicates that the signal is proportional to I^n where n=2.5. This observation is in agreement with Tjossen et al. (1989). Figure 5.5.6.2 shows the laser off resonance intensity dependence close to 230.1 nm. The power law shows n=1.2 in the middle range of the laser energy. The highest pulse energies in the figures correspond to a laser intensity of approximately $3x10^8$ W/cm^2. The data were obtained at the room temperature and at atmospheric pressure for the gas sample of 20 ppm CO seeded in the air.

5.6 Concluding remarks

A 2+1 REMPI process of the CO molecule at 230 nm for the transition of B $^1\Sigma^+\leftarrow$X $^1\Sigma^+$ has been studied by recording the optical spectrum and laser intensity dependence. The limits of the detection (LODs) using a simple ionisation chamber working at atmospheric pressure have been determined for the gas of both 20 ppm CO in the air and the gas 200 ppm CO in nitrogen. The optical spectrum for the gas of 200 ppm CO in nitrogen shows some extra unknown peaks compared with the one for the gas of 20 ppm in the air. In order to work out the identity of these unknown peaks, i.e. to try to find out the impurities in the mixture gas, mass spectra were taken at several wavelengths on the peaks. The results unfortunately shows no extra mass peaks other than background. Possibly explanations for this have been suggested. Finally a real time measurements of the CO content in an urban air sample has been made and this was compared with published CO pollution levels in Glasgow.

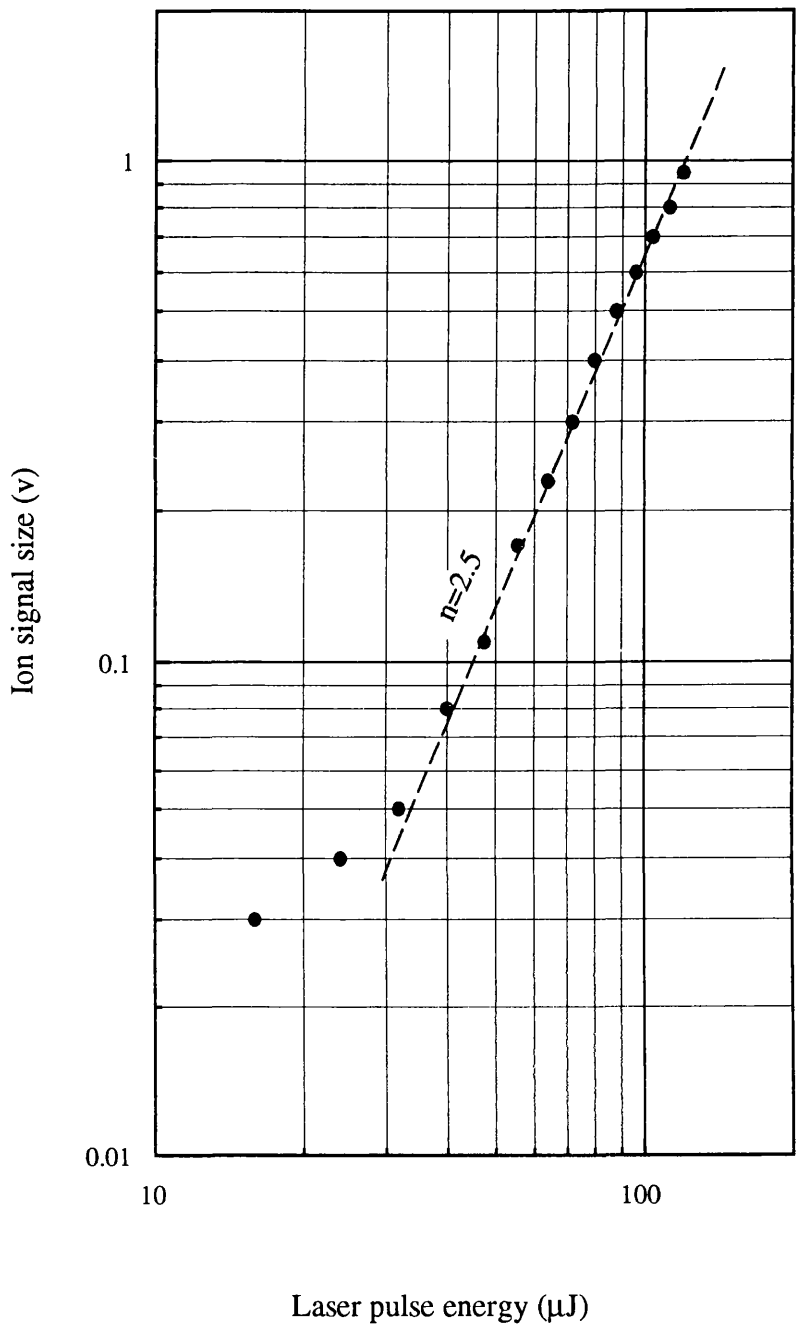

Figure 5.5.6.1 Laser power dependence of the gas of 20 ppm CO in the air whrn the dye laser was set on a wavelength at on resonanace. The power law shows n=2.5 (the slope of the deshed line).

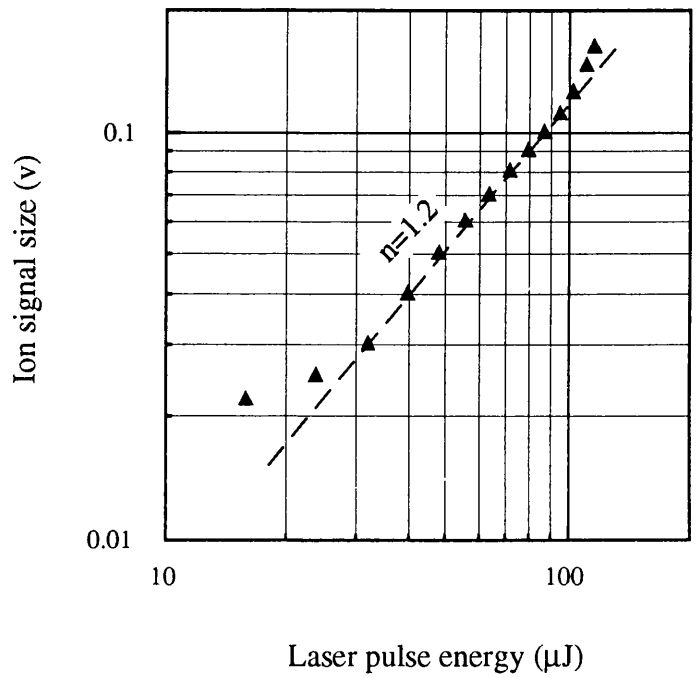

Figure 5.5.6.2 Laser power dependence of the gas of 20 ppm CO in the air when the laser was set on a wavelength at off resonance. In the midle range of the laser energe, the power law shows n=1.2 (the slope of the deshed line)

References:

Baker, J., Lamaire, J.L., Couris, S., Vient, A., Malmasson, D., Rostas, F. (1993)
A 2+1 REMPI study of the E-X transition in CO-indirect predissociations in the E $^1\Pi_1$ state, *Chemical Physics,* **178,** pp. 569-579

Baldacchini, G., D'Amato, F. , De Rosa, M., Nadezhdinskii, A.I., Lemekhov, N. and Sabolev,N. (1996)
Measurement of atmospheric CO concentration with tunable diode lasers *Infrared Physics and Technology,* **37**, No.1, pp. 1-5

Bray, R.G. and Hochstrasser, R.M. (1976)
Two-photon absorption by rotating diatomic molecules, *Mol. Phys.*, **31**, pp. 1199-1211.

Bernheim, R.A., Kittrell, C., and Veirs, D.K. (1978)
Doppler-free two-photon laser excitation of the vacuum ultraviolet absorption spectrum of CO, *J. Chem. Phys.* **69**, pp. 1308-1309

Chen, K-M and Yeung, E.S., (1978)
Rovibric two-photon transitions of symmetric top molecules, *J. Chem. Phys.* **69**, pp.43-52

Dianov-kolokov, V.I. and Yurganov, L.N., (1989)
Spectroscopic measurements of atmospheric carbon monoxide and methane-2. Seasonal variations and long-term trends. *J. Atoms. Chem.*, **8**, pp. 153-164

DiMauro, L.F. and Miller, T.A. (1987)
Laser-induced fluorescence of CO^+ and the CO a $^3\Pi_i$ state produced by multiphoton absorption in a supersonic jet, *Chemical Physics Letter,* **138,** pp. 175-180

Drabbels, M., Heinze,J., Meulen, J.J. and Meets, W.L. (1993)
High resolution double-resonance spectroscopy on Rydberg states of CO, *J. Chem. Phys.* **99**(8), pp. 5701-5711

Ferrell, W.R., Chen, C.H., Payne, M.G. and Willis, R.D. (1983)
Two-resonance step ionisation spectroscopy of CO, *Chem. Phys. Lett.* **97**, pp. 460-466

Fishman J. and Crutzen P.J. (1977)
A numerical study of tropospheric photon chemistry using a one-dimensional model, *J. Geophys. Res.* **82**, pp 5897-5906

Fishman J. , Solomon, S. and Crutzen P.J. (1979)
Observational and theoretical evidence in support of a significant in situ photochemical source of tropospheric ozone. *Tellus,* **31**, pp. 432-446

Fried, A. , Herry, B. , Parrish, D.D., Carpenter, J.R. and Buhr, M.P. (1991)
Inter comparison of tunable diode laser and gas filter correlation measurements of ambient carbon monoxide, *Atmospheric Environment,* **25A**, pp. 2277-2284

Fujii, A., Ebata, T., and Ito, M. (1989)
production of rotationally state selected ions by resonant enhanced multiphoton ionisation of CO in a supersonic free jet, *Chem. Phys. Lett.,* **161**(2), pp. 93-97

Halpern, J.B., Zacharias, H. and Wallenstain, R. (1980)
Rotational linestrengths in two- and tree-photon transition in diatomic molecules, *J. Mol. Spectrosc.*, **79**, pp. 1-30

Haumann, J., Seitzman, J.M., and Hanson, R.K. (1986)
Two-photon digital imaging of CO in combustion flames using planar laser-induced fluorescence, *Opt. Lett.*, **11**, pp. 776-778

Herzberg, G. (1950)
Molecular spectra and molecular structure, 1, Spectra of diatomic molecules, Van Nostrand, Prinston, N.J.)

Hines, M.A., Michelson, H.A., and Zare, R. N. (1990)
2+1 resonantly enhanced multiphoton ionisation of CO via the E $^1\Pi$-X $^1\Sigma^+$ transition: From measured ion signals to quantitative population descriptions, *J. Chem. Phys.* **93**(12), pp. 8557-8564

Hinkley, E.D., and Kelly, P.L. (1971)
Detection of air pollutants with tunable diode lasers. *Science* , **171**, pp. 635-639

Jiang, B., Sha, G., Sun, W., Zhang, C., He, J., Xu. S., and Zhang, C., (1992)
Xenon enhancement and third harmonic generated lines in the 3+m-photon ionisation spectroscopy of CO (A $^1\Pi \leftarrow$ X $^1\Sigma^+$) in CO+Xe mixture, *J. Chem. Phys.* **97**(7), pp. 4697-4703

Khalil, M.A.K. and Rasmussen (1988)
Carbon monoxide in the earth's atmosphere: Indications of a global increase. *Nature,* **332**, pp. 242-245

KlKarim, M.A.A., Khogali, M. and Zeqlam, H., (1991)
Traffic air pollution in Kuwait: preliminary results for nitrogen oxides and carbon monoxide, *The science of the Total Environment,* **106**, pp. 111-119

Kloptek, P. and Vidal. C.R. (1985)
Two-step vacuum-ultraviolet visible excitation spectroscopy on the CO molecule, *J. Opt. Soc. Am.* **2s**, pp. 869-876

Koehoven, S.M., Buma, W.J. and Lange, C. A. (1993)
A (3+1) resonance enhanced multiphoton ionisation study of the C $^1\Sigma^+$ and E $^1\Pi$ states of CO: polarisation dependence used to probe electronic excitation route and electronic character, *J. Chem. Phys.* **99**(7), pp. 5061-5070

Kosmidis, C., Ledingham, K W D, Clark, A., Marshall, A., Jennings, R., Sander, J., Singhal, R. P. (1994)
On the dissociation pathways of nitrobenzene, *Int. J. mass spec. and Ion proc.*, **135**, pp. 229-242

Ku, R.T., Hinkley, E.D., and Sample, J.O. (1975)
Long-path monitoring of atmospheric carbon monoxide with a tunable diode laser system, *Appl. Opt.* **14,** pp. 854-861

Krupenie, P.H. (1966)
The band spectrum of carbon monoxide, Nat. Bur. Stand., NBS 5, Washington, D.C.

Halpern, J.B., Zacharias, H. and Wallenstein, R. (1980)
Rotational line strengths in two- and three-photon transitions in diatomic molecules, *J. Mol. Spectr.*, 79, PP. 1-30

Huber, K.P., and Herzberg, G. (1979)
Molecular Spectra and Molecular Structure, IV, constants of diatomic molecules, Vannostrand-Reinhold, Prinston, N.J.

Loge, G.W., Tiee, J.J. and Wampler, F.B., (1983)
Multiphoton induced fluorescence and ionisation of carbon monoxide (B $^1\Sigma^+$),*J. Chem. Phys.* **79**(1), pp. 196-202

Looney, J.P., Harrington, J.E., Smyth, K.C., O'Brain, T.R. and Lucatorto, T.B. (1993)
Measurement of CO pressure in the ultrahigh vacuum regime using

resonance-enhanced multiphoton-ionisation time-of-flight mass spectroscopy, *J. Vac. Sci. Technol. A* **11**(6), pp. 3111-3120

Meyer, P.M. and Sigrist, M.W. (1990)
Atmospheric pollution monitoring using CO_2-laser photoaccoustic spectroscopy and other techniques, *Rev. Sci. Instrum.* **61(7)**, pp. 1779-1807

Metz, F., Howard, W.E., Wunsch, L. Neusser, H.J. and Schlag, E.W. (1978)
Proc. R. Soc. London Ser. A **363,** pp. 381-

Peng, W.X., Ledingham, K.W.D., and Singhal, R.P. (1997)
Trace CO detection at 230 nm, proceedings of RIS-96, AIP, pp. 219-222

Pratt, S.T., Dehmer, P.M., Poliakoff, E.D. and Dehmer, J.L. (1983)
Photoelectron studies of resonant multiphoton ionisation of CO via the $A^1\Pi$ state, *J. Chem. Phys.* **78**(1), pp. 65-72

Pratt, S.T., Dehmer, P.M. and Dehmer, J.L. (1983)
Two photon resonant, four photon ionisation of CO via the A $^1\Pi$ state with photoelectron energy analysis, *J. Chem. Phys* .**79**(7), pp. 3234-3239

Parrish, D.D., Trainer, M., Buhr, M.P., Watkins, B.A. and Fehsenfeld, F.C. (1991)
Carbon monoxide concentrations and their relation to total reactive nitrogen concentrations at two rural U.S. sites. *J. Geophys. Res.* **96**, pp. 9309-9320

Rinsland, C.P. and levine, J.S. (1985)
Free tropospheric carbon monoxide concentrations in 1950 and 1951 deduced from infrared total column amount measurements, *Nature*, **318,** pp. 250-254

Rottke, H and Zacharias, H (1985)
Sensitive detection of CO by tunable VUV laser excitation of the $B^1\Sigma^+$ state, Opt. Comm., 55, pp.87-90

Sachse, C.W., Hill, G.F., Wade, L.O. and Perry, M.G. (1987)
Fast-response, high-precision carbon monoxide sensor using a tunable diode laser absorption technique, *J. Geophys. Res.* , **92**, pp. 2071-2081

Seitzman, J.M., Haumann, J., and Hanson, R.K. (1987)
Quantitative two-photon LIF imaging of carbon monoxide in combustion gases, *Appl. Opt.*, **26**, pp. 2892-2899

Sha, G., Zhong, X., Zhao, S., and Zhang, C. (1984)
Two-colour resonant multiphoton ionisation study of CO spectroscopy of CO $B^1\Sigma^+ \leftarrow A^1\Pi \leftarrow X^1\Sigma^+$ transitions, *Chem. Phys. Lett.* **110**, pp. 405-409

Spiglanian, T.A., Perry, R.A. and Chandler, D.W. (1987)
Internal state distributions of CO from HNCO photodissociation, *J. Chem. Phys.* **87**, pp.1568-1576

Tilford, S.G. and Simmons, J.D. (1972)
Atlas of the observed absorption spectrum of carbon monoxide between 1060 and 1900 A, *J. Phys. Chem. Ref. Data* **1**, pp. 147-187

Thompson, A. and Cicerone, R.J. (1986)
Possible perturbations to atmospheric CO, CH_4, and OH, *J. Geophys. Res.*, **91**, pp. 10853-10864

Tjossem, P. J.H., and Smyth, K. C. (1989)
Multiphoton excitation spectroscopy of the B $^1\Sigma^+$ and C $^1\Sigma^+$ Rydberg states of CO, *J. Chem. Phys.* **91**(4), pp. 2041-2048,

Warneck, P. (1988)
Chemistry of the natural Atmosphere, Academic Press, San Diago, CA

Westberg, K., Cohen, N. and Wilson, K.W. (1971)
Carbon monoxide: its role in photochemical smog formation, *Science,* **171,** pp. 1013-1015

Wofsy, S.C. (1976)
Interactions of CH_4, and CO in the Earth's atmosphere, *Ann. Rev. Earth Planet. Sci.*, **4,** pp.441-469

Wolk, G.L. and Rich, J.W. (1983)
Observation of a new electronic state of carbon monoxide using LIF on highly vibrational excited CO (X $^1S^+$), *J. Chem. Phys.*, **79**(1), pp. 12-18

Zacharias, H, Rottke, H and Wldge, K.H. (1980)
Photoionisation of CO and NO by tunable VUV laser radiation, Opt. Comm., 35, pp. 185-188

Zander, R., Demoulin Ph., Ehhalt, D.H., Schmidt, U. and Rinsland C.P. (1989)
Secular increase of the total vertical column abundance of carbon monoxide above central Europe since 1950., *J. Geophys. Res.*, **94,** pp. 11021-11028

Chapter 6

Ionisation of Small Molecules in Intense Laser Fields

6.1 Introduction

The study of the interaction of atoms, molecules and clusters with high intensity laser fields is a subject of extensive current interest. Most atoms and molecules ionise rapidly when subjected to laser intensities greater than about 2 x 10^{13} W/cm^2, regardless of the wavelength of the light (Freeman and Bucksbaum, 1991). In intense laser fields, some new phenomena arise, e.g. simple molecules behave like structureless atoms, the ionising of a molecule only depends on the ionisation potential similar to atoms (Ilkov et al, 1992), dissociation takes place after ionisation (Walsh et al., 1993), etc. With the availability of short pulse lasers (picosecond or femtosecond) producing intensities above 10^{13} W/cm^2 in many laboratories, a wide variety of such phenomena have begun to be experimentally explored.

A number of diatomic and triatomic molecules such as H_2 (Codling et al, 1988; Luk and Rhodes, 1988), N_2 (Boyer et al. 1989; Frasinski et al. 1989; Cornaggia et al. 1990; 1991), O_2 (Normand et al. 1991 and Cornaggia, et al. 1991), CO (Cornaggia et al, 1991; Coding et al., 1990; L'Huillier, and Mainfray, 1984; Kumar et al., 1994), NO (He and Becker, 1997), CO_2 and NO_2 (Mathur et al, 1992; Frasinski et al., 1994; Kumar et al., 1994, Vijaylakshmi, et al., 1997) have been ionised using intense laser fields over a range of wavelengths using Nd:YAG, dye and CO_2 lasers, and pulse duration from several tens fs to a few tens nanoseconds.

Experimentally, attention has been focused on fragmentation patterns and the dynamics of the dissociative ionisation process, charge-symmetric and charge-asymmetric fragmentation of multiply charged molecular ions, the kinetic energies of the fragment ions, and measurement of photoelectron spectra (see, for example, Codling and Frasinski, 1993; Cornagia et al 1991; Ditrich and Corkum 1992; Luk et al., 1993 Normand et al., 1992; Zavriev et al., 1990, 1993 and the references therein).

Some applications of intense laser fields to surface analysis have also been reported (see, e.g. He and Becker, 1996).

Since the research with respect to trace analysis in the intense laser fields hasn't reached the stage of quantitative analysis yet, to perform quantitative analysis using intense laser mass spectroscopy, one needs to study the phenomena of molecules in the ultra strong laser fields first. One needs to study ion yields dependence on laser intensities and pulse widths, molecular dissociation pathways, the branching ratio of direct ionisation and dissociation etc.

In recent years, several research groups in the world have directed their efforts at investigating the competition between photoionisation and dissociation in molecular systems, e.g. Becker, Johnson, Ledingham, Mathur and Schlag and their co-workers (References mentioned previously).

Based on a simple kinetic rate picture, it should be possible to increase the intensity of the laser and make the ionisation process compete with dissociation in neutral levels. The photoabsorption rate depends on the intensity of the light used, while the dissociation rate does not. This model predicts that it should be possible to defeat the molecular dissociation process with direct ionisation. Ledingham et al have recently proved this by studying a number of small molecules (NO_2, CO, CO_2, CS_2, etc.).

Besides laser intensity, pulse duration is another factor which effects the competition between direct ionisation and dissociative ionisation. It is known that the dissociation rate of neutral molecules is in picosecond or subpicosecond regime. If the laser pulse duration is longer than the lifetime of the dissociative energy level involved in the interaction of laser and molecules, then the ions from photofragments can be dominant over their parent ions. The effect of the laser pulse duration on the multiphoton ionisation-dissociation (MPID) of benzaldehyde has been investigated by Yang et al (1985), and was carried out by comparing the MPID mass spectra obtained at the excitation wavelengths of 266 nm and 355 nm by a picosecond pulse laser with those obtained previously with a nanosecond pulse laser. Their results suggest that the relative importance of ionisation mechanisms changes with the laser pulse duration.

The small molecule NO_2, with a number of different high intensity laser systems, has been analysed at FORTH (Crete) and at RAL(UK) (Ledingham et al., 1995; Singhal

et al., 1996). In the former experiments, the multiphoton ionisation and dissociation of NO_2 at 248 nm and 496 nm (FORTH) have been carried out for a number of different laser pulse widths from 15 ns - 300 fs with laser intensity up to 2 x 10^{11} W/cm^2 coupled to a time-of-flight mass spectrometry in a molecular beam.

This thesis reports some results concerning the ionisation of small molecules, NO_2 CO, and CO_2, using a femtosecond laser in RAL and a linear mass spectrometer from Glasgow. The ionisation and dissociation patterns at 750 nm and 375 nm, both in vertical and horizontal polarisation have been studied and analysed. (Singhal et al, 1996). The polarisation direction is defined with respect to the plane containing the direction of laser beam and the mass spectrometer axis.

6.2. The femtosecond laser system

The whole experimental system consists of a femtosecond laser system, a linear mass spectrometer system and a digital oscilloscope LeCroy 9304, see figure 6.2. The laser system has been described in chapter 3. Essentially pulses of 45 fs duration are derived from a mode-locked titanium sapphire oscillator pumped with about 7W from an all-lines 'Beamlok' argon-ion laser (both Spectra physics, Mountain View, CA, USA). A simple stretcher, comprising two pairs of BK7 prisms in a double pass arrangement, was used to negatively chirp the pulses to about 700 fs prior to amplification in a three stage dye laser. The dye LDS 751 was used in preference to the higher gain rhodamine 700, normally used at this wavelength, because only the former dye was founded to have sufficient gain bandwidth to support 50 fs pulses. A 4 cm block of SF10 glass served to recompress the pulses down to 50 fs after the amplifier.

Pulses at 375 nm were generated by focusing the output of the laser with a 1m lens (f/50) into a 200 micron thick, type I BBO crystal cut at 28.7 degrees. The 375 nm light was re-collimated with a 0.5 m fused silica lens to give a beam diameter of 1 cm. The 375 nm pulses were directed towards the mass spectrometer with broad band UV mirrors. It was not possible to obtain directly the duration of 375 nm pulses, but spectral measurements give a FWHM bandwidth of 10 THz which is sufficient to support a Gaussian pulse of about 45 fs duration. Before enter the TOF chamber, the 375 nm pulse energy was typically 10 μJ before being focused with a 30 cm fused silica lens. Estimated intensities as high as 5 x 10^{13} W/cm^2 could thus be generated, although smaller pulse intensities were generally used.

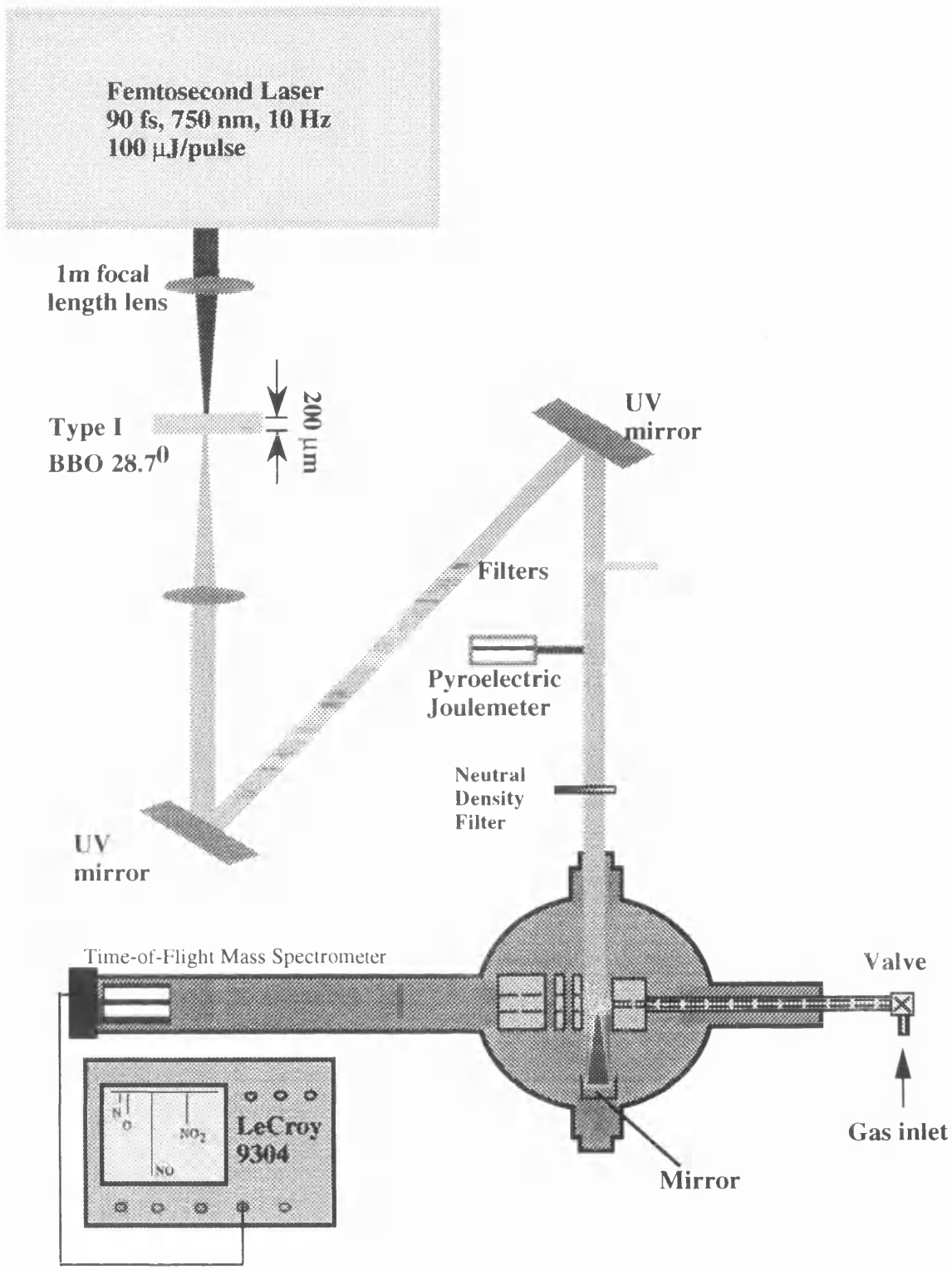

Figure 6.2. Femtosecond Laser Experimental Setup

The mass spectrometer used for femtosecond experiments is the same one which was used in nanosecond experiments as is described in chapter 3 and chapter 5. The only difference is an on-axis reflection mirror with a focal length of 10 cm placed inside the vacuum chamber to focus the incident laser radiation and to produce a laser spot with diameter of 9.15 μm for 750 nm laser beam and 4.75 μm for 375 nm laser beam.

The time-of-flight mass spectra were recorded by taking the electron multiplier output directly into a LeCroy (Chestnut Ridge, NY, USA) 9304 digital oscilloscope and averaging over hundreds of shots.

6.3. Ionisation of NO_2 in femtosecond laser fields

6.3.1. Introduction

The motivation for studying the ionisation of NO_2 in intense laser fields in this work was two fold: firstly to increase the dissociative information above the NO + O threshold and secondly for analytical purpose to determine the ionisation yields for different laser parameters, e.g. laser intensity, wavelength, polarisation etc. The lowest dissociative energy of the NO_2 molecule is 3.11 eV (at the energy level of 25130 cm^{-1}). In the UV and visible region, the molecule is easy to dissociate to its fragments NO plus $O(^3P)$ and NO plus $O(^1D)$. It has been shown that using a nanosecond laser, NO_2 ion signals can never be observed in mass spectra since the maximum laser intensity of a nanosecond laser is not high enough (it is only about 10^{10} W/cm^2) and the lifetimes of the dissociative energy levels are in sub-picosecond regime, see figure 6.3.1. However, in the pico- and femto-second regimes, NO_2 ion signals are detected and increase in size as the laser intensity increases (Ledingham et al, 1995; Kumar et al, 1994). It is easy to reach the higher laser intensities of 10^{12}-10^{15} W/cm^2 using pico- or femto-second lasers which are known to generate large parent signals.

If it is assumed that a laser pulse has both a perfect 'top-hat' cross-sectional spatial and temporal distribution, then the ion yields of non-resonant multiphoton ionisation of a given species scales below saturation has a simple dependence on the ionisation cross-section, laser power intensity and pulse duration, which can be expressed as (He and Becker, 1996)

$$N_{ions} = \rho \sigma I^n \tau \qquad (6.3.1)$$

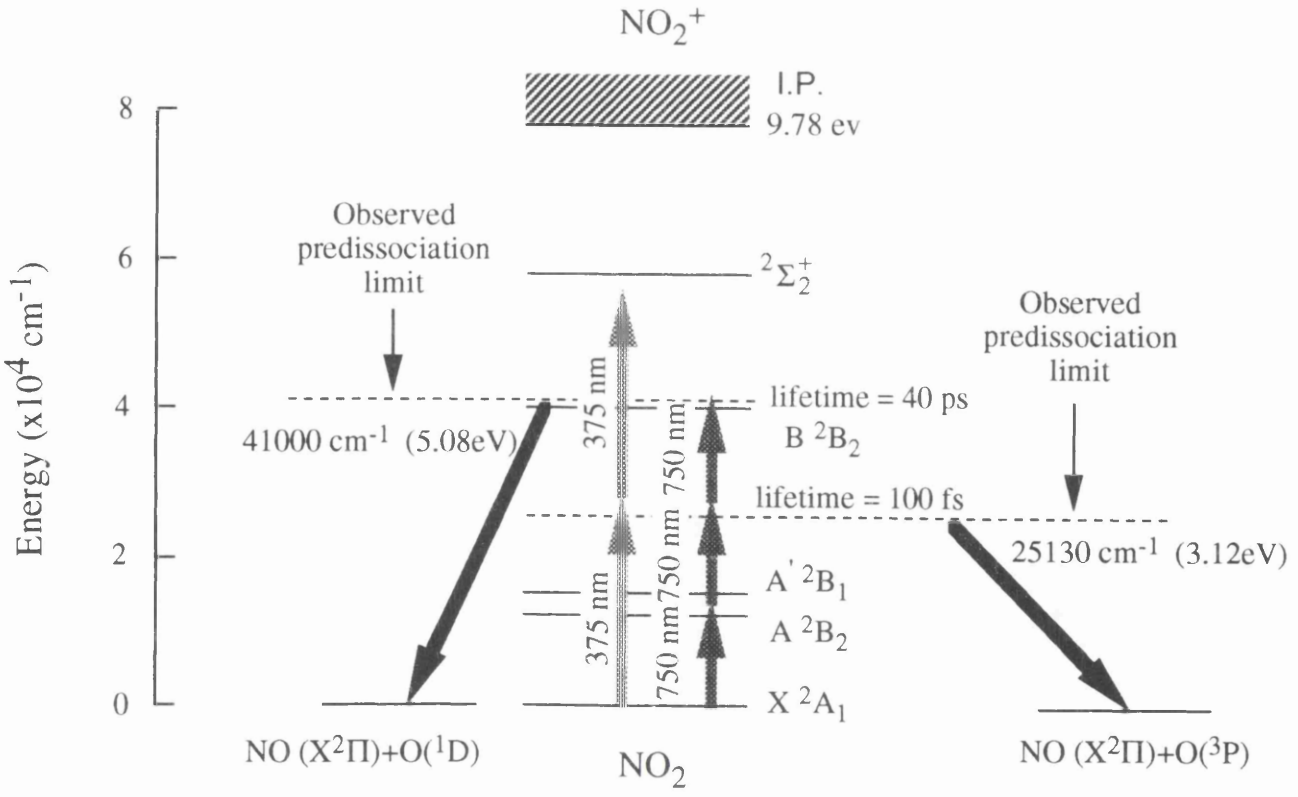

Figure. 6.3.1. Photodissociation of NO_2 molecule at two lower electronic energy levels. One 375 nm photon resonantly excites ro-vibrational levels in ^2B band in NO_2 which has a lifetime in the range of 100 fs.

where, N_{ions} is the number of photons created per unit volume, ρ is the density of the species, σ is the cross-section, I is the laser intensity (power density), n is the order of the process (the number of the non resonant photons absorbed) and τ is the duration of the laser pulse.

For resonant ionisation, the order of the process depends on the degree of saturation, the n number is often smaller then the one for the corresponding non-resonant process in a transition between the same upper and lower energy levels. This effect appeared in the ionisation processes of NO_2.

6.3.2. Experimental results

The results presented below show that the NO_2 molecule can be ionised directly to ions with less dissociation in intense laser fields. The ratio of NO_2^+/NO^+ depends upon the competition between the direct ionisation process and the dissociation process.

There are two possible ionisation pathways for the ionisation of NO_2: (1). Ionisation followed by dissociation (ID); (2). Dissociation followed by ionisation (DI). For the NO_2 molecule, the excited state B $^2B_2$, with term value of 40125.9 cm^{-1} and the transition from ground state to this state is $B^2B_2 \leftarrow X^2A_1$, is a resonant electronic energy level for 750 nm photons. For the NO molecule, the excited state D $^2\Sigma^+$, with term value of 53083 cm^{-1} and the transition from ground state to this state is $D^2\Sigma^+ \leftarrow X^2\Pi$, is a resonant electronic energy level for both 750 and 375 nm photons. The ionisation potential for the NO_2 molecule is 9.78 eV, a minimum of 6 photons is needed to ionise it. The same is true for NO since the I.P. for NO molecule is 9.36 eV, the minimum photon number needed is also 6. The multiphoton ionisation and dissociative ionisation pathways of NO_2 molecule in 750 nm and 375 nm can be seen in figure 6.3.2.1 and figure 6.3.2.2 respectively. In the figures, the black arrow series denote the dominant pathways. In figure 6.3.2.1, B $^2B_2$ is a resonant electronic energy level for the NO_2 molecule with 3 photons at 750 nm and D $^2\Sigma^+$ is a resonant electronic energy level for the NO molecule with a laser wavelength of 750 nm, duration of 90 fs. In figure 6.3.2.2, ro-vibrational levels of B $^2B_2$ are resonant for NO_2 molecule at 375 nm, while D $^2\Sigma^+$ is a resonant electronic energy level for NO molecule at 375 nm. Because 90 fs lasers have a linewidth of $3.3\text{x}10^{12}$ Hz (laser linewidth is $\Delta\nu = \frac{0.3}{90fs} = 3.3\times10^{12}Hz$, or $\Delta\lambda = -\frac{\lambda^2\Delta\nu}{c}$. For 375 nm wavelength,

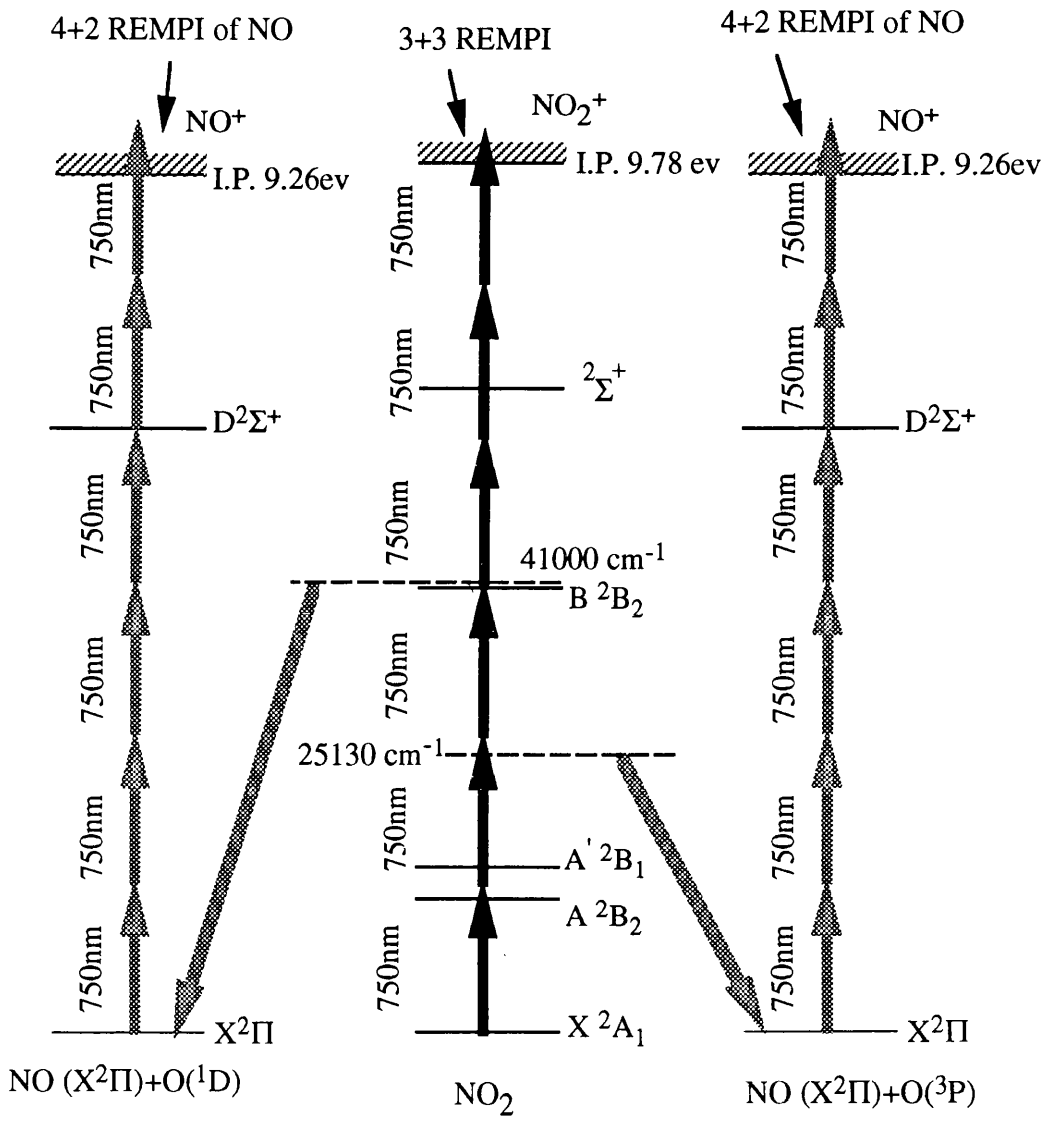

Figure 6.3.2.1 A diagram of multiphoton ionisation of NO_2 gas in a femtosecond laser field with a laser wavelength of 750 nm and horizontal polarisation, the black arrows show the preferable ionisation route which is an ID process. The light arrows denote the dissociative ionisation which are DI processes.

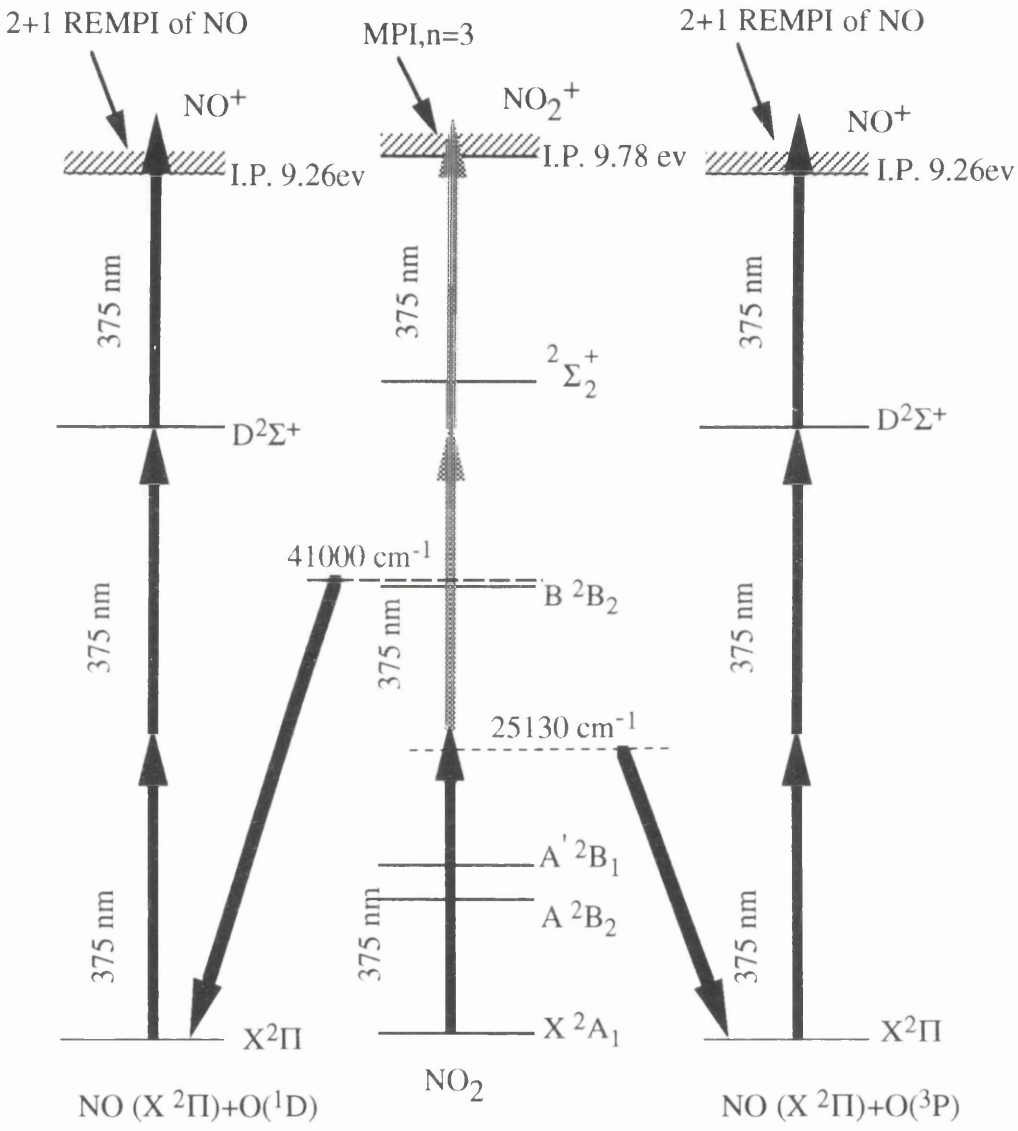

Figure 6.3.2.2 A diagram of multiphoton ionisation of NO_2 in the femtosecond laser field with a wavelength of 375 nm, duration of 90 fs and horizontal laser beam polarisation. The black arrows denote the processes of DI which are dominant over ID at 375 nm.

$\Delta\lambda$=0.15 nm and for 750 nm, $\Delta\lambda$=0.62 nm), the high density of states allows resonant excitation of 2 or 3 photons.

Figure 6.3.2.3 shows four time-of-flight spectra of NO_2 gas in a TOF mass spectrometer at different laser intensities and at the same gas pressures with a laser wavelength of 750 nm, a duration of 90 fs and with horizontal polarisation. In the figure, all the peaks denote ions. From this figure, it can be seen that the intensities of the NO_2 ion (parent) are always greater than the NO ion peaks. That means in the competition of ionisation and dissociation, the ionisation process is dominant. Alternatively, using laser pulses at wavelength 375 nm, the intensity of the NO ions (fragments) are always greater than the parent peaks which means that dissociation wins over direct ionisation, as is shown in figure 6.3.2.4. The intensity of the NO_2 parent ions is dominant over the fragment ions in figure 6.3.2.3 suggesting the following preferable sequential ionisation pathway of NO_2 molecules in the interaction with laser pulses:

$$\begin{aligned} NO_2 &\rightarrow NO_2^+ \\ NO_2^+ &\rightarrow NO^+ + O \,/\, NO + O^+ \end{aligned} \qquad (6.3.2.1)$$

This is an ID process and it is the process expected for trace analysis by femtosecond laser mass spectrometry.

Alternatively in figure 6.3.2.4, the fragment ion peaks are always stronger then the parent ions peaks and this phenomenon suggests that the DI process is more important than the ID process.

The small peaks of O and N ions appearing in the spectra of this figure suggest that there is dissociation to NO neutrals or NO ions i.e.

$$\begin{aligned} NO &\rightarrow NO^+ + e \\ NO^+ &\rightarrow N^+ + O \\ NO^+ &\rightarrow N \; + O^+ \end{aligned} \qquad (6.2.3.2)$$

The laser power dependence of ion signal size has been investigated at different laser wavelengths and polarities. Figure 6.3.2.5 shows the laser intensity dependence of the ion signal size for the laser wavelength of 750 nm and duration 90 fs with both vertical horizontal polarisation. In the figure, squares denote NO ion signals, circles denote NO_2 and crosses denote the ratios of NO_2/NO. All blank symbols denote the

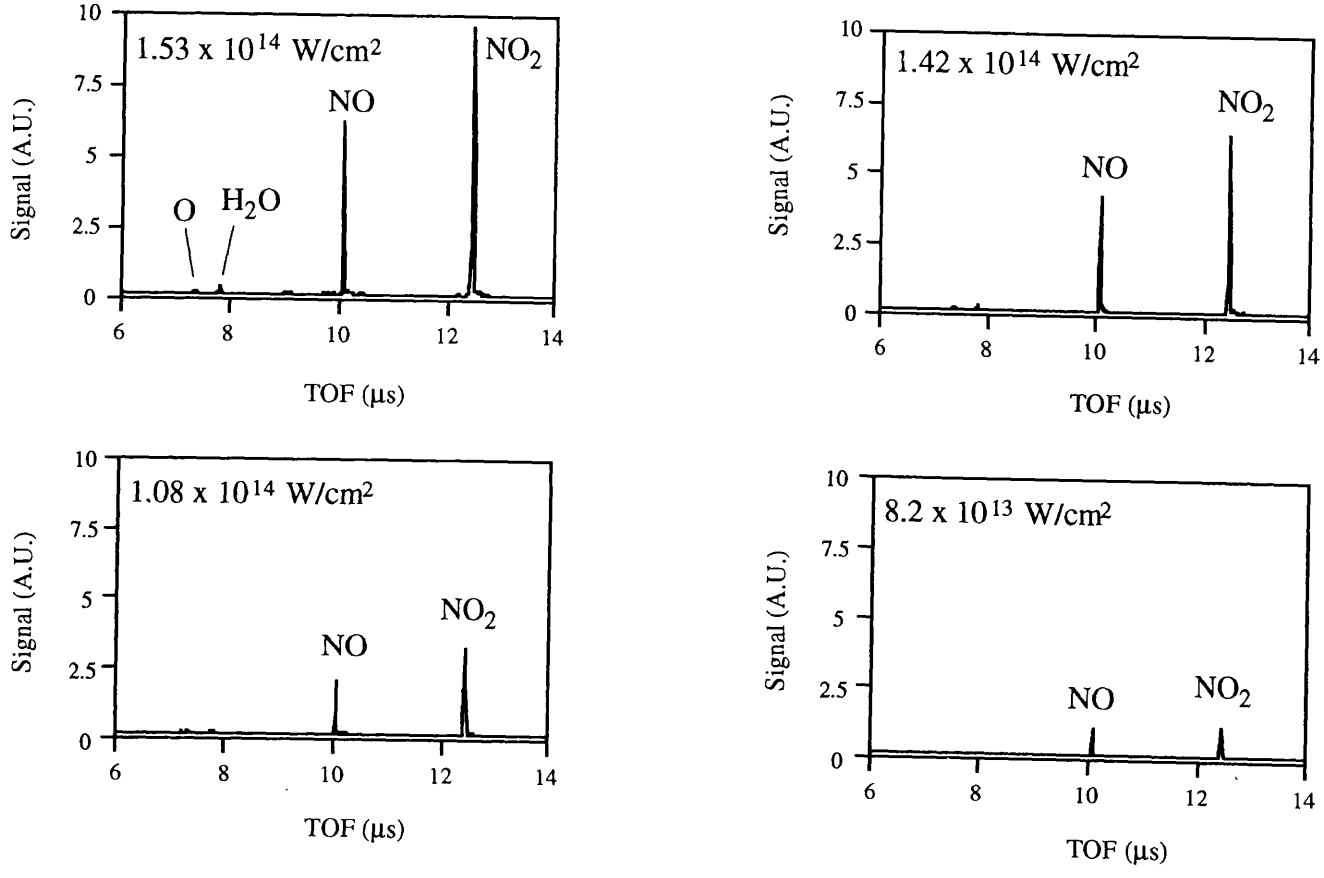

Figure. 6.3.2.3. Time-of-flght (TOF) spectra of NO_2 gas in a TOF mass spectrometer at different laser intensities and at approximately the same pressures. The laser wavelength is 750 nm and the laser pulselength is 90 fs. All the peaks in the graphs denote ion peaks.

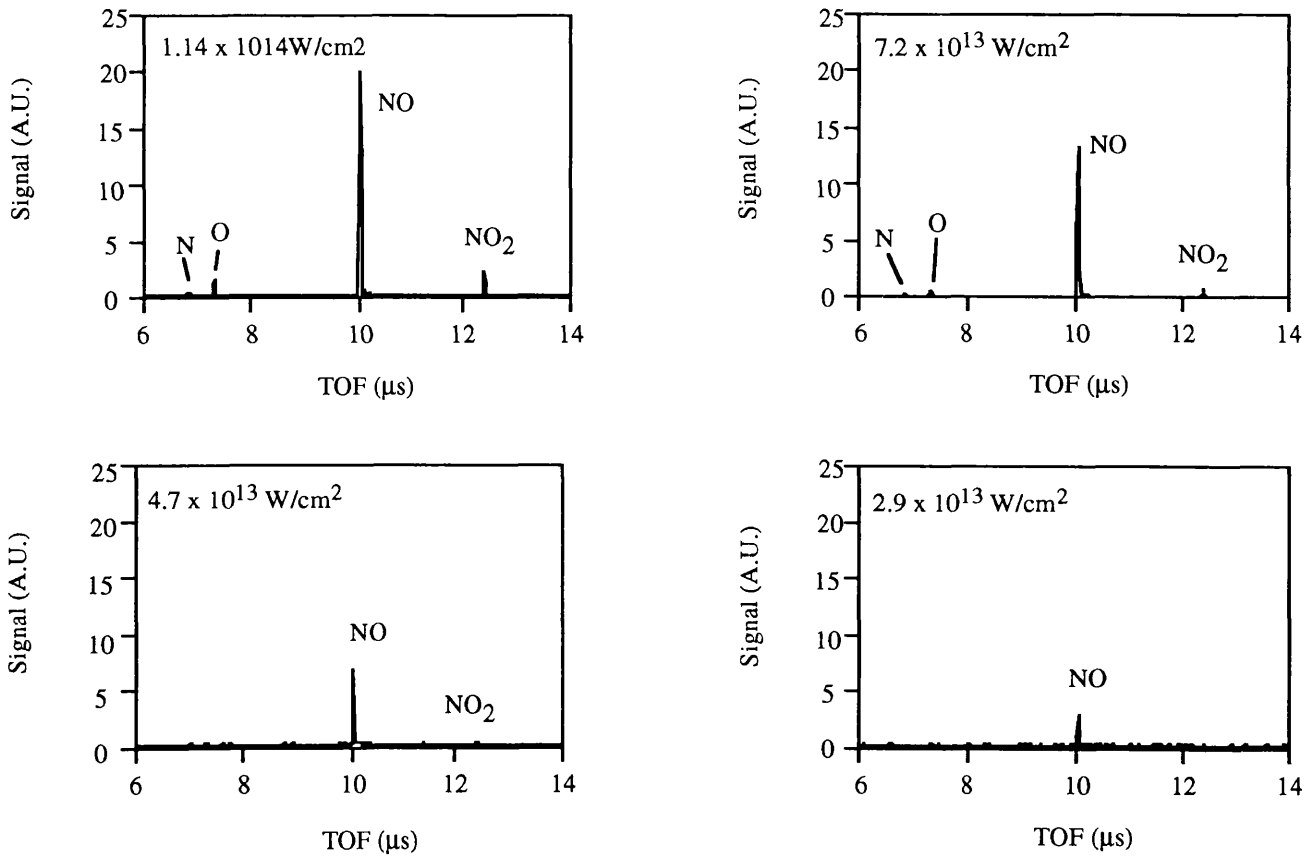

Figure. 6.3.2.4. Time-of-flght (TOF) spectra of NO_2 gas in a TOF mass spectrometer at different laserintensities and at the same pressures. The laser wavelength is 375 nm and the laser pulse length is 90 fs.All the peaks in the graphs denote ion peaks.

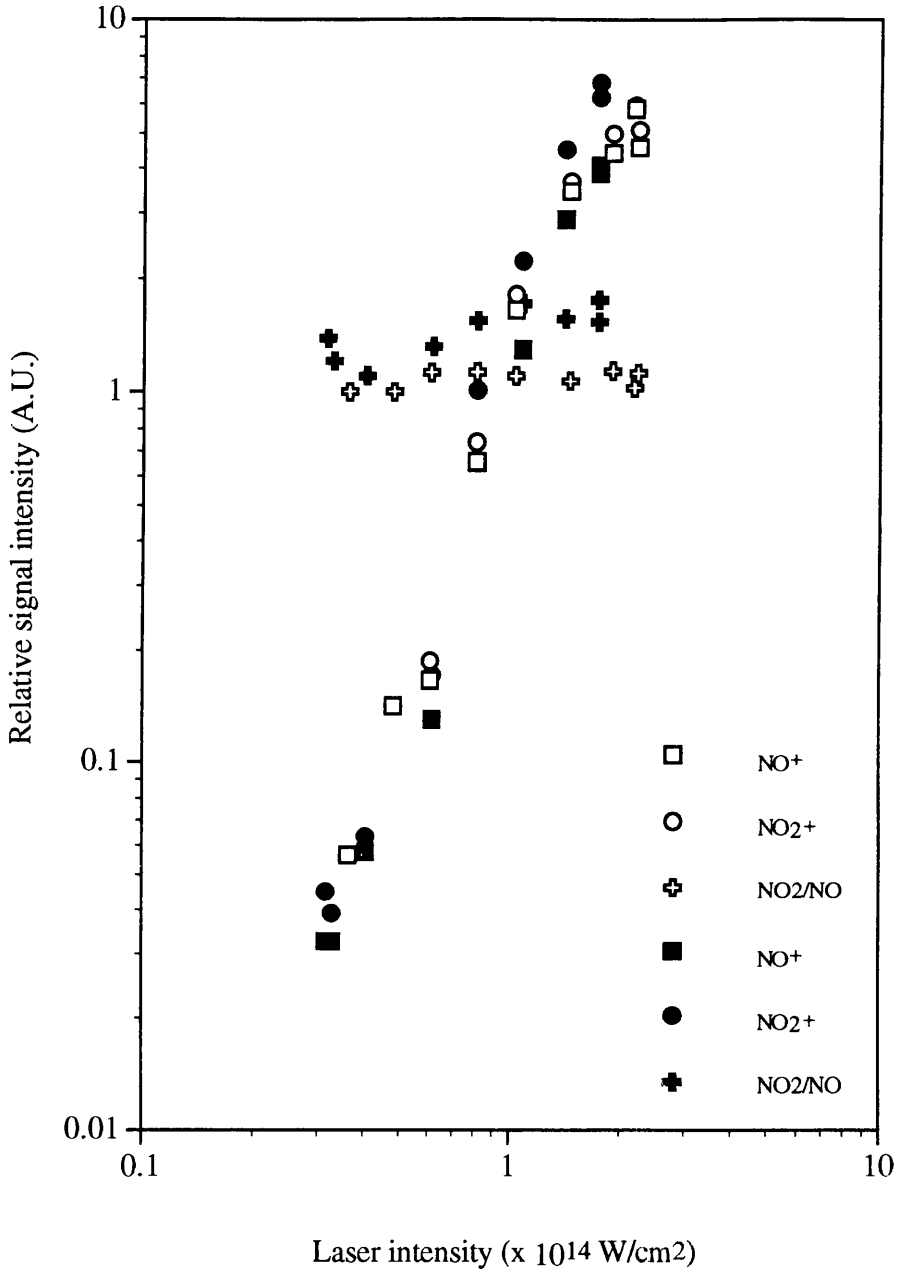

Figure 6.3.2.5 Laser power dependence of ions produced from NO_2 gas obtained at laser wavelength of 750 nm and pulse duration of 90 fs. In the figure, squares denote NO ions, circles denote NO_2 ions and crosses denote the ratio of NO_2/NO. All the empty attributers correspod to vertical polarisation and filled attributers correspod to horizontal polarisation.

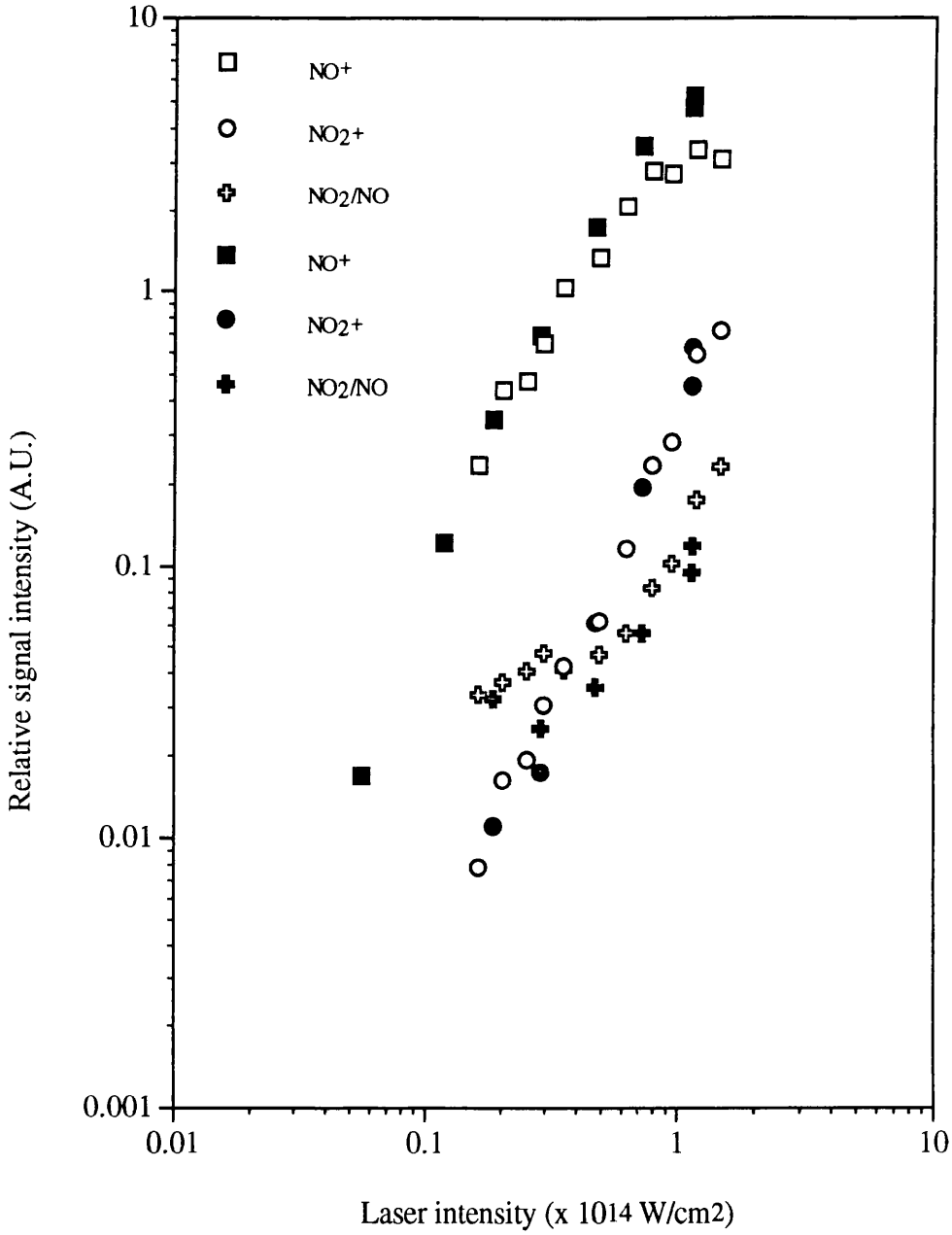

Figure 6.3.2.6 Laser power dependence of ions produced from NO_2 gas obtained at laser wavelength of 375 nm and pulse duration of 90 fs. In the figure, squares denote NO ions, circles denote NO_2 ions and crosses denote the ratio of NO_2/NO. All the open symbols correspond to vertical polarisation and filled symbols correspod to horizontal polarisation.

ions produced using vertical polarised laser beam and all filled symbols denote the ion signals produced using horizontal polarised laser beam. Two features can be seen from this figure: (1). The laser beam polarity doesn't influence the yields of NO and NO_2 very much, the data point scatter is the magnitude of experimental errors. (2). The ratios of NO_2/NO ions basically keep constant with a value of unity at 750 nm with vertical polarisation in the range of laser intensities employed, that means the possibilities of ID and DI process are almost equal.

Either for the ID or DI process the fragmentation ion yields of NO and O should have equal intensities, however they are not. It can be seen from figure 6.3.2.3 and figure 6.3.2.4 that the NO^+ intensity is always much larger than O^+ intensity due to the ionisation potential of oxygen being much higher than NO.

Figure 6.3.2.5 shows the laser power dependence of ions produced from NO_2 gas at 750 nm in a laser intensity range of (3×10^{13} - 2×10^{14}) W/cm^2 and figure 6.3.2.6 shows the laser power dependence of ions produced from NO_2 gas at 375 nm in a laser intensity range of (5×10^{12} - 1×10^{14}) W/cm^2. Each figure shows two data series taken at both vertical and horizontal polarisation at 375 nm. The data in figure 6.3.2.6 shows the same behaviour for the ions with respect to the laser polarisation as figure 6.3.2.5 (at 750 nm), however the laser intensity dependence is somewhat different from the one at 750 nm. At 375 nm, the ratio of NO_2^+/NO^+ is always less than one, which means in the processes of ionisation and dissociation the NO^+ signal intensity is always greater then the intensity of NO_2^+, i.e., dissociation rate is larger than ionisation rate. Below the laser intensity of 6×10^{13} W/cm^2, this ratio changes little ; while above this value, this ratio gets larger as the laser intensity increases. This is because the NO^+ signal begins to saturate above this value of laser intensity, while the NO_2^+ signal does not.

From figure 6.3.2.5 and figure 6.3.2.6, it also can be seen that polarisation does not influence either the NO^+ or NO_2^+ yields, since the curves fitting the data points taken with different polarisation of laser pulse nearly overlap.

Using figure 6.3.2.5 and 6.3.2.6, and fitting the data points of NO_2 and NO to curves, the slopes of the linear segments of each curve are calculated and are taken as the power law of non-resonant multiphoton transition, i.e. the photons absorbed. A compilation of the power laws of NO_2 gas at 750 and 375 nm and at both vertical and horizontal polarisation of laser fields is listed in table 6.3.1.

From table 6.3.1, one can see that:

Table 6.3.1. NO_2 gas ionisation laser power laws

	Laser wavelength , 750 nm		Laser wavelength , 375 nm	
Polarisation	Vertical	Horizontal	Vertical	Horizontal
NO_2	3.5	3.2	2.0	2.3
NO	3.4	3.0	2.0	2.0

(1). For the laser wavelength of 750 nm, both NO^+ and NO_2^+ power law indices $n \geq 3$. From figure 6.3.2.1, it is known that the ID process of NO_2 is a 3+3 REMPI process and the DI process is a 4+2 REMPI process from the ground state of NO. At 750 nm the NO_2^+ power law $n \approx 3$ suggests that for the ID route, either the resonant transition of $B^2B_2 \leftarrow X^2A_1$ or the ionisation from B $^2B_2$ is saturated. Alternatively some of the transitions involved in these two steps are saturated (Singhal, 1997). While the NO^+ power law $n \approx 3$ suggests that in the DI process, the ionisation is saturated. Singhal has proved theoretically that for the ID route, the first two photon absorption is saturated and the remaining four photons absorption is unsaturated. For the DI route, the first four photon absorption is nearly saturated and the two photon absorption is saturated.

(2) The power law for NO_2^+ at 375 nm $n \geq 2$ suggests that, at 375 nm, the ID process is a non-resonant multiphoton process with no saturation, while the DI process is saturated, either in transition step of $D^2\Sigma^+ \leftarrow X^2\Pi$ or in the ionisation step.

Form figure 6.3.2.6, it can be seen that the NO^+ signal becomes gradually saturated while the NO_2^+ signal does not.

6.3.3 Comparison with rate equation model for 375 nm , 90 fs laser pulses

The rate equation formalism described in section 2.8.2 was applied (Singnal et al, 1997) to obtain the predictions for the ion yield curves for NO and NO_2 and the ratio of the two ions as a function of laser intensity for 375 nm and 90 fs laser pulses. These results are compared with the experimental measurements in figure 6.3.3.1 (for NO_2), figure 6.3.3.2 (for NO) and figure 6.3.3.3 (for the ratio of NO_2/NO). The parameters used for the calculations were exactly those which were applied in the

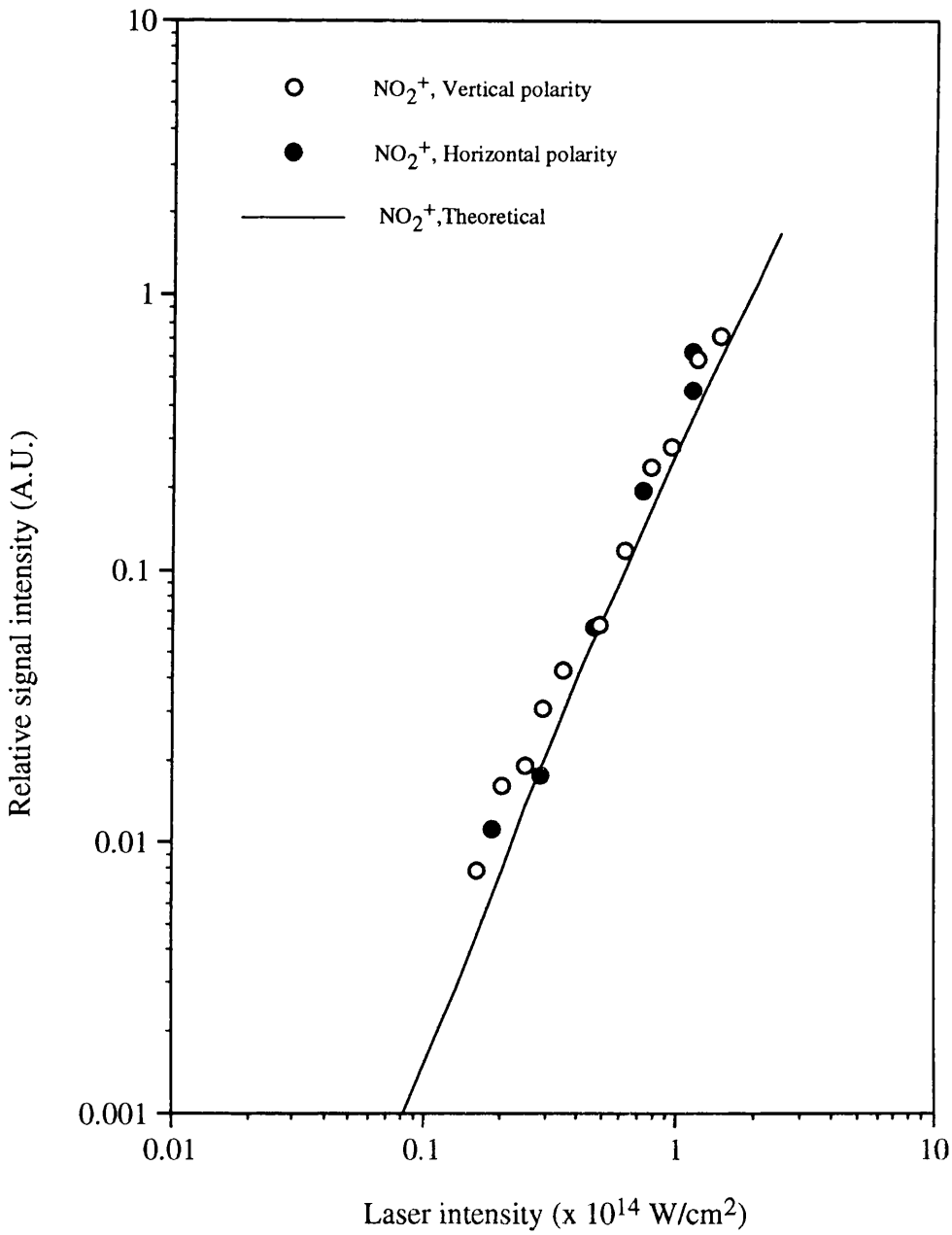

Figure 6.3.3.1 Comparison between experimental and theoretical results forlaser power dependence of NO_2 ions produced from NO_2 gas obtained atlaser wavelength of 375 nm and pulse duration of 90 fs. In the figure, all thecircles denote the experimental data points of NO_2 ions, the same as in figure6.3.2.6 used. The theoretical curve is obtained from the rate equations givenin section 6.3.3.

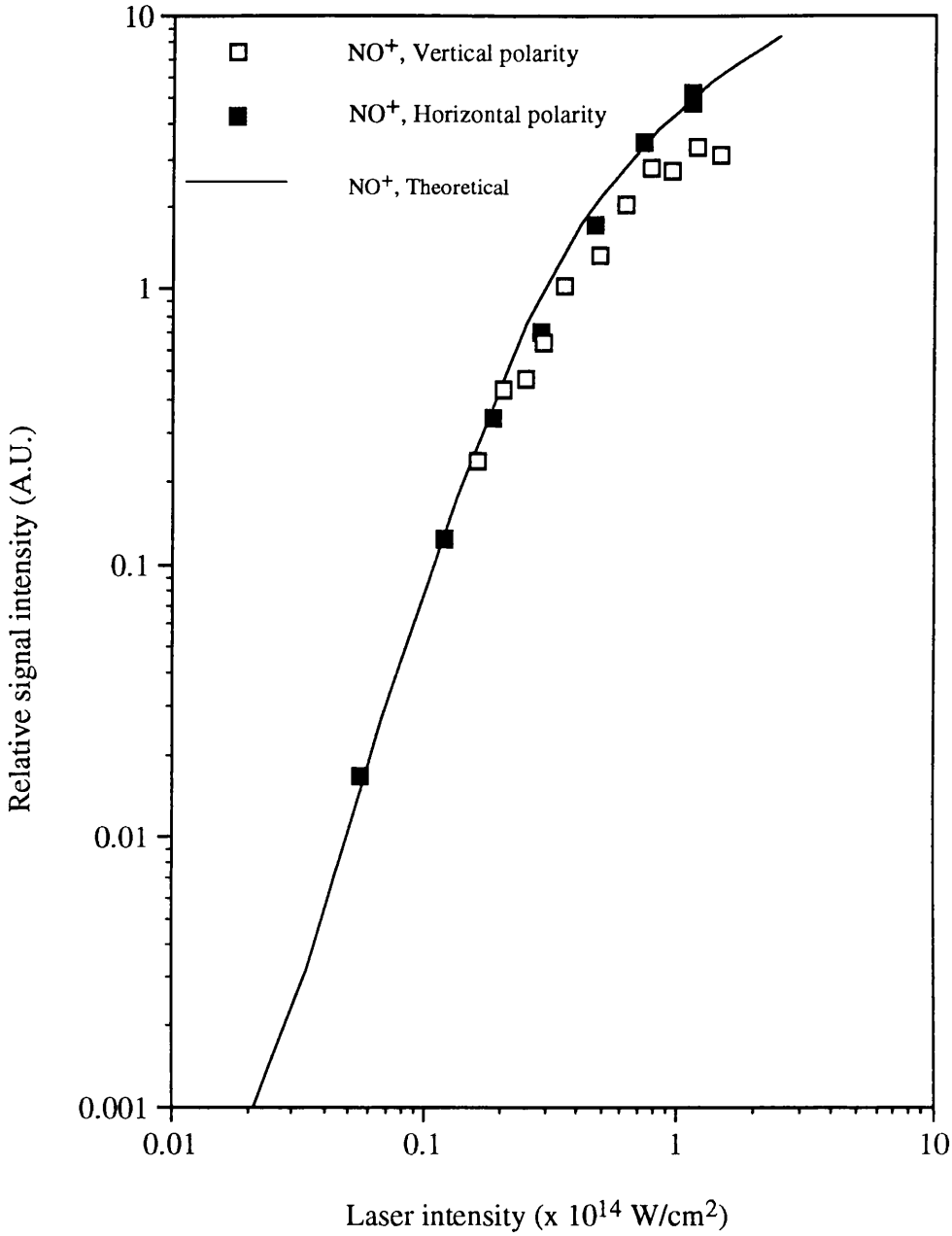

Figure 6.3.3.2 Comparison between experimental and theoretical results for laser power dependence of NO ions produced from NO_2 gas obtained at laser wavelength of 375 nm and pulse duration of 90 fs. In the figure, all the squares denote the experimental data points of NO ions for both vertical and horizontal polarisations, the same as in figure 6.3.2.6 used. The theoretical curve is obtained from the rate equations given in section 6.3.3.

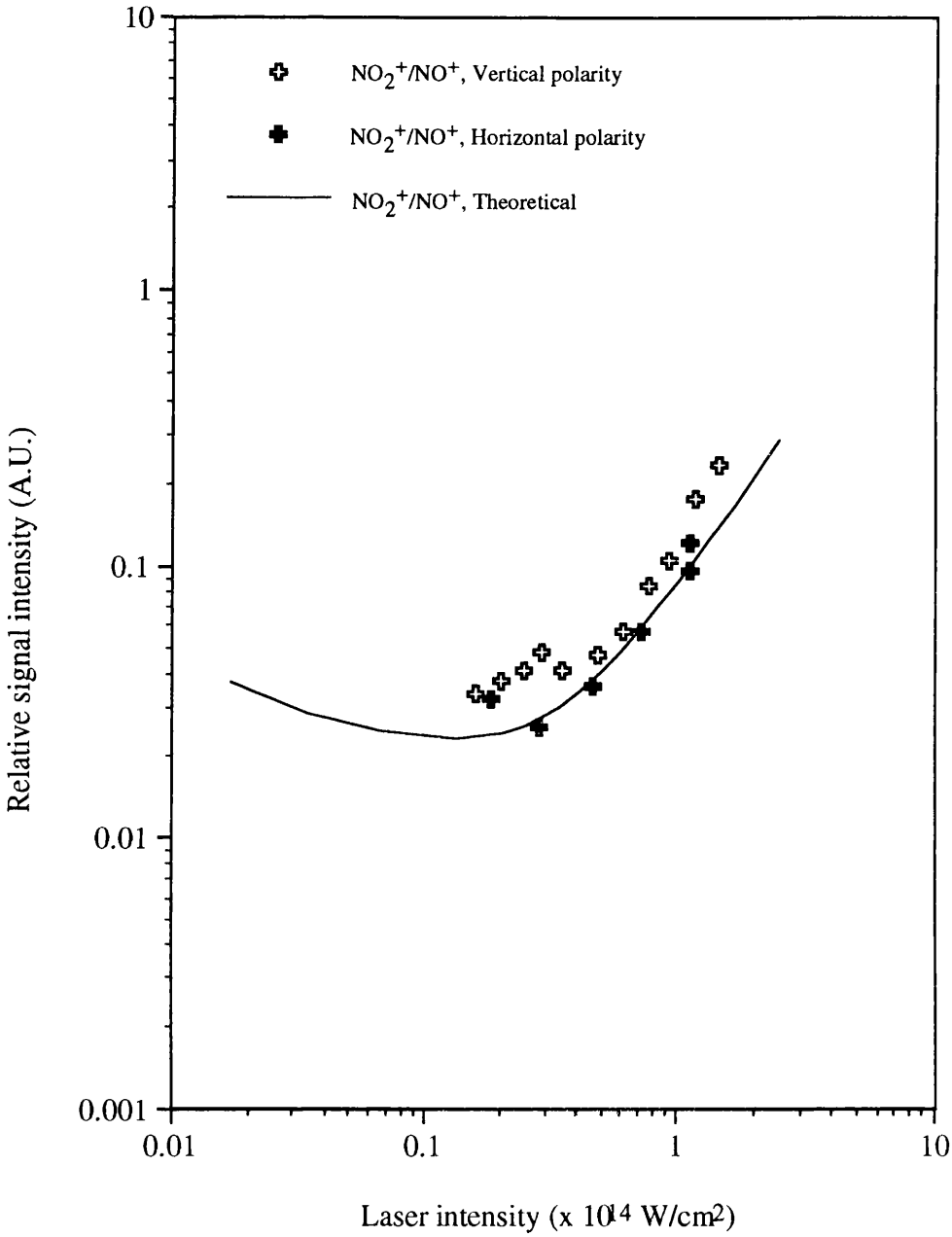

Figure 6.3.3.3 Comparison of laser power dependence of ion yields ratioNO_2/NO for NO_2 gas obtained at laser wavelength of 375 nm and pulseduration of 90 fs. In the figure, all the symbols denote the experimental datapoints, the same as in figure 6.3.2.6 used. Theoretical curve is the resultsobtained from the rate equations model given in section 6.3.3.

analysis of the previous lower intensity data by Singhal et al. (1996). These are listed in the following:

$$\sigma_{01} = 3.2 \times 10^{-19} cm^2$$

$$\sigma_{12} = 10^{-53} cm^4 s$$

$$\sigma_{34} = 4.8 \times 10^{-51} cm^4 s$$

$$\sigma_{45} = 9 \times 10^{-8} cm^2$$

$$k_p = 2.76 \times 10^{12} s^{-1}$$

The time profile of the laser pulse was assumed to be $Sech^2$ and the spatial profile was taken to be a Gaussian of waist size 4.75 microns.

It is apparent from Figure 6.3.3 (1-3) that the parameters appropriate to describe the low intensity data also provide an acceptable description of the new higher intensity data. however there is some improvement which could be obtained as the strengths of NO and NO2 ions is not exactly reproduced. This may be either because of the deficiency in the parameters used in the calculation or may reflect a deficiency in the model assumptions. For example, the direct ionisation route in both NO and NO2 was not considered in the calculations and at the high intensities employed in the new measurements, this route might contribute significantly. Extension of the model to include this route is being undertaken.

6.4. Ionisation of CO_2 in femtosecond laser fields

The detection of carbon dioxide (CO_2) is of general interest since this gas is ubiquitous in the atmosphere as a product of photochemical processes, playing an important role in the life cycle, the greenhouse effect, and combustion process.

Carbon dioxide is transparent in the visible and near-ultraviolet regions. The lowest energy absorption falls into two regions, 175-140 nm and 139-124 nm (Herzberg, 1966), however the absorption spectrum in the vacuum ultra-violet region is quite complex. Obviously, it is not possible to detect CO_2 using conventional optical absorption spectroscopy. REMPI is a good technology to detect and study molecules, but for CO_2 only a few energy levels can be used as intermediate states with nanosecond lasers in the visible or UV region (e.g. Wu and Johnson, 1989). This is

because the ionisation potential of CO_2 is rather high and almost all of its excited states are predissociative. Therefore a relatively high laser power is needed for ionisation to proceed on the same time scale as dissociation.

The ionisation of CO_2 in intense laser fields has been studied by Walsh et al (1993) to explain the ionisation mechanisms, Cornaggia (1994) et al for investigating the laser-induced Coulomb explosion, Frasinski et al (1994) for the multielectron dissociative ionisation in intense laser fields, Becker et al (1996) for surface analysis and Kumar et al (1994) for the dissociation by intense laser fields. The motivation for the present work is directed at the trace analysis of carbon dioxide.

6.4.1. About the CO_2 molecule

A schematic diagram of the potential energy curves for the ground state and the lowest excited states (modified from a paper by Harding et al, 1988) is shown in figure 6.4.1. It can be seen from this figure that the lowest dissociative electronic energy level is at 43983 cm^{-1} which is equivalent to 5.45 eV and a higher one is at 59873 cm^{-1} equivalent to 7.42 eV. If photodissociation proceeds, a minimum number of four 750 nm photons or two of 375 nm photons are needed. The photodisociation mechanisms are:

$$CO_2 + nh\nu \rightarrow CO(^1\Sigma^+) + O(^1D) \qquad (6.4.1.1)$$

and/or

$$CO_2 + nh\nu \rightarrow CO(^1\Sigma^+) + O(^3P) \qquad (6.4.1.2)$$

To determine which reaction is the dominant one, the measurements of the quantum yields of $O(^1D)$ and (^3P) ions are needed and that work is beyond the scope of this thesis.

In intense laser fields, the direct ionisation can dominate photodisociation and the CO_2 molecules can be ionised directly, i.e.

$$CO_2 \rightarrow CO_2^+ + e \qquad (6.4.1.3)$$

The ionisation mechanism will be discussed in next paragraph

6.4.2. The studies of the mass spectra in femtosecond laser fields

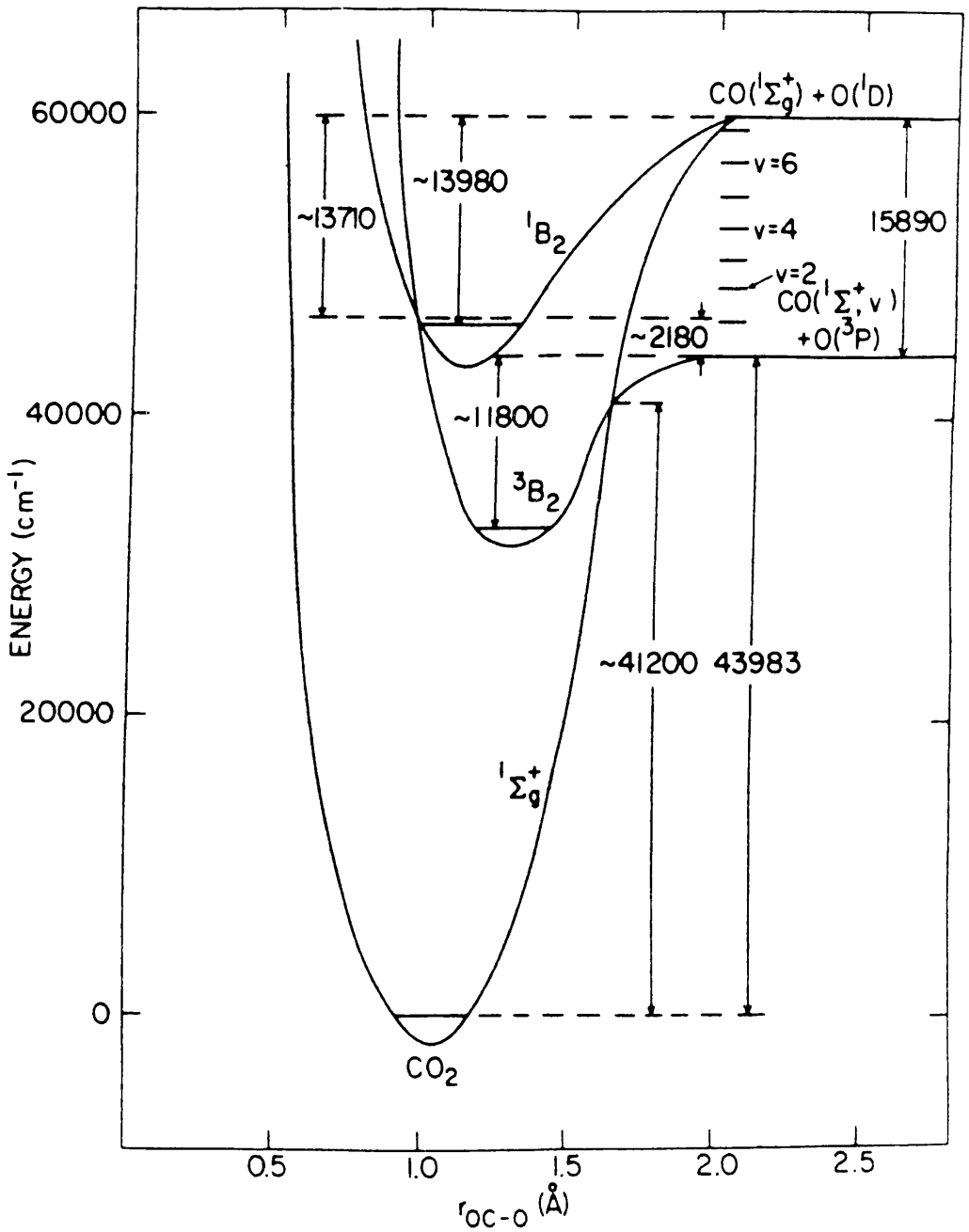

Figure 6.4.1 Potential energy curves of CO_2, taken from Harding et al (1988).

Figure 6.4.2.1 shows a time-of-flight spectrum and its two magnified spectra (10 times and 100 times respectively). This spectrum was obtained at a laser intensity of 2.1 x 10^{14} W/cm^2 with a wavelength of 750 nm, pulse duration 90 fs and vertical beam polarisation under a pressure of 6.9 x 10^{-5} Torr. All the ion products are shown on figure (a), (b) and (c). From figure 6.4.2.1 (a), it can be considered that the H_2O^+ and O_2^+ peaks came from the background gas in the vacuum chamber since these two peaks appears on all mass spectra. The peak corresponding to m/z=40 and marked by "?" will be explained in the section of discussion. All other ion peaks came from the ionisation of CO_2 gas. In figure 6.4.2.1 (b), the two small peaks situated on the shoulder of CO_2 peak are from the isotope molecules of carbon and oxygen. In figure 6.4.2.1 (c), a tiny C^+ peak can be seen (only at a magnification factor of 100).

Figure 6.4.2.2. shows the time-of-flight spectra of CO_2 gas obtained at the three laser intensities, 2.1 x 10^{14} , 1.4 x 10^{14} and 5 x 10^{13} W/cm^2 respectively at a wavelength of 750 nm and with a pulse duration of 90 fs. Figure 6.4.2.2 (a) and (b) are the same spectrum, but with different magnification factors; for (a) the factor is 1 and for (b) is 10. Figure 6.4.2.2 (c) was taken at a laser intensity of 1.4 x 10^{14} magnified x10 and (d) at 5 x 10^{13} W/cm^2 magnified x100.

Comparing figure 6.4.2.2 with a CO_2 mass spectrum (figure 6.4.2.3), obtained by Becker at all, 1996, using a 32 ps laser it can be seen that in the present case the parent CO_2^+ peaks always dominate over fragment CO^+ peaks. However in Becker's work, there is no significant difference between the heights of these two ion peaks, even at a higher laser intensity (1.39 x 10^{15} W/cm^2) than in the present work. A conclusion can be drawn from this comparison that for CO_2 molecules, ID dominates over DI when using a femtosecond laser.

In addition, double charged CO_2 ions appeared in our experiments, which suggest the following pathway:

$$\begin{aligned} CO_2 + nh\nu &\rightarrow CO_2^+ + e \\ CO_2^+ + nh\nu &\rightarrow CO_2^{2+} + e \end{aligned} \qquad (6.4.2.1)$$

Figure 6.4.2.4. shows the laser intensity dependence of the ion signal sizes of the CO_2 parent ions and CO fragment ions. The data were obtained using 750 nm laser pulse with a duration of 90 fs. In the figure, all the empty symbols denote the data taken using vertically polarised laser beam and all the filled symbols denote the data taken

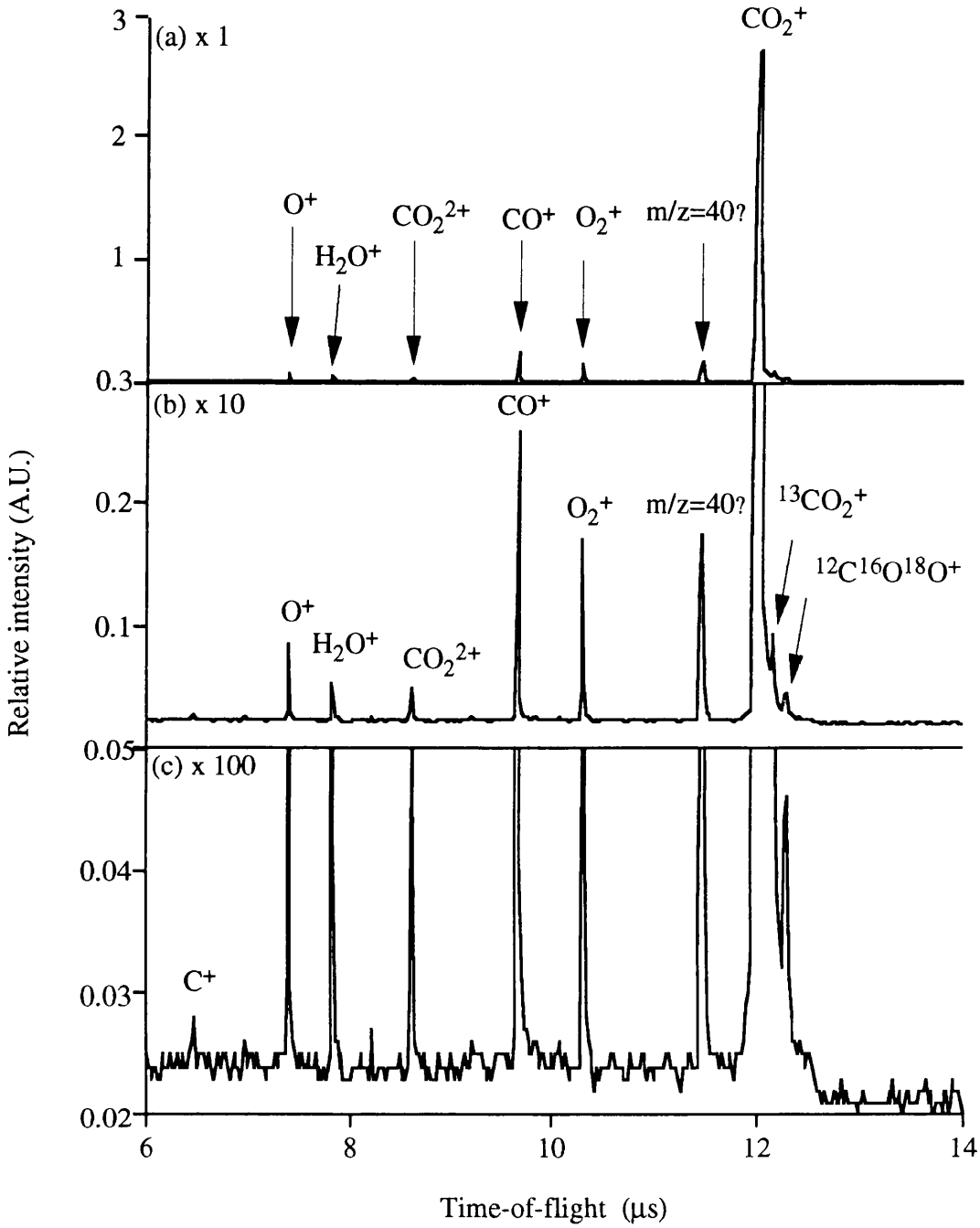

Figure 6.4.2.1 The time-of-flight spectra of CO_2 gas obtained at laser intensity of 2.1 x 10^{14} W/cm^2 with a wavelength 750 nm, duration 90 fs and vertical beam polarisation under a pressure of 6.9 x 10^{-5} Torr. (a) without magnification. (b) with a magnification of 10 times. (c) with magnification of 100 times. Only from (c) one can see the tiny C^+ peak. The two small peaks situated on the shoulder of CO_2 peak are the isotope molecules of carbon and oxygen.

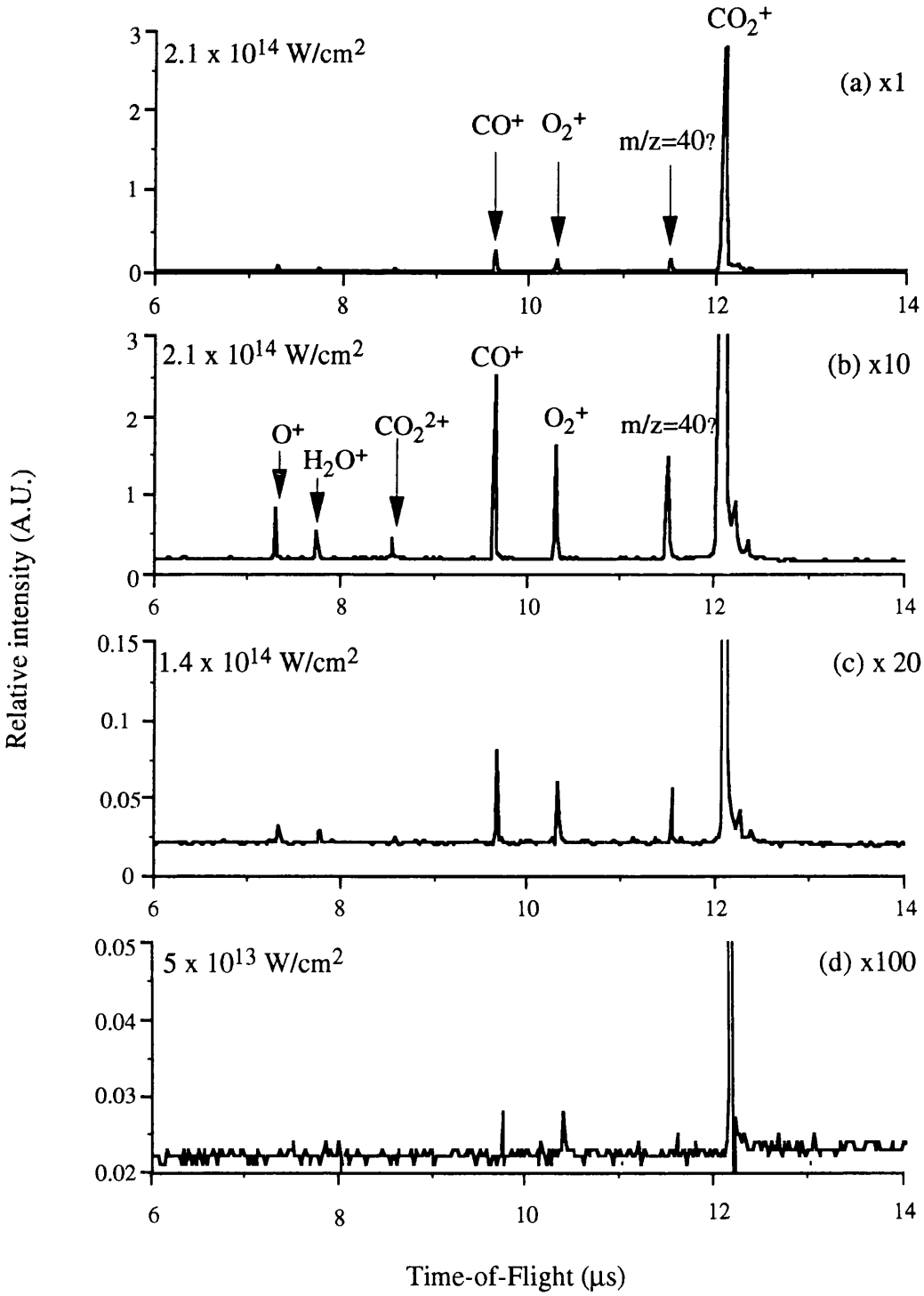

Figure 6.4.2.2. Time-of-Flight spectra of CO_2 obtained at three laser intensities with laser wavelength of 750 nm and pulse duration of 90 fs. All spectra were taken under almost the same pressure of 7.0×10^{-5} torr. Spectrum (b) is a 10 times magnified diagram of (a).

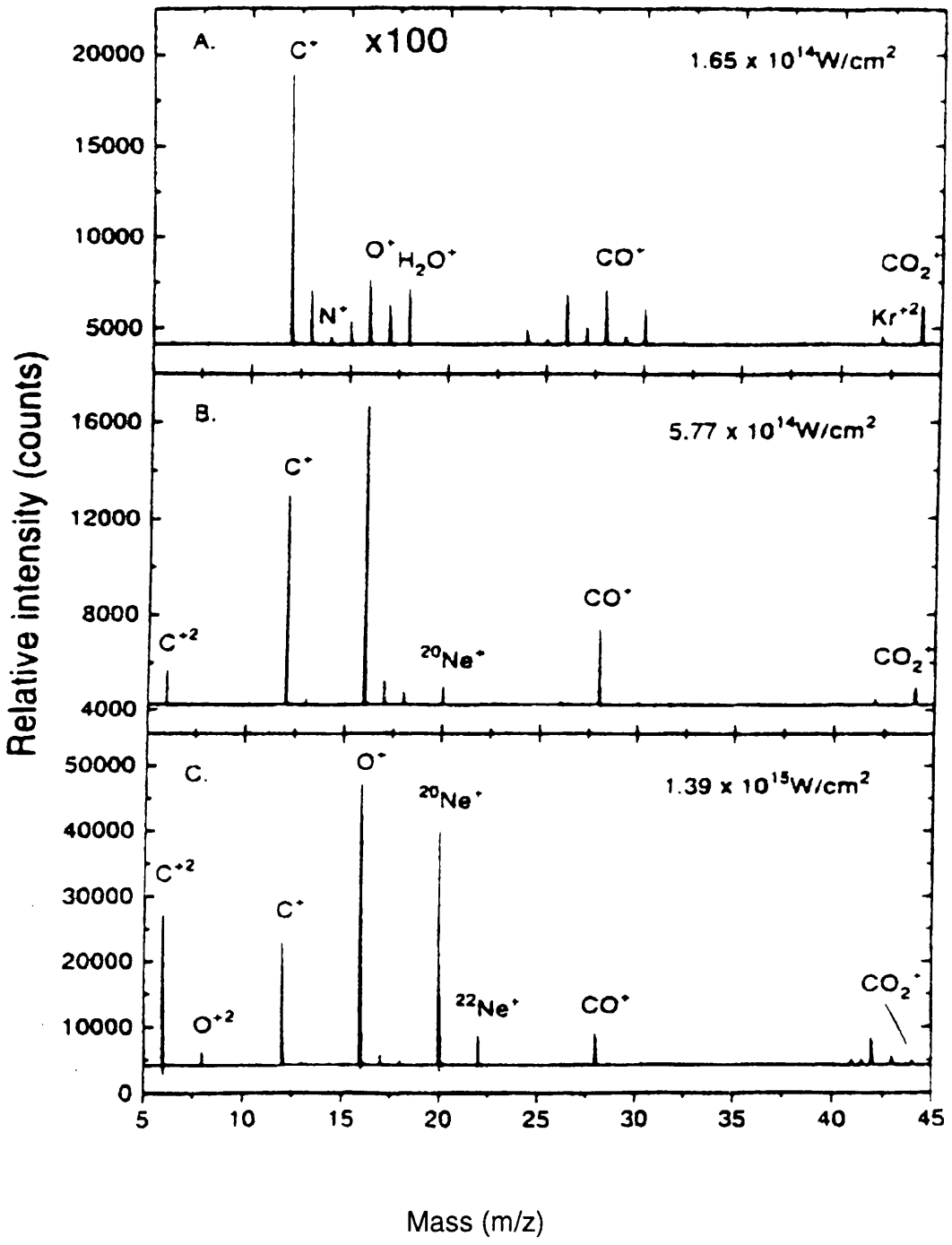

Figure 6.4.2.3. Time-of Flight spectra of CO_2 taken from He and Becker (1996) The spectra were obtained at three different laser power densities. Spectrum (a) was taken under the same conditions as spectra and (c) but with an increased sensitivity factor of 100.

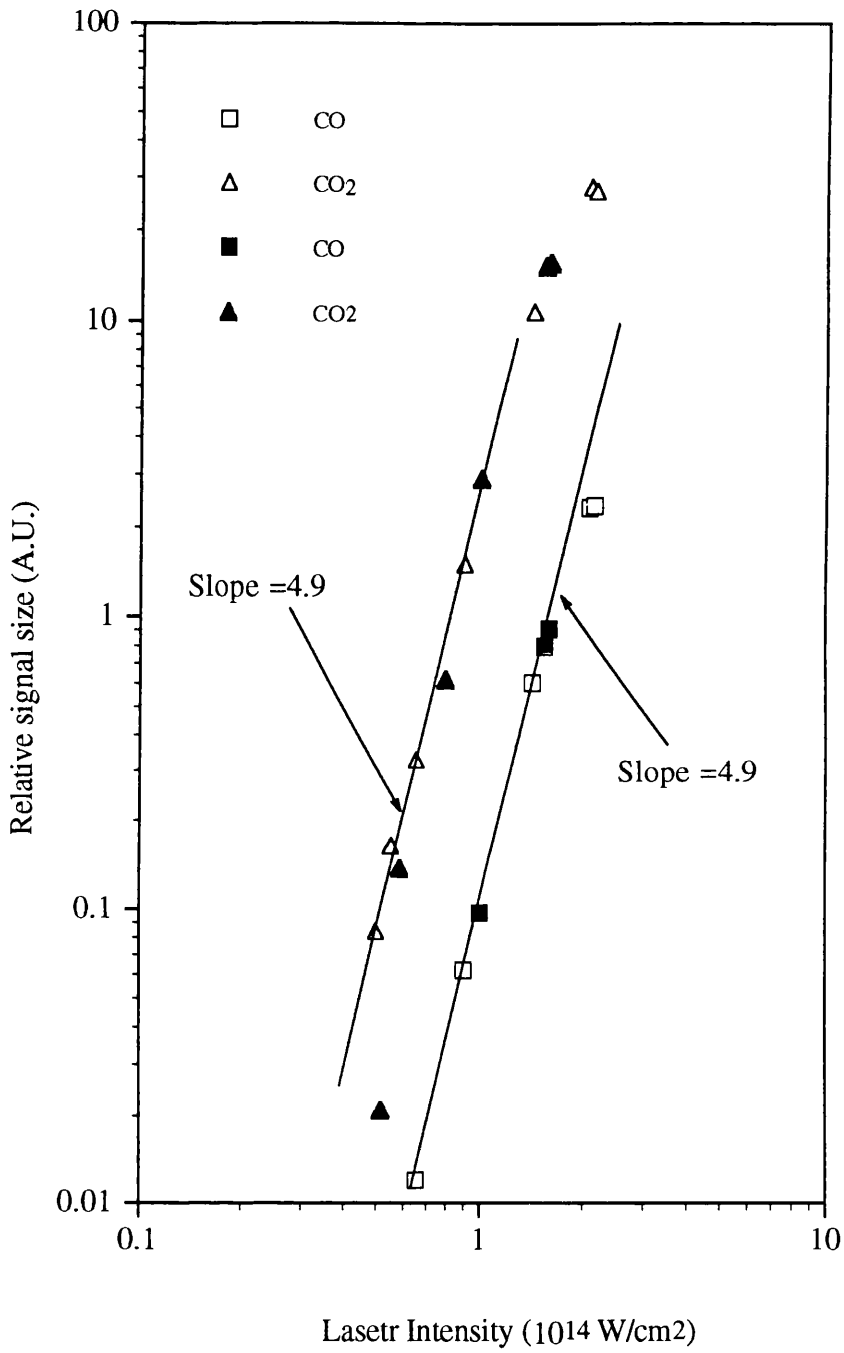

Figure 6.4.2.4 Laser intensity dependence of CO_2 parent ions and CO gragment ions from CO_2 gas obtained using 750 nm laser pulse with duration of 90 fs. In the figure all open symbols denote the data taken with vertical polarised laser beam and all filled symbols denote the data taken with horizontal polarised laser beam.

using horizontally polarised laser beam. It can be seen that the data points obtained using the laser beams with different polarisation follow the same trend i.e. both the empty symbols and the filled symbols lie on the same curves for either CO_2 or for CO ions. The slopes of the segments of the straight line of the CO_2^+ and CO^+ laser power dependence curves (which means the orders of the ionisation processes) are nearly the same (approximately equal 4.9), which implies that CO^+ comes directly from CO_2^+, i.e. this figure suggests an ID process

$$CO_2 + nh\nu \rightarrow CO_2^+ \Rightarrow CO^+ + O \qquad (6.4.2.2)$$

The ionisation potential of the CO_2 molecule is 13.77 eV and therefore at least 9-photons at 750 nm are needed for directly ionising CO_2 neutrals for the non-resonant multiphoton process, while here only a gradient of 5 is recorded. The reason why the gradient is less than the number of the photons needed can be explained by analysing the mechanisms of the involved ionisation. Two possibilities exists for the ID process of CO_2 at 750 nm: (1) saturated multiphoton ionisation (MPI); (2) tunnelling ionisation. For the situation of saturated MPI, the process order (the slope of the laser power density curve) can be any value which depends on the degree of saturation. Close to saturation fewer photons are apparently needed. For the situation of tunnelling ionisation, 9-photons are not needed either. The criterion for tunnelling ionisation is that the Keldysh parameter $\gamma<0.5$.

As mentioned in chapter one the Keldysh parameter is defined by

$$\gamma = \left(\frac{V}{2U}\right)^{1/2} \qquad (6.4.2.3)$$

where V is the zero-field ionisation potential and U is the ponderomotive potential of the laser. The ponderomotive potential is the average kinetic energy of an electron and is given by

$$U(eV) = 9.33 \times 10^{-14} I(W/cm^2)\lambda(\mu m) \qquad (6.4.2.4)$$

In this work, the γ-value changes from 1.4 to 0.6, that is to say that at the highest laser intensity the ionisation is very close to tunnelling ionisation.

Figure 6.4.2.5 shows the laser intensity dependence of CO_2^+ and the main fragment ion products CO^+ and O^+ and of the summation of all fragment ions from the ionisation at 750 nm, with laser duration of 90 fs and vertical polarisation. In the

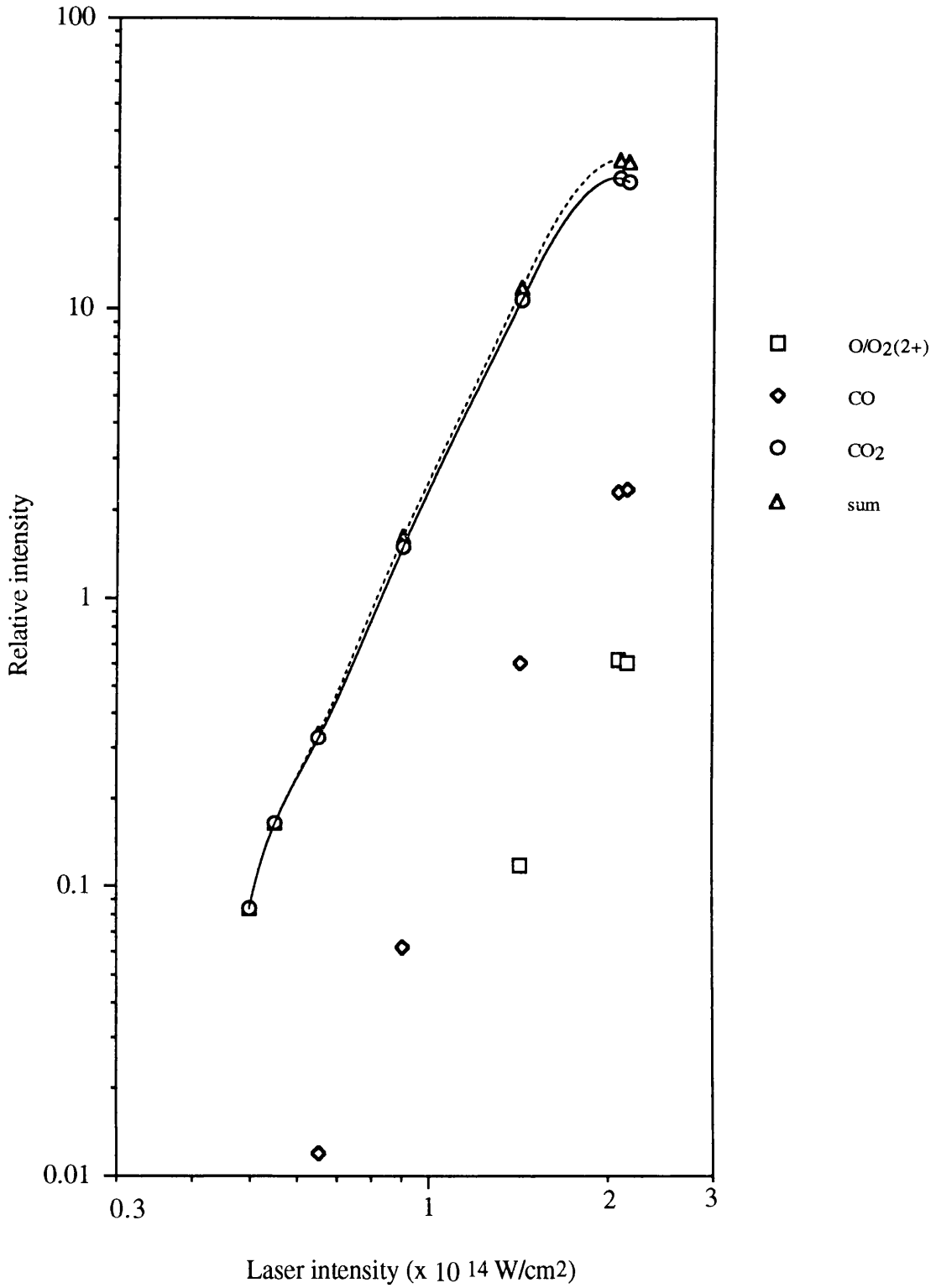

Figure 6.4.2.5 The laser power dependence of CO_2 parent ions (denoted by circles), fragment CO (denoted by diamond) and O (denoted by squares) ions as well as of the sum of all of fragments (denoted by triangles).

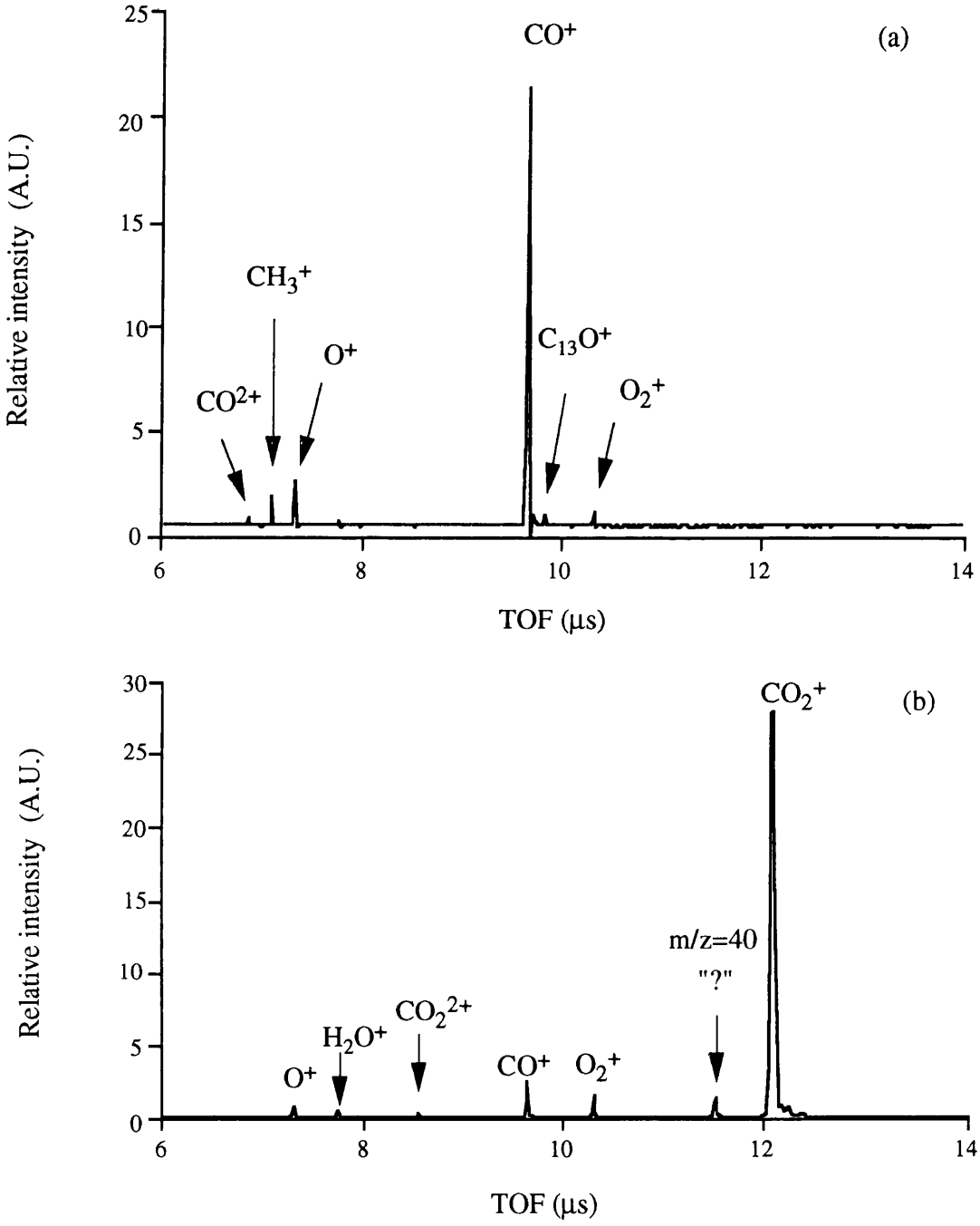

Figure 6.4.2.6. (a) A Time-of-flight spectrum of CO gas obtained at the laser intensity of 1.0 x 10^{14} W/cm^2, wavelength 750 nm and pulse width 90 fs. (b) A Time-of-flight spectrum of CO_2 gas obtained at the laser intensity of 1.0 x 10^{14} W/cm^2, wavelength 750 nm and pulse width 90 fs.

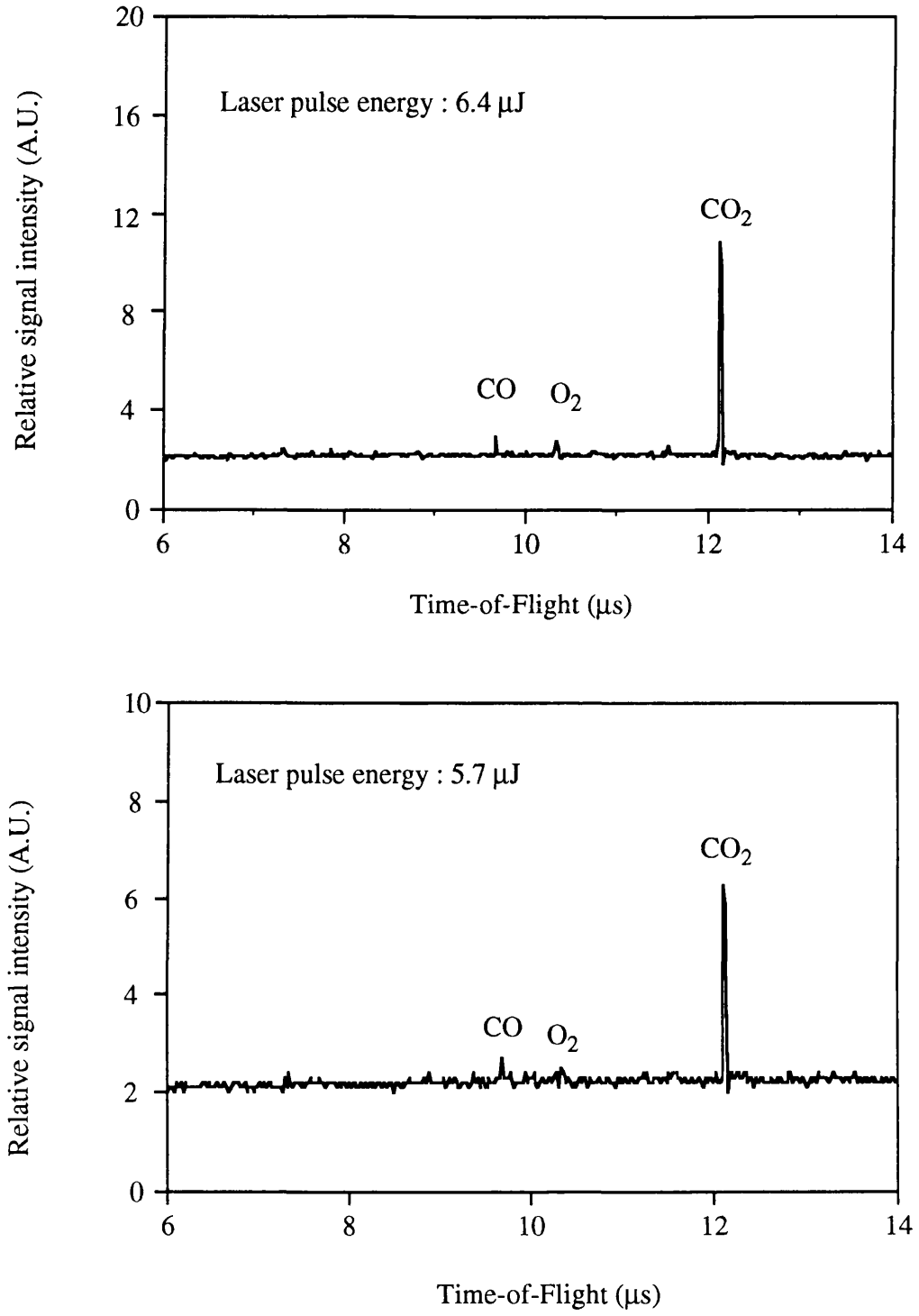

Figure 6.4.2.7. Time-of-flight spectra of CO_2 gas obtained using 375 nm, 90 fs laser pulses but at different polarisation. The upper spectrum wastaken at a laser pulse energy of 6.4 μJ and for vertical polarisation and the lower one was taken at a laser pulse energy of 5.7 μJ and for horizontal polarization. These energies were the largest values for each case under the experimental conditions. In the figure all peaks denote ion peaks.

figure, diamonds denote CO^+, squares denote O^+ and triangles denote the summation of all ion species. The triangles are linked by a dashed line. It can be seen that the intensities of the summation are very close to the CO_2 ion yields which means that nearly all CO_2 molecules in the laser field were ionised directly, therefore ID process is by far the dominant process.

There are two possibilities to explain the ion peak of m/z=40. Firstly, this peak maybe recognised as Ar^+, since Ar was used as a gas calibrant for the experiment previous to the CO and CO_2 gas analysis. The order of using the gas species is: Ar, CO and then CO_2. In order to find out if the unknown ion peak is due to the remaining resident Ar molecules, a TOF spectrum of CO and a spectrum of CO_2 is shown in figure 6.4.2.6 for a comparison. The laser intensities used are the same for both CO and CO_2. From figure 6.4.2.6 (a), it can be seen that there is no peak in the position corresponding to m/z=40. If say some Ar molecules remained in the vacuum chamber after performing the Ar experiment, then an Ar^+ peak should be seen in the CO TOF spectrum too. However this is not the case. A possible explanation is that when the CO_2 gas cylinder was put into use, the same cylinder head was used as the one used for the Ar experiment without extensive purging. Secondly, the "?" peak (with mass 40 a.m.u) probably can also be denoted as a product C_2O^+, which has been discussed by other authors (McNesby and Okabe, 1964).

From figure 6.4.2.6, it also can be seen that double charged CO ions appeared on the TOF mas spectrum which suggests the further ionisation of CO^+ following the ionisation of CO molecules, e.g.:

$$CO^+ + nh\nu \rightarrow CO^{2+} + e \qquad (6.4.2.5)$$

The experiment of CO_2 ionisation has been also carried out at the frequency doubled wavelength of 375 nm with the same pulse duration 90 fs.

Figure 6.4.2.7 shows the time-of-flight mass spectra of CO_2 taken at 375 nm with both vertical (upper trace) and horizontal (lower trace) laser beam polarisation. It can be seen that the structure of the spectra are very similar to the situation of 750 nm, but that all the peaks are much smaller than that at 750 nm since the laser pulse energies are much lower at 375 nm.

Figure 6.4.2.8 shows the laser intensity dependence of CO_2 in the laser field of 375 nm. The process order is about 4.6 which is very close to the number at 750 nm.

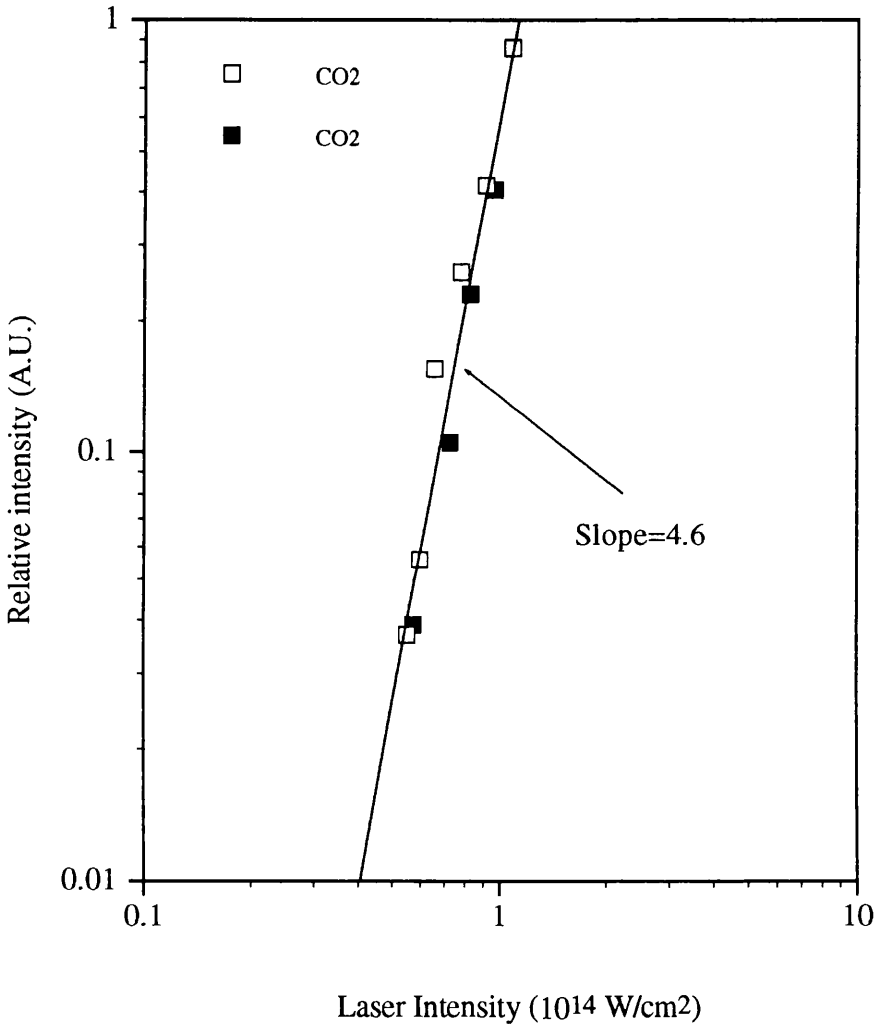

Figure 6.4.2.8. Laser intensity dependence of CO_2 ions from CO_2 gas obtained using 375 nm laser pulses with duration of 90 fs. All the empty squares denote the data taken with vertical polarised laser beam and all the filled attributers denote the data taken with horizontal polarised laser beam.

This result suggests that the ionisation of CO_2 is not wavelength dependent. From this point of view, the ionisation mechanism may be considered as saturated multiphoton ionisation.

6.5. Concluding remarks

6.5.1. For NO_2

The ionisation of NO_2 gas in intense laser fields has been investigated using a pulse laser in an intensity range of (3.2 x 10^{13} - 2.2 x 10^{14}) W/cm^2 at 750 nm and (5.6 x 10^{12} - 1.5 x 10^{14}) W/cm^2 at 375 nm with a pulse duration of 90 fs and both vertical and horizontal beam polarisation. The following conclusions can be drawn:

(1). Polarisation doesn't effect the ion yields.

(2). At 750 nm, the ratio of NO_2/NO ions is constant and at 375 nm this ratio remains constant below the saturation of the NO ions, after the saturation this ratio increases.

(3). At 750 nm, ID is the dominant process over DI, while at 375 nm DI is the process which is the more important. The competition between ID and DI depends on the laser wavelength, power density and the lifetime of the dissociate energy levels.

6.5.2. For CO_2

The ionisation of CO_2 gas in intense laser fields has been investigated using pulse laser in a power density range of (5.6 x 10^{13}-2.2 x 10^{14}) W/cm^2 at 750 nm and (5.7x 10^{13} - 1.1 x 10^{14}) W/cm^2 at 375 nm with a pulse duration of 90 fs and both vertical and horizontal beam polarisations. The following conclusions may be drawn:

(1). For CO_2, in femtosecond laser fields, in all cases the ID process is always the dominant process which defeats the DI process completely.

(2). There is no difference of process order between the ionisation at 750 nm and 375 nm which might suggest either partial saturation or tunnelling.

(3). There is no polarisation effect on the ionisation of the CO_2 molecules in femtosecond laser fields.

(4). Double charged ions can be observed at high laser power densities which might be indicative of tunnelling ionisation.

6.5.3. General conclusion

For the molecules with high ionisation potential and higher dissociation energy, e.g. CO and CO_2, it has been shown that the ID defeats DI and that doubly charged parent ions can be observed because of the very high intensity of parent ions compared to its fragment ions. A similar observation has also been made by Kumar et al (1994).. There is no polarisation effect on the ion yields.

References:

Boyer, K., Luk, T.S., Solem, J.C. and Rhodes, C.K. (1989)
Kinetic energy distribution of ionic fragments produced by subsecond multiphoton ionisation of N_2. *Phys. Rev. A,* **39**, pp. 1186-1192

Codling, K. and Frasinski, L.J. (1993)
Dissociative ionisation of small molecules in intense laser fields, *J . Phys. B: At. Mol. Opt. Phys.*, **26,** pp. 783-809

Codling, K., Frasinski, L.J. and L.J., Hatherly, P.A. (1988)
Multiphoton ionisation of H_2 and D_2 using an intense sub-picosecond laser, *J . Phys. B: At. Mol. Opt. Phys.*, **21,** pp. L433-L438

Codling, K., Frasinski, L.J., Hatherly, P.A. and Stankiewicz, M. (1987)
New triple coincidence technology applied to multiple ionisation of molecules, *Phys. Scr.*, **41**, pp. 433-439

Cornaggia, C., Lavacier, J., Normand, D., Morellec, J. and Liu, H. X. (1990)
Intensity dependence of the multielectron ionisation of N_2 at 305 and 610 nm, *Phys. Rev. A*, **42**, pp. 5464-5472

Cornaggia, C., Lavacier, J., Normand, D., Morellec, and Agostini, P. (1991)
Multielectron dissociative ionisation of diatomic molecules in an intensive femtosecond laser field, *Phys. Rev.*, **44**, pp. 4499-4505

Cornaggia, C., Schmidt, M., and Normand, D. (1994)
Coulomb explosion of CO_2 in an intense femtosecond laser field, *J. Phys. B: At. Mol. Opt. Phys.*, **27,** pp. L123-L130

Dietrich, P. and Corkum, P.B. (1992)
Ionisation and dissociation of diatomic molecules in intense infrared laser fields, *J. Chem. Phys.*, **97**, pp. 3187-3198

Dyer, M.J., Jusinski, L.E., Helm, H. and Becker, C.H. (1991)
Surface analysis by phtoionisation of sputtered species with intense picosecond laser radiation, *Applied Surface Science*, **52**, pp. 151-157

Freeman, R.R. and Bucksbaum, P.H. (1991)
Investigations of above-threshold ionisation using subpicosecond laser pulses, *J. Phys. B: At. Mol. Opt. Phys.*, **24,** pp. 325-327

Frasinski, L.J., and Hatherly, P.A , Codling, K., Larsson, M., Persson, A. and Wahlstrom, C-G (1994)
Multielectron dissociative ionisation of CO_2 in intense laser fields, *J. Phys. B: At. Mol. Opt. Phys.*, **27,** pp. L109-L114

Frasinski, L.J., Codling, K., and Hatherly, P.A. (1989)
Multiphoton multiple ionisation of N_2 probed by covariance mapping, *Phys. letter A* , **142,** pp. 499-503

Goppert-Mayer, M. (1931)
Ann. Phys. **9**, 273-294

Harding, D.R., Weston, Jr. R.E., Flynn, G.W. (1988)
Energy transfer to CO(v) in the $O(^1D)+CO(^1\Sigma_g^+)$ reaction, *J. Chem. Phys.* **88**, pp. 3590-3598

He, C. and Becker, C. H., (1997)
Absolute nonresonant multiphoton ionisation cross section of NO at 532 nm, *Phys. Rev. A*, **55,** pp. 1300-1306

He, C. and Becker, C. H., (1996)
Surface analysis with 10^{14}-10^{15} Wcm^{-2} laser intensities, *Surface and interface analysis,* **24,** pp.79-85

Ilkov, F.A., Decker, J.E. and Chin, S.L. (1992)
Ionisation of atoms in the tunnelling regime with experimental evidence using Hg atoms. *J. Phys. B: At. Mol. Opt.*, **25**, pp. 4005-4020

Kumar, G.R., Safvan, C.P., Rajgara, F.A., and Mathur, D. (1994)
Dissociatve ionisation of molecules by intense laser fields at 532 nm and 10^{12}-10^{14} Wcm^{-2}, *J. Phys. B: At. Mol. Opt. Phys.*, **27**, pp. 2981-2991

Lavancier, J., Normand, D., Cornaggia, C., Morellec, J. and Liu, H.X. (1991)
Laser intensity dependence of the multielectron ionisation of CO at 305 and 610 nm, *Phys. Rev. A.* **43**, pp. 1461-1469

Ledingham, K.W.D., Kosmidis, C., Georgou, S., Courris, S. , Singhal. R.P. (1995)
A comparison of the femto-pico- and nano-second multiphoton ionisation

and dissociation process of NO_2 at 248 nm and 496 nm, *Chem. Phys. Lett,* **247**, pp. 555-563

Luk, T.S. and Rhodes, C.K. (1988)
Multiphoton dissociative ionisation of molecular deuterium *Phys. Rev. A.* **38**, pp. 6180-6184

Luk, T.S., Tate, T.A., Boyer, K., and Rhodes, C.K. (1993)
Comparison of kinetic-energy distributions and ionic fragment yields of CO_2 and N_2O arising from Coulomb explosions induced by mulyiphoton ionisation and fast ion impact, *Phys. Rev. A*, **48**, pp. 1359-1363

L'Huillier, A. and Mainfray, G. (1984)
Multiphoton ionisation versus dissociation of diatomic molecules irradiated by an intense 40 ps laser pulse, *Chem. Phys. Lett.*, **103**, pp. 447-450

Mathur, D., Krishnakumar, E., Rajgra, F.A., Raheja, U.T. and Krishnamurthi, V. (1992)
Energy-distributions of recoil ions produced in 100 MeV collisions of SI_8^+ with CO_2 and CS_2 molecules. *J. Phys. B: At, Mol, Opt. Phys.*, **25**, pp. 2997-3008

Normand, D., Cornaggia, C., Lavancier, J., Morellec, J. and Liu, H. X. (1991)
Multielectron dissociative ionisation of O_2 in an intense picosecond laser field, *Phys. Rev. A*, **44**, pp. 475-482

Normand, D., Lompre, L.A. and Cornaggia, C. (1992)
Laser-induced molecular alignment proved by a double-pulse experiment, *J. Phys. B: At, Mol, Opt. Phys.*, **25**, pp. L497-L503

Safvan, C.P., Vijyalakshmi, K., Gajgara, F.A., Kumar, G.R., Marathe, V.R. and Mathur, D. (1996)
Dissociation dynamics of NO_2 in intense laser fields: directional specificity of O^+ and NO^+ fragments

Singhal, R.P., K.W.D. Ledingham, Kilic, H.S., McCanny, T., Smith, D.J., Peng W.X., Kosmidis, C. and Langley, A. J. (to be published)
On the ionisation and dissociation of NO_2 by short intense laser pulse

Singhal, R.P. (1997)
Private communication.

Singhal, R.P., Kilic, H.S., Ledingham, K.W.D., Kosmidis, C., McCanny, T (1996)
Multiphoton ionization and dissociation of NO_2 by 50 fs laser pulses, *Chem. Phys. Lett*, **253**, pp.81-86

Singhal, R.P. (1997)
Private communications.

Szaflarski, D.M. and El-Sayed (1988)
Multiphoton absorption fragmentation mechanisms of CH_3I by picosecond and nanosecond laser mass spectrometry, ed. by Bandrauk. A.D., Atomic and molecular process with short intense laser pulses, Pleenum press, New York and London

Vijayalaskshmi, K., Safvan, C.P., Kumar, G.R., Mathur, D. (1997)
On the proposal for femtosecond parent-ion mass-spectrometry, *Rap. Comm. Mass Spectr.*, **10**, pp. 1626-1628

Walsh, T.D.G., Decker, J.E. and Chin, S.L.(1992)
Tunnel ionisation of simple molecules by an intense CO_2 laser, *J. Phys. B: At, Mol, Opt. Phys.*, **25**, L85-L90

Wu. M and P. M. Johnson (1989)
A study of some Rydberg states of CO_2 by (3+1) multiphoton ionisation spectroscopy, *J. Chem. Phys.* ,**91**, pp. 7399-7407

Yang, J.J., Gobeli, D.A., and El-Sayed, M.A. (1985)
Change in the mechanism of laser multiphoton ionisation-dissociation in benzaldehyde by changing the laser pulse width, *J. Phys. Chem.*, **89**, pp. 4326-3429

Zavriyev, A., Bucksbaum, P.H., Muller, H.G., and Schumacher, D.W. (1990)
Ionisation and dissociation of H_2 in intense fields at 1.064 μm, 532 nm, and 355 nm, *Phys. Rev. A*, **42**, pp. 5500-5513

Zavriyev, A., Bucksbaum, P.H., Squier, J. and Saline, F.
Light-induced vibrational structure in H2+ and D2+ in intense laser fields, *Phys. Rev. lett.* **70**, pp.1077-1080

Chapter 7

Future Research Plan

7.1 Introduction

The research work of this thesis is divided into two categories: (1). To carry out trace analysis using the REMPI technique in the nanosecond regime. (2). To develop a new research area particularly the physics for trace analysis in the femtosecond regime. The future plan will outline further research in the femtosecond regime and its applications to trace analysis.

REMPI is a very mature technique requiring the condition of resonance which limits the applications of REMPI. Moreover, it is difficult to detect intact molecular ions since most molecules have low dissociation energy levels. Therefore the physicists and chemists working in the area of trace analysis have turned their research interests to the development of a new analysis tool called Femtosecond Laser Mass Spectrometry (FLMS) for the ultra-trace analysis of atoms and molecules. The research in both the physics of ultrafast phenomena and the applications to trace analysis have been carried out by a number of research groups in the world (see the references in chapter 6). Although a lot of papers in this field have been published, so far there is no work goes beyond the laser intensity of 10^{15} Wcm^{-2}. Ledingham has predicted (1997) that above this laser intensity threshold, some attractive phenomena would take place, e.g. ion yields would be independent of laser wavelength, independent of laser intensity and even independent of the ionisation potentials of the molecules under study. As a result, the ion yield is only dependent on the density of the molecules under study or the pressure of the sample in the vacuum. Therefore for the analysis of a gas mixture, the only thing needed to do is to measure the ion signal size for the different ion species by analysing the mass spectra taken using FLMS technique.

The mechanism of such a kind of ionisation would be at the interface between multiphoton ionisation and tunnelling ionisation and the research in this aspect will be another interesting activity for atoms and molecules in intense laser fields.

A consequence of ionisation above the laser intensity threshold of 10^{15} Wcm^{-2} can be deduced from figure 7.1 (from He et al, 1996): In this figure, a number of curves corresponding to a group of species to be analysed are plotted by taking relative sensitivity factors (RSFs) as a function of laser power densities (laser intensities). The definition of the relative sensitivity factor (RSF) is as follows:

For a multi-element sample containing a group of species A,B, and C, the RSFs of species A and B, with reference to species C, are

$$RSF(A) = \frac{I_A / [A]}{I_C / [C]} \tag{7.1.1}$$

and

$$RSF(B) = \frac{I_B / [B]}{I_C / [C]} \tag{7.1.2}$$

where I_A, I_B and I_C are the signal intensities of species *A*, *B* and *C*; and [A], [B] and [C] are the concentrations of species A,B and C in the sample.

From figure 7.1, it can be seen that above the value of laser intensity (10^{15} Wcm^{-2}), the RSFs (compared to Ar) do not change very much and gradually approach to unity at about 5 x 10^{15} Wcm^{-2}. This means that the ionisation sensitivity for each element is the same and it is independent of laser intensity and ionisation potential. The signal size of the ionisation is only a function of the gas pressure i.e. 100% ionisation efficiency.

To reach the goal of realising quantitative analysis using FLMS, only a laser intensity > 10^{15} Wcm^{-2} is needed. The upgrading of the laser facilities at RAL is underway and hence to perform the experiments with such a laser power density will be possible. The proposed future programme will be described in the next paragraph.

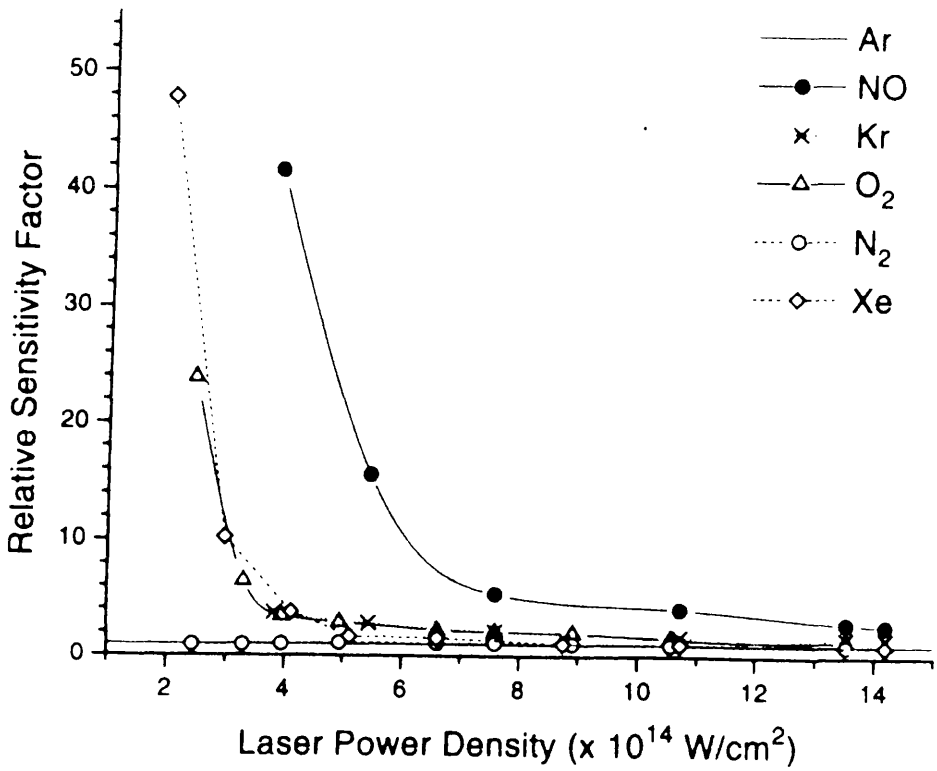

Figure 7.1 A diagram from He at al, 1996. RSFs of the gases studied versus power density of the ionising laser beam. The values are obtained with reference to Ar. Gases are studied in groups with no mass interference fron single- and charged parent species and fragments. Gas composition is accurately determined by absolute capatance monometer pressure gauges at the source with a known leak rate into the chamber. Influences due to differences in pumping speed were eliminated by temporarily closing the gate valve to the cryopump.

7.2 Future research plan

7.2.1 Research work in pure physics

To verify the prediction proposed by Ledingham et al, the following studies investigating the physics of atoms and molecules in ultra-intense laser fields will be performed. Those are:

(1). The studies on the ionisation of small molecules, e.g. H_2, D_2, N_2, O_2, CO, CO_2, NO, NO_2 and CS_2, with laser intensity up to 1 x 10^{15} Wcm^{-2}, using three wavelengths 800, 400, 200 nm at different pulse widths from 100 fs up to 2 ps.

(2). The studies on the ionisation of aromatic and nitroaromatic gas samples with different laser wavelengths and pulse widths and laser intensities up to 10^{15} Wcm^{-2}.

(3). The studies on the interference from the species with the same or close mass to charge ratios.

7.2.2 Research work in the applications of ultra-trace analysis

As is mentioned in section 7.1, above the laser intensity of 10^{15} Wcm^{-2} ionisation efficiency for different gas species will approach 100% and the ionisation signal size will only depend on the gas pressure, therefore the simultaneous quantitative analysis of gas mixtures will become possible. Hence experiments will be carried out in the near future to varify this.

Reference:

He, C. and Becker, C. H., (1996)
Surface analysis with 10^{14}-10^{15} Wcm^{-2} laser intensities, *Surface and interface analysis,* **24,** pp.79-85

Ledingham, K.W.D., Singhal, R.P., Langly, A.J. and Towrie, M. (1997)
The potential of femtosecond laser mass spectrometry for ultra-trace analysis of atoms and molecules, A research proposal to the Engineering and Physical Sciences Research Council (EPSRC)